AMERICAN UNIVERSITY OF BEIRUT

POLYOXOMETALATES IMMOBILIZED ONTO MESOPOROUS ORGANICALLY-MODIFIED SILICA AEROGELS FOR SELECTIVE OXIDATION CATALYSIS OF ANTHRACENE

by
RAMI GHASSAN AL-OWEINI

A thesis
submitted in partial fulfillment of the requirements
for the degree of Master of Science
to the Department of Chemistry
of the Faculty of Arts and Sciences
at the American University of Beirut

Beirut, Lebanon
October 2009

AMERICAN UNIVERSITY OF BEIRUT

POLYOXOMETALATES IMMOBILIZED ONTO MESOPOROUS ORGANICALLY-MODIFIED SILICA AEROGELS FOR SELECTIVE OXIDATION CATALYSIS OF ANTHRACENE

by
RAMI GHASSAN AL-OWEINI

Approved by:

Dr. Houssam El-Rassy, Assistant Professor Chemistry	Advisor
Dr. Rabih Sultan, Professor Chemistry	Member of Committee
Dr. Faraj Hasanayn, Associate Professor Chemistry	Member of Committee

Date of thesis defense: October 9, 2009

AMERICAN UNIVERSITY OF BEIRUT

THESIS RELEASE FORM

I, Rami Ghassan Al-Oweini

☐ authorize the American University of Beirut to supply copies of my thesis to libraries or individuals upon request.

☐ do not authorize the American University of Beirut to supply copies of my thesis to libraries or individuals for a period of two years starting with the date of the thesis defense.

_____
Signature

_____
Date

ACKNOWLEDGMENTS

First and foremost, I would like to express my sincere appreciation to my advisor, Dr. Houssam El-Rassy, for his prolific, insightful, generous, enthusiastic support throughout this research project, which enabled me to finish this thesis and make my stay at AUB one of the most rewarding in my life.

Genuine gratitude is also expressed to the committee members Dr. Rabih Sultan and Dr. Faraj Hasanayn, for their time, valuable comments and suggestions on my thesis work.

I wish to take this opportunity to earnestly thank Mr. Shant Aghyarian for his much recognized help and assistance. Especially, I wish to thank former and current members in Dr. El-Rassy's research group, Miss Hiba Ramadan, Miss Joelle Akl, and Mrs. Lara Abramian for their friendship and help. Without their enthusiastic contribution and great effort, this work would not have been possible. I thank all the faculty, staff, and colleagues in the Department of Chemistry, who have made my academic experience rich and memorable.

We are most grateful to the American University of Beirut Research Board for funding and support of the projects in this thesis. My particular acknowledgment and thanks also go to the personnel at the Central Research Science Laboratory for their assistance in the technical work.

Finally, I wish to express my deepest appreciation to my family and friends, for their love, understanding, patience, and full support throughout the past five years.

AN ABSTRACT OF THE THESIS OF

Rami Ghassan Al-Oweini for Master of Science
Major: Chemistry

Title: Polyoxometalates Immobilized onto Mesoporous Organically-Modified Silica Aerogels for Selective Oxidation Catalysis of Anthracene

Novel surface organically-modified silica aerogels were synthesized and characterized by FTIR spectroscopy and nitrogen adsorption/desorption experiments. The surface modification of the silica aerogels was conducted with the help of a two-step sol-gel process where various silicon precursors and co-precursors were used. The silicon precursors have identical methoxy and ethoxy groups, while the co-precursors have a substituted non-hydrolysable alkoxy group (methyl, ethyl, n-propyl, *iso*-butyl, octyl, vinyl, or phenyl) substituted instead. The functional groups that were functionalized on the surface of these silica aerogels have been identified and appealing physicochemical properties were identified. The aerogels synthesized with a very fine mesoporous nature possessed high specific surface areas and pore volumes. The analysis of the structure of these synthesized silica materials were chemically very comparable with only some differences due to the nature of the various silicon precursors.

Such highly qualified mesoporous materials were used as the very suitable supports onto which two types of polyoxometalates were loaded. In this thesis, inorganic-organic hybrid silica aerogel materials were synthesized by the immobilization of two molybdovanadophosphoric acids onto the mesoporous silica aerogels synthesized through an amine organic linker. All the catalyst materials were characterized by atomic absorption spectroscopy, FTIR, nitrogen sorption measurements, XRD, and DR UV-Vis for their structural nature and physicochemical properties. These techniques revealed that the polyoxometalates were retained inside the pores of the mesoporous silica aerogels. The catalytic activities of these supported POMs on silica aerogel materials were tested in liquid-phase oxidation of anthracene with 70% tert-butylhydroperoxide as the oxidant in benzene. Immobilized molybdovanadates onto amine-functionalized silica aerogel materials was highly active in the oxidation of anthracene to 9, 10-anthraquinone, where an improvement of the catalytic activity was noticeable with 100% selectivity for 9, 10-anthraquinone. Finally, oxidant and solvent effects were evaluated and analyzed.

CONTENTS

ACKNOWLEDGEMENTS….. v

ABSTRACT…..... vi

LIST OF ILLUSTRATIONS xi

LIST OF TABLES xvii

Chapter……..... Page

1. INTRODUCTION 1

1.1. The Sol-Gel Process 1

1.1.1. Overview 2
1.1.2. Chemistry..... 2
1.1.3. Advantages and disadvantages 4

1.2. Silica 6

1.2.1. Overview 6
1.2.2. Theory..... 6
1.2.3. Synthesis of Inorganic Gels 7
1.2.4. Applications..... 9

1.3. Aerogels 10

1.3.1. Overview 10
1.3.2. Theory..... 11
1.3.3. Synthesis of Silica Aerogels 12
1.3.4. Applications..... 22

1.4. Organically-Modified Silica Materials 25

1.4.1. Overview 25

1.4.2. Chemistry 25
1.4.3. Advantages and disadvantages 26

1.5. Polyoxometalates 27

1.5.1. Overview 27
1.5.2. Theory 27
1.5.3. Preparation 32
1.5.4. Application 34

1.6. Polyoxometalates in Catalysis 35

1.6.1. Overview 35
1.6.2. Theory 36
1.6.3. Applications 37

1.7. Supported Polyoxometalates 37

1.7.1. Overview 37
1.7.2. Chemistry 38
1.7.3. Advantages and disadvantages 39

1.8. Aim of Present Work 40

2. SILICA AEROGELS SYNTHESIS 42

2.1. Silica aerogels synthesis 42

2.1.1. Materials 42
2.1.2. Procedure 43

2.2. Results and discussion 45

3. FTIR SPECTROSCOPY 47

3.1. Infrared spectroscopy 47

3.1.1. Overview 47
3.1.2. Theory 50
3.1.3. Sample preparation and characterization 52

3.2. Results and discussion 53

3.2.1. TMOS and TEOS aerogels 53
3.2.2. Methyl aerogels 55
3.2.3. Ethyl aerogels 56

3.2.4. Propyl aerogels 58
3.2.5. Isobutyl aerogels 59
3.2.6. Octyl aerogels 60
3.2.7. Vinyl aerogels 61
3.2.8. Phenyl aerogels 62

3.3. Conclusion 63

4. SURFACE CHARACTERIZATION 66

4.1. Nitrogen sorption experiments 66

4.1.1. Overview 66
4.1.2. Theory 68
4.1.3. Sample preparation and characterization 74

4.2. Results and discussion 76

4.2.1. TMOS and TEOS aerogels 76
4.2.2. Methyl aerogels 79
4.2.3. Ethyl aerogels 82
4.2.4. Propyl aerogels 82
4.2.5. Isobutyl aerogels 83
4.2.6. Octyl aerogels 85
4.2.7. Vinyl aerogels 86
4.2.8. Phenyl aerogels 88

4.3. Conclusion 89

5. ATALYSIS 92

5.1. Overview 92

5.1.1. Acid catalysis 92
5.1.2. Oxidation catalysis 95

5.2. POM synthesis 97

5.2.1. Materials 98
5.2.2. Procedure 98
5.2.3. Characterization 100
5.2.4. Results and discussion 101
5.2.4.1. FTIR spectroscopy 102
5.2.4.2. Nitrogen physisorption experiments 103
5.2.4.3. X-ray diffraction 104
5.2.4.4. DR UV-Vis spectroscopy 105

5.3. POM immobilization 106

5.3.1. Materials 106
5.3.2. Procedure 106
5.3.3. Characterization 109
5.3.4. Results and discussion 110
5.3.4.1. AAS spectroscopy 111
5.3.4.2. FTIR Spectroscopy 112
5.3.4.3. Nitrogen physisorption experiments 114
5.3.4.4. X-ray diffraction 117
5.3.4.5. DR UV-Vis spectroscopy 119

5.4. Catalysis 121

5.4.1. Reaction significance 121
5.4.2. Materials 123
5.4.3. Procedure and analysis technique 123
5.4.4. Results and discussion 125
5.4.4.1. Catalysis 125
5.4.4.2. Oxidant and solvent effects 129
5.4.4.3. Catalyst reuse 132

5.5. Conclusion 133

6. CONCLUSION 134

Appendix

APPENDIX A 137

APPENDIX B 141

APPENDIX C 149

REFERENCES 170

ILLUSTRATIONS

Figure..……..... Page

1. 1. Sol-gel techniques and their products; modified from Ref. [5, 18] 4

1. 2. Different kinds of silica aerogels prepared by drying under supercritical CO_2 in our laboratory 11

1. 3. pH rate profile for hydrolysis in aqueous solution; taken from Ref. [69] 13

1. 4. Dissolution rate and relative gel time as a function of pH; taken from Ref. [5]... 15

1. 5. Schematic representation of gel surface at the end of drying; modified from Ref. [78]..... 19

1. 6. A possible cold supercritical drying path in the Pressure (P) Temperature (T) phase diagram of CO_2 (Shown in dashed arrows); modified from Ref. [36] ... 21

1. 7. Stardust capsule and canister with a close up view of a cometary impact (yellow arrow) into the aerogel collector; modified from Ref. [98, 99]..... 23

1. 8. Scanning electron micrograph of ammonium phosphomolybdate; taken from Ref. [132]..... 28

1. 9. Ball-and-stick and polyhedral representations of the fundamental unit MO_6, whereby the M atom is displaced off the geometrical centre of the octahedron towards one of the oxygens giving rise to a distorted C_{4v} unit; modified from Ref. [133]..... 29

1. 10. The polyhedral models represent the three possible unions between two MO_6 octahedral units, whereby each corner represents an oxygen position; taken from Ref. [133] 29

1. 11. Polyhedral representation for the different structures of heteropolyanions; modified from Ref. [138]..... 31

1. 12. Polyhedral representation of the five rotational isomers of the Keggin anion, in which the shaded region are the edge-sharing octahedra involved in the isomerism; taken from Ref. [140-142] 32

1. 13. Preparation schemes of two POMs: $H_3PMo_{12}O_{40}.nH_2O$ (Left), $H_3PW_{12}O_{40}.nH_2O$ (Right); modified from Ref. [143] 33

1. 14. Hierarchical structure of heteropoly compounds; modified from Ref. [146] 34

2. 1. Silica aerogel synthesis 45

3. 1. A simple FTIR spectrometer layout; modified from Ref. [224] 49

3. 2. Various vibrational modes; the arrows represent the vibration direction of the atoms bound to the atom A; + and – represent the vibrational motions in two opposite directions: inwards and outwards; modified from Ref. [222, 225] 51

3. 3. FTIR spectra of the silica aerogels from TMOS and TEOS 55

3. 4. FTIR spectra of the methyl-modified silica aerogels 57

3. 5. FTIR spectra of the iso-butyl-modified silica aerogels 60

3. 6. FTIR spectra of the vinyl-modified silica aerogels 62

4. 1. Types of physisorption isotherms (Left), Types of hysteresis loops (Right); modified from Ref. [88] 69

4. 2. Pore types a) open pore b) closed pore c) ink-bottle pore d) cylindrical, open-ended pore; taken from Ref. [243] 71

4. 3. NOVA 2200 Quantachrome surface area analyzer, Long Sample Cells; modified from Ref. [242] 75

4. 4. Nitrogen adsorption/desorption isotherms of the silica aerogels from TMO and TEOS 78

4. 5. Pore size distribution of the silica aerogels from TMOS and TEOS 79

4. 6. Nitrogen adsorption/desorption isotherms of the methyl-modified silica aerogels 81

4. 7. Pore size distribution of the methyl-modified silica aerogels 81

4. 8. Nitrogen adsorption/desorption isotherms of the iso-butyl-modified silica aerogels 84

4. 9. Pore size distribution of the iso-butyl-modified silica aerogels 85

4. 10. Nitrogen adsorption/desorption isotherms of the vinyl-modified silica aerogels87

4. 11. Pore size distribution of the vinyl-modified silica aerogels 88

5. 1. The heteropoly etherate layer (Left) and the obtained orange crystals of 11-MVPA (Right), as prepared in our laboratory 99

5. 2. 10-MVPA (Dark Orange) and 11-MVPA (Orange) mixtures before extraction (Left), the extraction with diethyl ether with the heteropoly etherate layer as the middle layer (Center), and the crystallization in a vacuum dessicator over concentrated sulfuric acid (Right); during MVPA synthesis in our laboratory 100

5. 3. FTIR spectra of the 10-MVPA and 11-MVPA 102

5. 4. Nitrogen adsorption/desorption isotherms of the 10-MVPA and 11-MVPA 103

5. 5. Pore size distribution of the 10-MVPA and 11-MVPA 104

5. 6. X-ray diffraction patterns of the 10-MVPA and 11-MVPA 105

5. 7. DR UV-Vis spectra of the 10-MVPA and 11-MVPA 106

5. 8. The change in color from orange to green after immobilization, as prepared in our laboratory 109

5. 9. FTIR spectra of the M1 immobilized materials 113

5. 10. FTIR spectra of the E1 immobilized materials 113

5. 11. Nitrogen adsorption/desorption isotherms of the M1 immobilized materials .. 115

5. 12. Pore size distribution of the M1 immobilized materials 116

5. 13. Nitrogen adsorption/desorption isotherms of the E1 immobilized materials ... 116

5. 14. Pore size distribution of the E1 immobilized materials 117

5. 15. X-ray diffraction patterns of the M1-10 and M1-11 118

5. 16. X-ray diffraction patterns of the E1-10 and E1-11 119

5. 17. DR UV-Vis spectra of the M1-10 and M1-11 120

5. 18. DR UV-Vis spectra of the E1-10 and E1-11 121

5. 19. Anthraquinone production as a function of time with the 10-MVPA immobilized materials 127

5. 20. Anthraquinone production as a function of time with the 11-MVPA immobilized materials 128

A. 1. FTIR spectra of the ethyl-modified silica aerogels 137

A. 2. FTIR spectra of the propyl-modified silica aerogels 137

A. 3. FTIR spectra of the octyl-modified silica aerogels 138

A. 4. FTIR spectra of the phenyl-modified silica aerogels 138

B. 1. Nitrogen adsorption/desorption isotherms of the ethyl-modified silica aerogels 141

B. 2. Pore size distribution of the ethyl-modified silica aerogels 141

B. 3. Nitrogen adsorption/desorption isotherms of the propyl-modified silica aerogels 142

B. 4. Pore size distribution of the propyl-modified silica aerogels..... 142

B. 5. Nitrogen adsorption/desorption isotherms of the octyl-modified silica aerogels 143

B. 6. Pore size distribution of the octyl-modified silica aerogels 143

B. 7. Nitrogen adsorption/desorption isotherms of the phenyl-modified silica aerogels 144

B. 8. Pore size distribution of the phenyl-modified silica aerogels 144

B. 9. BET plots of the silica aerogels from TMOS and TEOS 145

B. 10. BET plots of the methyl-modified silica aerogels..... 145

B. 11. BET plots of the ethyl-modified silica aerogels..... 146

B. 12. BET plots of the propyl-modified silica aerogels 146

B. 13. BET plots of the iso-butyl-modified silica aerogels 147

B. 14. BET plots of the octyl-modified silica aerogels..... 147

B. 15. BET plots of the vinyl-modified silica aerogels 148

B. 16. BET plots of the phenyl-modified silica aerogels..... 148

C. 1. Calibration curve for Mo AAS..... 150

C. 2. FTIR spectra of the M9 immobilized materials 150

C. 3. FTIR spectra of the E9 immobilized materials 151

C. 4. FTIR spectra of the M10 immobilized materials 151

C. 5. FTIR spectra of the E10 immobilized materials 151

C. 6. FTIR spectra of the E11 immobilized materials 152

C. 7. FTIR spectra of the E12 immobilized materials 152

C. 8. FTIR spectra of the E13 immobilized materials 152

C. 9. FTIR spectra of the E14 immobilized materials 153

C. 10. FTIR spectra of the E15 immobilized materials 153

C. 11. BET plots of the 10-MVPA and 11-MVPA..... 153

C. 12. BET plots of the M1 immobilized materials..... 154

C. 13. BET plots of the E1 immobilized materials..... 154

C. 14. Nitrogen adsorption/desorption isotherms of the M9 immobilized materials . 154

C. 15. Pore size distribution of the M9 immobilized materials 155

C. 16. BET plots of the M9 immobilized materials..... 155

C. 17. Nitrogen adsorption/desorption isotherms of the E9 immobilized materials... 155

C. 18. Pore size distribution of the E9 immobilized materials 156

C. 19. BET plots of the E9 immobilized materials..... 156

C. 20. Nitrogen adsorption/desorption isotherms of the M10 immobilized materials 156

C. 21. Pore size distribution of the M10 immobilized materials 157

C. 22. BET plots of the M10 immobilized materials..... 157

C. 23. Nitrogen adsorption/desorption isotherms of the E10 immobilized materials. 157

C. 24. Pore size distribution of the E10 immobilized materials 158

C. 25. BET plots of the E10 immobilized materials..... 158

C. 26. Nitrogen adsorption/desorption isotherms of the E11 immobilized materials. 158

C. 27. Pore size distribution of the E11 immobilized materials 159

C. 28. BET plots of the E11 immobilized materials..... 159

C. 29. Nitrogen adsorption/desorption isotherms of the E12 immobilized materials. 159

C. 30. Pore size distribution of the E12 immobilized materials 160

C. 31. BET plots of the E12 immobilized materials..... 160

C. 32. Nitrogen adsorption/desorption isotherms of the E13 immobilized materials. 160

C. 33. Pore size distribution of the E13 immobilized materials 161

C. 34. BET plots of the E13 immobilized materials 161

C. 35. Nitrogen adsorption/desorption isotherms of the E14 immobilized materials. 161

C. 36. Pore size distribution of the E14 immobilized materials 162

C. 37. BET plots of the E14 immobilized materials 162

C. 38. Nitrogen adsorption/desorption isotherms of the E15 immobilized materials. 162

C. 39. Pore size distribution of the E15 immobilized materials 163

C. 40. BET plots of the E15 immobilized materials 163

C. 41. DR UV-Vis spectra of the E1 and E1-N 163

C. 42. DR UV-Vis spectra of the M9-10 and M9-11 164

C. 43. DR UV-Vis spectra of the E9-10 and E9-11 164

C. 44. DR UV-Vis spectra of the M10-10 and M10-11 164

C. 45. DR UV-Vis spectra of the E10-10 and E10-11 165

C. 46. DR UV-Vis spectra of the E11-10 and E11-11 165

C. 47. DR UV-Vis spectra of the E12-10 and E12-11 165

C. 48. DR UV-Vis spectra of the E13-10 and E13-11 166

C. 49. DR UV-Vis spectra of the E14-10 and E14-11 166

C. 50. DR UV-Vis spectra of the E15-10 and E15-11 166

C. 51. Typical HPLC chromatograms as obtained during our analyses 167

C. 52. HPLC calibration curve for AN 168

C. 53. HPLC calibration curve for AQ 168

C. 54. HPLC calibration curve for AT 169

TABLES

Table..……. ..... Page

1. 1. Types of heteropoly compounds 30

2. 1. Precursor/co-precursor composition of the different surface-modified silica aerogels 43

4. 1. Physicochemical properties of the materials 90

5. 1. Some important oxidants, showing the available oxygen and their reactive by-products 95

5. 2. AAS data for the immobilization of 10-MVPA and 11-MVPA on the different silica aerogel materials 111

5. 4. Catalytic activity of 10-MVPA 128

5. 5. Catalytic activity of 11-MVPA 129

5. 6. Effect of oxidant and solvent on the catalytic activity of E1-10 131

5. 7. Catalytic activity for the reuse of E1-10 132

A. 1. Characteristic vibration frequencies (cm^{-1}) in FTIR spectra of synthesized silica aerogels 139

C. 1. Physicochemical properties of the different immobilized materials 149

CHAPTER ONE

INTRODUCTION

This research originates back to the early 19th century when it came to the notice of early investigators by mere mistake and coincidence the discovery of silica glass-like material which later flourished by the exploitation of interesting properties of aerogels. At around the same era of time and in another place on this planet, a well-devoted research group has come to the innovation of polyoxometalates. Now, after nearly 200 years from then, the entrapment of the polyoxometalates inside the aerogels is investigated in order to enhance their action in catalysis and to further understand their physicochemical principles.

1.1. The Sol-Gel Process

In the mid-19th century the so-called "Sol-Gel Process" has gained vast interest especially in the field of processing inorganic ceramics and glass materials [1-3], mainly through the investigations into its governing physical and chemical principles [4, 5]. It has later demonstrated to be an essential method for producing amorphous porous materials [6].

The chemical and molecular design of molecular precursors such as metal alkoxides or hydroxylated metal ions in aqueous solutions provides an interesting and powerful means to mold the nanostructure of the oxide materials and to control their condensation reactions [7]. Conclusively, the hydrolysis and condensation of these precursors are the basis of the sol-gel process [5].

1.1.1. Overview

The term "Sol-Gel Process" designates the formation of a porous three-dimensionally well-organized homogeneous gel of a colloidal suspension that develops in an established manner in a liquid medium [4, 8]. The most widely used class of precursors for the preparation of such colloids are metal alkoxides which are metal-organic compounds of a metal center with an attached organic ligand [5]. Metal alkoxides, as such, are seemingly interesting in chemistry because they readily react with water in a hydrolysis reaction leading to the formation of either completely hydrolyzed $M(OH)_n$ or partially hydrolyzed $M(OR)_{n-z}(OH)_z$ molecules, depending on the amount of water available for this reaction [5]. The latter would react together in a condensation reaction leading to the formation of a dimer. This reaction will continue even further to promote larger and longer silicon-networked molecules by polymerization of these dimers into larger chains and rings of silicon oxides [5].

Ultimately, many attempts have been conducted to construct a well-defined definition of the sol-gel process, some of which only account for oxides that are homogeneous at the atomic level [9]; others restrict it to the gels synthesized solely from alkoxides or the production of inorganic oxides [9, 10]. However, the process also includes the production of hybrid organic-inorganic materials synthesized from other components such as nitrides, sulfides [4], chlorides, organosilanes [11], and other organic molecules.

1.1.2. Chemistry

The fundamental idea of sol-gel processing is to gradually generate an oxide network by polymerization reactions of chemical precursors dissolved in a liquid

medium [4]. Sols and gels are two different kinds of matter that are present in nature, which include a variety of forms and substances such as clays, inks, blood, serum, and milk [12]. Ever since, sols and gels have brought up considerable scientific interest by the research led by Graham in colloidal sciences and sols investigations in 1861 [3] and by the synthesis of the first silica and alumina gels by Ebelmen in 1846 [1, 2, 13, 14] and Cossa in 1870 [15], respectively. Thereafter, many forms of inorganic gels have been proposed and progressively synthesized by the aid of several innovative techniques. The research was then directed into a new direction by the prominent supercritical drying introduced by Kistler in 1931 [16], which led to the production of the first silica, alumina, zirconia, stannic and tungsten oxide aerogels [4, 17].

A vast scope of procedures and processing techniques have been developed to minimize shrinkage and prevent cracking in order to retain more of the original properties of the initial gel. Subsequently, many alterations can be brought to the sol-gel process as a synthesis technique [4]. A summarizing scheme such as that in Figure 1.1 shows that the first step of any sol-gel process is the mixing of the precursors into a metal alkoxide solution *(A)* which would lead to the formation of either a sol *(B)* or a xerogel film *(C)* [18]. Depending on the way of treatment here and henceforth, sols and gels are treated in various synthetic routes to acquire the desired properties of the final form [4]. Hence by the use of surfactants or by supercritical drying as explained earlier, the size of pores in the network could be controlled as well as to avoid fracturation, both of which are remarkably valuable and advantageous in the field of catalysis [4].

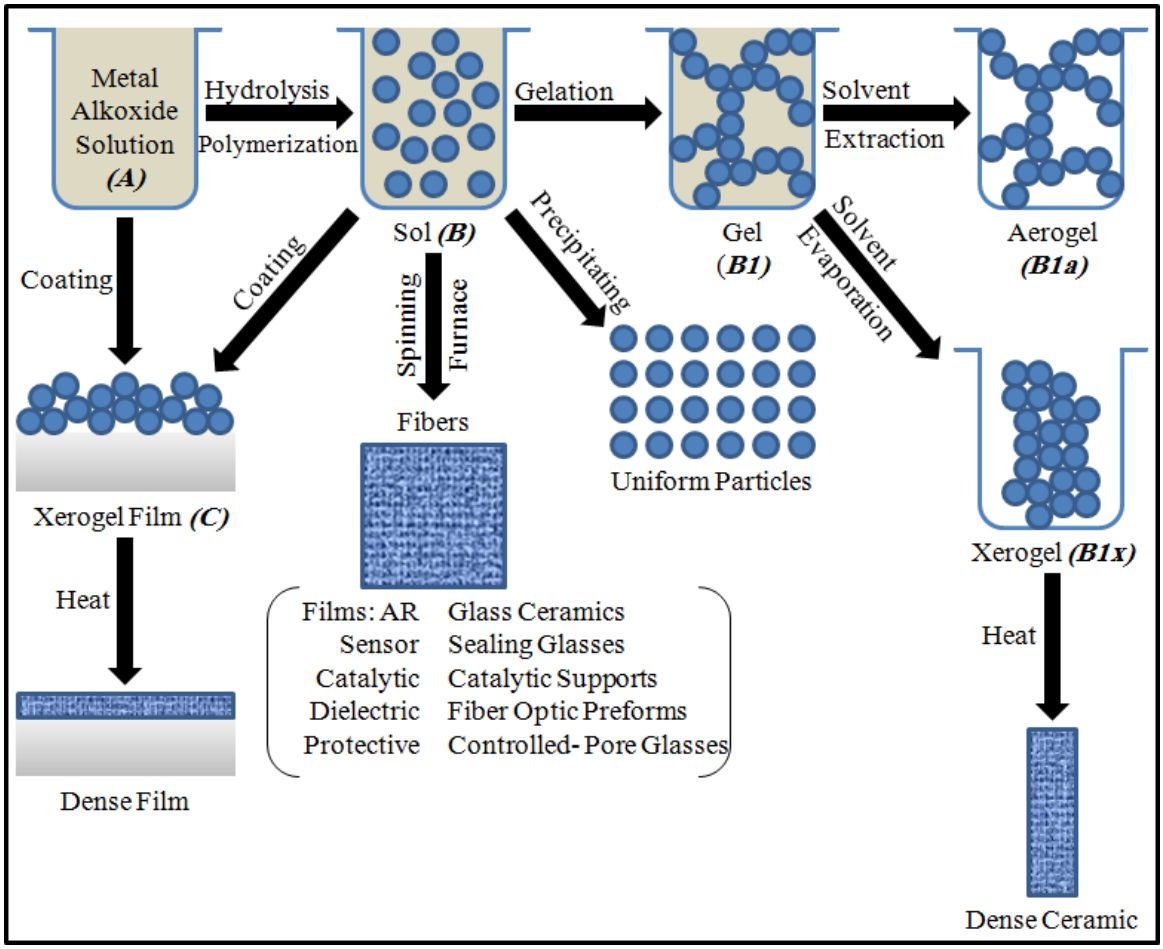

Fig. 1. 1. Sol-gel techniques and their products; modified from Ref. [5, 18]

1.1.3. Advantages and disadvantages

The applications of the sol-gel process a decade ago were not very well pronounced except in areas such as glass and ceramics fabrication and manufacture [4]. Though its exploitation is still during the developing stages, yet new interesting organic-inorganic sol-gel materials for photochromic and laser dyes uses, as well as controlled pore structured gels aided by micellar surfactants were recently synthesized [19, 20]. Other interesting applications of the materials produced by the sol-gel process is for example the use of silica monoliths in high-energy physics [21, 22], their use as thermal insulators in double windows [23-25], their promising biological applications as

biosensors [26] and biocatalysts [27], and their use for comet dust collection [28, 29]. These applications and much more will be discussed in further details in Section 1.3.4 where the scope of aerogel applications in particular is reviewed.

The sol-gel process is an innately advantageous technique with a very broad range of enhancing and facilitating procedures not only for the production of better ceramics but also for making new hybrid organic-inorganic materials. The process also allows the formation of very pure products by simple purification of the initial precursors [4]. While comparing the primitive techniques of ceramics and glass production with their high temperature, increased energy demands, and pollutant byproducts, the sol-gel process emerges as a drastic enhancing eco-friendly system that combined with its low processing temperatures function as a control for chemical reaction kinetics as well as to command the shape, size, and pore distribution of the particles [4, 30].

However, this meticulous control and careful tailoring of the pores and crystalline or amorphous structure of the processed material comes at very expensive costs of the precursors especially the alkoxides [4]. Nonetheless, lowered temperatures of processing for both the amorphous and the crystalline material are thus needed. This cooling would result into a disadvantage in the form of energy that could limit their action in some domains and may well be critical in some areas of their application [31]. Another fundamental shortcoming of the sol-gel process is that it fails to stay on par with the mass production of large scale ceramics and glass materials production that rely on much cheaper starting material and much faster processing times. The sol-gel process is nonetheless restricted to the fabrication and innovation of highly sophisticated scientifically-controlled material [4].

1.2. Silica

1.2.1. Overview

Silica is originally known as the common silicon dioxide whether in its crystalline, amorphous, or hydrated forms. However, silica does not only comprise material composed of SiO_2 solely but it also designates all kinds of silicates that are formed through simple polymerization and foremost the development of a network composed from $(SiO_2)_n$ [32]. The nature of clays and silica-based rocks present in oceans, since the beginning of time, has resulted into silica being the most abundant constituent of the earth's crust, whereby 28% is silicon, 47% is oxygen, and 75% is the combined silica in all its occurring forms from silicates, glasses, and sand [33, 34]. The chemistry of its molding into quartz crystals remains inconclusive, thus more studies has to be directed toward understanding its solubility behavior in water [32].

1.2.2. Theory

Silica plays a very important role in industrial and commercial use in building materials, ceramics, glasses, and concretes as it is the sole source for elemental silicon [33]. The basic building block of most silicates and silica material is a tetrahedral SiO_4 structural subunit weaved tightly in a three dimensionally chained network [32]. Although silica are chemically and thermally inert, its reactivity and chemical transformations is dependent on its form and state under suitable conditions [33].

The uniqueness of silica is instantly linked up with water as a unique liquid itself and thus comprehending the system of silica-water is critical in our understanding of the underlying problems and applications [32]. Most natural silica are essentially insoluble in water and hence exist as crystalline material with a highly ordered

geometrical structure. On the same basis, amorphous silica has a similar basic structure yet it lacks a well-ordered geometry [33]. The presence of silanol groups is the directing agent in the physical properties of amorphous silica as oxide adsorbents [35]. Conversely, amorphous silica are less toxic and innately inclined to form aggregates with intersecting characteristics such as low surface tension and good dielectric strength [33].

1.2.3. Synthesis of Inorganic Gels

Generally, gels lie on the borderline between three sub-groups of chemistry organic, inorganic, and biological [36]. In their sol-gel processing, silica gels were fist synthesized from metallic salts MX_n, where M is a metal and X is the anions [1, 2]. However, these metal atoms are in a solvated cationic state $M[H_2O]_n^{z+}$ when the precursors are present in aqueous solutions. The first step in the synthesis is the formation of sols and gels consists of the hydrolysis reactions in which the OH groups replace the water molecules. These deprotonation and condensation reactions with water loss give either “ol” bridges as M–OH–M or “oxo” bridges as M–O–M [36]. One proposed mechanism comprises the direct substitution of the H_2O ligand by an OH^- followed by a proton exchange as Livage *et al.* have suggested according to the following equation [37].

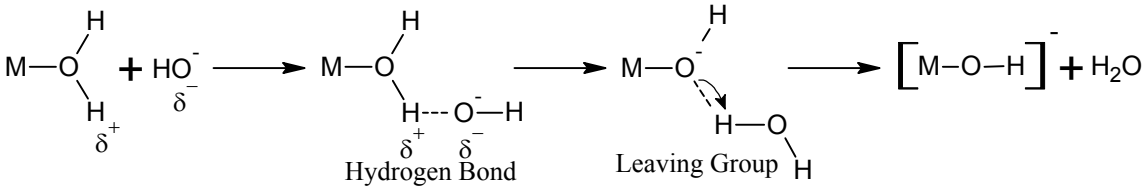

Equation 1. 1

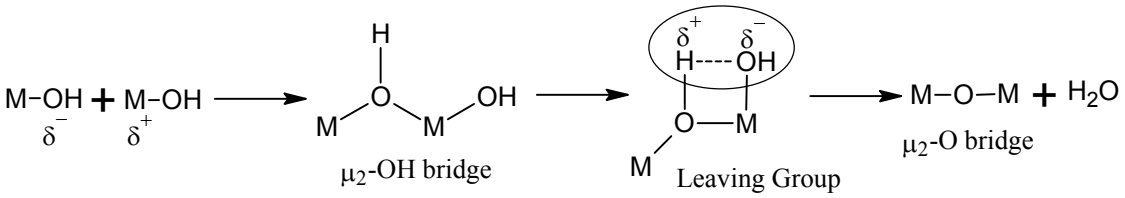

Equation 1. 2

Several condensation reactions will subsequently lead to the formation of "ol" or "oxo" bridges according to Equation 1.2 [37].

Another extensively used type of precursors is alkoxides $M(OR)_n$. These precursors are constructed by the combination of a metal M with an alkoxide group OR, whereby R is an alkyl group [36]. Such precursors are often characterized by the presence of M–O polar covalent bonds. The initial step towards the formation of gels is the hydrolysis reactions of the precursors that comprise a nucleophilic chemical attack on the metal M, which is dependent on the partial positive charge carried by M. Consequently, this step is facilitated by the partial negative charge carried by the oxygen atom of the water molecule as seen in Equation 1.3 [36]. Water is being utilized in this case as a reactant taking part in the hydrolysis reactions, by replacing OH ligands instead of the OR followed by condensation [36].

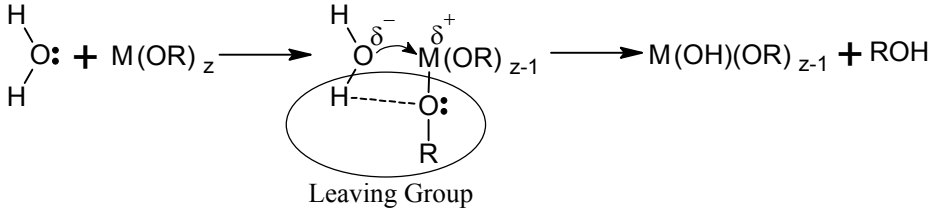

Equation 1. 3

Nevertheless, the reaction of hydrolysis and condensation together occur instantaneously and are thus difficult to decipher between the two and thus their kinetics are studied simultaneously in order to effect the production of oligomers resulting into packed clusters, as in the case of some alumina gels [36]. Conversely, silicon precursors, specifically alkoxides, pose an exception in that the hydrolysis and condensation reactions are slow. In view of that, they need to be catalyzed by either an acidic or a basic medium depending on the choice to control their kinetics of formation in addition to suiting the desires of their applications [36].

1.2.4. Applications

Owing to their interesting properties and characteristics of being malleable and increasingly versatile, silica materials with the vast array of forms, shapes, and structures that it can embrace are considered and employed in many situations ranging the whole micro to macro scale of implementations and applications. Namely raw glass and basic ceramics can be utilized in daily life and could also be used in building, sound proofing, green houses, protection, lighting, and engineering.

On the other hand, silica polymers may well be used for optical resolution of chiral molecules [38]; separation or enrichment of drugs [39], pesticides and herbicides [40]; mimicking antibody and receptor binding sites [41], catalytic enzyme sites [42],

and chemical and biochemical sensing [43]. In a recent study, silica gels were used in high performance liquid chromatography separations, whereby a column packed with newly synthesized molecularly-imprinted polymers on silica gel showed higher column efficiency and better resolution for selected enantiomers relative to a traditionally-packed column [44].

In addition, looking at more sophisticated forms of these silica materials such as amorphous materials, mesoporous molecular sieves, xerogels, and aerogels have an outstanding range of applications from biology and medicine to synthesis and catalysis. Such materials could be used in supporting and incorporating other materials, some examples are the entrapment of biopolymers into sol-gel derived silica nanocomposites used in enzymatic and biological synthetic routes [36, 45-49], the immobilization of biomolecules on mesoporous structured materials being exploited in the medical field [50-53], and the immobilization and encapsulation of metal complexes or polyoxometalates in mesoporous solids as approaches in advancing chemical catalytic means [54-58].

1.3. Aerogels

1.3.1. Overview

As explained and illustrated in previous sections, aerogels (aero: a Greek prefix relating to air) [59] are gels prepared by the low temperature well-known sol-gel process with drying under supercritical conditions in order to preserve the porous structure which they had originally in their gel *(B1)* form as seen earlier in Figure 1.1. These materials have interesting and distinctive properties such as very high relative pore volume. Additionally, some other distinctive physical properties of these aerogels

are very high specific surface areas (600–1000 $m^2.g^{-1}$), evident low densities (0.003–0.35 $g.cm^{-3}$), high thermal tolerance up to 500°C with melting points greater than 1200°C, very low values for a solid material with index of refraction (1.0–1.05) and dielectric constant (~1.1 for a density of 0.1 $g.cm^{-3}$), and their fascinating amorphous structure with high porosity (80–99.8%) [36, 60-64].

1.3.2. Theory

First and foremost, aerogels *(B1a)* and xerogels *(B1x)* (xero: from the Greek *xeros* meaning dry) [59] (Figure 1.1) are essentially similar since the supercritical drying only affects larger pores. Xerogels are easily utilized as coatings on ceramic supports unlike aerogels which have limited application in filtration membranes affected by their fragility [65]. Silica aerogels specifically are considered to be extremely light with very low densities as seen earlier and are brittle material. Such flexibility would entitle the aerogels to be used in kinetic energy absorber materials [66]. In due course, aerogels have unique adaptable structures and characteristics that entitle them to a vast scope of applications [36].

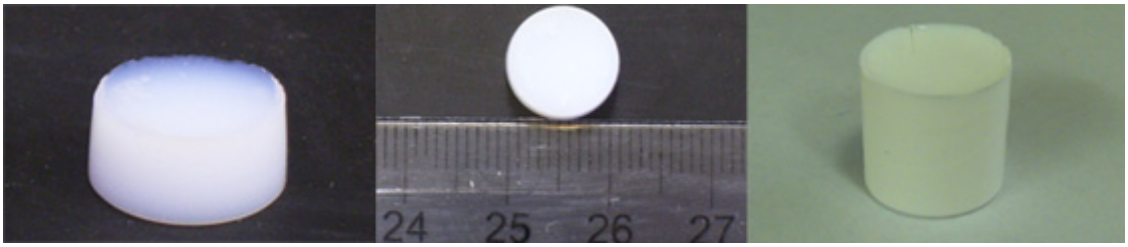

Fig. 1. 2. Different kinds of silica aerogels prepared by drying under supercritical CO_2 in our laboratory

Theoretically, every material could be converted to glass from its solution and a random- network gel could be easily obtained with any sol-gel precursor, on condition

that the hydrolysis and condensation rates can be lowered to controllable magnitudes [36]. However, this is experimentally much easier with silicon precursors than with other alkoxides [67]. In the following sections, specific factors that influence the hydrolysis and condensation reactions of the sol-gel process will be discussed and primarily focused on the influences of pH.

1.3.3. Synthesis of Silica Aerogels

The synthesis of silica aerogels is of prime interest and importance for the purpose and aim of this work, and thus the following representative synthetic schemes for tetramethoxysilane (TMOS) will be regarded as a synthesis template that is followed throughout.

Mixing

Iler argued that sols are formed by mixing colloidal particles in water while avoiding any possible precipitation at suitable pH values [32]. As previously discussed, other routes comprise the hydrolysis of an alkoxide precursor, such as $Si(OR)_4$, where R is CH_3, C_2H_5, C_3H_7, or others according to the scheme in Equation 1.4 [67].

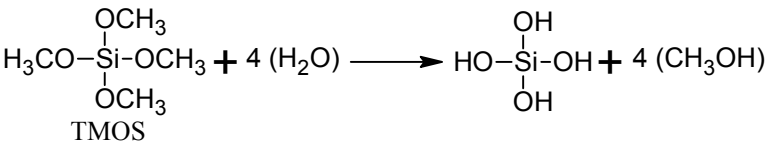

Equation 1. 4

Iler classified the polymerization process into three pH domains of which less than pH 2, between pH 2-7, and greater than pH 7 [32]. Unbiased hydrolysis takes place by the nucleophilic attack of the oxygen contained in water on the silicon atom regardless of pH as concluded by the reaction of isotopically labeled water with TEOS

giving purely unlabelled alcohol in both the acid- and base-catalyzed reactions as in Equation 1.5 [68].

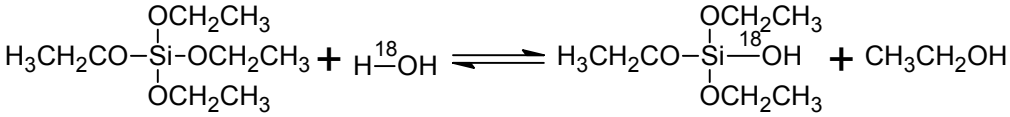

Equation 1. 5

Moreover, the pH effect can be clearly noted from studying the hydrolysis rate profile seen in Figure 1.3 [69].

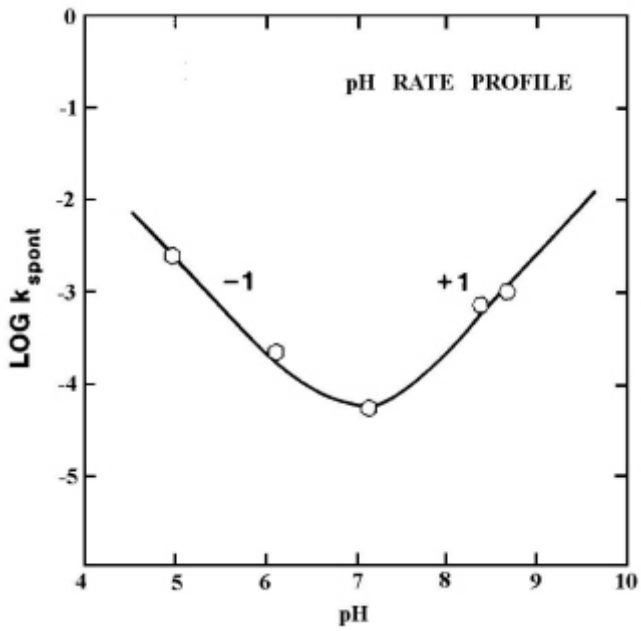

Fig. 1. 3. pH rate profile for hydrolysis in aqueous solution; taken from Ref. [69]

After the hydrolysis of these bonds, the condensation reaction of the silanol tetrahedra forming ≡Si–O–Si≡ bonds commences as in Equation 1.6 [67].

Equation 1. 6

Engelhardt *et al.* [70] showed that the hierarchal sequence of condensation products is monomer, dimer, linear trimer, cyclic trimer, cyclic tetramer, and higher order rings, which necessitates both depolymerization that involves ring opening and the availability of monomers in the synthetic medium with the oligomeric species which could be easily generated by reverse reactions [67].

The rate of such ring opening polymerizations, and monomer addition reactions are dependent on pH. At pH values below 2, the condensation rates are proportional to the proton concentration [18]. The solubility of silica as seen in Figure 1.4 is low when the pH is less than 2, thus the formation and arrangement of silica particles occur simultaneously while aging merely contributes to the growth after the particles exceed 2nm in diameter. Therefore, gel networks develop remarkably small particles [69].

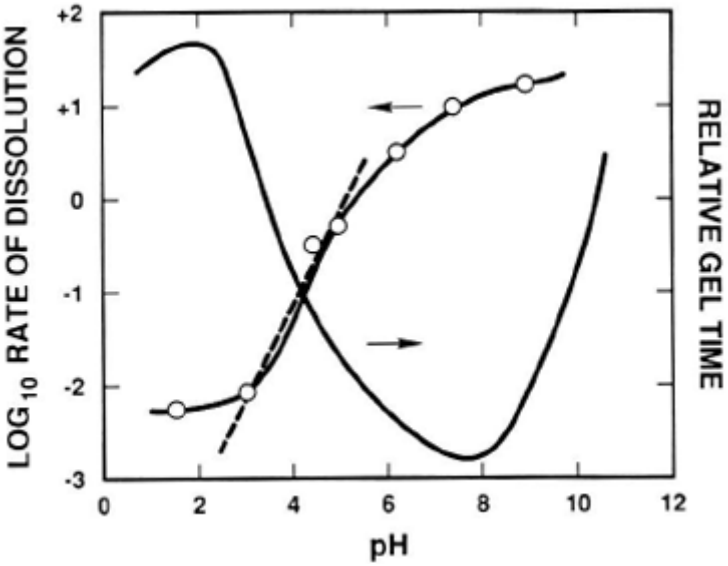

Fig. 1. 4. Dissolution rate and relative gel time as a function of pH; taken from Ref. [5]

It is commonly agreed that the condensation rates are proportional to [OH^-] for a pH ranging from 2 to 7. Condensation preferably occurs between more highly condensed species and those less highly condensed suggesting a low rate of dimerization. Accordingly, once the dimers are formed, they directly react with monomers to form trimers which in turn react with other monomers to form tetrameters as explained earlier [69, 71]. Due to the increased proximity of the chain ends and the subsequent decrease of the monomers, then the cyclization would occur leading to further growth by addition of lower molecular weight species to more highly condensed species and thus forming chains and networks. Undesirably, particle growth stops at 2–4 nm as particle diameter owed to the low solubility of silica in this pH range [71].

The polymerization occurs similarly to that between pH 2 and 7 for pH values greater than 7. In this pH range, the growth starts to take place with the addition of monomers to the more highly condensed ionized particles rather than by aggregation [69]. Owed to the greater solubility of silica and the greater size dependence of

solubility above pH 7, particles grow in size and decrease in number as highly soluble small particles dissolve [5]. Particle growth ceases when the solubilities of the smallest and largest particles become identical in a process known by Ostwald ripening [72]. Hence, at this pH, particle size in addition to growth are affected by the particle size distribution and the temperature, with the larger particles obtained at higher temperatures [5, 18].

In a further polycondensation reaction as in Equation 1.7, linkage of additional ≡Si–OH tetrahedra would ultimately result into a SiO_2 network where the H_2O and alcohol expelled from the reaction are retained in the pores of the network [67].

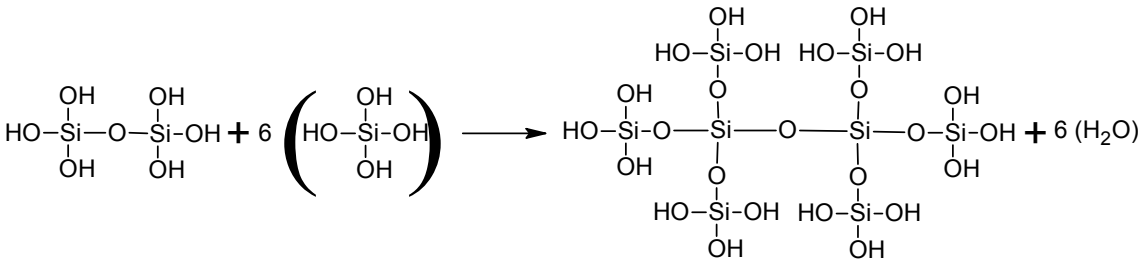

Equation 1. 7

Further mixing of the TMOS and water in solution tends to initiate several sites for the hydrolysis and polycondensation. Sols are then formed at these sites when Si–O–Si bonds colloid cooperatively in that region [67]. Eventually, the resulting silica network of these sols being its size and internal cross-linking depends on pH and the H_2O/Si molar ratio (R) [32].

Gelation

It is quite difficult analytically to measure a gelation point of any system, including that of sol-gel silica; however it is easily identified and purely conceived qualitatively. As the sol particles grow and collide, condensation occurs and macroparticles form. The macroparticles resulted from the condensation within a sol

then become a gel when it can elastically resist a stress [67]. When this kind of support and resistance is attained, gelation is complete at this point and the gelation time (t_{gel}) would be calculated. Gelation is a gradual process of forming an elastic gel from the viscous sol material when more and more particles are being interconnected, and thus the activation energy cannot be defined. The subsequent steps of the gel processing primarily depend on the ancestor structure of the wet gel formed by gelation [67].

Brinker and Scherer explained that the gelation point being considered as a fast solidification process would tend to cease the increasing viscosity of the material during the entire gelation procedure [73]. Consequently, the rigid structure of the gel could only be subject to change with time, depending on either temperature, solvent, pH, or upon solvent removal as detailed shortly [67]. Iler noted as well that the gel time increases under more basic conditions [32].

Aging

The structure and properties of any processed gel continue to change long after the gelation point in a process called aging. Four processes can occur individually or simultaneously during aging including polycondensation (Equations 1.6 and 1.7), synerisis which is the natural shrinkage of the gel as the result of solvent expulsion from the gel pores, coarsening which is the irreversible decrease in surface area caused by dissolution and reprecipitation processes, and phase transformation [67]. Regrettably, there is insufficient knowledge of aging mechanisms, kinetics, and quantitative analysis of the aging process although it is well theoretically documented [32, 74-77].

Drying

The drying behavior of porous solids has been explained solely by classical concepts as that endured in ceramics production. During the first stage of drying, the gel volume decreases relative to the liquid volume that is lost by evaporation. At the beginning, the surface area of the gel comprises free water separated by a gel network with bound water at the interface [67]. The retained gel network is deformed by large capillary stress and forces resulting in its shrinkage. The greatest changes in volume, weight, density, and structure occur during this drying stage which ends when the shrinkage ceases at the critical point depicted in Figure 1.5 [78]. Then the internal liquid would flow to the surface where the evaporation takes place. However, the rate of evaporation decreases as a consequence of the decrease in the effective pore radius driven by the capillary stress. In the last step of drying, the pores can no longer be emptied, yet the remaining liquid can now only escape by evaporation from within the pores by diffusion of vapor to the surface. No more structural changes would occur but minor weight changes can take place until internal equilibrium is attained[67].

Supercritical carbon dioxide drying (SCCD) is the most prominent and established technique of drying to obtain the desired aerogel. The liquid-vapor meniscus which retreats during the emptying of the pores is easily avoided by employing such technique in the wet gel drying. In order to avoid the collapse of the pore volume due to the capillary pressure created by the surface tension of the solvent, there is a need to eliminate this surface tension by transforming the liquid into a supercritical fluid [36]. Such drying technique would relatively maintain the desired interesting porous structure as it is by avoiding the collapse. Long after Kistler *et al.* [16] has initially investigated the technique, it was largely developed yet it still comprises heating the wet gel in a

closed container, to pressures and temperatures exceeding the critical temperature, T_c, and critical pressure, P_c, of the liquid entrapped in the pores inside the gel [16, 17].

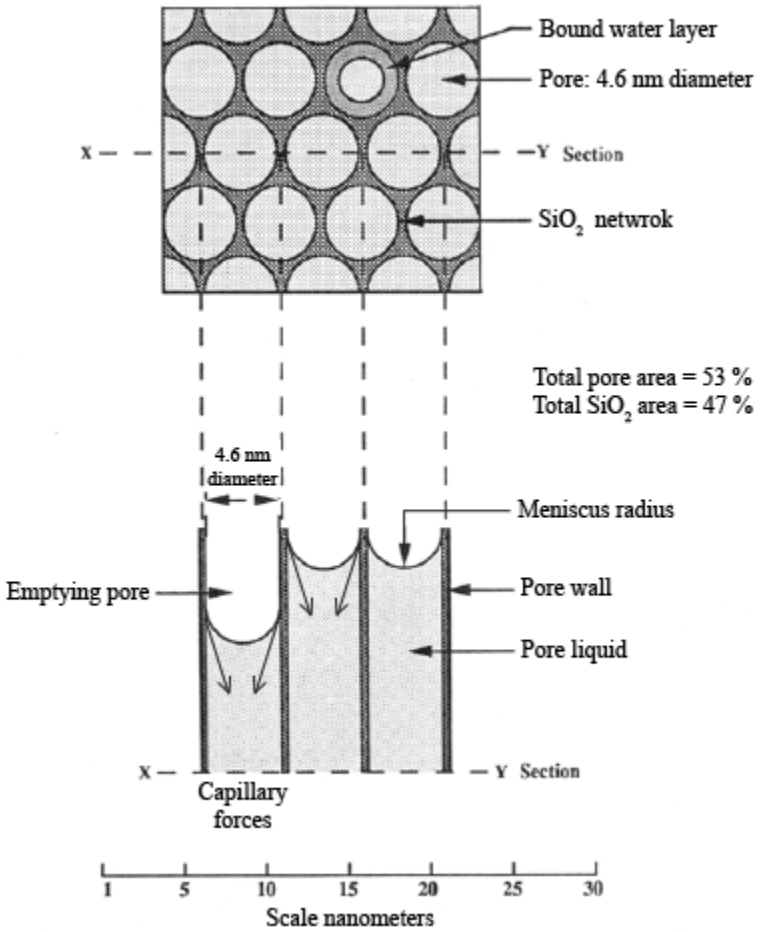

Fig. 1. 5. Schematic representation of gel surface at the end of drying; modified from Ref. [78]

The supercritical drying methods that will be shortly described in further details are quite expensive due to the high pressures involved. In view of that, drying at ambient and subcritical conditions is hence favored due to lower costs [79]. Aerogels synthesized by either alkoxysilanes [80] or are waterglass-based [81, 82] can be prepared by ambient pressure drying. This kind of drying however involves surface modification and network strengthening by chemical modification of the inner surface

in order to minimize the capillary forces, as well as several solvent exchange processes [79]. Another drying method is the freeze-drying which involves freezing and sublimation under vacuum of the liquid existing in the pores, giving a material known by cryogel [83]. Yet disadvantages of this method arise from the fact that long stabilization time for the network is needed and in certain cases a destruction of the network may take place [79]. One newly implemented drying routine for the production of aerogel powder is the fluidized bed drying technique [84-86], which encompasses the drying of the wet-gel slurry at the ambient pressure by passing a gas through them. This technique is believed to be promising for the large scale production [87].

Accordingly, two types of supercritical drying could be distinguished. One way is the high-temperature supercritical drying (hot) in alcohol accompanied by a difficult controllable aging process. Achieving these supercritical conditions of increased temperature and pressure, the materials would usually have a hydrophobic character owed to alkoxy groups on their surfaces. During silica aerogel synthesis, such alkoxy groups are generated by the reaction of the alcohol with the silanol groups. Another way is the low temperature supercritical drying (cold) in CO_2 which leads to more hydrophilic solids by avoiding such processes [36].

A possible supercritical drying path in the phase diagram of CO_2 under supercritical conditions of T_c=304.1 K and P_c=73.8 bar is presented in Figure 1.6 [36]. Silica aerogels obtained under such conditions characteristically have a pore volume above 90% of the sample volume and a specific surface area that could exceed 1000 $m^2.g^{-1}$. Conversely, other oxides usually have lower specific pore volume and surface area than the silica with the carbon aerogels being an exception [36].

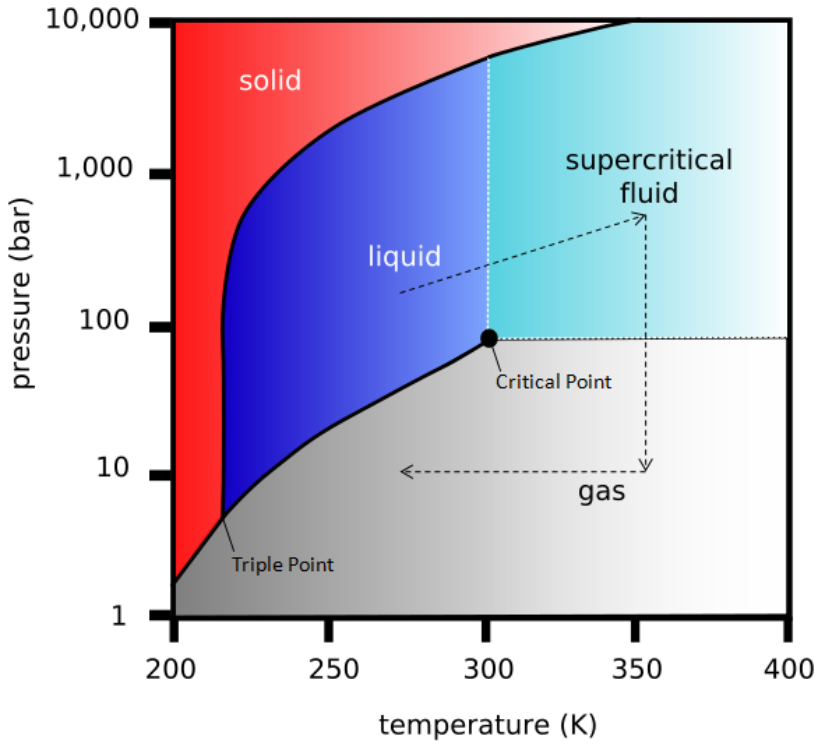

Fig. 1. 6. A possible cold supercritical drying path in the Pressure (P) Temperature (T) phase diagram of CO_2 (Shown in dashed arrows); modified from Ref. [36]

Consequently, the aerogels obtained after SCCD would acquire an amorphous structure, with empty pores within the intercalations of the network, and thus are deemed as porous materials. Porous materials in chemistry are utilized as adsorbents, catalysts and catalytic supports attributed to their high specific surface areas and large pore volumes. Porosity develops when the gel network with its additional cross-linking becomes well strengthened to resist the forces of surface tension. Solvent removal at its critical point as just explained with no liquid-vapor interfaces occurs with no capillary pressure [5], and therefore much less driving force for shrinkage exists in aerogels compared to xerogels. This leads to expanded structures in the aerogels that are of better resemblance of the wet gel attained at the gelation point.

Porous materials are classified according to IUPAC based on their predominant pore size as either microporous having pore sizes below 2 nm, macroporous with pore

sizes exceeding 50 nm, or mesoporous with intermediate pore sizes between 2 and 50 nm [88]. Zeolites, with a crystalline aluminosilicate network, having pore sizes ranging from 0.2-1.0 nm are one the best microporous catalytic supports, yet with such small pores its scope of applications would be limited [89]. Accordingly, mesoporous materials are one of the most active research areas being explored, owing to their larger pore sizes and extremely articulate pore structures.

1.3.4. Applications

Aerogels were originally used in applications such as storage of rocket fuels [90], thermal window insulation, acoustic barriers, supercapacitors, nuclear waste storage [36, 66, 91], Cherenkov radiation detectors [22], shock wave studies at high pressures [92], inertial confinement fusion [93], micrometeorites [94], and radioluminescent devices [95]. More importantly, with the increasing interest in planetary science, these same aerogels with their interesting properties listed in previous sections are being used by the NASA Jet Propulsion Laboratory in a new technique for collecting comet dust. Owing to their capability of withstanding magnetic and UV radiation with very high thermal stability, the aerogels were successfully engaged in the NASA Stardust project in 2006 to collect samples of the deflected comet named Wild-2 [96]. The Stardust capsule came back to Earth on January 15, 2006 with the cometary and contemporary interstellar grains, which are kept intact without melting or destruction, trapped inside the aerogel collectors [97, 98]. In the recent PATHFINDER MARS mission, the aerogels were used to insulate the Sojourner Mars Rover and to protect the very sensitive electronics from freezing by maintaining the temperature at 21°C, while the temperature outside dropping to -67°C at night [96].

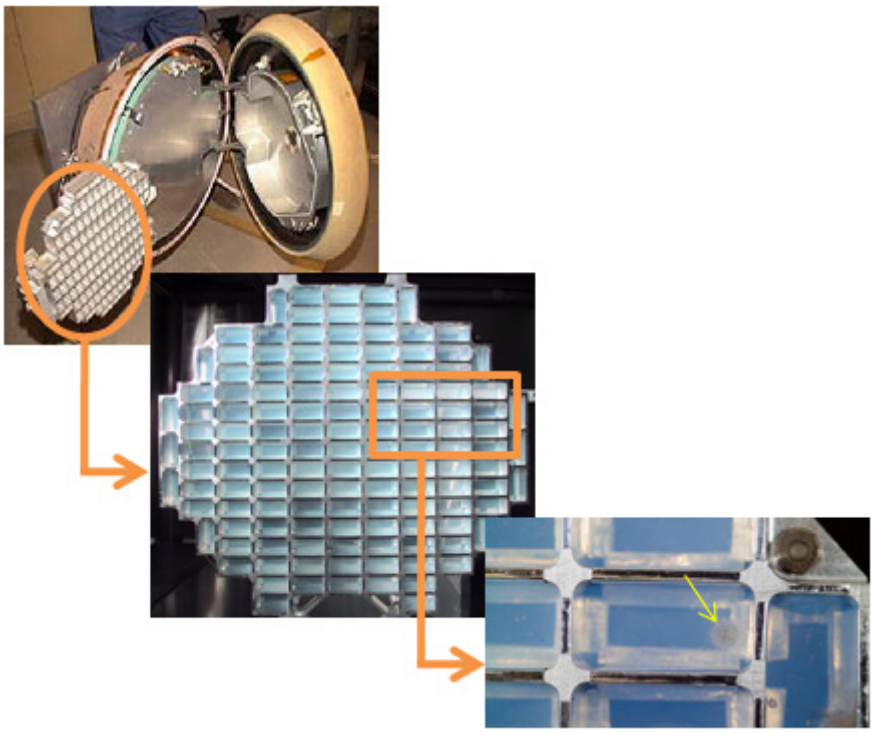

Fig. 1. 7. Stardust capsule and canister with a close up view of a cometary impact (yellow arrow) into the aerogel collector; modified from Ref. [98, 99]

Aerogels are now employed as chambers that house other materials to provide them with shelter in the form of rigidness, resistance to water and to austere thermal conditions, stiff characteristics [36], as well as being expected to provide increased specific surface areas that directly enhances the activity of these guest materials. Some interesting biological applications are the encapsulation of enzymes in silica aerogels and their application in biocatalysis [100, 101] as well as studying aerogel-supported lipid bilayers [102]. Aerogels have significant properties that are exploited in catalysis. In addition, a recent study by Pierre and co-workers [47] has achieved the encapsulation of the enzyme lipase in unique aerogel networks for use in a transesterification reaction and managed to leave them intact, due to the uniqueness achieved by the SCCD.

The most recent aerogel applications are investigated at our laboratory. In one study, Abramian and El-Rassy [103] showed that titania aerogel is a highly efficient adsorbing material for azo-dyes from aqueous solutions. In another study, El-Rassy and co-workers [104] have utilized newly synthesized porous cobalt ferrite aerogels as efficient catalysts for the hydrolysis of 4-nitrophenyl phosphate. In order to broaden the scope of the aerogel applications even further and to avoid drawbacks, such as being fragile, brittle and moisture sensitive, newly synthesized flexible and superhydrophobic silica aerogels by Rao *et al.* [105] and ionogels synthesized from ionic liquids used in sol-gel chemistry by Vioux *et al.* [106] have increased the potential of aerogel usage as electrolyte membranes, optical devices, catalysts and sensors. Moreover, a recent investigation in an interesting area of research is the preparation of a novel silica aerogel used as an adsorbent for toxic organic compounds [107].

Away from chemistry and the extensive applications in science, aerogels, with their thermal insulation properties, could well be used in the newly developed aerogel-insulated Antarctic expedition jacket created by NASA [108], the new aerogel winter boot manufactured by Red Wing's Vasque, the Laken aerogel-enhanced aluminum bottles, LapDesk for laptop heat protection and comfort by LapLogic [109], and much more aerogel-embedded products from Aspen [110]. One captivating use of aerogels is in the Dunlop Aerogel Technology project [111] for manufacturing a new generation of racket and sports equipment, which delivers unmatched strength to weight ratio for enhanced stiffness, increased power, and thermo protection.

1.4. Organically-Modified Silica Materials

1.4.1. Overview

Despite their interesting properties and chemically fascinating characteristics, the fact that silica aerogels being fragile and hygroscopic make them unstable for long-time reactions [112]. Therefore, there is an extreme urgency to mold better sustainable and durable material without such limitations [113]. These restrictions are due to the presence of polar silanol groups at the surface of these networks which would easily absorb water leading to a hydrophilic character [114]. Several studies and projects have been put forth in the attempt to achieve a hydrophobic-oriented surface instead. One intriguing approach is the organic modification of the surface of these silica materials [115], which are prepared by combining various silicon precursors having four identical hydrolysable alkoxy groups and co-precursors with at least one non-hydrolysable alkyl group. Previous organo-functionalization techniques were conducted under basic catalyzed hydrolysis and condensation of tetramethoxysilane $Si(OMe)_4$ (TMOS) and methyltrimethoxysilane $MeSi(OMe)_3$ (MTMS) [112, 116], and the hydrophobic surface nature of the obtained organically-modified silica were fully studied and characterized [117].

1.4.2. Chemistry

In order to attain these organically-modified silica materials, the H of the Si–OH could be replaced by hydrolytically stable Si–R groups (R is CH_3, C_2H_5, C_3H_7, etc.) in order to repel the water molecules and give it a more hydrophobic character [118]. One technique is that during the preparation of the sol-gel, silicon precursors having one organic group as well as three alkoxy groups $R''Si(OR')_3$ are used as co-precursors

during the synthesis, whereby R'' and R' being organic groups [113-115, 118-121]. The structure and surface chemistry of these newly synthesized organically-modified aerogels were characterized by various techniques such as Fourier Transform Infrared spectroscopy and nitrogen adsorption/desorption experiments, respectively [115, 117].

1.4.3. Advantages and disadvantages

The sound advantages of such modified silica materials with organic groups existing at their surface give them very interesting features that could be easily exploited in suitable areas of application of which is the attractively high specific surface areas (333–779 $m^2.g^{-1}$) and a pore volume between 0.40 and 1.60 $cm^3.g^{-1}$ as reported in the present thesis project. The synthesis of hydrophobic silica materials has been investigated in various modes of applications and procedures [117]. The surface of silica aerogels made from mixtures of two silica precursors dried under supercritical CO_2 conditions was notably different from that dried in methanol at higher temperatures [117].

One disadvantage of such organically-modified silica materials arises from the complication of drying these gels. If the drying is done following the hot method in an organic solvent such as methanol this make them highly hydrophobic [117]. However if the drying is done near room temperature, this would result into hydrophilic materials instead [22] that could be attributed to the hydrophilic property of the silica [122]. The addition of silicon precursors containing at least one non-polar side group during the synthesis is a way to prevent such effects [117]. Another advantage lies in using these materials as an expedient medium for the Cherenkov counter [21], used in physics for the identification of electrically charged particles [123]. In the present thesis, various

organically-modified silica aerogels were synthesized and dried under SCCD, and used as supports for the immobilization of polyoxometalates due to their beneficial characteristics of high surface areas and pore sizes being the most promising.

1.5. Polyoxometalates

1.5.1. Overview

Most inorganic compounds are formed from atoms of a metallic nature as their basic building units. Polyoxometalates (POMs) are nano-sized metal-oxygen clusters of high oxidation state early transition metals, principally molybdenum, tungsten, and vanadium [34, 124]. They are versatile structures with instinct properties in nano-sized dimensions, shape, charge density and surface reactivity owed to the flexibility of their chemical composition, charge and counterions [34, 124, 125]. Consequently, essentially tailored and controlled synthetic routes could be desirably employed to create a medium for catalytic diversity [126]. This is achieved by other substituted hetero-transition metals or by the formation of a hybrid organic-inorganic structure flexibility that would eventually cause a noticeable improvement in their catalytic performance and selectivity [127].

1.5.2. Theory

Berzelius has discovered in 1826 [128] a yellow precipitate produced by the addition of ammonium molybdate to phosphoric acid. This precipitate is known today as ammonium 12-molybdophosphate seen in Figure 1.8, and was later introduced into analytical chemistry. Nevertheless, Marignac has precisely determined in 1862 [129] the compositions of such heteropoly acids by the development of tungstosilicic acids

and their salts [130]. Subsequently, the field developed rapidly so that a variety of POMs and salts had been identified and discovered. The first attempts to elucidate the composition of POMs were put forth by Werner's coordination theories [124]. These compounds continually posed conceptual and experimental challenges to the founding fathers of the coordination chemistry and many other investigators. Only until recently with the introduction of modern high-resolution and sophisticated instrumentation that the fundamental chemistry of these compounds has been advanced [34, 131].

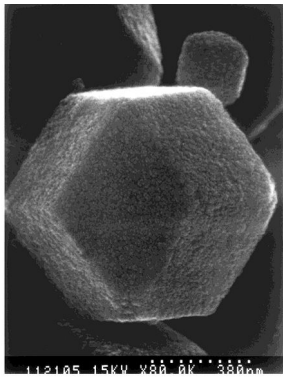

Fig. 1. 8. Scanning electron micrograph of ammonium phosphomolybdate; taken from Ref. [132]

POMs constitute an important sector of inorganic molecules in the field of coordination chemistry, whereby they are characterized by a basic building unit having a metallic atom M at its center surrounded by oxygen atoms or other ligands [34]. Therefore, two major forms of polyoxoanions directed by electrostatic and radius-ratio principles normally observed for extended ionic lattices are known. The first type is constituted by silicates and oxoanions of neighboring main-group elements and the second type is formed from the early transition metals [34]. Both forms are governed by constellations of metal-centered MO_n polyhedra with n=4–6 that are linked by shared

corners, edges, and faces. POMs are however predominantly characterized by MO_6 octahedra with terminal M=O bonds directed outwards that result in discrete structures [34, 124]. POMs are highly structured materials and these structure entities are their fundamental structural units, similar to $–CH_2–$ units when compared to organic chemistry.

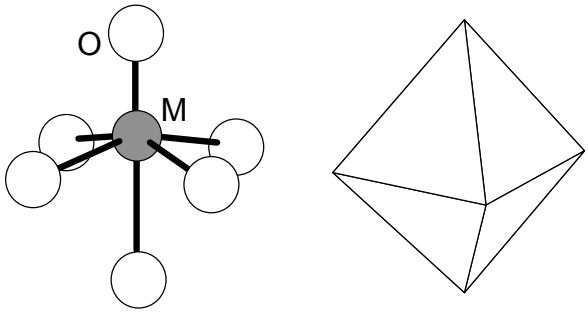

Fig. 1. 9. Ball-and-stick and polyhedral representations of the fundamental unit MO_6, whereby the M atom is displaced off the geometrical centre of the octahedron towards one of the oxygens giving rise to a distorted C_{4v} unit; modified from Ref. [133]

These fundamental structural units are then packed into forming countless shapes shown in Figure 1.10, noting that the most stable unions between two octahedra are the corner- and edge-sharing models, in which the M^{n+} ions are far enough from each other. Thus the face-sharing model is less common due to closer metallic centers causing more repulsion and decreased stabilization [124, 134, 135].

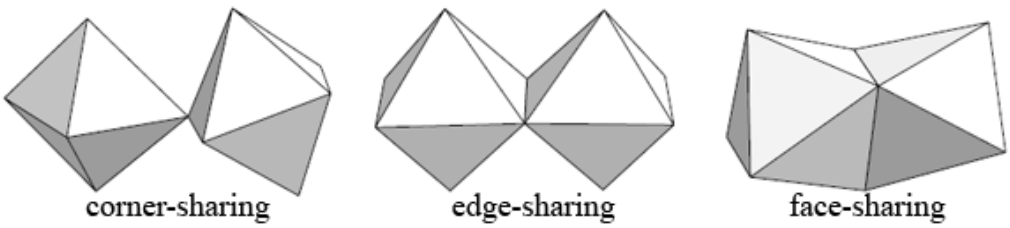

Fig. 1. 10. The polyhedral models represent the three possible unions between two MO_6 octahedral units, whereby each corner represents an oxygen position; taken from Ref. [133]

POMs could hence be categorized into the following groups: Isopolyanions $[M_nO_y]^{p-}$, produced by acid condensation of pure MoO_{2-4} or WO_{2-4}, e.g. Mo_7O_{6-24} and $W_{10}O_{4-32}$; Heteropolyanions $[X_zM_nO_y]^{q-}$, produced by acid condensation of the mixed solution of MoO_{2-4} or WO_{2-4} and a heteroatom X (P, Si, As, Fe, Co, etc.), e.g. Keggin ion $PW_{12}O_{3-40}$ and Wells-Dawson ion $P_2W_{18}O_{6-62}$; Mixed heteropoly compounds containing both Mo and W in different ratios produced by acid condensation of the solution containing both of MoO_{2-4} or WO_{2-4} and a heteroatom, e.g. $P_2W_{15}Mo_3O_{6-62}$; Transition metal substituted POM produced by replacing M–O moieties by transition metals of various ligands, e.g. $[PW_{11}O_{39}Mn(H_2O)]^{6-}$ [136].

The most representative POM is the Keggin HPA of the formula $[XM_{12}O_{40}]^{n-}$ such as the newly synthesized molybdovanadophosphoric acids of the general formula $H_{3+x}PMo_{12-x}V_xO_{40}$(x=0–3).$nH_2O$ [137]; made of an assembly of twelve MO_6 octahedrons sharing their corners or edges with a central XO_4 tetrahedron as seen in Figure 1.11 alongside some other types of heteropoly compounds differentiated in the following comparative table [34].

Table 1. 1. Types of heteropoly compounds

Types	**Molecular formula**	**Building units**	**Type of sharing**	**Central groups**
Keggin	$X^{n+}M_{12}O_{40}{}^{(8-n)-}$	M_3O_{13}	Edge	XO_4
Dawson	$X_2{}^{n+}M_{18}O_{62}{}^{(16-2n)-}$	M_3O_{13}	Edge	XO_4
Waugh	$X^{n+}M_9O_{32}{}^{(10-n)-}$	M_3O_{13}	Edge	XO_6
Anderson	$X^{n+}M_6O_{24}{}^{(12-n)-}$	M_2O_{10}	Edge	XO_6
Silverton	$X^{n+}M_{12}O_{42}{}^{(12-n)-}$	M_2O_9	Face	XO_{12}

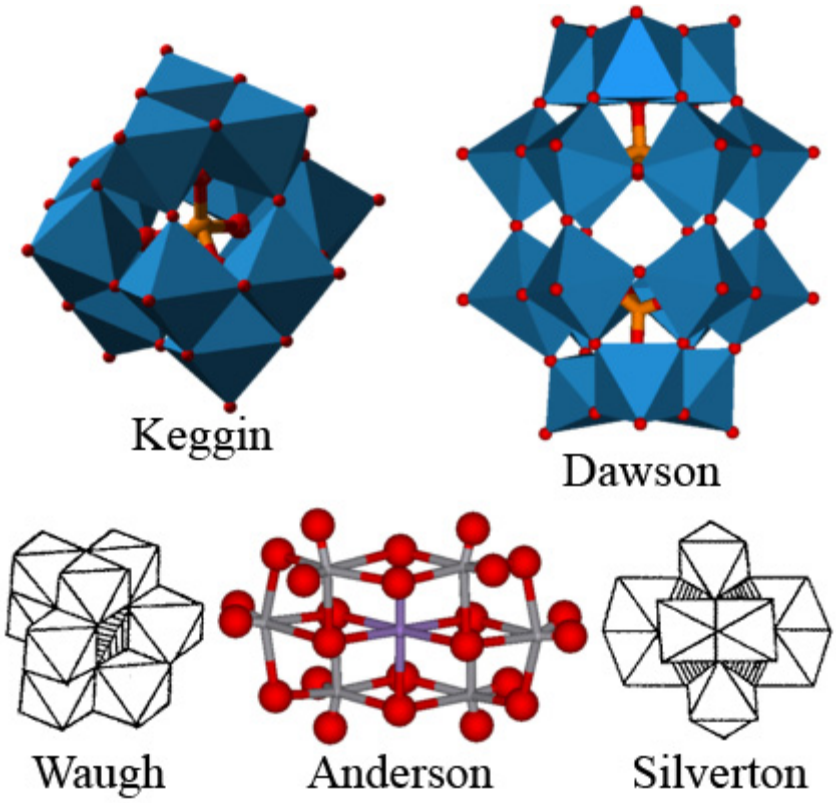

Fig. 1. 11. Polyhedral representation for the different structures of heteropolyanions; modified from Ref. [138]

These highly structured compounds are very well organized and described, so there is a need to look at their rotational isomers that are themselves highly symmetric materials. So far, the α-Keggin form of T_d symmetry is constructed from equivalent metal centers, however the β structure could be generated by a 60º rotation of one of the M_3O_{13} triad about a 3-fold axis of the α anion and thus the rotation of the remaining triads would result into three additional isomers, γ, δ and ε all seen in Figure 1.12 [139-142]. Such flexibility and versatility would result into an unmatched range of physical properties and the ability to form structures that can stretch the scopes of POMs' applications in chemical industry and catalysis.

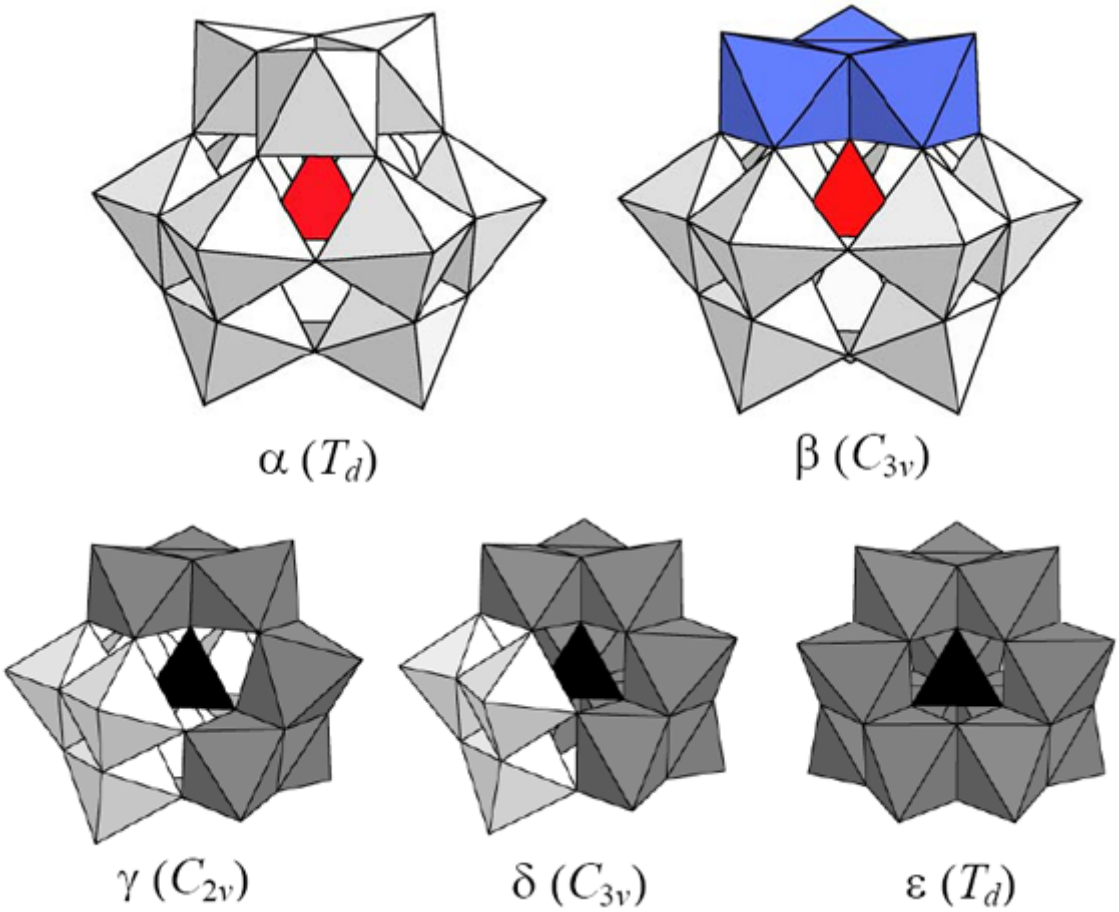

Fig. 1. 12. Polyhedral representation of the five rotational isomers of the Keggin anion, in which the shaded region are the edge-sharing octahedra involved in the isomerism; taken from Ref. [140-142]

1.5.3. Preparation

POMs have been synthesized and isolated from both aqueous and nonaqueous solutions. Correspondingly, POMs that are water soluble have been prepared from metals, even though this might lead to the infinite polyanion or mixed oxide structures [124].

The most widely used method of preparation comprises the acidification of aqueous solutions of simple oxoanions and the necessary heteroatoms [143]. Figure 1.13 exemplifies two schematic representations of the preparation of the two most common POMs experiencing high catalytic activities in various organic acid catalysis

reactions [144]. In many cases as in the above examples, the equilibrium constants and rates of formation should be large enough that the POMs be easily crystallized as salts from acidic mixtures at room temperature [145]. In order to achieve the acidification needed for crystallization, some mineral acids, electrolytic oxidation of the solvent, or addition of the appropriate anhydride might be used [143]. Accordingly, the isolation of polyanions from solution is generally achieved by addition of an appropriate counteraction, commonly an alkali metal, ammonium or tetralkyl ammonium. Some larger alkylammonium salts which are insoluble in water could be recrystallized from solvents such as diethyl ether, acetonitirile, and acetone [143].

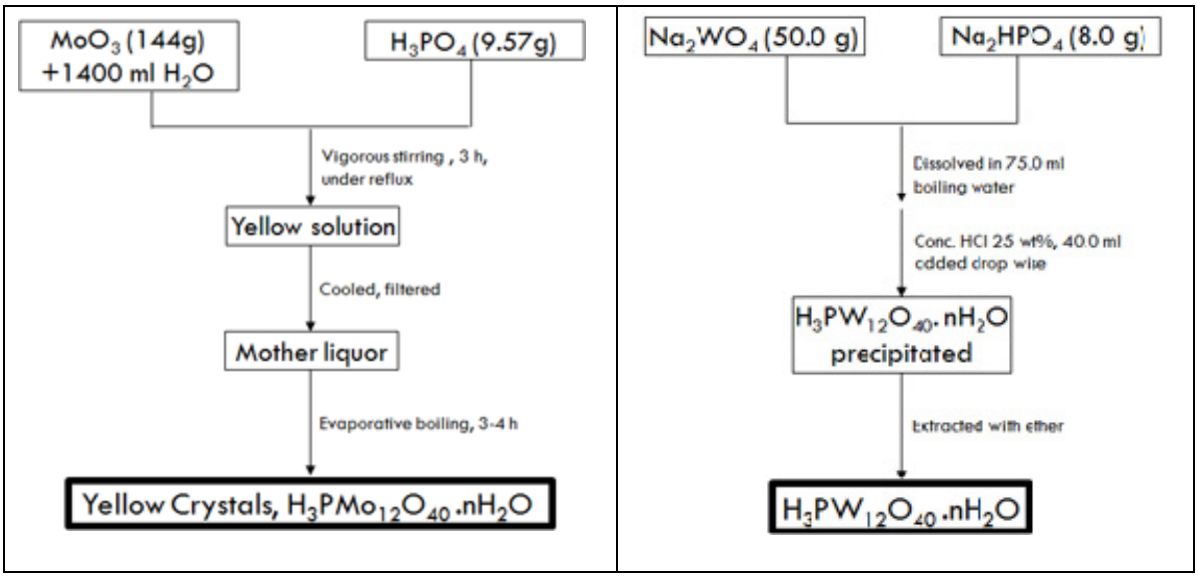

Fig. 1. 13. Preparation schemes of two POMs: $H_3PMo_{12}O_{40}.nH_2O$ (Left), $H_3PW_{12}O_{40}.nH_2O$ (Right); modified from Ref. [143]

In order to have a better picture and to fully understand the heterogeneous catalysis of POMs, it is very important to distinguish between the two classes of structures. As a reference to the differences, the hierarchical structure of the Keggin POM is shown in Figure 1.14. POMs in the solid state are ionic crystals which are sometimes amorphous. They consist of large polyanions as the primary structure,

cations, water of crystallization, and other molecules. All of these combined would give a three-dimensional arrangement which is the secondary structure. A tertiary structure was later realized to take part in their catalytic function, which is the structure of assembled POMs comprising the distribution of protons, particle size, surface area, and pore.

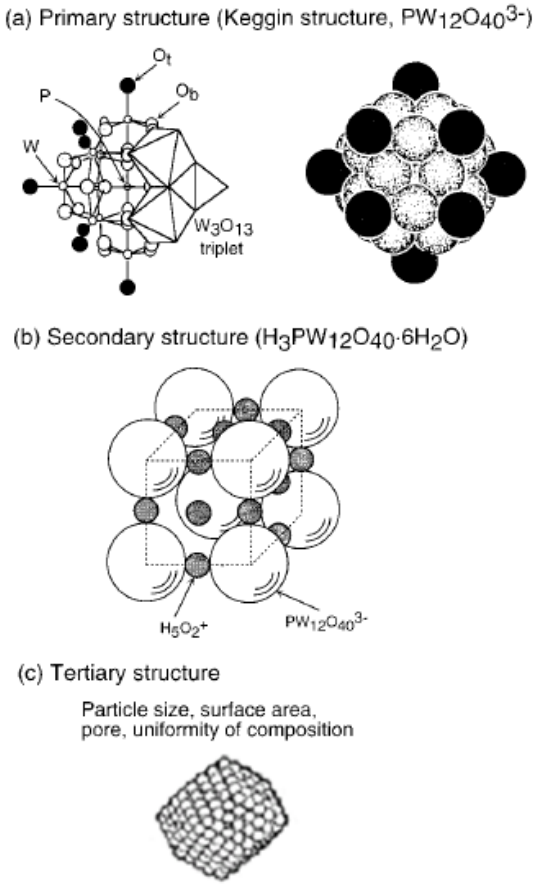

Fig. 1. 14. Hierarchical structure of heteropoly compounds; modified from Ref. [146]

1.5.4. Application

The major part of POMs' molecular science in chemistry, physics, biology, and materials science has just been recently reported and investigated [131]. POMs could be broadly modified in such a way, all molecular properties such as composition, size, shape, charge density, acidity, solubility, and redox potentials, which affect the

usefulness of a class of compounds in catalysis, medicine, and materials science, can be altered by approaches and techniques that are now affordable and justifiable [34, 131].

In 1998, a special issue of Chemical Reviews has published a thematic edition on POMs [125] providing a comprehensive coverage of studies, and the broad research and applications conducted in this area thus far. Katsoulis [147] has provided a survey of POMs' applications, some of are worth mentioning such as coatings [148], processing radioactive waste [149, 150], membranes [151], sensors [152, 153], dyes and pigments [154, 155], electrooptics [156], electrochemistry and electrodes, capacitors [157, 158], dopants in sol-gel matrixes [159, 160], bleaching of paper pulp [161], food chemistry [162, 163], in addition to appealing implications for catalysis [144, 146, 164] and medicine [165]. Practically, several profitable processes involving POMs in both homogeneous and heterogeneous catalysis are being exploited [131]. Moreover, other technologies based on POM derivatives are in development, yet so much work, efforts, and perseverance are still required to ensure a complete and comprehensive view of the chemistry, synthesis, and applications of POMs.

1.6. Polyoxometalates in Catalysis

1.6.1. Overview

Among numerous applications of heteropoly compounds, catalysis is by far the most important [57, 144, 166-174]. The first attempts to use POMs as catalysts can be traced back to the early 1900s, whereby heteropoly compounds have several advantages in this area, the most important of which is their multifunctionality and structural mobility [144]. POMs with a very strong Brönsted acidity are considered to be efficient oxidants that undergo fast reversible multielectron redox transformations under mild

conditions [144]. As explained in earlier sections, changing the chemical composition of these POMs would vary their acid-base and redox properties to a great extent [144]. In liquid-phase oxidation for instance, the occurrence of a certain number of vanadium ions in the POMs is essential for their oxidative reversibility under milder conditions compared to $[PMo_{12}O_{40}]^{3-}$ which lack such potential [144]. Their overall structure is usually maintained upon substitution or oxidation/reduction and thus would result into an appealing exceptionally high proton mobility [175, 176]. Additionally, as hinted in previous sections, many heteropoly compounds have very high solubilities in polar solvents and an effectively high thermal stability in the solid acid state which equally would facilitate their action as catalysts [144].

1.6.2. Theory

Provided their unique properties, heteropoly compounds are outstanding acid, redox, and bifunctional acid-redox catalysts [144]. Their catalytic reactions can be performed in both homogeneous and heterogeneous systems [34]. Moreover, they are employed as model systems for basic research and investigation into mechanistic studies on the molecular level, as well as their importance in applied catalysis [20, 144, 166-169].

Due to the fact that these POMs with such favorable characteristics and alluring properties of being inert to thermal and oxidative degradation [34], as well as their adjustable solubility by counterion metathesis, polyelectrolyte pursuit, and photocatalytic activity has caused them to become pioneers in oxidative catalysis [177]. Moreover, the importance of POMs as effective catalysts relies in their ability of acid-

redox bifunctionality, in addition to their fascinating balance between their oxidizing capacity on one hand and their catalytic activity on the other [146, 167].

1.6.3. Applications

Such bespoke POMs are generally implemented as efficient catalysts for environmentally friendly oxidation reactions under aerobic conditions [34, 124, 131, 178, 179]. Some transition metal substituted POMs were employed by Bonchio *et al.* for the aerobic oxidation of cyclohexane [180] and *cis*-cyclooctene [173], and bio-oriented catalysis [174], giving high selectivity and unmatched turnover frequencies with unique robustness in their structural and coordination properties. It is usually advisable to acquire heterogeneous catalysis, because of the advantages in product separation, catalyst recycling, and in order to use these POMs as ideal catalysts under mild conditions while avoiding extensive use of reducing agents and solvents [34, 124, 131, 178, 179, 181, 182]. Later on, it was well documented that supported POM catalysts on solid materials, such as silica for instance, gave it better yielding amounts with improved catalytic activities in comparison with the same free POM [183].

1.7. Supported Polyoxometalates

1.7.1. Overview

Well-ordered mesoporous silica materials as those highlighted in earlier sections such as MCM-41, SBA-15, as well as silica aerogels are being used as supports for the immobilization of various solid catalysts [184-188]. In particular, silica aerogels gained a high interest due to their large internal surface area (~1000 $m^2.g^{-1}$) facilitating the distribution of a large number of catalytically active sites [189, 190]. Furthermore,

the large pores (~20 nm mean pore diameter) allow the dispersal of substrates and products. Correspondingly, their high optical transmission, low densities and low thermal conductivities make it thermally and hydrothermally much more robust than other supports [117, 189, 190].

1.7.2. Chemistry

One of the most important approaches towards implementing a reliable catalytic system with 100% selectivity to the desired product with much less energy demands while maintaining the innate activity is to encapsulate or immobilize these metal POM clusters onto mesoporous supports; and thus would enhance their reactivity by acting in a sterically controlled manner [191, 192]. In such systems, the steric effect is a consequence of the geometry acquired by the mesoporous solids. Additionally, linking up with the surface functional groups causes a decrease in its freedom when compared to that in the bulk yet leading towards improved and better aimed ends [191, 192]. Recent studies have reported the immobilization of POMs and their derivatives on a variety of supports such as silica, carbon, mesoporous silica MCM-41 [193], MCM-48 [54], SBA-15 [194] and SiO_2-xerogel [195] hooked up to an organic amine group linkage, and their uses in different scopes of catalytic, organic, and chemical activity and reactivity has been profusely explored and studied [196-199]. Results of such catalysis reactions with the POMs immobilized onto these different silica supports have yielded higher catalytic activity with enhanced selectivity. Moreover, one important advantage of this heterogeneous catalysis is that the catalyst is readily recyclable by filtration without any loss of activity [194].

Limited research has been conducted on heteropoly compounds, however the most important of which are heteropolymolybdovanadates. An important heteropolymolybdovanadate is the 10-molybdo-2-vanadophosphate(V) anion synthesized by Kokorin [200]. Krivy and Krtil assigned in 1964 [201] a basicity of 3 to the l0-molybdo-2-vanadophosphoric acid based on radiometric titration studies aided by cesium-137, resulting into the salt of formula $Cs_3H_4[P(Mo_2O_7)_5V_2O_6]$. In 1964, Souchay and co-workers [202, 203] have managed to produce heteropolymolybdovanadates such as 9-molybdo-3-vanadophosphoric acid, 10-molybdo-2-vanadophosphoric acid (10-MVPA), and 11-molybdo-1-vanadophosphoric acid (11-MVPA). Tsigdinos and Hallada [137] later on investigated the methods of preparation and characterization of these POMs in well documented procedures. In the current thesis investigation, these highly active heteropoly compounds with effective catalytic behavior [54] are immobilized in the synthesized organically-modified silica aerogels.

1.7.3. Advantages and disadvantages

POMs have always been limited by disadvantages such as very low surface areas with less than 10 $m^2.g^{-1}$ [204], and as seen for 10-MVPA and 11-MVPA in the present investigation with surface areas of 4 and 8 $m^2.g^{-1}$ respectively. In some cases, POMs might experience low decomposition temperatures causing a decrease in the number of active sites on its surface rendering their activity less effective [205]. POMs also suffer from being non-recyclable after use in the reactions because they are water soluble, where it is quite complicated to rejuvenate the used solid for future use [206]. Thereafter, a huge and important leap is by their immobilization and/or encapsulation in

mesoporous solids, achieved in this area of exploration, in order to optimize the feedback from these highly active solids. In such a step, less energy is being demanded while maintaining the POMs' catalytic activities in an attempt to accomplish a selectivity up to 100% of the desired product [192].

1.8. Aim of Present Work

Increasing interest has been oriented towards 9, 10-anthraquinone (AQ) and its derivatives that were employed as antioxidants and antitumor agents in the chemotherapy treatment of cancer [207-210]. Due to its crucial use as a carrier of H_2 in the commercial production of hydrogen peroxide, 9,10-Anthraquinone is regarded as the chief derivative of anthracene (AN) [211, 212]. Additionally, AQ plays a crucial role in the preparation of dyes and pigments [213], papers, and molecular switches used in electrical devices [214-218]. However, this broad range of profitable applications comes at a very high cost of production. Some expensive means of AQ production encompass the oxidation of AN with chromic acid, vapor-phase oxidation of AN by air [219], benzene condensation, and via the Diels-Alder reaction [220].

During the past 200 years or so, many homogeneous catalytic systems for the oxidation of AN were employed but are now rendered ineffective due to their drawbacks. Immobilized chelates [221], enzymes [45-47], and supported clusters for the oxidation of AN with results of high catalytic activity (21 mole AN converted per mole of catalyst per hour, as the turnover frequency) and 100% selectivity to AQ have been reported [54]. Here, the immobilization of various POMs onto highly porous amino-modified silica aerogels is studied where the aminoalkyl silicon precursors are grafted on the surface of the gels. The synthesized solid supports were characterized by FTIR

spectroscopy, N_2 adsorption, powder X-Ray diffraction, diffuse-reflectance UV-Visible spectroscopy, and atomic absorption spectroscopy. The impetus of this research includes both the effect of the immobilization of POMs onto mesoporous inorganic supports for their use in heterogeneous catalysis and to develop a novel catalytic system adapted for the highly selective oxidation of AN to AQ, compared to the homogeneous catalyst. The design and fabrication of such highly active, cost-effective, less energy demanding, eco-friendly complex catalytic system for the 100% selectivity of the oxidation of AN to AQ is a gargantuan step into a new era of technology and power.

CHAPTER TWO

SILICA AEROGELS SYNTHESIS

2.1. Silica aerogels synthesis

2.1.1. Materials

The chemicals were used in this study as received and without further purification. Tetramethoxysilane (TMOS – $Si(OCH_3)_4$) was provided from Merck. Tetraethoxysilane (TEOS – $Si(OC_2H_5)_4$), Methyltrimethoxysilane (MTMS – $CH_3Si(OCH_3)_3$), Methyltriethoxysilane (MTES – $CH_3Si(OC_2H_5)_3$), Ethyltriethoxysilane (ETES – $C_2H_5Si(OC_2H_5)_3$), Propyltrimethoxysilane (PrTMS – $C_3H_7Si(OCH_3)_3$), Isobutyltriethoxysilane (isoBTES – $(CH_3)_3CSi(OC_2H_5)_3$), Vinyltriethoxysilane (VTES – $CH_2{=}CHSi(OC_2H_5)_3$) were supplied from Fluka. Ethyltrimethoxysilane (ETMS – $C_2H_5Si(OCH_3)_3$), Propyltriethoxysilane (PrTES – $C_3H_7Si(OC_2H_5)_3$), Isobutyltrimethoxysilane (isoBTMS – $(CH_3)_3CSi(OCH_3)_3$), Octyltrimethoxysilane (OTMS – C8H17Si(OCH3)3), were provided from Aldrich. Octyltriethoxysilane (OTES – $C_8H_{17}Si(OC_2H_5)_3$), Vinyltrimethoxysilane (VTMS – $CH_2{=}CHSi(OCH_3)_3$), Phenyltrimethoxysilane (PhTMS – $C_6H_5Si(OCH_3)_3$), Phenyltriethoxysilane (PhTES – $C_6H_5Si(OC_2H_5)_3$) were from Acros Organics. Methanol, hydrochloric acid (37%), and ammonium hydroxide were from Riedel-de-Haen, Panreac and Fischer Scientific, respectively. Double deionized water was prepared in our laboratory.

2.1.2. Procedure

The silica aerogels were synthesized similar to the representative scheme in Section 1.3.3, where tetraalkoxysilanes ($Si(OR)_4$; R = CH_3 or C_2H_5) were used solely in the preparation of the pure silica aerogels. Other than being combined according to a molar ratio of 1:0.25 with other silicon co-precursors ($R''Si(OR')_3$; R' = CH_3 or C_2H_5; R'' = CH_3, C_2H_5, n-C_3H_7, iso-C_4H_9, n-C_8H_{17}, C_2H_3, C_6H_5) to produce the desired surface-modified silica aerogels with non-hydrolysable alkyl groups on their surface. Table 2.1 gives a naming system used for identifying the different silica aerogel materials obtained.

Table 2. 1. Precursor/co-precursor composition of the different surface-modified silica aerogels

Sample	Composition	Sample	Composition
M1	TMOS	E1	TEOS
M2	TMOS / MTMS	E2	TEOS / MTMS
M3	TMOS / ETMS	E3	TEOS / ETMS
M4	TMOS / PrTMS	E4	TEOS / PrTMS
M5	TMOS / isoBTMS	E5	TEOS / isoBTMS
M6	TMOS / OTMS	E6	TEOS / OTMS
M7	TMOS / VTMS	E7	TEOS / VTMS
M8	TMOS / PhTMS	E8	TEOS / PhTMS
M9	TMOS / MTES	E9	TEOS / MTES
M10	TMOS / ETES	E10	TEOS / ETES
M11	TMOS / PrTES	E11	TEOS / PrTES
M12	TMOS / isoBTES	E12	TEOS / isoBTES
M13	TMOS / OTES	E13	TEOS / OTES
M14	TMOS / VTES	E14	TEOS / VTES
M15	TMOS / PhTES	E15	TEOS / PhTES

Following a two-step sol–gel process, the first step was to mix the silicon precursors in a polypropylene vial with methanol, 0.2 M hydrochloric acid (HCl) solution and deionized water, and kept stirring at room temperature for 24 hours. A 0.5 M ammonium hydroxide solution (NH_3[aq]) was then added to the mixture and stirring

continued for a further 5 minutes to ensure a well homogenous solution. The gelation of the sol was then observed in the next 24 hours and the obtained gels were kept for aging for one day at the same conditions.

The current process has resulted into the production of a wet silica alcogel according to the following set of synthetic molar ratios $Si(OR)_4$:Methanol:H_2O:HCl:NH_3 were 1:12:6:3×10^{-3}:6×10^{-3} for the pure silica aerogels, and $Si(OR)_4$:R''$Si(OR')_3$:Methanol:H_2O:HCl:NH_3 were 0.8:0.2:12:6:3×10^{-3}:6×10^{-3} for the organically-modified silica aerogels.

The obtained silica alcogels were then drenched in acetone for a 24 hour solvent-exchange, by which the acetone replaces the residual water and methanol within the pores of the alcogel. This step was a necessary routine in order to ensure better and increased miscibility of the solvent present inside the pores and the liquid carbon dioxide used in the drying step next. Later on, the drying of these treated wet alcogels in carbon dioxide under supercritical conditions, as explained previously in Section 1.3.3.4, led to the desired final silica aerogels after solvent evacuation. For a better understanding of the whole synthetic picture, a schematic diagram of the silica aerogels synthesis is presented in figure 2.1.

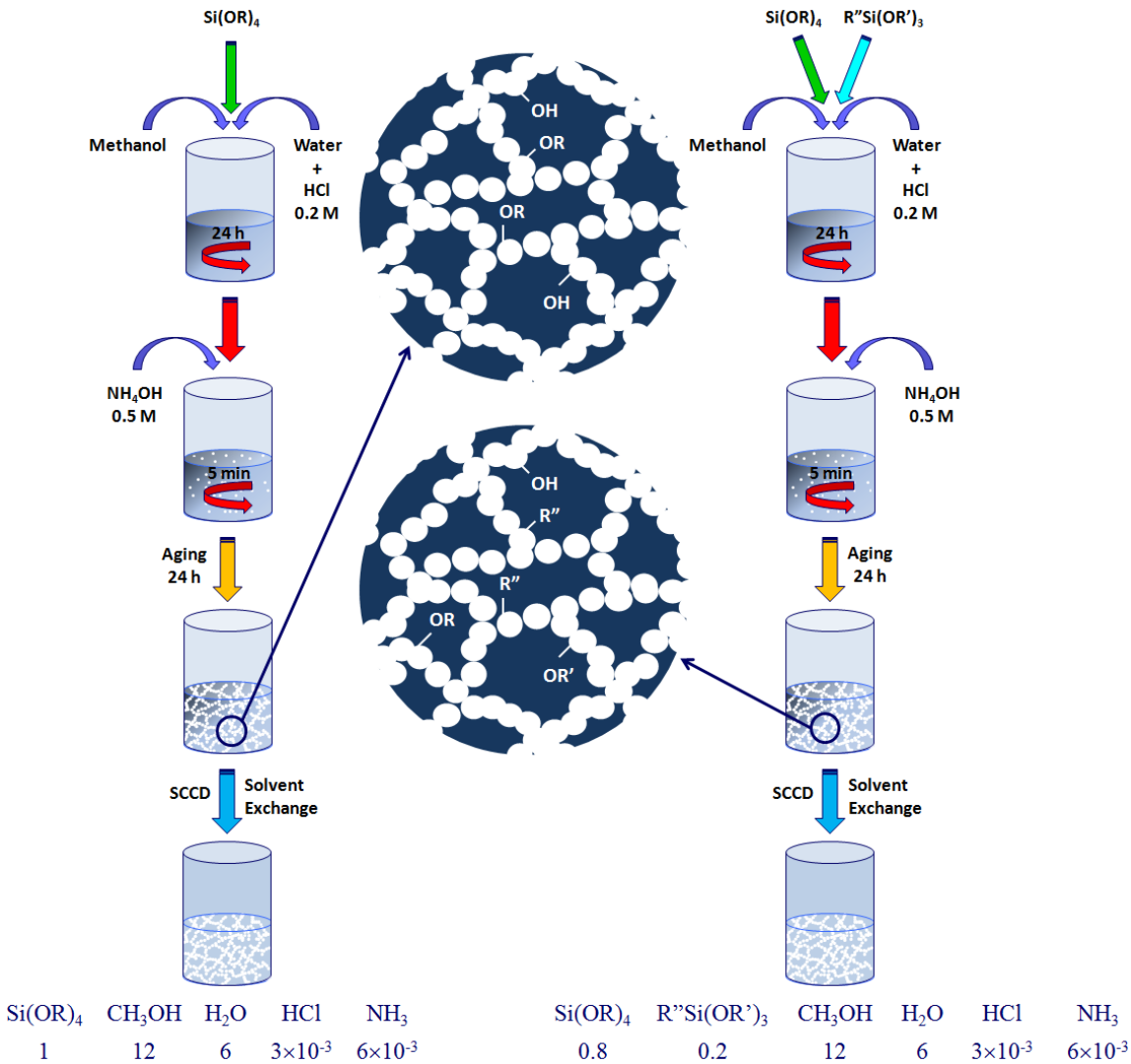

Fig. 2. 1. Silica aerogel synthesis

2.2. Results and discussion

The described synthetic procedure allowed the formation of hard and low-density white non-transparent silica aerogels. As explained in Section 1.3.3, the first step is the hydrolysis of the alkoxy groups of the silicon precursors leading to the formation of silanol groups (Si–OH), where the H^+ ions of the hydrochloric acid solution play the role of the catalyst.

While, the silicon precursors are expected to be totally hydrolyzed after 24 hours of reaction, the non-hydrolysable silicon precursors R'' groups however remain unmodified according to Equation 2.1.

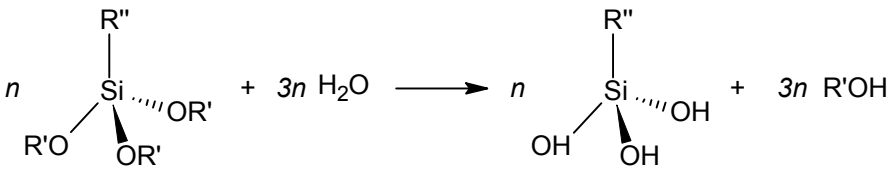

Equation 2. 1

The utility of the ammonia solution in the following step, the poly-condensation (Equation 2.2), is to neutralize the pH of the mixture and to shift it towards basic conditions where the hydroxide anions (OH^-) play the role of basic catalysts. This step led to the formation of oxobridged Si–O–Si groups and therefore to the interconnectivity of the silica network. The unhydrolyzed R'' groups are expected to exist on the surface of the solids' pores, giving to these solids their hydrophobic character.

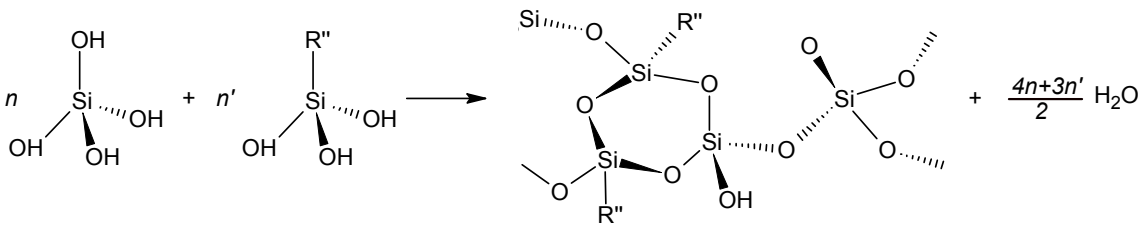

Equation 2. 2

CHAPTER THREE

FTIR SPECTROSCOPY

In order to cover the entire scope of this research, the host silica materials were first synthesized according to the two-step sol-gel process explained in Chapter Two of this thesis. However, there was a great urge to understand and to really qualify and quantify the material that was obtained. The organically surface-modified silica aerogels that were synthesized need to be tested for purity and characterized to make sure that what is proposed is exactly what was achieved. One important analytical tool that has been a powerful technique for materials analysis in the chemistry laboratory since a decade is infrared (IR) spectroscopy. Thus, IR spectroscopy was employed as an analytical tool to elucidate the structures and identify the materials that were obtained [118], the results of which are already published in a paper in the Journal of Molecular Structure [115] prior to the completion of this thesis; yet they will be deliberately revisited.

3.1. Infrared spectroscopy

3.1.1. Overview

IR spectroscopy is particularly an important structural characterization technique because of the high information that could be abstracted from a spectrum and the wide range of possible sample preparation and measurement [222]. IR spectroscopy has thus emerged as one of the most important analytical spectroscopic techniques used by inorganic chemists, in particular, for preparative purposes [223]. In simple terms, it comprises the measurement of the amount of absorbed IR radiation by a sample situated

in the path of an IR beam at different IR frequencies [224]. Different functional groups were found to absorb characteristic frequencies of the IR radiation, and thus possess a distinctive fingerprint. Therefore, the key objective of the IR spectroscopic analysis is to determine the chemical functional groups in a sample [223].

For a qualitative feel, IR spectroscopy can result in a positive identification of every different kind of material, as just explained. Additional information could as well be derived on the amount of material present and one direct indication for that is the intensity of the peaks in the spectrum [225]. With innovative integrated software algorithms, IR may well be an excellent quantitative tool for a better comprehension of the behavior of the tested materials in different environments [223]. Hence, Fourier transform spectrometers (Figure 3.1) have recently replaced the old technology for most applications due to their superior speed and sensitivity [224]. The use of an interferometer, a newly developed simple optical device, allows a quick and simultaneous measurement at all frequencies. One complication though is that the data acquired from this is in the form of an interferogram signal, which is an encoded information over the entire IR region [222]. Fourier transformation is a mathematical operation that decodes the information and converts the interferogram from a time domain spectrum displaying intensity versus time to the final IR spectrum of the familiar frequency domain spectrum showing intensity versus frequency [224]. This has momentously stretched the potentials of IR spectroscopy and has been applied to many areas that are very difficult to analyze by older instruments. In Fourier transform infrared (FTIR) spectroscopy, all frequencies are examined simultaneously instead of viewing each component frequency sequentially, as in a dispersive IR spectrometer [222].

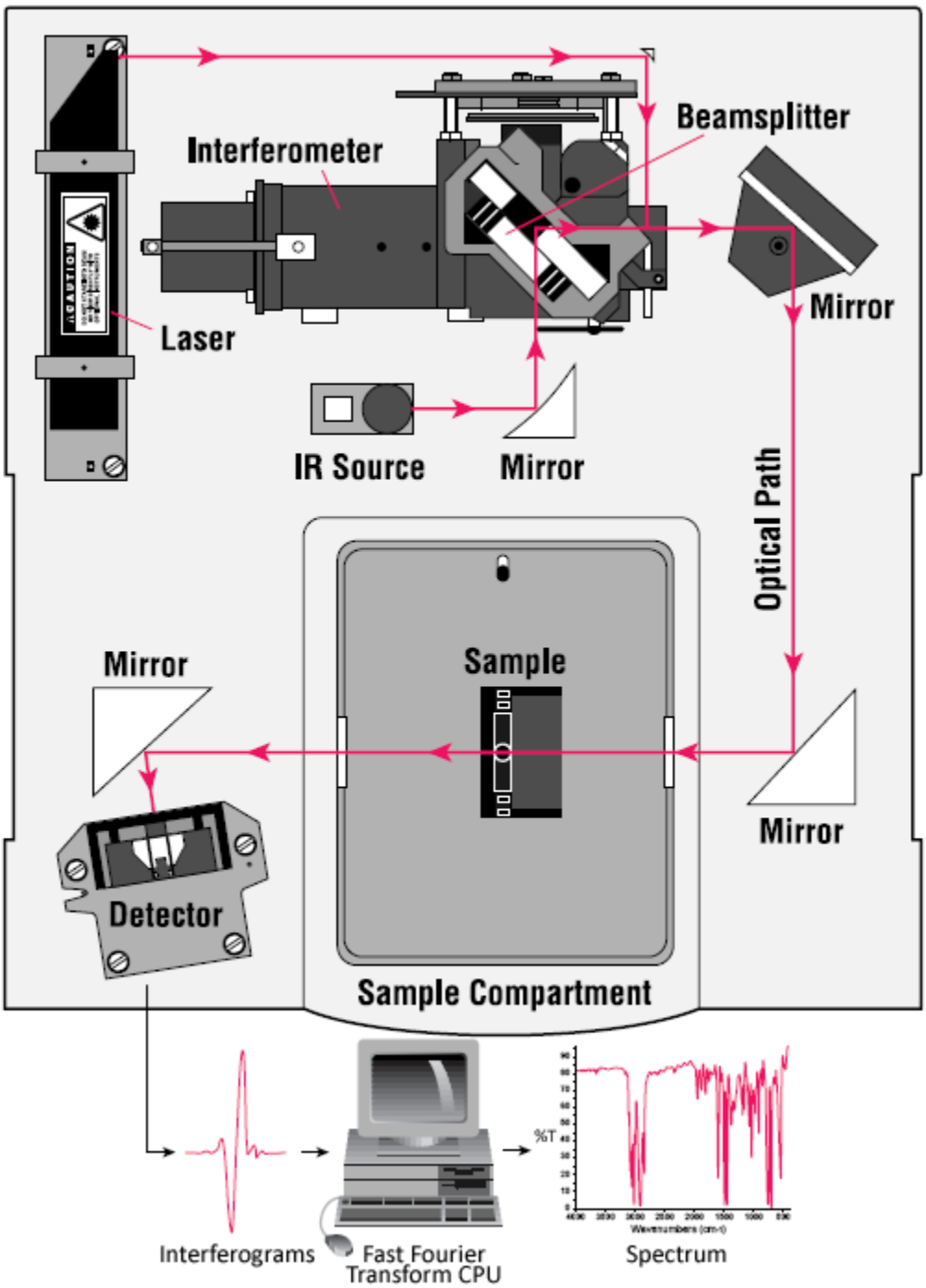

Fig. 3. 1. A simple FTIR spectrometer layout; modified from Ref. [224]

Using various sampling equipment and accessories, FTIR spectrometers can accept a wide range of sample material such as gases, liquids, and solids [225]. The IR

region of the electromagnetic spectrum spans from 14,000 cm^{-1} to 10 cm^{-1}. However, the region of most interest for chemical analysis is the mid-IR region (4,000–400 cm^{-1}) which corresponds to changes in vibrational energies within the molecules. The far IR region (400–10 cm^{-1}) is nonetheless useful for investigating molecules such as inorganic compounds with heavy atoms but rather necessitates specialized experimental techniques [222]. For the purpose of this work, the mid-IR region was enough to fully characterize the samples and to provide the information needed.

3.1.2. Theory

All the atoms in molecules are in continuous vibration motion with respect to each other at temperatures above absolute zero. Having some idea or a representation of the physical process involved when a molecule interacts with the IR radiation is extremely helpful in interpreting IR spectra [222]. The molecule would absorb the radiation when the frequency of a specific vibration is exactly equal to the frequency of the directed IR radiation [223]. Two types of molecular vibrations are known, stretching and bending. The various types of vibrations are illustrated in Figure 3.2.

Since bond lengths and angles represent the average positions about which atoms vibrate, a molecule consisting of N atoms has a total of 3 N degrees of freedom corresponding to the Cartesian coordinates of each atom in the molecule. In a nonlinear molecule, 3 of these degrees are rotational, 3 are translational, and the remaining would correspond to fundamental vibrations; in a linear molecule however, one of the rotational degrees of freedom is redundant [223]. The net number of normal modes of vibration for nonlinear and linear molecules is therefore 3n-6 and 3n-5 respectively,

those of which produce a net change in the dipole moment may experience an IR activity [222].

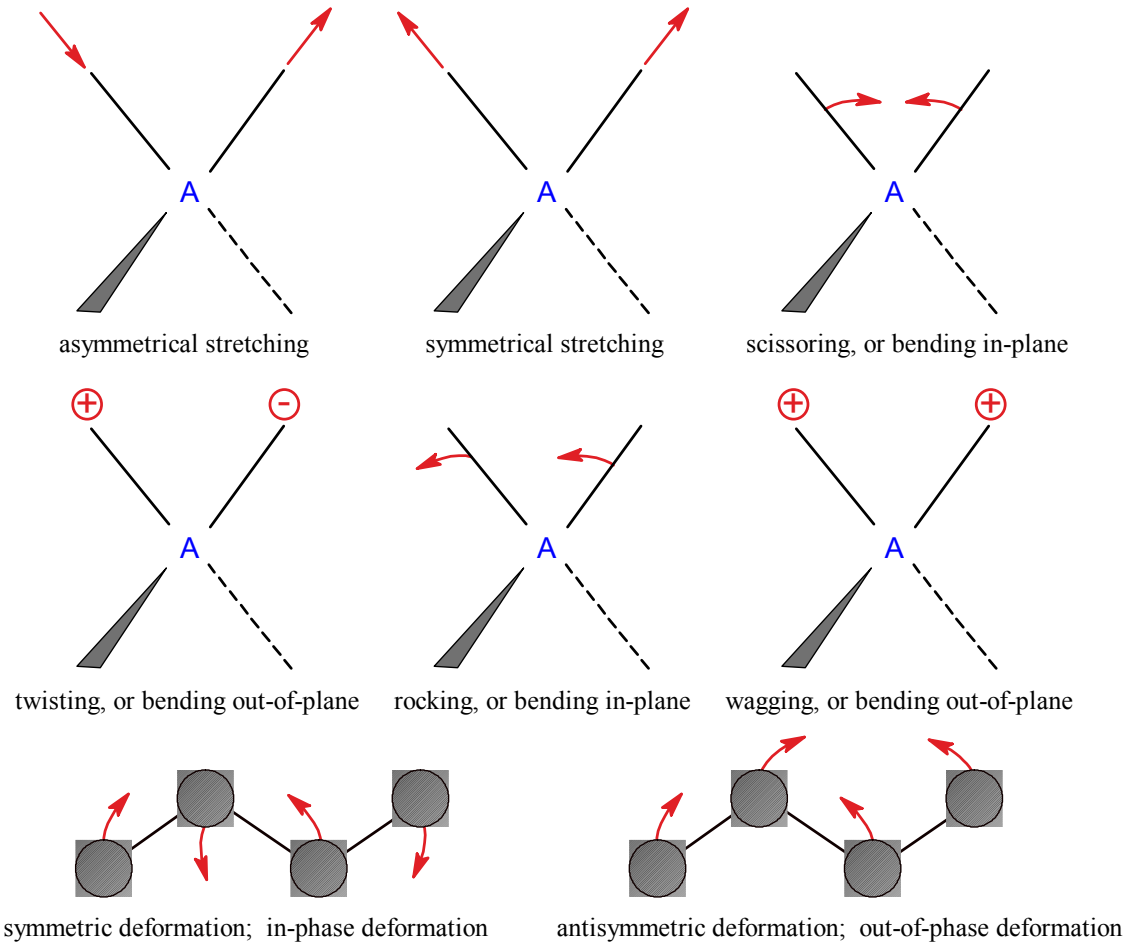

Fig. 3. 2. Various vibrational modes; the arrows represent the vibration direction of the atoms bound to the atom A; + and – represent the vibrational motions in two opposite directions: inwards and outwards; modified from Ref. [222, 225]

The total number of observed absorption bands is not necessarily the same as the total number of fundamental vibrations. This is because some modes could be IR inactive and one frequency could cause more than one mode of motion. On the other hand, additional bands may appear as overtones of the fundamental absorption frequencies, combinations or differences of fundamental frequencies, or an interactive

combination between the two [223]. The merging and arrangement of all the aspects, that were just highlighted, would eventually create a unique resemblance IR spectrum for each compound [225]. With the aim of obtaining a more detailed interpretation of an IR spectrum, it is necessary to refer to correlation charts and tables of infrared data. Many different tables available for references [222, 226-233] were employed here to facilitate the process of deciphering the data acquired from their respective IR spectra.

3.1.3. Sample preparation and characterization

A variety of techniques for sample preparation exists depending on the physical form of the sample to be analyzed, as it might be already known by now. The main two methods for sampling involve the use of Nujol mull or potassium bromide disks [222]. Additionally, preparing a solution in a suitable solvent may also be used, but nevertheless this could result into spectrum bands of its own which may mask bands in the sample spectrum [225]. The latter of the two main methods has proven to be much easier and would return better results. Using this method, a very small amount of the solid (approximately 1–2 mg) is added to pure potassium bromide powder (approximately 200 mg) and ground up into very fine powder (theoretically < 2 microns) [234] to minimize IR light scattering. The powder is then made into a disk by pressing it in a mechanical pellet presser, where the pressure is maintained for several minutes before removing the formed KBr disk. The disk is then ready for scanning, while a 100% KBr disk is also prepared for use as the background.

The FTIR spectroscopy conducted in this thesis was performed on a Nicolet™ 4700 FTIR spectrometer. The transmittance measurements were carried out according to the KBr technique, as explained earlier, where 1% in weight aerogel powder-

containing potassium bromide pellets were used. The success of this technique is dependent on the powder being ground as fine as possible to minimize IR light scattering off the surface of the particles [223]. It is also important that the sample be dry before preparation, since KBr is easily hygroscopic. Potassium bromide has been chosen because it has no infrared absorption in the region of desired study and therefore the peaks collected in the mid-IR range belong solely to the analyzed sample [222].

3.2. Results and discussion

The FTIR spectra of the synthesized silica aerogels show several bands corresponding to various structural units of the solid network. Some of the obtained spectra are included in this section, which are color-coded into those prepared in TMOS shown in blue and those prepared in TEOS shown in red, while the rest are shown in the Appendix. However, a complete list of the vibration frequencies and their assignments are regrouped in Appendix A, Table A.1.

3.2.1. TMOS and TEOS aerogels

The FTIR spectra of the M1 and E1 silica aerogels obtained, respectively from TMOS or TEOS (Figure 3.3) show common bands assigned to various vibrations in the solid network. The analysis of these spectra revealed the broad band centered at around 3470–3450 cm^{-1} corresponding to the overlapping of the O–H stretching bands of hydrogen-bonded water molecules (H–O–H···H) and SiO–H stretching of surface silanols hydrogen-bonded to molecular water (SiO–H···H_2O) [5]. Furthermore, the Si–O in-plane stretching vibrations of the silanol Si–OH groups appear at around 960 cm^{-1} [229] and the absorption bands corresponding to the adsorbed water molecules

deformation vibrations appear at 1653–1634 cm^{-1} [227]. The adsorption of water molecules on the surface of the aerogels is due to the existence of the surface silanol groups and therefore to the hydrophilic nature of these sol–gel materials. The intense silicon–oxygen covalent bonds vibrations appear mainly in the 1200–1000 cm^{-1} range revealing the existence of a dense silica network, where oxygen atoms play the role of bridges between each two adjacent silicon atoms. The very intense and broad band appearing at 1095–1089 cm^{-1} and the shoulder at around 1200 cm^{-1} are assigned, respectively to the transversal optical (TO) and longitudinal optical (LO) modes of the Si–O–Si asymmetric stretching vibrations [231]. Conversely, the symmetric stretching vibrations of Si–O–Si appear at 800 cm^{-1} [5] and its bending mode appears at 469–467 cm^{-1} [230]. The low energy band at around 560 cm^{-1} is assigned to Si–O stretching of the SiO_2 network defects [5]. It was noticed that the spectra of M1 and E1 show no peaks corresponding to C–H vibrations, except a very weak peak appearing at 1384 cm^{-1} in the M1 spectrum. This peak was easily assigned to the C–H symmetric deformation of $–CH_2$ groups [222]. These latter groups are expected to correspond to residual non-hydrolyzed alkoxy groups (–OR) on the surface of the silica aerogels. Accordingly, we can easily conclude that the surface alkoxy groups are in very small quantities as their corresponding stretching vibrations did not appear in the E1 spectrum and therefore the hydrolysis step for the E1 aerogel is faster than for the M1 where no methoxy groups appear. The absence of these bands is a proof that: (a) the mixing time before the addition of ammonia during the synthesis was enough for the silicon precursors to be totally hydrolyzed; (b) the produced alcohol during the hydrolysis step was totally evacuated during the solvent exchange and the SCCD. Therefore, the hydrolyzed silanols condensed and participated in the formation of the silica network.

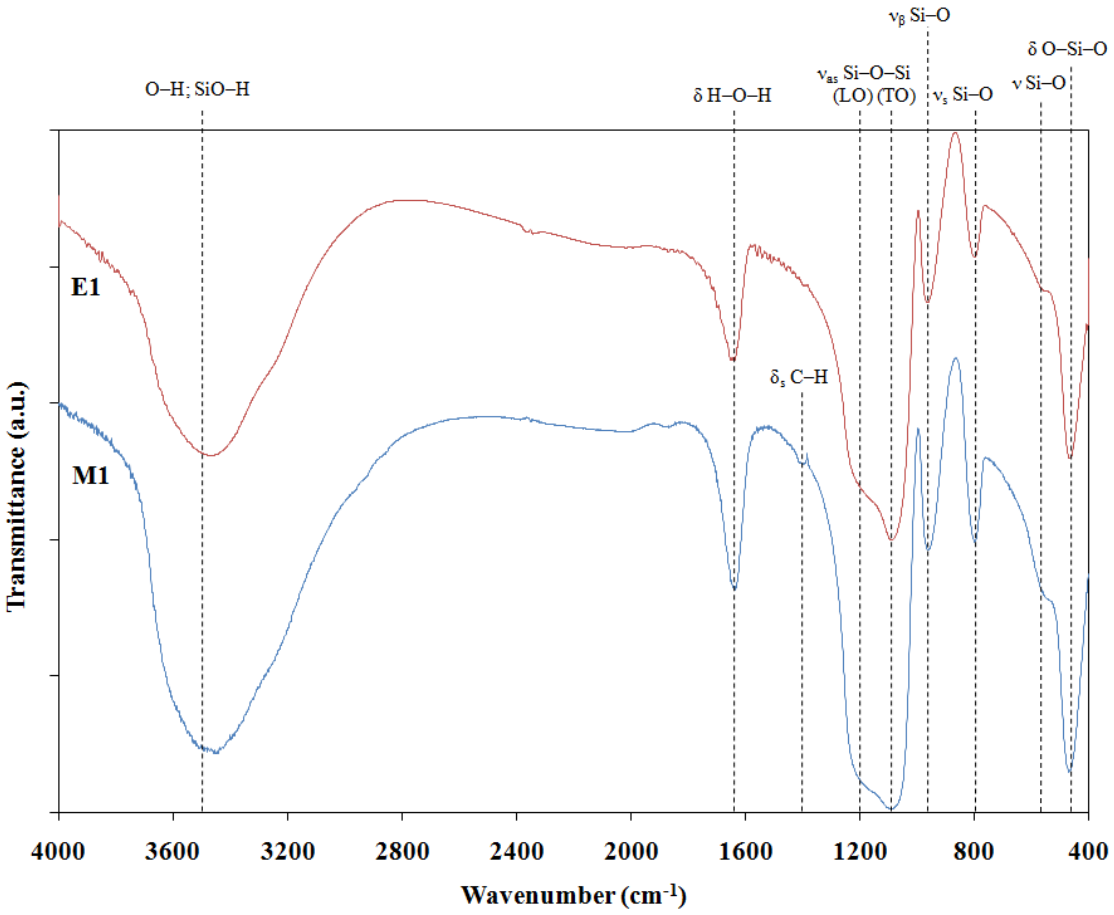

Fig. 3. 3. FTIR spectra of the silica aerogels from TMOS and TEOS

3.2.2. Methyl aerogels

The use of silicon precursors having three alkoxy and one methyl groups in addition to TMOS or TEOS (samples M2, E2, M9 and E9) led to the formation of surface methyl-functionalized silica aerogels. The corresponding IR spectra (Figure 3.4) show several peaks in the 2980–2850 cm^{-1} range assigned to the C–H symmetric and antisymmetric stretching vibrations of $–CH_3$ and $–CH_2$ groups [222]. These surface groups exist after the hydrolysis and poly-condensation of the methyl-silicon precursors used in the synthesis. The samples M2 and M9 show slightly more intense bands than E2 and E9.

The bands corresponding to the antisymmetric stretching vibrations of $–CH_3$ groups did not appear for the four samples, and thus we can conclude that the antisymmetric stretching vibrations have lower sensitivity than the symmetric ones appearing at 2977 cm^{-1}. The spectra show also C–H symmetric and antisymmetric deformation vibrations at 1385–1384, 1280–1279 and 1413–1407 cm^{-1}, respectively, [222, 227] with the absence of differences in the intensities for the various aerogels. The peaks at 834–831 cm^{-1}, having approximately the same intensities, are assigned to the Si–C stretching vibrations [227]. As the vibrations appearing at 1280–1279 cm^{-1} are specific of the silicon-bonded alkyl groups C–H bending, the coexistence of these peaks with those at 835 cm^{-1} confirmed the surface modification of the aerogels according to the Equation 2.2. Accordingly, the obtained materials are surface methyl-functionalized silica aerogels with no significant difference in their spectra regardless of the methyl group source. The comparison between the intensities of the symmetric and antisymmetric deformation vibrations revealed that the symmetric peaks are much more intense than the antisymmetric.

3.2.3. Ethyl aerogels

Surface ethyl-functionalized silica aerogels were obtained through the use of ethyltrialkoxysilane in addition to TMOS or TEOS. The FTIR spectra (Appendix A, Figure A.1) of these materials show C–H stretching vibration peaks between 2971 and 2854 cm^{-1} and C–H deformation vibrations at 1464–1462 cm^{-1} [222] owing similar intensities but neatly more intense than their equivalent in the methyl-modified silica aerogels. This difference is due to the existence of a larger number of CH_2 and CH_3 groups in the ethyl-modified aerogels. However, the C–H bending vibrations appearing

at 1258– 1256 cm^{-1} are less intense than those of the methyl-functionalized samples. This decrease in the intensity could be attributed to the steric hindrance of the ethyl groups compared to the methyl groups.

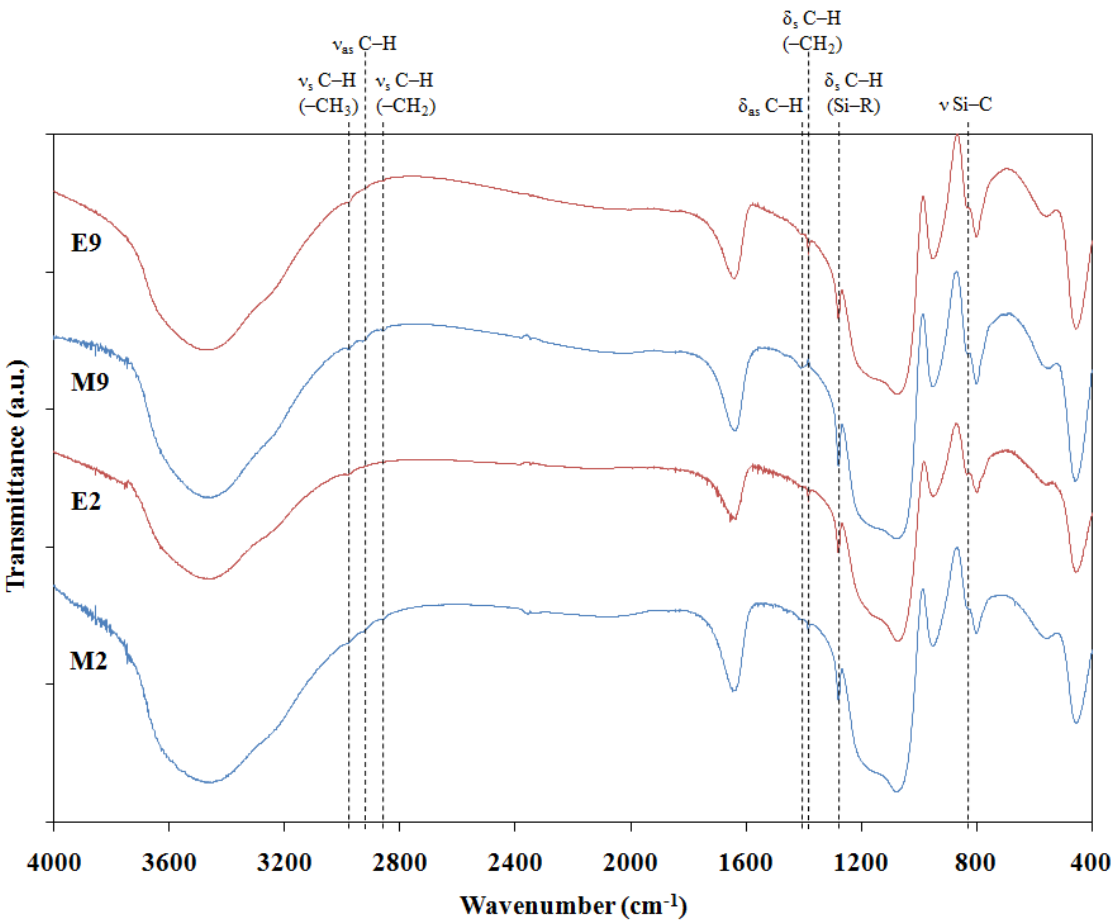

Fig. 3. 4. FTIR spectra of the methyl-modified silica aerogels

The Si–C stretching vibration appearing at 834–831 cm^{-1} for the methyl-functionalized aerogels did not appear for the ethyl-functionalized aerogels at the same frequency. The ethyl-functionalized aerogels spectra show a large band centered at 788–783 cm^{-1} which is probably an overlapping of the Si–C and Si–O stretching vibrations.

In addition to the peak appearing at 1464–1462 cm^{-1} assigned to the C–H deformation vibration, the ethyl-spectra show two peaks that do not exist in the methyl-spectra. The first one at 698–692 cm^{-1} is assigned to the Si–O symmetric stretching vibration [229] and the second is a shoulder at around 910 cm^{-1} corresponds to the in-plane stretching vibration of free $Si–O^-$ [228]. This latter vibration did not appear clearly for the methyl-modified aerogels. It is believed that the broad band centered at 951 cm^{-1} for the methyl-modified aerogels is a combination of the Si–O in-plane stretching vibrations in Si–OH and free $Si–O^-$. This is explained by the fact that the band centered at 951 cm^{-1} for methyl-aerogels is larger than the corresponding one for the ethyl-aerogels. The overall comparison of the vibration bands of the ethyl silicates having various sources of silicon precursors showed a great similarity in the band frequencies as well as in their intensities. This resemblance is directly correlated to an analogous behavior of the silicon precursors in the reaction media during the diverse synthesis steps of hydrolysis and condensation.

3.2.4. Propyl aerogels

More developed C–H stretching vibration peaks in the range 2965–2876 cm^{-1} than the methyl- and ethyl-modified aerogels where shown in the propyl-modified aerogels FTIR spectra. The increase in the intensities of these peaks is coupled to the increase of the intensities of the C–H deformation peaks appearing between 1466 and 1379 cm^{-1}. The propyl-aerogels spectra (Appendix A, Figure A.2) showed peaks at 1341 cm^{-1} that could be assigned to the $–CH_2$-deformation vibrations of the propyl group [235]. While taking into consideration the existence of these vibrations as well as their relative intensities, the four different propyl-modified aerogels were found to exhibit

similar surface groups with approximately the same ratio Si–C_3H_7 surface groups/bridging-oxygen tetracoordinated Si atoms. It is also worth noting that the Si–O in-plane stretching vibrations of the silanol Si–OH groups at around 950 cm^{-1} are more intense for M4 and M11 than for E4 and E11. The difference in the intensities of these peaks is coupled to the intense peaks appearing at 1634 cm^{-1} for M4 and M11 corresponding to the adsorbed water molecules deformation vibrations. In addition, some residual unhydrolyzed alkoxy groups were observed for the E11 samples evident by the existence of a band at 1384 cm^{-1}.

3.2.5. Isobutyl aerogels

Besides the Si–O and adsorbed water vibrations, the spectra corresponding to the samples M5, E5, M12 and E12 show intense peaks assigned to the C–H stretching and deformation vibrations (Figure 3.5). These vibrations were found in these samples due to the existence of a large number of CH_2 and CH_3 groups in the solid network having the isobutyl-silicon precursors as sources. Bands at 1369 cm^{-1} assigned to the deformation vibration of –CH_2– in the methyl groups [222] appear for all samples with the M5 and M12 samples showing more intense peaks than the E5 and E12 samples. However, the C–H stretching deformation peak appearing at 1384 cm^{-1} is much more intense for the E5 than the three other samples, with the corresponding peak more intense in E12 than M5 and M12. These intense peaks are due to the subsistence of unhydrolyzed isobutoxy groups in the silica network resulting from a slower hydrolysis of the ethyl-silicon precursors than the methyl-silicon precursors. Therefore the poly-condensation of the silanol groups started before the hydrolysis was completed. The

vibration peaks appearing at 740–735 cm^{-1} could be easily assigned to the CH_2 rocking [222].

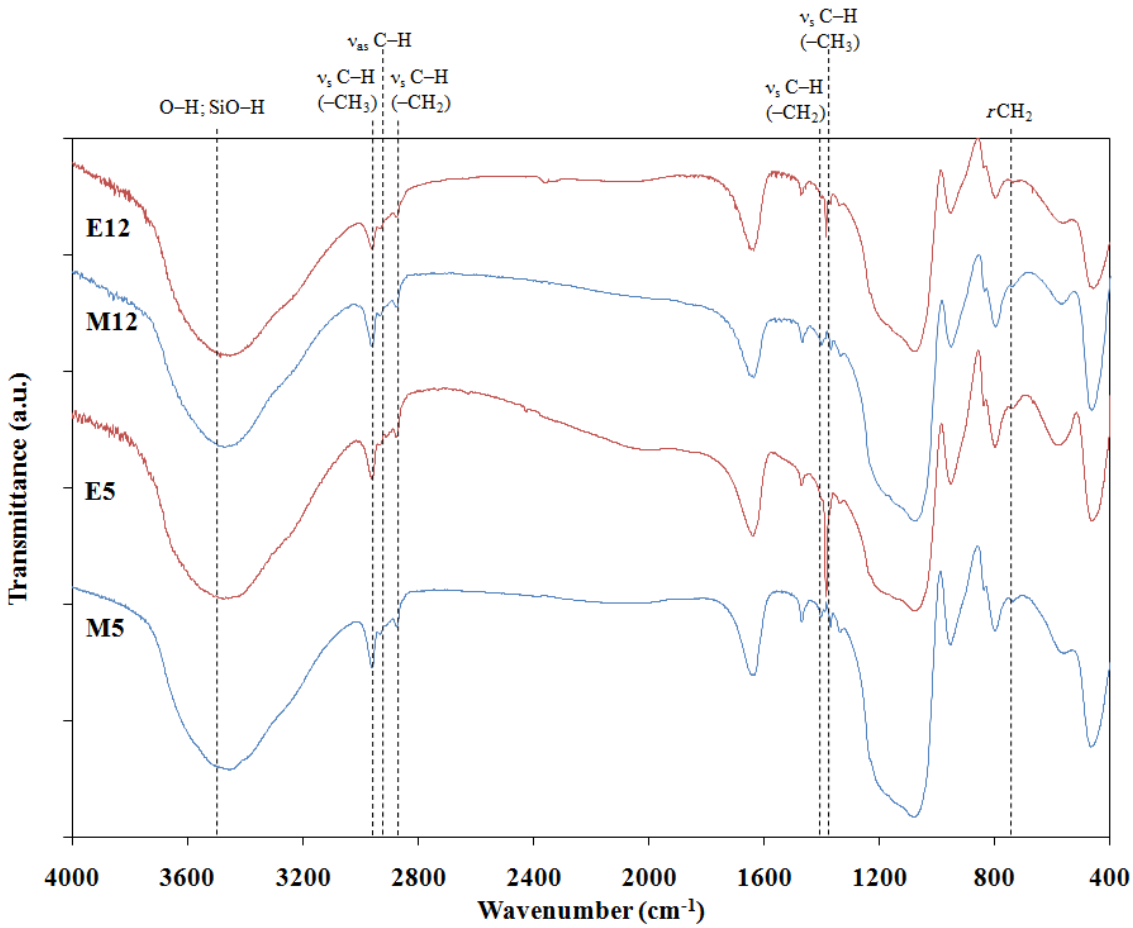

Fig. 3. 5. FTIR spectra of the iso-butyl-modified silica aerogels

3.2.6. Octyl aerogels

The octyl silicates FTIR spectra (Appendix A, Figure A.3) show very intense asymmetric and symmetric C–H stretching vibrations between 2930 and 2858 cm^{-1}. The existence of these intense bands (more intense for M6 and M13 than the others) is due to the large number of $-CH_2$ groups in the octyl-modified silica aerogels, showing their rocking vibrations at 723 cm^{-1}. The existence of these octyl-surface groups is coupled

with an increase of the hydrophobicity of the samples shown by the decrease of the intensities of the surface-adsorbed water at 3450 and 1635 cm^{-1}. These results revealed a difference in the hydrolysis and poly-condensation kinetics of the different silicon precursors. The hydrolysis rates of the OTMS and OTES are comparable to the one of the TMOS and thus the silica network is obtained by the poly-condensation of the hydrolyzed silicon entities. Thereafter, this led to a higher octyl-surface functionalization for M6 and M13 than for E6 and E13 where surface silanols and adsorbed water are shown to exist in abundance.

3.2.7. Vinyl aerogels

The vinyl-modified silica aerogels M7, E7, M14 and E14 show comparable FTIR spectra (Figure 3.6). Very weak peaks (shoulders) have been shown at 1605 cm^{-1} that are typical of C=C vibrations [232] and intense peaks appearing at 1413 cm^{-1} were easily assigned to the in-plane C–H deformation vibrations of the $=CH_2$ groups [232]. The out-of-plane $Si–CH=CH_2$ hydrogen deformation vibrations occur at around 540 cm^{-1} [227]. In spite of the similarities in the peaks' positions, the spectra did not show the same vibration band intensities for the various samples. M7 and M14 spectra show more intense peaks at 955 and 784 cm^{-1} than those of E7 and E14, while E7 and E14 spectra show better resolved peaks at around 1160 and 1078 cm^{-1} than M7 and M14. These results reveal the existence of more developed silica networks for the samples M7 and M14 than the others showing weak asymmetric stretching vibrations (LO mode). Furthermore, it was noticed the absence of any vibration band at 1384 cm^{-1} in the M7 aerogel spectra corresponding to residual alkoxy groups in the network. Therefore, the silicon precursors were thought to be totally hydrolyzed before undertaking the poly-

condensation. However, some remaining alkoxy groups exist for the three other aerogels showing vibration bands at this frequency with the M14 band being weaker than those appearing for E7 and E14.

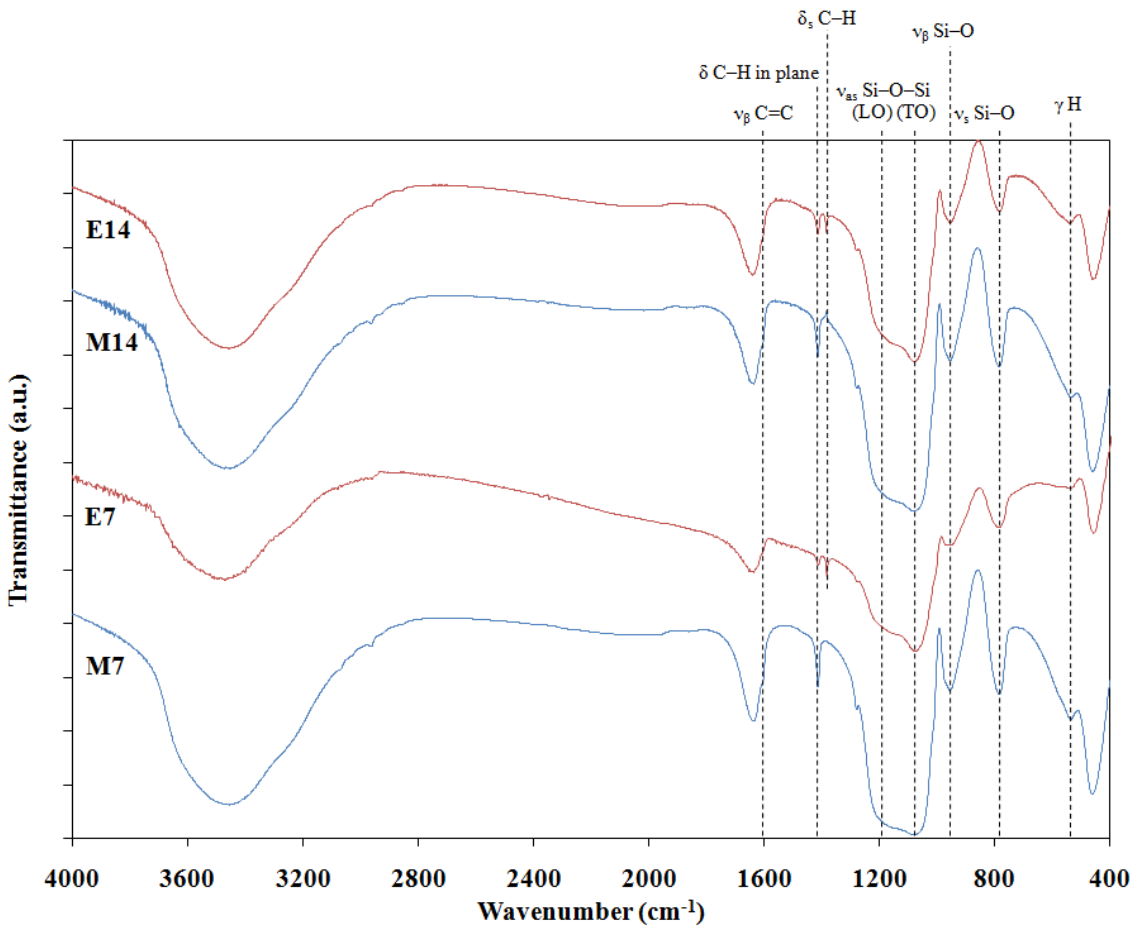

Fig. 3. 6. FTIR spectra of the vinyl-modified silica aerogels

3.2.8. Phenyl aerogels

The FTIR spectroscopy performed on the phenyl-modified silica aerogels showed weak peaks in the C–H symmetric and asymmetric stretching vibrations range except for the E8 sample that exhibits more intense peaks at these frequencies (Appendix A, Figure A.4). This could be attributed to some residual precursors. Weak

peaks appearing at 1596 cm^{-1} are assigned to the in-plane stretching vibrations of phenyl groups C=C bonds [232]. Moreover, the E8 and E15 spectra show weaker peaks than M8 and M15 at 1491 cm^{-1} corresponding to the combination of two vibrations: the phenyl C=C stretching and in-plane C–H deformation [226, 232]. These peaks are directly related to the intense peaks appearing at 1432 cm^{-1} assigned to the same vibrational combination. It is worth to note that the M8 exhibits an intense peak assigned to this vibration. The combination of these various vibrations as well as their intensities indicates that the silica networks of the samples synthesized starting from TMOS contain more phenyl-surface groups. The typical broad band corresponding to the asymmetric Si–O stretching vibrations is resolved into two separated peaks centered at 1137 and 1081 cm^{-1} with the samples E8 and E15 displaying better bands than the other two. The peaks appearing at around 700 cm^{-1} are assigned to the phenyl H out-of-plane ring deformation vibration [226], more intense for TMOS samples. On a similar basis, this asserts the conclusion about the existence of phenyl groups on the surface of the aerogels. In addition, the four spectra show peaks at 1000 cm^{-1} assigned to the symmetric phenyl groups C=C stretching vibrations [233].

3.3. Conclusion

Surface organo-modified silica aerogels were obtained from combinations of various silicon precursors and co-precursors, and dried under supercritical conditions. The synthesized sol–gel materials were successfully studied by FTIR spectroscopy that revealed the existence of different chemical groups corresponding to the silicon precursors and co-precursors that constituted the structure of the aerogels, as well as groups achieved after the reaction of the precursor's molecules with water in the

hydrolysis and with other precursors and co-precursors in the poly-condensation. Vibration bands at the same frequencies were found for similar aerogels, with some differences in their intensities. This dissimilarity is believed to be directly related to unequal concentrations of the corresponding chemical groups within the solid network due to variation in the hydrolysis rates of the used silicon precursors. Large ethoxy-based silicon precursors were found to undertake slow hydrolysis reactions leading to the formation of silica network where some alkoxy groups remain on the surface of the aerogels. This observation was not seen for methoxy-based aerogels showing more developed silica networks and significant alkyl-surface groups responsible of the hydrophobic character of the synthesized silica aerogels. Accordingly, the synthesized silica aerogels expected to have same silica networks were found to have comparable but not identical structures. Therefore, they will understandably have similar but not identical physical and chemical properties when used in various applications.

It is quite hard and even impossible to identify an unknown compound by solely using IR spectroscopy. This characterization technique is quick, relatively cheap, and useful for identifying certain functional groups in molecules resulting into unique IR spectra serving as a fingerprint for that compound. However, in order to be able to set these newly surface-modified silica aerogels into action in various applications, there is a greater aim of characterization to be thus studied and investigated. Therefore, to be able to employ these synthesized organo-modified silica aerogels, with such hydrophobic surface, as a host material for immobilizing the POMs, as suggested by the aim of the present work, hence a complete study of the effect of the silicon precursors and co-precursors on the surface chemistry of these silica aerogels should be investigated. In the next chapter, nitrogen adsorption/desorption experiments will be

discussed and analyzed as a further tool to characterize and study the surface chemistry of the different synthesized and FTIR-characterized silica aerogel materials.

CHAPTER FOUR

SURFACE CHARACTERIZATION

Surface chemistry is a rapidly developing area of particular significance to the newly developing nanotechnologies and material science orientations. Surface chemistry can be simply defined as the study of chemical reactions at the interfaces between states of matter [236]. Solid surfaces are particularly important in areas of industrial and economic emphasis, whereby heterogeneous catalysis has long been the pioneer in the world's industrial output of materials such as plastics and fertilizers [237].

4.1. Nitrogen sorption experiments

4.1.1. Overview

Much effort has been dedicated to studies in this field which all started by the work of Sabatier on hydrogenating organic compounds in 1912 and by the Haber process for the synthesis of ammonia in 1918 [238]. After roughly two decades from then, Langmuir, with his many advancements and investigations in surface chemistry, has managed to develop an equation as a model for monolayer adsorption [238]. Moreover, Brunauer, Emmett, and Teller [239] were capable of generalizing Langmuir's theory to multimolecular adsorption and have identified the BET method which is the most widely used procedure for the determination of the surface area of solid materials. Since then, the field has immensely flourished and attracted many devoted scientists. The most recent development is the work of the Nobel Prize laureate in Chemistry 2007, Gerhard Ertl [240], who received this prize for his thorough

investigation of the gas-solid interface, specifically the interaction between carbon monoxide molecules and platinum surfaces.

A great amount of work is usually carried out towards transferring the reaction of a newly developed homogeneous catalytic process onto a suitable surface in order to achieve the utmost gain from such highly advantageous surface reactions [237]. As scientists and investigators, we should be ready to make the most of every similar opportunity that might arise. Such is the aim of this thesis project in attempting to transfer the homogeneous reaction of the anthracene oxidation catalyzed by POMs onto a highly mesoporous silica aerogel surface. The work of heterogeneous catalysis is done so that to take advantage of the increased porosity and relatively high specific surface area of these surfaces, in the aim of achieving better catalytic activity and selectivity. Therefore, the surface of these silica materials need to be studied and analyzed, and thus will be explored in the following sections.

Numerous experimental techniques are available for the surface and pore size characterization of porous materials. Among these, it is worth to highlight the importance of small angle x-ray and neutron scattering, mercury porosimetry, scanning and transmission electron microscopy, nuclear magnetic experiments, and others involving diffraction or scanning tunneling microscopy [241]. However, nitrogen adsorption has emerged as the most popular method used to identify surface properties because it is quite feasible compared to other methods, and it also encompasses the evaluation of a wide range of pore sizes, from micropores to macropores and the mesopores in between [88]. Liquid nitrogen adsorption is thought of as the interaction taking place between the adsorbate, the adsorbing molecule, and a substrate (adsorbent), the surface, at the adsorbate-solid interface [236].

4.1.2. Theory

When an atom or a molecule hits a surface, this would result into several possible outcomes of which are elastic scattering, inelastic scattering, and the retention of the molecule on the surface [237]. In studying surface chemistry, the last outcome is thus of greater importance and interest. Two types of interactions that hence can occur are the physical adsorption (physisorption) by the van-der-Waals forces of interaction or a much stronger interaction resulting into some chemical bonding (chemisorption) between the adsorbate and the adsorbent [236].

Achieving an understanding of the surface area and porosity of an adsorbent, accomplished by constructing an adsorption-desorption profile as the adsorbate pressure changes [236]. In other words, an adsorption isotherm is the amount of adsorbate adsorbed, in terms of coverage or uptake, over a broad range of relative pressures, at constant temperature [88]. Adsorption/desorption profiles are regrouped into one of the six types shown in Figure 4.1 (Left), in which the measurements of these isotherms could be conducted with the help of gravimetric or volumetric techniques. As a result of that, types I and II are of considerable interest to studies of surface chemistry. It is worth noting that, desorption isotherms are consequently acquired in the same way by the measurement of the amount of gas removed while decreasing the adsorbate pressure [88, 236, 237].

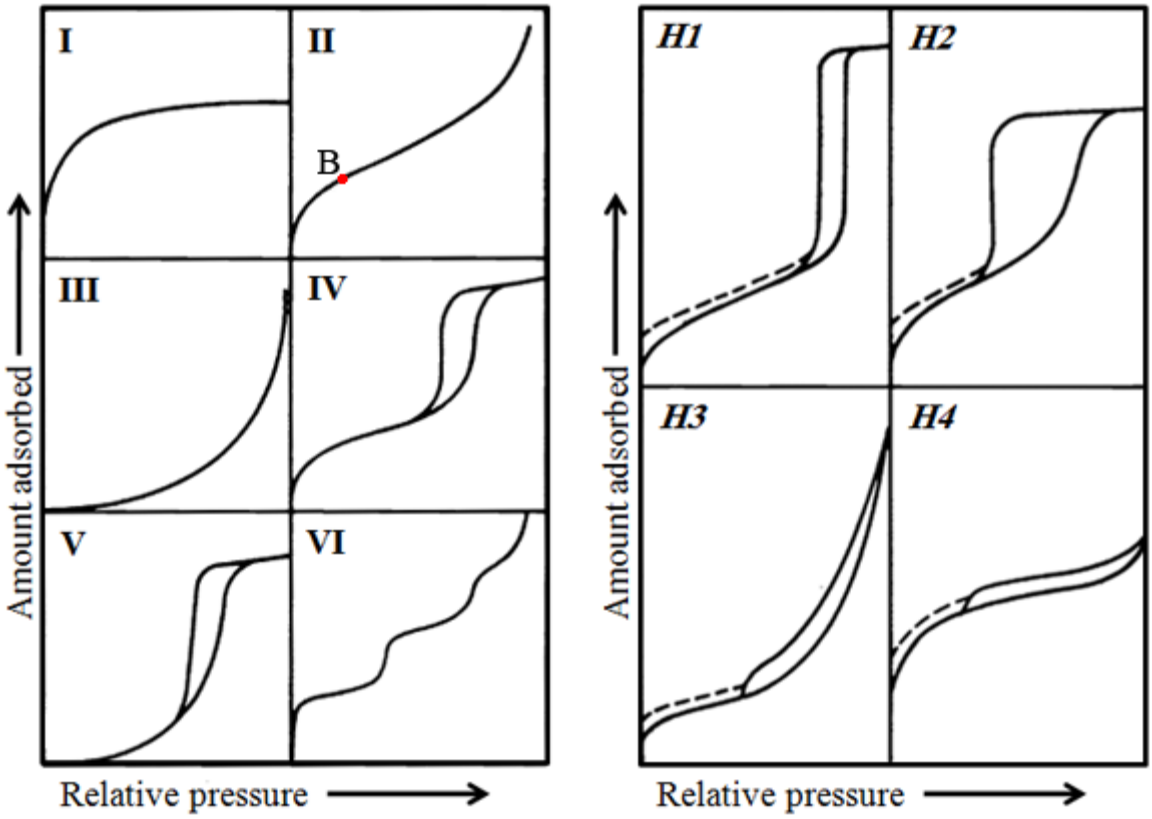

Fig. 4. 1. Types of physisorption isotherms (Left), Types of hysteresis loops (Right); modified from Ref. [88]

Chemisorption is ideally described by isotherms of type I (Langmuir), whereby the amount adsorbed increases until it results into a plateau as P/P_0 approaches 1 when the surface becomes saturated with adsorbate and thus absorption ceases. Such isotherms govern the behavior at interfaces of microporous solids with relatively small external surfaces such as activated carbons, molecular sieve zeolites, and certain porous oxides. Therefore, the gas uptake is clearly limited by the accessible micropore volume rather than by the internal surface area [88].

Physisorption on the other hand is usually associated with isotherms of type II (BET), whereby there is a further increase in the amount adsorbed beyond the monolayer plateau when many layers are ultimately adsorbed [239]. The point at which the monolayer coverage is complete and the multilayer adsorption begins to take place

is indicated by the inflection point B [88]. Such isotherms often govern the behavior at interfaces of non-porous or macroporous adsorbents [236].

Type III sorption isotherms are associated with multilayer formation from the start, and thus do not exhibit any inflection point and remains convex to the relative pressure axis all over. This is a direct indication of weaker adsorbate-adsorbent interactions and more pronounced adsorbate-adsorbate interactions [88]. Such isotherms are quite rare, and only govern some systems such as the adsorption of nitrogen on polyethylene or water vapor on graphite [236].

Type IV isotherm is of considerable interest in the study of real catalysts as it implies a hysteresis loop which is indicative of an increase in pressure to a certain level resulting in different coverage when compared to the coverage formed while decreasing the pressure [88]. The initial part is similar to that in type II and is thus attributed to a monolayer-multilayer adsorption. This behavior is associated with the occurrence of evaporation and capillary condensation in pores similar to those commonly found in catalysts [236]. Such isotherms govern the behavior at interfaces of many mesoporous industrial adsorbents. Therefore, the shape of the hysteresis can often indicate the size and type of pore in the catalyst itself [237].

Type V isotherms show pore condensation and hysteresis indicative of pores in the mesoporous range. Additionally, they experience weak adsorbate-adsorbent interactions such as those of type III, however are relatively uncommon. Type VI isotherms are however a special case describing a multilayer adsorption on a uniform non-porous surface by a non-polar adsorbate, whereby the steps depend on the system and temperature [236]. The height of these steps is therefore indicative of the monolayer

capacity for each adsorbed layer. Some examples of this last type are the adsorption of argon or krypton on graphitized carbons at liquid nitrogen temperature [88].

It is widely accepted that there is a correlation between the shape of the hysteresis loop and the texture of a mesoporous adsorbent, which is its pore size distribution, geometry, and connectivity [236]. An empirical classification of hysteresis loops was given by IUPAC based on de Boer's earlier classification as presented in Figure 4.1 (Right) [88]. According to this classification, type *H1* is attributed to cylindrical pores; type *H2* loop is associated with pores of narrow necks and wide bodies or "ink-bottle" pores; type *H3* is attributed to slit-shaped pores; and type *H4* hysteresis is produced by wedge-shaped pores with a shade of similarity to the slit-shaped pores, but in this case having a slight microporosity character [88].

Characteristically, the hysteresis loops in all isotherms close before reaching a certain relative pressure in the desorption process except when microporosity is present. The closure point occurs at a relative pressure that which is almost independent of the nature of the porous adsorbent but mainly depends on the nature of the adsorbate; for example, $P/P_0 \approx 0.42$ for nitrogen at its boiling point (77K) and $P/P_0 \approx 0.28$ for benzene at 298K [88, 242].

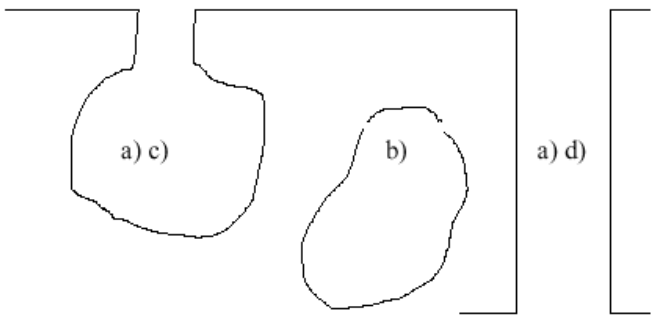

Fig. 4. 2. Pore types a) open pore b) closed pore c) ink-bottle pore d) cylindrical, open-ended pore; taken from Ref. [243]

The Langmuir isotherm is limited to the adsorption of one monolayer of adsorbate. In a system where the heat of evaporation of the adsorbate is much smaller than the heat of adsorption, then adsorption could take place at temperatures well above the boiling point of the adsorbate thus limiting any further formation of layers [237]. However, if both heats are similar, a very low temperature would be sufficient to produce enough adsorption for the coverage of the first layer, would facilitate the formation of further layers above it [237]. Several isotherms are largely based on the Langmuir theory, all of which have been developed to take into account the limitations of the Langmuir model [88]. The formation of multilayers is thus modeled by the BET isotherm which essentially uses the basis of Langmuir's theory and extends it to encompass further physisorption of multilayers [239].

The BET equation is usually applied in the linear form:

$$\frac{1}{W\left(\left(P_o / P\right)-1\right)} = \frac{1}{W_m C} + \frac{C-1}{W_m C}\left(\frac{P}{P_0}\right)$$

Equation 4. 1

in which W is the weight of gas adsorbed at a relative pressure P/P_0, and W_m is the weight of adsorbate constituting a monolayer of surface coverage. The term C is the BET constant related to the energy of adsorption in the first adsorbed layer; consequently its value is an indication of the magnitude of the adsorbent/adsorbate interactions [242].

The BET equation requires a linear plot of $1/[W((P_0/P)-1)]$ versus P/P_0 which for most solids, using nitrogen as the adsorbate, is restricted to a limited region of the adsorption isotherm, usually in the P/P_0 range of 0.05–0.30 [88]. This region is shifted

to lower relative pressures for microporous materials. Typical BET plots of the silica aerogel materials synthesized are shown in Appendix B. The specific surface area S of the solid can be calculated from the total surface area S_t and the sample weight w, according to the following equations:

$$S = \frac{S_t}{w}; \quad S_t = \frac{W_m \quad N \quad A_{cs}}{M}; \quad W_m = \frac{1}{s+i}$$

Equation 4. 2

whereby N is the Avogadro number (6.023×10^{23} molecules.mol^{-1}), A_{cs} is the molecular cross-sectional area of the adsorbate (for nitrogen = 16.2 Å^2), M is the molecular weight of the adsorbate, and s and i are respectively the slope and intercept of the BET plot [242].

The method to calculate the pore size distribution has been manifested by Barett, Joyner, and Halenda (BJH) in a complex numerical integration method making use of all the data from either the adsorption of desorption isotherms. The desorption curve however is usually employed except in cases where pore blocking would affect the desorption from taking place normally. There are many schemes that have been suggested based upon some assumptions regarding pore shape [236]. Among these different approaches, the BJH method can be considered the most popular for mesopores size analysis and will be employed in the current investigation. If the sorption isotherm exhibits a distinct plateau as in the case of type IV and V isotherms, then the total specific pore volume (by gram of material) would be defined as the liquid volume at a certain P/P_0, usually at P/P_0=0.95 or higher closer to 1 in such a way it is always located after the pore condensation step. The pore volume would be: $V_p=W_a/\rho_l$, where W_a is the adsorbed amount in grams and ρ_l is the liquid density of the volume

adsorbed at saturation. The average pore radius $\bar{r}_p$ would thus be calculated from the ratio of the total pore volume and the BET surface area from the following equation: $\bar{r}_p = 2V_p/S$ [236].

The porosity of powders and other porous solids can be conveniently characterized by gas adsorption studies as explained in details previously. Two common techniques for describing porosity are the determination of total pore volume and pore size distribution. Nitrogen at 77 K is the most suitable adsorbate for the evaluation of the porosity of most solid materials [242]. Making use of all these extensively clarified and exemplified powerful tools would enable the easy elucidation and surface study and characterization of the silica aerogels. This was obtained by determining their specific surface area, total pore volume, porosity structure, and pore size distribution. Interpretation and discussion of the nitrogen sorption experiments conducted for the silica materials will follow in the coming sections.

4.1.3. Sample preparation and characterization

The adsorption isotherm is obtained point-by-point on a NOVA 2200 Quantachrome surface area analyzer (Figure 4.3) by admitting to the adsorbent successive known volumes of nitrogen and measuring the equilibrium pressure [242]. Before any prior use of the instrument, the calibration of the manifold and the cell where the sample is introduced, need to be done to ensure good reproducible results. The sample cell chosen for the analysis in this project is the 9 mm step diameter with the larger bulb (Figure 4.3) in order to prevent elutriation, or loss of powder out of the sample cell, caused by a rapid gas flow out of the cell [242]. It is especially problematic

for low-density samples, which is the case for our samples of very low density silica aerogels.

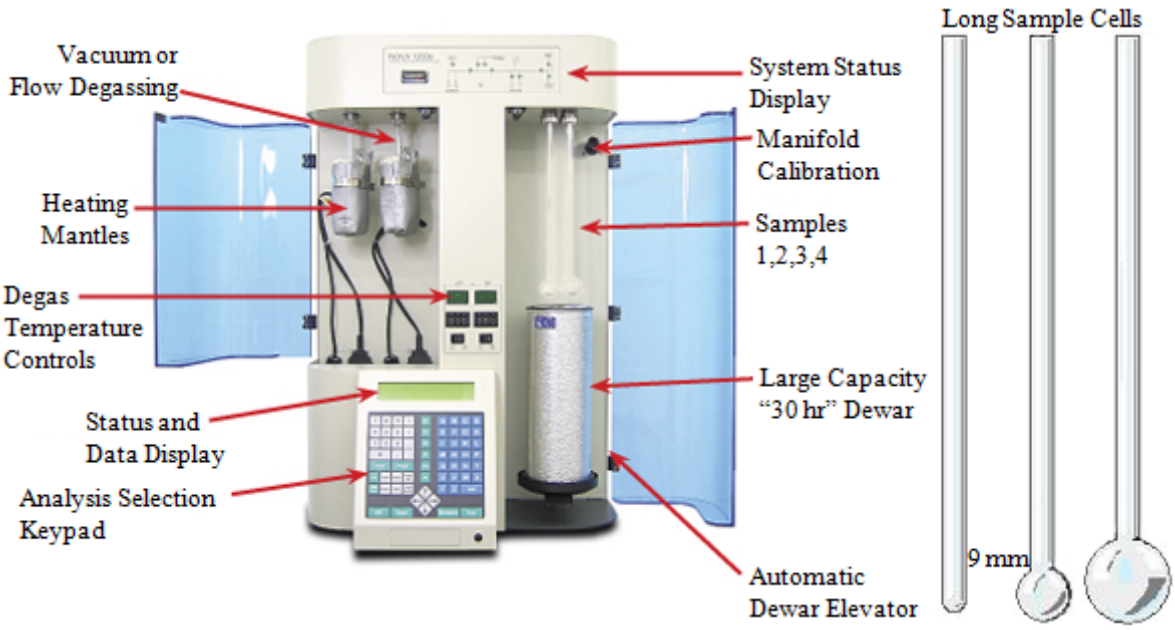

Fig. 4. 3. NOVA 2200 Quantachrome surface area analyzer, Long Sample Cells; modified from Ref. [242]

In order to run a complete nitrogen adsorption/desorption experiment, approximately 100 mg of the aerogel powder was introduced in a sample cell. The sample was degassed for 2 hours at 120°C. The temperature has to be sufficiently high but not too high to avoid any structural change of the sample, since too high temperatures can cause irreversible damage to the sample and result in a decrease in surface area due to sintering, or an increase in surface area due to a thermally induced decomposition. The degassing time has to be enough to completely remove unwanted vapors and gases adsorbed on the sample surface. The conditions are chosen in this way after conducting a series of tests to optimize the conditions of temperature and time that would yield reproducible data. After unloading the degasser, the cell is removed and

reweighed to obtain dry, outgassed sample weight w, which is used in calculating the specific surface area, since some powder could be inevitably lost by elutriation [242].

Data points are then selected by relative pressure (P/P_0) on the NOVAWin2 software. Once the measurements are completed, NOVAWin2 offers a powerful data analysis and archiving platform that are used to construct graphical plots and tables of isotherms, pore size distributions, and information of specific surface area and porosity [242].

4.2. Results and discussion

The nitrogen adsorption/desorption experiments of the synthesized silica aerogels conducted at 77 K have resulted into sorption profiles and pore size distributions, in addition to valuable information such as specific surface area, total pore volume, volume of mesoporosity and microporosity, and average pore radius. Some of the obtained adsorption-desorption isotherms and pore size distributions are included in this section, which are color-coded into those prepared with TMOS shown in blue and those prepared with TEOS shown in red, while the rest are shown in Appendix B. Besides, a complete comparative list of the specific surface areas, pore volumes and radii are regrouped in Table 4.1.

4.2.1. TMOS and TEOS aerogels

The nitrogen adsorption/desorption experiments conducted for the M1 and E1 silica aerogels, obtained from TMOS and TEOS respectively, have resulted into comparable profiles where isotherms of type IV are observed for both samples revealing a mesoporous nature of these aerogels (Figure 4.4). The adsorption process exhibit also

for the two aerogels adsorption hysteresis of type H2 as the adsorption and desorption curves do not coincide. As mentioned earlier, these H2 loops are associated with "ink-bottle" pores with the E1 showing a broader desorption plateau that might be due to larger body/neck ratio than for the M1 aerogel where less capillary condensation takes place. Calculations of the specific surface area according to the BET model revealed comparable values for both samples. Such a result was expected as the two isotherms show very similar behavior at low partial pressures ($P/P_0 < 0.5$). Calculated values were 574 and 545 $m^2.g^{-1}$ for M1 and E1, respectively. Derived pore volumes from the highest relative pressure are 1.31 $cm^3.g^{-1}$ for M1, of which 89% (1.16 $cm^3.g^{-1}$) is the total volume of mesopores and 11% that of micropores. Doing the same calculation for E1 revealed a pore volume equal to 0.94 $cm^3.g^{-1}$ with 0.82 $cm^3.g^{-1}$ (87%) that of mesopores. While comparing these values, we can see that the M1 has larger surface area and pore volume than the corresponding TEOS aerogel with a similar distribution of meso- and micro-porosity. The pore size distribution derived from the BJH theory revealed a difference between the two samples with the M1 having larger pore diameters than E1. The pore diameter maxima are 73 and 46 Å for M1 and E1, respectively. The calculation of the average pore radius $\bar{r}_p$ revealed values equal to 46 and 35 Å for M1 and E1, respectively. The difference between these latter values and those calculated from the desorption curve (BJH) is due to the fact that micro- and mesopores are considered in the average pore radius calculation, not only mesopores for BJH.

Regrouping all the calculated data from the adsorption-desorption isotherms as well as what was derived from the BJH model, we can conclude that the synthesis of silica aerogels from TMOS (M1) can lead to materials exhibiting higher surface area, pore volume and pore diameters than those prepared from TEOS (E1). These aerogels

did not show a noticeable difference in their structural characterization (FTIR spectroscopy), however an evident difference in their surface properties was noted. These differences are attributed to unequal hydrolysis and poly-condensation reaction rates affecting directly the network formation and therefore the surface physic-chemical properties.

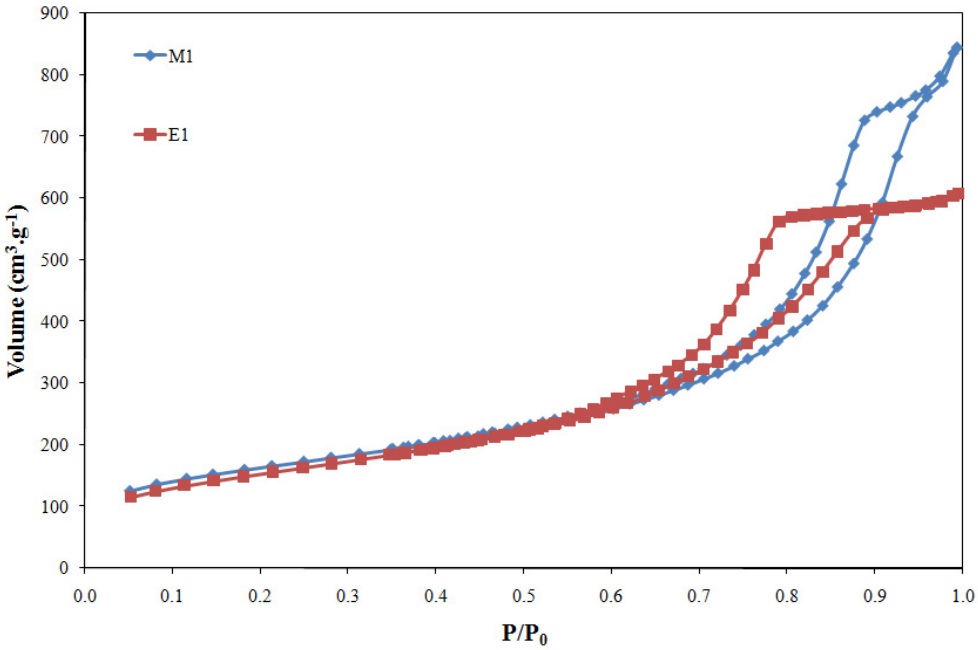

Fig. 4. 4. Nitrogen adsorption/desorption isotherms of the silica aerogels from TMOS and TEOS

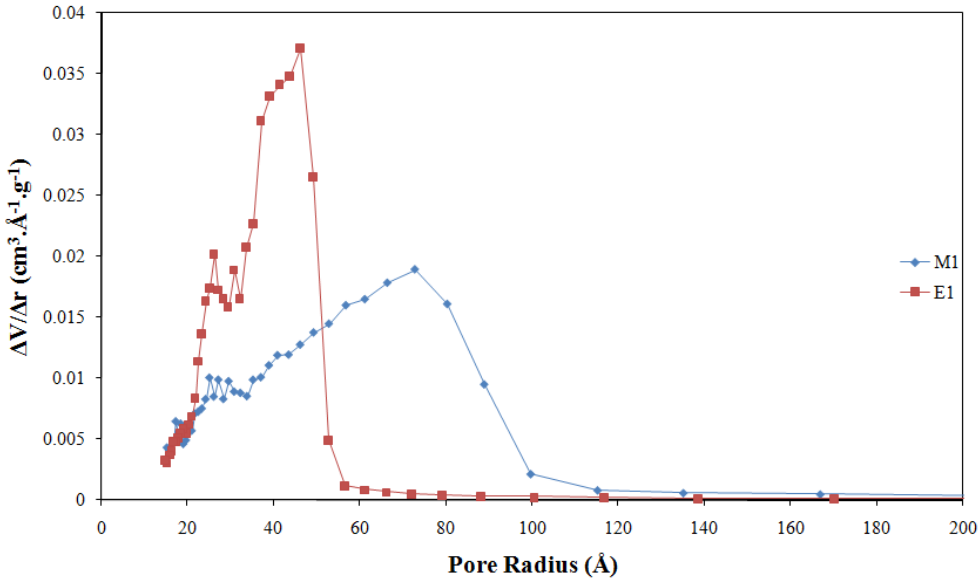

Fig. 4. 5. Pore size distribution of the silica aerogels from TMOS and TEOS

4.2.2. Methyl aerogels

The nitrogen sorption experiments performed for the methyl-functionalized silica aerogels (M2, E2, M9 and E9) resulted into different specific surface area values calculated from the nitrogen adsorption curve for P/P_0 ranging between 0.05 and 0.30. These areas are 598, 649, 693, and 599 $m^2.g^{-1}$ for M2, E2, M9 and E9, respectively. Comparing these values to those obtained for M1 and E1, we can easily see that the methyl-functionalized silica aerogels show constantly greater surface areas than unfunctionalized aerogels regardless of the precursors' nature. The isotherms shown in figure 4.6 revealed a mesoporous nature for the four aerogels due to the existence of the hysteresis loop being of type IV. We can clearly notice the capacity of E2 and M9 to adsorb a larger volume of liquid nitrogen than the two other aerogels, which reflects larger pore volumes and hence more mesoporosity. Among these aerogels, the largest pore volume was found for the sample revealing the largest surface area (M9) and found

to be equal to 1.24 $cm^3.g^{-1}$ of which 82% are due to the existence of mesopores. The total pore volume for E2 is 0.92 $cm^3.g^{-1}$ (74% mesopores), for E9 0.62 $cm^3.g^{-1}$ (48% mesopores), and for M2 0.55 $cm^3.g^{-1}$ (36 % mesopores). Existing microporosity is due to the existence of some organic groups (methyl, methoxy or ethoxy groups) on the surface of the pores that will occupy a certain volume and therefore reduce the accessible cavity by the nitrogen molecules.

While comparing the SSA values and their relations with the total pore volumes and those of mesopores, we can clearly notice that the decrease of the SSA is coupled with a decrease of the pore volume and the percentage of volume due to the mesoporosity. The same trend was also seen for the average pore radius $\bar{r}_p$ equal to 36, 28, 21, and 18 Å for M9, E2, E9 and M2, respectively. The pore size distribution derived from the BJH model (Figure 4.7) revealed comparable profiles with the mesoporosity being expressed clearly for the E2 and M9 aerogels with maxima around 50-60 Å.

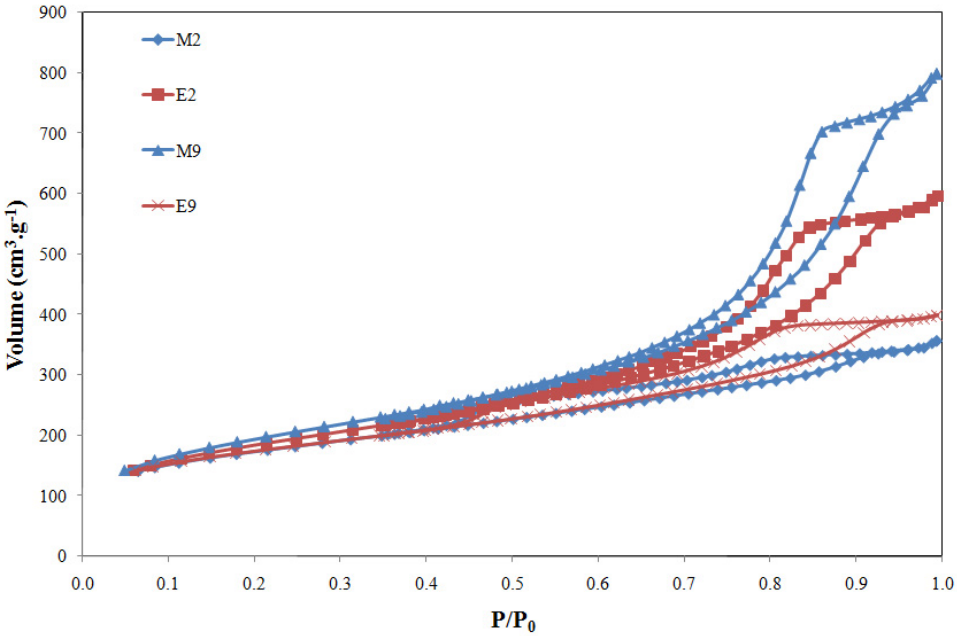

Fig. 4. 6. Nitrogen adsorption/desorption isotherms of the methyl-modified silica aerogels

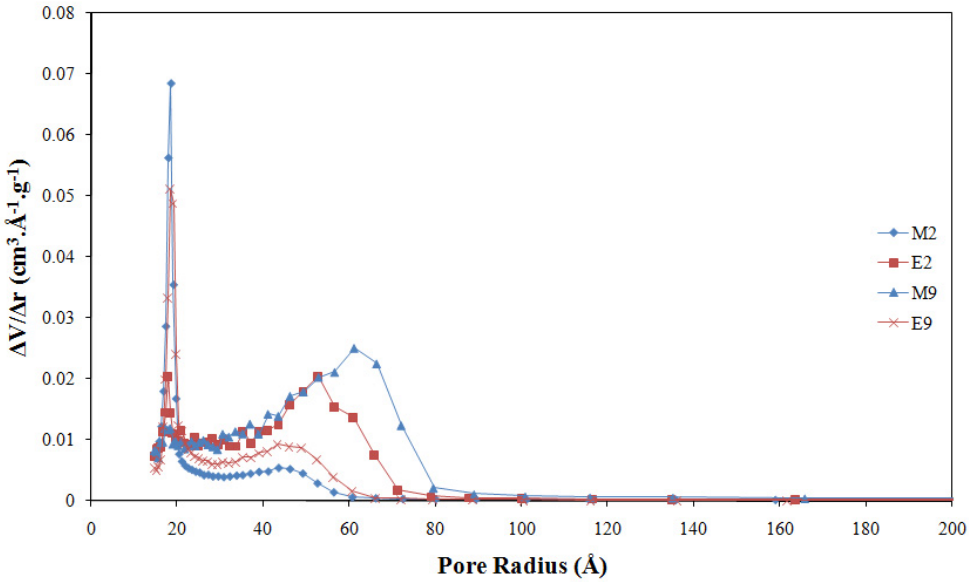

Fig. 4. 7. Pore size distribution of the methyl-modified silica aerogels

4.2.3. Ethyl aerogels

Ethyl-functionalized silica aerogels synthesized from ethyltrialkoxysilanes in addition to TMOS and TEOS have resulted into materials of specific surface area equal to 730, 598, 779, and 635 $m^2.g^{-1}$ for M3, E3, M10, and E10, respectively. The adsorption-desorption type IV isotherms revealed H2 hysteresis reflecting the existence of mesopores within the gels networks. However, the total and mesopores pore volumes disclosed the exact distribution of the aerogels pores. M3 has a total pore volume equal to 0.86 cm^3 g^{-1} of which 62% are due to mesopores; E3 has a V_p equal to 0.65 cm^3 g^{-1} of which 57% are mesopores; M10: 1.38 cm^3 g^{-1} with 81% are due to mesopores; E10 has 0.66 cm^3 g^{-1} of which 53% are due to mesopores. As mentioned earlier, the microporosity is due to organic surface groups. The pore size distributions bare the pore natures where the distribution for E3 and E10 are very similar with close maxima (35 and 41 Å) with no pores larger than 60 Å. In the other hand, M3 does not show a clear maximum while M10 has a maximum around 72 Å with all the pres being smaller than 100 Å. Although the FTIR spectroscopy did not find a remarkable difference in the structure of these aerogels, surface measurement techniques such as nitrogen adsorption show eminent differences in the surface area and porosity of these materials. Such a difference is attributed mainly to non-identical reactions at the precursor's level as well as the cluster's one.

4.2.4. Propyl aerogels

The adsorption-desorption isotherms (Appendix B, Figure B.3) of the propyl-modified silica aerogels show type IV isotherms with H2 hysteresis for M4, M11 and E11 revealing "ink-bottle" shaped pores, while that of E4 is of type H4 corresponding to

wedge-shaped pores. The loop of the isotherm of E4 displays an increased microporosity character compared to the other samples where the microporous pore volume corresponds to 80% of the total pore volume of this aerogel (V_p= 0.40 $cm^3.g^{-1}$). The specific surface area equal to 727, 526, 549, and 568 $m^2.g^{-1}$ for M4, E4, M11, and E11, respectively. The total pore volumes for these aerogels were 0.97 $cm^3.g^{-1}$ (mesoporosity 68%), 0.40 $cm^3.g^{-1}$ (mesoporosity 20%), 0.64 $cm^3.g^{-1}$ (mesoporosity 61%), 0.79 $cm^3.g^{-1}$ (mesoporosity 77%), respectively. The pore diameter maxima are in the 40-45 Å range except for the E4 that has more micropores than mesopores and where the BJH method cannot give precise values.

4.2.5. Isobutyl aerogels

Besides the mesoporosity nature which has been proved to be the case for all the silica aerogel materials analyzed thus far, the samples E5 and M12 clearly have an increased microporosity character due to the type H4 looped isotherms (Figure 4.8), and as a result of that the wedge-shaped pores that they have. However, M5 and E12 have a richer mesoporosity character reflected by a pore size distribution in the mesoporous range, with the E12 having a clear maximum at around 35 Å (Figure 4.9). Calculated specific surface area for these isobutyl-modified silica aerogels were found 333, 463, 569, and 589 $m^2.g^{-1}$ for M5, E5, M12, and E12, respectively. Their pore volume values are respectively 0.47 $cm^3.g^{-1}$ (68% are mesopores), 0.44 $cm^3.g^{-1}$ (43% are mesopores), 0.53 $cm^3.g^{-1}$ (36% are mesopores), and 0.79 $cm^3.g^{-1}$ (76% are mesopores). Calculating the average pore radius showed 28 and 27 Å for M5 and E12, and 19 Å for both E5 and M12. Once again the surface measurements done were not conclusive about the behavior of the precursors during the synthesis (hydrolysis and poly-condensation) and

as it is known by now, the shape and nature of these pores is hugely affected by the way the silica network is formed. Hence, a certain tendency can be depicted where these aerogels exhibit, in general, lower pore volumes and average pore sizes than the previous ones whose surfaces were functionalized with smaller organic groups that occupy smaller volumes.

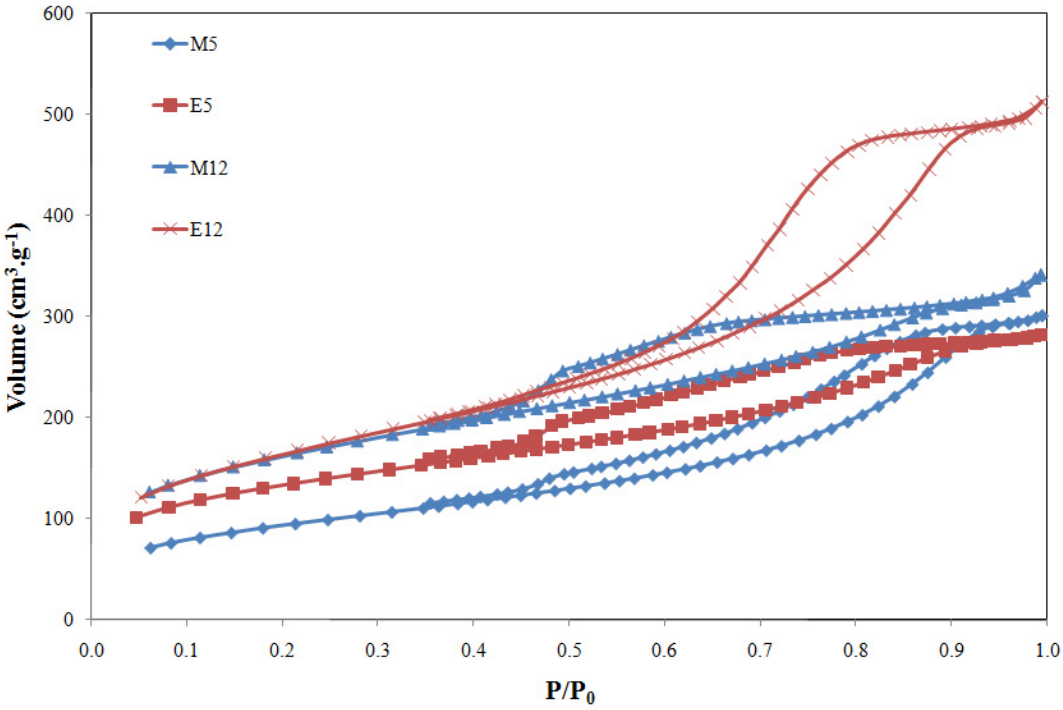

Fig. 4. 8. Nitrogen adsorption/desorption isotherms of the iso-butyl-modified silica aerogels

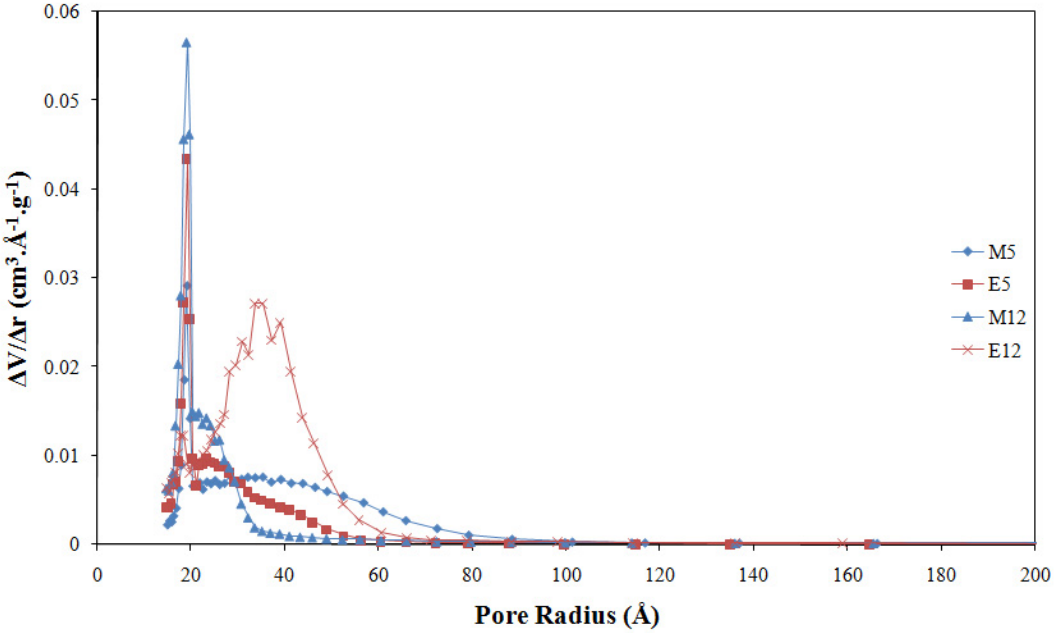

Fig. 4. 9. Pore size distribution of the iso-butyl-modified silica aerogels

4.2.6. Octyl aerogels

The nitrogen adsorption-desorption isotherms recorded for octyl-modified silica aerogels are quite distinctive from those recorded for the previous samples as they show different isotherm types depending on the silicon precursors used in their synthesis. While M6 and E6 show type I isotherms specific of microporous materials, M13 and E13 reveal type IV isotherms corresponding to mesoporous materials (Appenix B, Figure B.5). The hysteresis loops seen for these two latter samples are also different as M13 is showing a H1 type hysteresis attributed to cylindrical pores while E13 bares a H3 type attributed to wedge-shaped pores. The shapes of these aerogels pores are probably due to the octyl surface groups that, due to their lengths, will be arranged within the network in lamellar geometries than can be seen to a certain extent. This arrangement will create pores having perfect cylindrical shapes (M13) or wedge-

shaped pores that can be considered as derived from cylindrical pores after some disturbance. Calculated SSA for M13 and E13 are 225 and 388 $m^2.g^{-1}$ and V_p 0.61 $cm^3.g^{-1}$ (82% are mesopores) and 1.57 $cm^3.g^{-1}$ (92% are mesopores), respectively. These values reflect low SSA, however the mesoporosity of these aerogels is high because of the rearrangement of the octyl groups within the pores. An accent should be drawn to the very high pore volume of the E13 aerogel where cylindrical pores are depicted, and whose pore size distribution presents a maximum at 22 nm, however the average pore radii considering the totality of the pores are 54 and 81 Å for M13 and E13, respectively.

On the other hand, M6 and E6 isotherms present very low adsorption-desorption profiles and very low specific surface areas, as low as 6 and 4 $m^2.g^{-1}$ with essentially no calculated pore volume. Therefore, these materials are considered non-porous. This behavior might be due to the existence of the common precursor to these aerogels, the OTMS, which seems not be hydrolyzed during the process and thus condense within the pores of the silica network of the TMOS and TEOS. The pores would thus be completely closed by these bulky compounds like a knot, and thus the materials present only little or no porosity and hence very low specific surface area. Hence, the use of OTMS is not a good choice in the synthesis of octyl-modified silica aerogels.

4.2.7. Vinyl aerogels

The vinyl-modified silica aerogels show very similar nitrogen adsorption-desorption isotherms of type IV along with hysteresis type H2, and comparable pore size distributions with maxima in the 50-70 Å range, with no pores larger than 90 Å

(Figures 4.10 and 4.11). Calculated specific surface areas were found to be relatively high and are 673, 726, 633, and 645 $m^2.g^{-1}$ for M7, E7, M14 and E14, respectively. Comparing the porosity of these aerogels, we noticed large pores with values being 1.13 $cm^3.g^{-1}$ (81% are mesopores) for M7, 0.92 $cm^3.g^{-1}$ (62% are mesopores) for E7, 0.84 $cm^3.g^{-1}$ (67% are mesopores) for M14, 1.06 $cm^3.g^{-1}$ (78% are mesopores) for E14. The average pore radii derived from the specific surface area and the pore volume reflect also the high porosity with values being 34, 25, 27, and 33 Å for M7, E7, M14 and E14, respectively. The high porosity of these aerogels is due to the small size of the vinyl groups existing on the surface of the materials as verified by FTIR spectroscopy, contributing to the functionalization of the aerogels surface without affecting much their pore volumes.

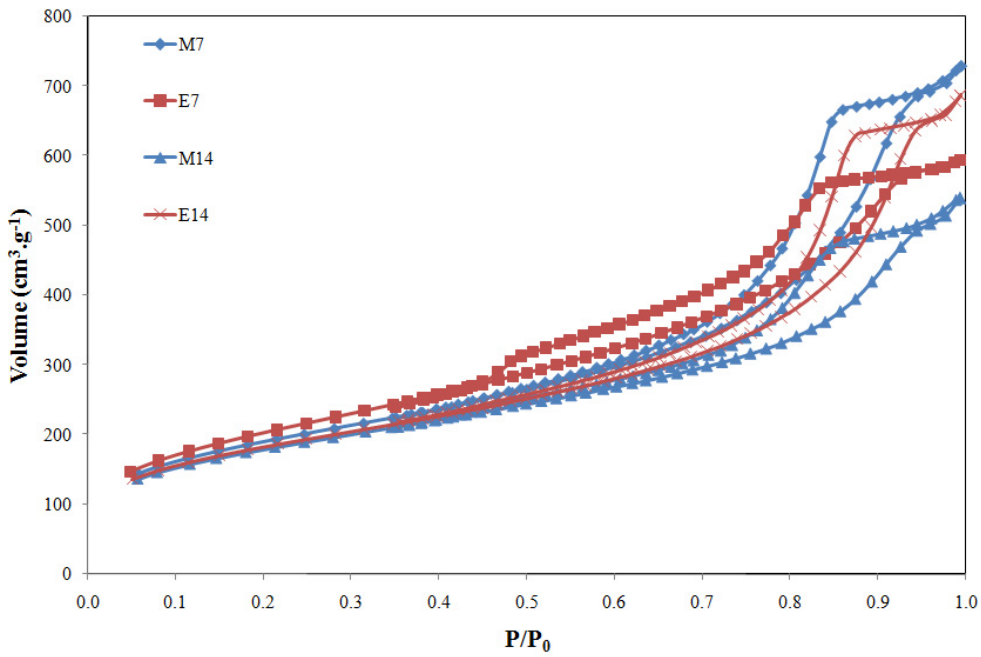

Fig. 4. 10. Nitrogen adsorption/desorption isotherms of the vinyl-modified silica aerogels

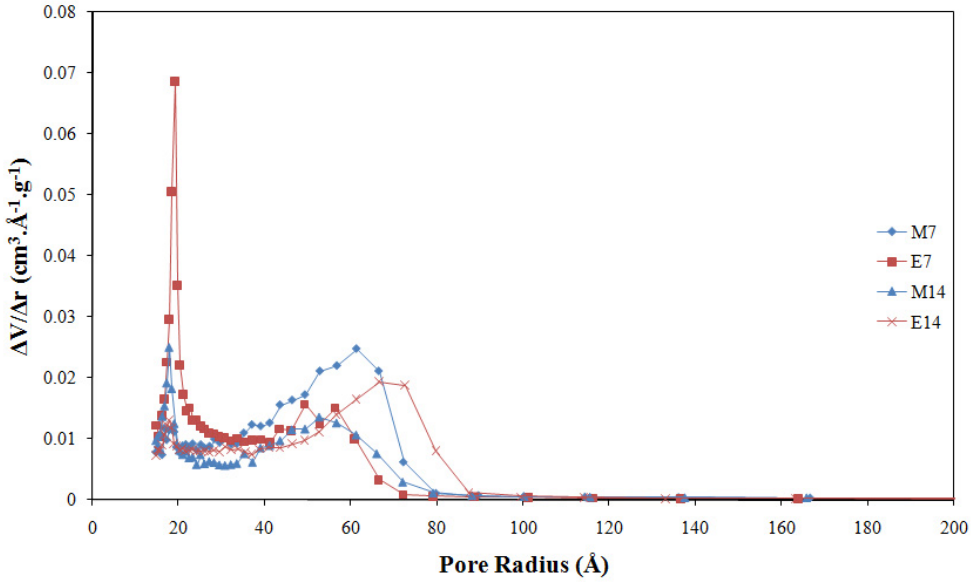

Fig. 4. 11. Pore size distribution of the vinyl-modified silica aerogels

4.2.8. Phenyl aerogels

The nitrogen isotherms obtained for the phenyl-modified silica aerogels (Appendix B, Figure B.7) have a strictly type IV isotherms with a clear type H2 hysteresis, thus the materials are easily identified as mesoporous materials with ink-bottle pores which are very comparable. The pore size distribution (Appendix B, Figure B.8) for these silica aerogels shows an evident distribution in the mesoporous range (61-72 Å) with the majority of the pores being smaller than 10 nm, except for M15 where some pores are in the 10-15 nm range. The specific surface area calculated for these aerogels and found 616, 517, 553, and 685 $m^2.g^{-1}$ for M8, E8, M15 and E15, respectively. Their pore volume values are respectively 1.12 $cm^3.g^{-1}$ (80% are mesopores), 0.88 $cm^3.g^{-1}$ (80% are mesopores), 0.88 $cm^3.g^{-1}$ (75% are mesopores), and 1.22 $cm^3.g^{-1}$ (84% are mesopores). Calculated average pore radii are very similar with

values equal to 36, 34, 32 and 36 Å for M8, E8, M15, and E15, respectively. The similarity in the pore radii is correlated with the similarity in the total pore volumes and specifically the percentage of mesopores.

4.3. Conclusion

As a summary of all the results obtained and discussed in previous sections, the results of specific surface areas, pore volumes and radii, in addition to percentage of mesoporosity are regrouped in a comparative way in Table 4.1.

Mesoporous surface organo-modified silica aerogels were successfully obtained with considerably high surface areas and high total pore volumes, the majority of which is mesoporous. Therefore, conducting the synthesis for obtaining these aerogels have resulted into material of high surface area and enough pore volume to act as promising substrates for the immobilization of polyoxometalates, with a target to increase their catalytic activity by increasing their exposure to the reactants. The reaction will take place at the solid-liquid interface where the POMs are suspected to be present.

Comparing the surface properties of all the different synthesized silica aerogels, those of which prepared from co-precursors of larger side chains experienced less specific surface areas and pore volumes. However, the results were not sufficient and conclusive to make conclusions about the reactivity of the precursors and co-precursors and the formation of the solid network after hydrolysis and condensation of the mother molecules. Important information found in this study is that the followed synthesis technique coupled with the SCCD drying allows the formation of materials where micropores and mesopores coexist in different ratios, with the percentage of

mesopores being directly proportional to the total pore volume. Increasing the pore volume leads immediately to an increase in the mesopores/micropores ratio.

Table 4. 1. Physicochemical properties of the materials

Silica Aerogel Materials	Specific surface area ($m^2.g^{-1}$)	Total pore volume ($cm^3.g^{-1}$)	Volume of mesopores ($cm^3.g^{-1}$)	Volume of micropores ($cm^3.g^{-1}$)	Percent Mesoporosity (%)	Average pore radius (Å)
M1	574	1.31	1.16	0.15	89	72.7
E1	545	0.94	0.82	0.12	87	46.1
M2	598	0.55	0.20	0.35	36	43.5
E2	649	0.92	0.68	0.25	73	52.7
M9	693	1.24	1.02	0.22	82	61.1
E9	599	0.62	0.30	0.32	49	43.2
M3	730	0.86	0.53	0.33	61	43.4
E3	598	0.65	0.37	0.27	58	35.3
M10	779	1.38	1.12	0.26	81	66.5
E10	635	0.66	0.35	0.31	52	41.3
M4	727	0.97	0.66	0.31	68	46.2
E4	526	0.40	0.08	0.32	20	27.0
M11	549	0.64	0.39	0.25	62	41.1
E11	568	0.79	0.61	0.18	77	41.1
M5	333	0.47	0.32	0.14	69	35.2
E5	463	0.44	0.19	0.25	43	23.3
M12	569	0.53	0.19	0.34	37	23.3
E12	586	0.79	0.60	0.20	75	35.3
M6	6	0.01	0.01	0.00	71	24.2
E6	4	0.01	0.01	0.00	82	28.2
M13	225	0.61	0.50	0.11	82	43.6
E13	388	1.57	1.44	0.13	92	72.5
M7	673	1.13	0.91	0.22	80	61.2
E7	726	0.92	0.57	0.35	62	49.3
M14	633	0.84	0.56	0.28	67	52.7
E14	645	1.06	0.83	0.24	78	66.4
M8	616	1.12	0.90	0.22	80	61.1
E8	517	0.88	0.70	0.18	80	72.8
M15	553	0.88	0.66	0.22	75	72.5
E15	685	1.22	1.02	0.20	83	66.3

After comparing the obtained results in this chapter, M1, E1, M9, E9, M10, E10, E11, E12, E13, E14 and E15 were chosen as the best aerogels after comparing their physicochemical properties (high specific surface area and high mesoporous volume) with the other synthesized silica materials. The POMs were immobilized onto these aerogels for a complete catalytic study where heterogeneous catalysts were compared to their corresponding homogeneous catalysts. This investigation is the subject of the next chapter.

CHAPTER FIVE

CATALYSIS

5.1. Overview

This chapter will present an in-depth investigation on the use of POMs as catalysts in heterogeneous reaction media. This is meant to reveal a newly synthesized heterogeneous catalyst by the immobilization of the active POMs onto the novel organic-modified silica aerogel materials. This is therefore an attempt to better describe the general principles involved in this important area of application of POM chemistry. The first sections will cover briefly the use of POMs as acid catalysts and then their use in oxidation catalysis. An advanced understanding of the entire catalysis picture would be achieved by looking first at the POM catalysis in homogeneous reaction media. Subsequently, these catalytic behaviors could be easily transformed onto a suitable surface, as explained earlier, to take advantage of their use in heterogeneous catalysis instead. The discussion of oxidation catalysis will highlight the general principles involved in the activation of oxidants and oxygen donors, as well as the use of POMs specifically for such purposes.

5.1.1. Acid catalysis

Acid catalysis by POMs in general and especially by Keggin heteropoly acids, is the oldest and most recognized fields of research where POMs have played an important role in application to catalysis [144]. The key to the effectiveness of POM catalysts is their high Brönsted type acidity, which has been emphasized earlier,

associated with the large negative charge polarization on the polyoxoanion species. The polyoxoanion species are therefore weak bases with increased softness, and a very low Lewis type acidity. The Brönsted acidity of POMs in general, can be considered as much more powerful than the strongest and most common mineral acid such as sulfuric acid. Accordingly, general trends may be formulated for a series of Keggin type POMs concerning their Brönsted acidity of the proton, the basicity of the polyoxoanion, and their hydrolytic stability [244].

Brönsted acidity:

$H_3PW_{12}O_{40} > H_4PVW_{11}O_{40} > H_4SiW_{12}O_{40} > H_3PMo_{12}O_{40} > H_3SiMo_{12}O_{40}$

Polyoxoanion basicity:

$[SiW_{12}O_{40}]^{4-} > [GeW_{12}O_{40}]^{4-} > [PW_{12}O_{40}]^{3-} > [PMo_{12}O_{40}]^{3-} > [SiMo_{12}O_{40}]^{4-}$

Hydrolytic stability:

$H_4SiW_{12}O_{40} > H_3PW_{12}O_{40} > H_4SiMo_{12}O_{40} > H_3PMo_{12}O_{40}$

In addition to these trends, polyoxomolybdates are superior oxidants than their equivalent polyoxotungstates. The former are therefore often used in oxidatitive systems such as those employed in this work. However, their use in such reaction conditions would often allow their reduction into heteropoly blues. All of the above trends should be carefully assessed and considered while investigating or developing new synthetic routes [244]. Consequently, most acid catalysis and synthetic procedures mediated by POMs have been carried out with either $H_3PW_{12}O_{40}$ or $H_4SiW_{12}O_{40}$ with their structures already explained in Chapter One.

POMs theoretically can be used in nearly all acid catalyzed reactions. POMs in homogeneous phase catalysis, compared to other well-known acids, especially the widely used sulfuric acid and hydrochloric acids, would acquire some advantages in

addition to some other disadvantages. The advantages are in three main aspects: There are fewer side reactions, such as sulfonation and chlorination, duo to the non-reactivity and low basicity of the polyoxo counter anion; their higher Brönsted acidity leads to significantly higher rates per proton, which might be attributed to the high molecular weight of the POMs. POMs are non-corrosive and in some cases tend to prevent corrosion. On the other hand, the high cost and lower availability are considerable disadvantages of POMs. Moreover, their difficult recovery from homogeneous media makes it impossible to recycle these cluster catalysts. In reactions such as Friedel-Crafts acylations, the low Lewis acid type acidity of POMs is thus a significant drawback. Even though POMs have a very strong Brönsted character, yet they are not considered as superacids. In addition to that, molybdates are often reduced leading to heteropoly blues and subsequent color contamination of the product [244].

Future developments in this area have to be set so to avoid all of these drawbacks and deficiencies of POMs in homogeneous reactions. Increasing the Brönsted acidity of POMs even further, which is now possible by partial exchange of protons on the POMs with cesium cations, is a very promising approach [245]. This leads to an insoluble POM that is being intensively examined for heterogeneous acid catalyzed reactions. Moreover, the preparation of POMs with enhanced Lewis activity could lead to their catalytic use in reactions presently carried out by stoichiometric amounts of $AlCl_3$. Another improvement would be the development of certain transformations leading to POMs with both oxidation and acid catalysis capabilities [244].

5.1.2. Oxidation catalysis

Since the oxidation chemistry is much more complicated and diverse compared to acid catalysis, as is the use of POMs in oxidation catalysis. The key importance of POMs in homogeneous oxidation chemistry is their oxidative stability and their ability to withstand high temperatures. POMs, in this area of study, would thus have practical advantages over widely investigated organometallic compounds. Modern studies into new catalytic reactions are thus oriented towards improving classic organic synthesis. Organic synthesis involving oxidative transformations, in the past, has been dominated by the use of environmentally damaging reagents that lead to large amounts of toxic and dangerous wastes, which are much more difficult and expensive to dispose. The present and future trend is the use of eco-friendly oxidants such as molecular oxygen, hydrogen peroxide, *tert*-butyl hydroperoxide, and others in sustainable catalytic procedures. The following table lists some desired "green" oxidants as well as others that are interesting and often studied [244].

Table 5. 1. Some important oxidants, showing the available oxygen and their reactive by-products

Oxidant	% Active Oxygen	By-product
O_2	50-100	H_2O or none
H_2O_2	47	H_2O
O_3	33	O_2
N_2O	36	N_2
NaOCl	21	NaCl
$(CH_3)_3COOH$	21	$(CH_3)_3COH$
$NaIO_4$	7.5	$NaIO_3$
PhIO	7.5	PhI

Other studies are discussed here in an attempt to comprehend the reactions taking place. The significance of the activation of the hydrocarbon by electron transfer was investigated by the excellent correlation of the reaction rate with the oxidation potential of the substrate. Researchers have attested the cation radical intermediate, in the case of AN, by ESR spectroscopy. A mechanistic scheme for anthracene oxidation is a convenient way to summarize the research [244].

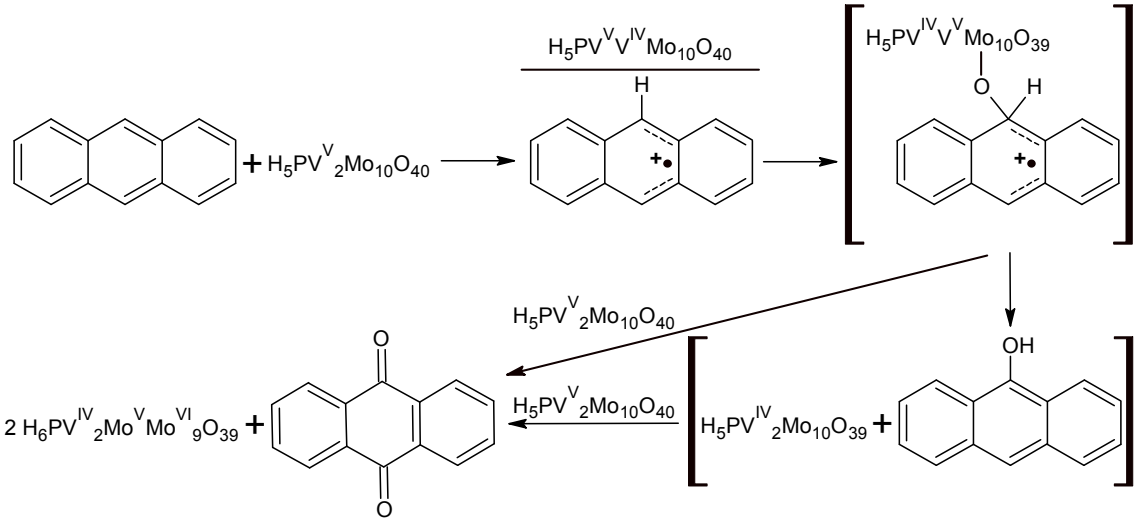

Scheme 5. 1

Though it remains an open question, two potential hypotheses (Equations 5.1 and 5.2) have been put forward in an attempt to describe the mode of re-oxidation of the reduced POM.

Hypothesis No.1:

$$[PV_2^{(IV)}Mo_{10}O_{39}]^{5-} + H_2O \longrightarrow [PV_2^{(IV)}Mo_{10}O_{40}]^{7-} \xrightarrow{1/2\ O_2} [PV_2^{(V)}Mo_{10}O_{40}]^{5-} + H_2O$$

Equation 5. 1

Hypothesis No.2:

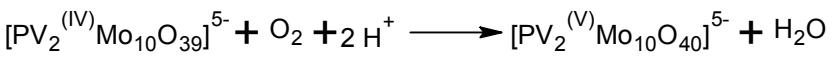

$$[PV_2^{(IV)}Mo_{10}O_{39}]^{5-} + O_2 + 2\,H^+ \longrightarrow [PV_2^{(V)}Mo_{10}O_{40}]^{5-} + H_2O$$

Equation 5. 2

The catalytic use of POMs along with benign oxidants is therefore an important branch of research. Furthermore, understanding the mechanisms of catalytic cycles in this area and developing new ways for the activation of oxidants is highly desirable [244]. After this brief overview of the homogenous based catalytic reactions of POMs and in order to enhance all of their limitations in such media, these POMs need to be transformed and applied in heterogeneous phase systems. This is achieved by immobilizing these POMs onto suitable solid materials, which are the newly synthesized surface-modified silica aerogels in the case of this thesis. The synthesis of these solid materials was already considered in Chapter Two. The current work has been oriented to study these POM clusters in heterogeneous mediated oxidation catalysis and by this to fully understand their behavior in such highly interesting and vastly growing systems. However, before doing so, the synthesis of the POMs that will be used and tested for the heterogeneous catalysis will be examined in the following section.

5.2. POM synthesis

The POM syntheses will be as seen in the procedure next are based on the synthetic methods that have been first put by Tsigdinos and Hallada [137].

5.2.1. Materials

Sodium phosphate dibasic anhydrous Na_2HPO_4 was obtained from Mallinckrodt, sodium metavanadate $NaVO_3$ was provided by Sigma Aldrich, sodium molybdate dehydrate and diethyl ether were purchased from Fluka, sulfuric acid was obtained from BDH. All the chemicals were used as is without further purification.

5.2.2. Procedure

11-Molybdo-1-vanadophosphosoric acid $H_4[PMo_{11}VO_{40}]\cdot 32.5H_2O$

11-Molybdo-1-vanadophosphosoric acid (11-MVPA) was synthesized by dissolving 0.71 g of Na_2HPO_4 (5 mmol) in 10 ml water and mixed with a solution of 0.61 g sodium metavanadate (5 mmol) in 10 ml boiling water. The mixture was then cooled and acidified to a red color by the addition of 0.5 ml concentrated sulfuric acid. Then a solution of 13.3 g $Na_2MoO_4\cdot 2H_2O$ (55 mmol) in 20 ml water was added to the first mixture. The last step was the slow addition of 8.5 ml of concentrated sulfuric acid to the mixed solution while ensuring vigorous stirring. The addition of H_2SO_4 in this step has caused a noticeable change in color from dark to light red. The water solution was left to cool and the MVPA was then extracted with 50 ml diethyl ether. The desired heteropoly etherate was present in the middle layer of this extraction, where the aqueous layer, remaining at the bottom, was of a yellowish color and probably contained some vanadyl species. A stream of air, using the compressed air gun, was passed over the heteropoly etherate layer (Figure 5.1, Left), after separation, to free it of diethyl ether. The orange solid that remained was later dissolved in 5 ml water and placed over concentrated sulfuric acid in a vacuum dessicator for 12 hours. Then the wet solid was

removed from the dessicator and air-dried for 12 more hours to permit further drying. These last two steps allowed for the complete drying and ensured good crystallization of the POM. The dry orange crystals that formed (Figure 5.1, Right) are now ready to be used in their respective catalytic application.

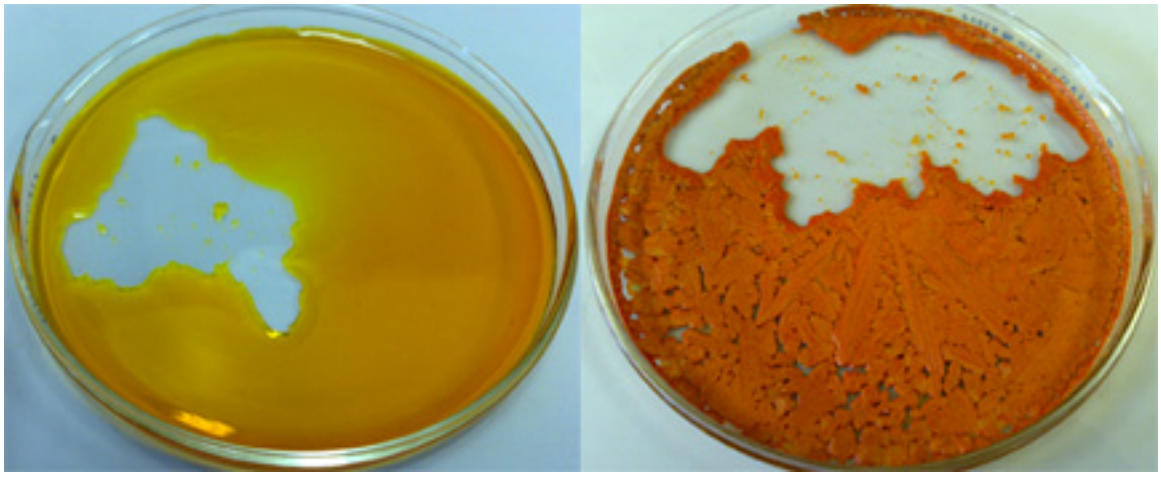

Fig. 5. 1. The heteropoly etherate layer (Left) and the obtained orange crystals of 11-MVPA (Right), as prepared in our laboratory

10-molybdo-2-vanadophosphoric acid $H_5[PMo_{10}V_2O_{40}]\cdot 32.5H_2O$

Similar to the synthesis just described, 10-molybdo-2-vanadophosphoric acid (10-MVPA) was synthesized by dissolving 2.44 g of sodium metavanadate (20 mmol) in 10 ml boiling water and were mixed with 0.71 g Na_2HPO_4 (5 mmol) in 10 ml water. After the solution was cooled, 0.5 ml concentrated sulfuric acid was added resulting into a similar red color. 12.1 g of $Na_2MoO_4\cdot 2H_2O$ (50 mmol) dissolved in 20 ml water was then added. While vigorously stirring the solution, 8.5 ml concentrated sulfuric acid was added slowly, and the obtained hot solution was allowed to cool back to room temperature. The MVPA was similarly extracted with 50 ml diethyl ether, and air was passed over the heteropoly etherate layer to free it of diethyl ether. The remaining solid

was again dissolved in water and crystallized, as already described for 11-MVPA. The large dark-orange crystals that formed were air-dried and made ready to be immobilized onto silica aerogels.

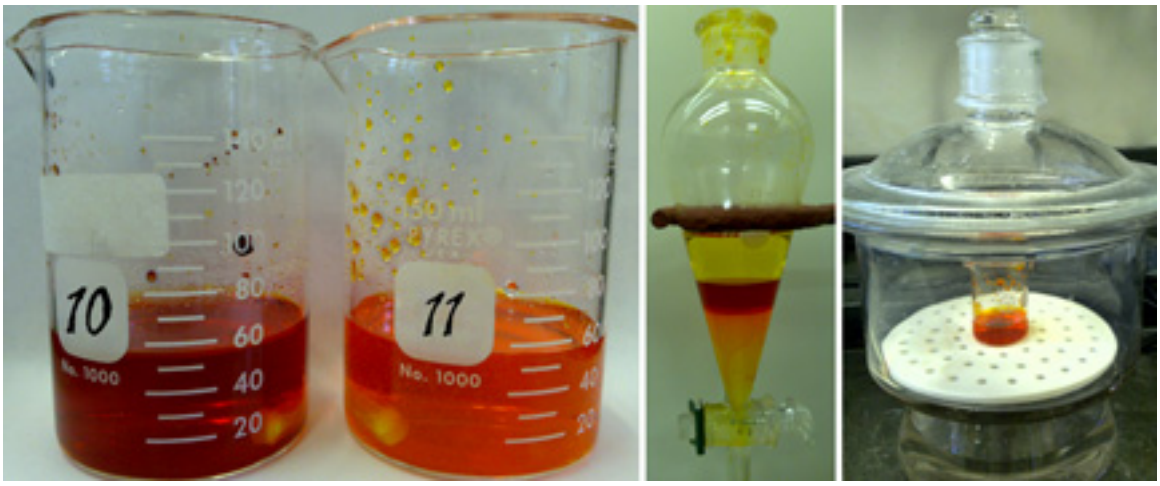

Fig. 5. 2. 10-MVPA (Dark Orange) and 11-MVPA (Orange) mixtures before extraction (Left), the extraction with diethyl ether with the heteropoly etherate layer as the middle layer (Center), and the crystallization in a vacuum dessicator over concentrated sulfuric acid (Right); during MVPA synthesis in our laboratory

5.2.3. Characterization

These obtained POMs 10-MVPA (10) and 11-MVPA (11) were characterized by FTIR spectroscopy using a Nicolet™ 4700 FTIR spectrometer, where the procedure is the same as that illustrated in Chapter Three. The specific surface areas of these clusters were measured by N_2 physisorption at liquid nitrogen temperature using a Quantachrome NOVA-2200 surface area analyzer and standard multipoint BET analysis methods, where the procedure is the same as that explained in Chapter Four. X-Ray diffraction (XRD) patterns of the POMs were obtained in detector scan mode with a BRUKER D8 Discover diffractometer equipped with a Cu-Kα radiation (λ=1.5405 Å), scanning in the range 2Θ = 20°–80°, with the generator operated at 40 kV and 150 mA.

Diffuse reflectance UV–Vis (DR UV–Vis) spectra of catalyst samples were obtained using a JASCO, V-570 UV/VIS/NIR spectrometer equipped with a 90° angle integrating sphere diffuse–reflectance accessory.

Conventional UV-Visible spectrophotometry is carried out in transmission mode with samples that allow the light beam to pass straight through without being diverted by refraction or spread out by scattering. In the case of powdered catalysts, such as the materials in this work, the incident light is almost completely diffused and it is necessary to use Diffuse Reflectance (DR) instead of transmission spectroscopy. The reflectance of a solid includes specular reflectance and diffuse reflectance. This latter, characterized by an angular distribution independent of the incident angle, prevails in the case of powdered solids. Moreover, diffuse reflectance depends on the particle size, which is when the particle size decreases would result into an increase of reflectance [246]. Generally, samples that are opaque may be analyzed by placing them at the back of an integrating sphere, reflecting light off them, and gathering the scattered light that bounces back. The DR UV-Visible spectroscopy conducted here is done by mounting our samples on a white non-reflecting holder and placed in the beams path to collect the desired spectra. The results of such an experiment would give us reflectance spectra that could be easily transformed into absorbance spectra with absorptions bands associated with the occurring internal transitions.

5.2.4. Results and discussion

All the obtained results for the characterization of the POMs 10-MVPA and 11-MVPA are labeled and color-coded as 10 (Dark Orange) for 10-MVPA and 11 (Orange) for 11-MVPA. The assigned color code is for a very specific reason, which is

corresponding to the color of the obtained materials themselves as seen the figures of section 5.2.2.

5.2.4.1. FTIR spectroscopy

FTIR spectra of 10-MVPA and 11-MVPA are depicted in figure 5.3. The characteristic bands of these POMs were observed at 1054, 959, and 882 cm^{-1}. The peak at 1054 cm^{-1} was attributed to the P–O vibration, the peak at 959 cm^{-1} was attributed to the Mo-O transition, and the peak at 882 cm^{-1} was attributed to Mo-O vibrations within the Mo-O-Mo entity [193, 247].

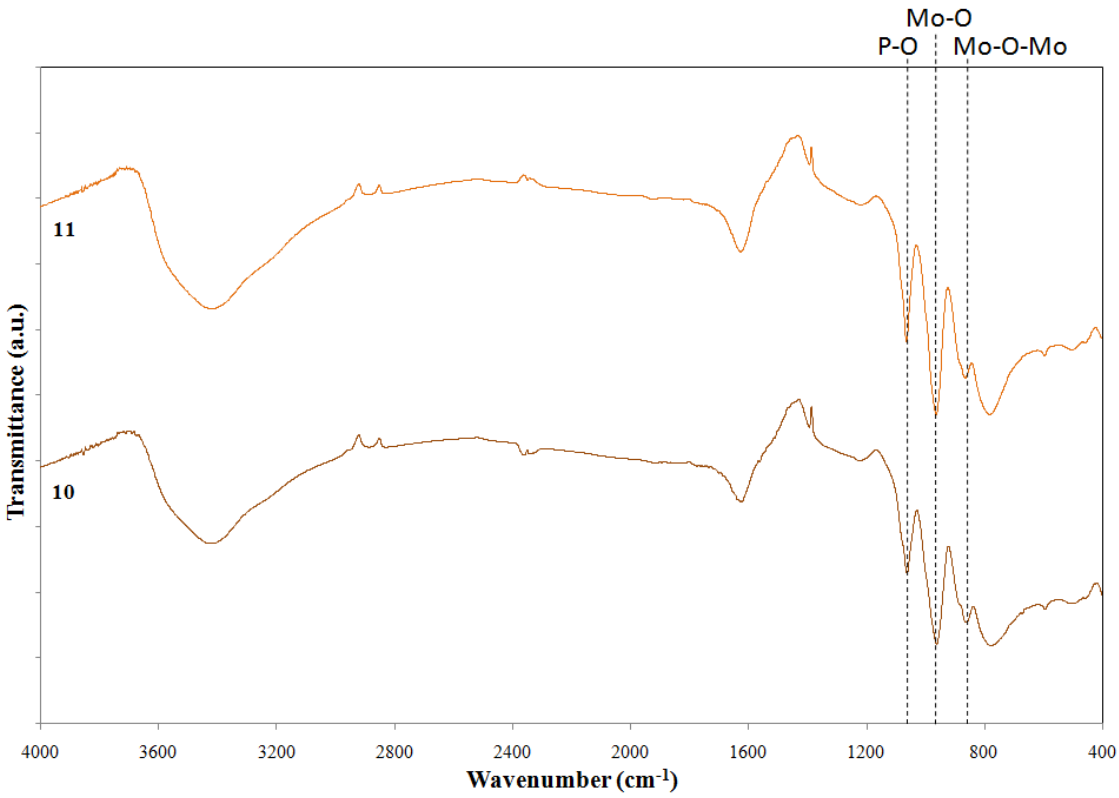

Fig. 5. 3. FTIR spectra of the 10-MVPA and 11-MVPA

5.2.4.2. Nitrogen physisorption experiments

The nitrogen adsorption/desorption experiments conducted on the 10-MVPA and 11-MVPA have resulted into relatively low specific surface areas of 4 and 8 $m^2.g^{-1}$ respectively. The total pore volume is 0.015 and 0.022 $cm^3.g^{-1}$ for the 10 and 11 respectively, which is again very low. The isotherms (Figure 5.4) show type III isotherms with some mesoporosity due to the appearance of a type H3 hysteresis. Therefore, one can conclude that these synthesized POMs do have some mesoporosity character, which is also emphasized by the pore size distributions (Figure 5.5) where some mesopores exist in the 20–40 Å range.

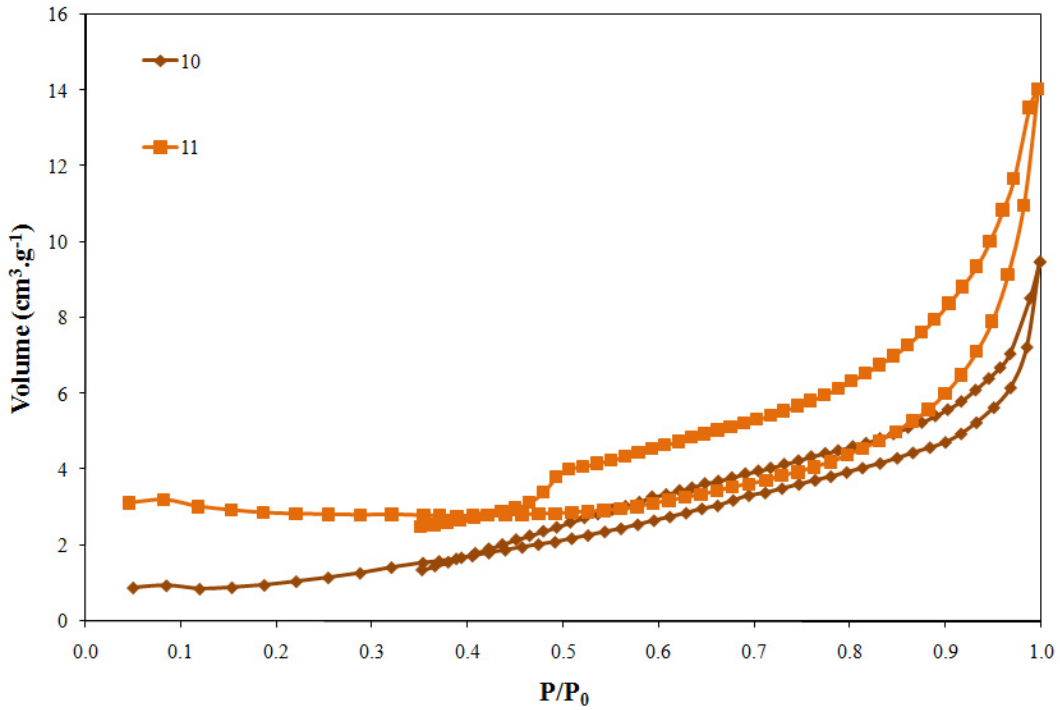

Fig. 5. 4. Nitrogen adsorption/desorption isotherms of the 10-MVPA and 11-MVPA

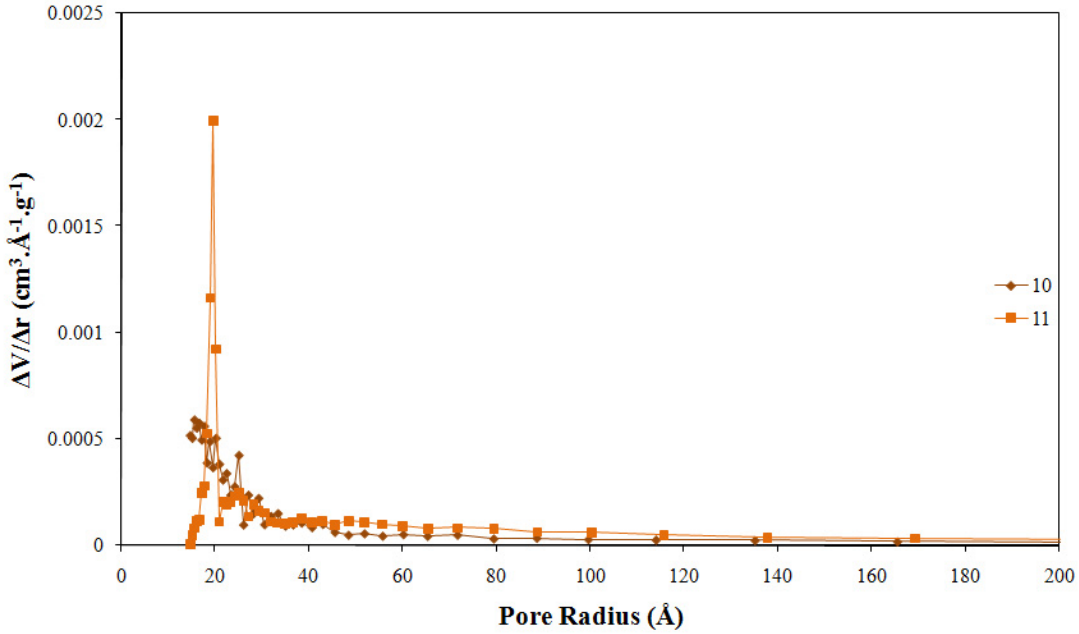

Fig. 5. 5. Pore size distribution of the 10-MVPA and 11-MVPA

5.2.4.3. X-ray diffraction

Contrary to the nitrogen physisorption experiments where little information may be abstracted on the structure of these POMs, the x-ray diffraction patterns obtained for the 10-MVPA and 11-MVPA (Figure 5.6) showed a rather conclusive picture about the nature of these POMs. As it is seen in the diffraction patterns the appearance of a sharp peaks at and 36° for 11, however the pattern for 10 is on the contrary non-conclusive since these peaks would later appear, with the same intensity, for the supported materials. Such peaks are very indicative and characteristic of a crystalline structure attained by these solid clusters.

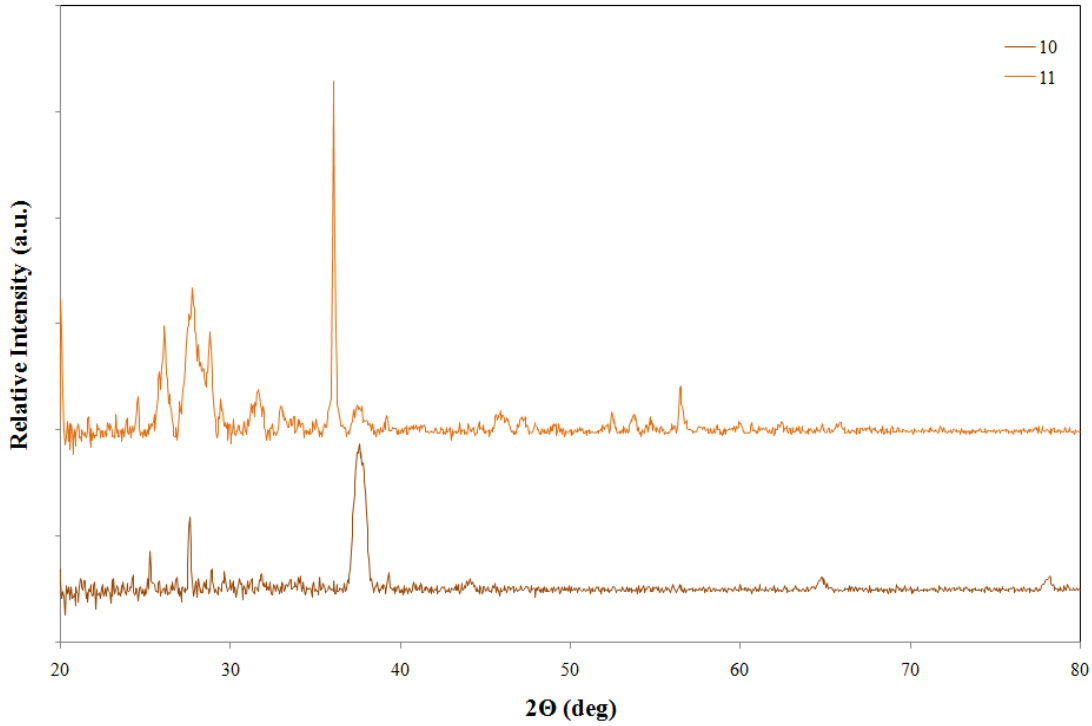

Fig. 5. 6. X-ray diffraction patterns of the 10-MVPA and 11-MVPA

5.2.4.4. DR UV-Vis spectroscopy

10-MVPA and 11-MVPA DR UV–Vis spectra are shown in figure 5.7. Because 10 and 11 exhibit characteristic absorption bands in UV–Vis region, their structures are often characterized by diffuse-reflectance UV–Vis spectroscopy. The spectra show two prominent bands at 234 and 322 nm in addition to a large absorption band starting from 422 nm until 560 nm. The former two peaks are clear cut proof of the value of these crystals as they are characteristic of the two POMs [54, 193, 247].

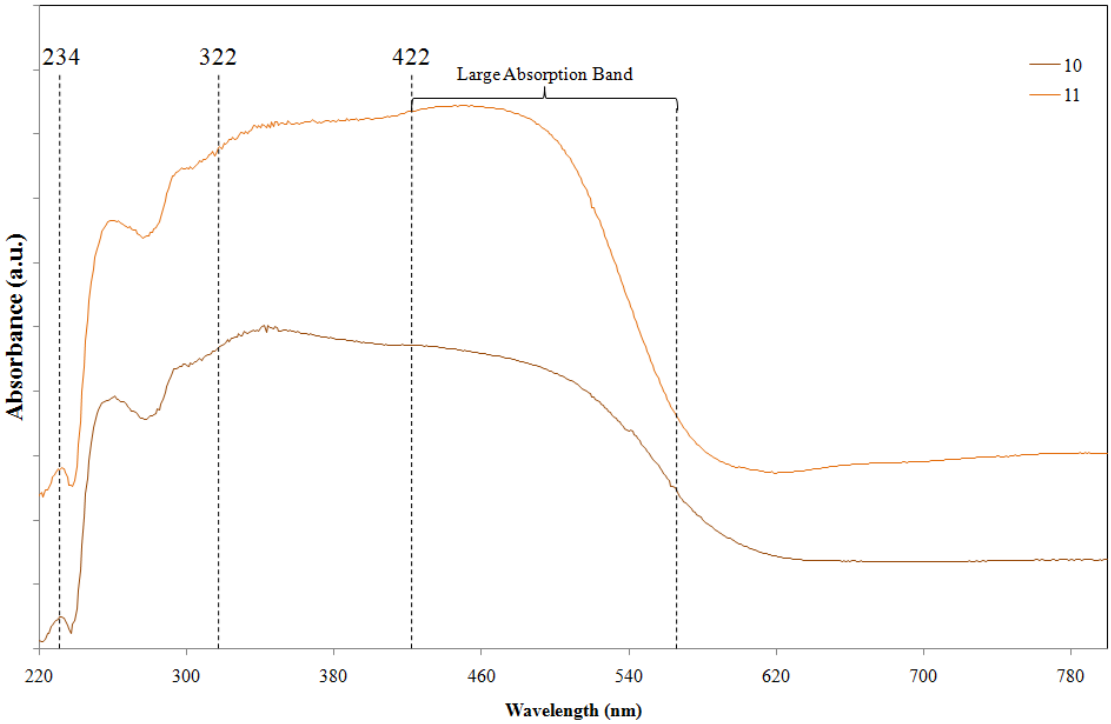

Fig. 5. 7. DR UV-Vis spectra of the 10-MVPA and 11-MVPA

5.3. POM immobilization

5.3.1. Materials

3-Aminopropyltriethoxysilane (APTES) was provided by Acros Organics, toluene was from Fluka, sulfuric acid was obtained from BDH, and all are used as received.

5.3.2. Procedure

After synthesizing and characterizing the surface-modified silica aerogel materials in previous chapters, and the POMs being successfully synthesized as seen in section 5.2, it is now the challenge to immobilize these highly active POMs onto the mesoporous materials. The procedure illustrated here was derived from the synthetic procedure that Bordoloi *et al.* [54] have conducted to produce their own type of

catalysts. This synthesis is a two step process, first the amino-functionalization of the silica aerogel materials in order to enhance the loading of the POM in the next step of immobilization, then these amine functionalized mesoporous materials were treated with a concentrated sulfuric acid so to minimize leaching and to allow more of the POM to be trapped within the network of the silica aerogels.

Amine-functionalization

The surface modification of the silica aerogels by (3-aminopropyl)triethoxysilane (APTES) was carried out using a grafting method as described previously [248]. In a typical preparation, freshly organically-modified silica aerogels (3 g), which were reduced to powder, were refluxed with 90 ml of toluene. To this, 1.5 g APTES (1608 μl; 6.7 mmol) was added and stirred under reflux conditions for 4 h. After the solvent was distilled off, the solid was filtered, washed, and then dried at room temperature. The product is designated with a letter 'N' next to the silica aerogel's name. Amine-functionalized silica aerogels were then treated with H_2SO_4 to minimize leaching and to enhance POM loading. Acidification was carried out by adding 15 ml of 1 mM sulfuric acid solution to 2 g of the amine-functionalized organo-modified silica aerogels, and is left in treatment for 24 hours. The more positively charged NH_3^+ groups on the support, the stronger is the electrostatic binding of the 10-MVPA and 11-MVPA to the support. The treated solution was later filtered to get the acid-treated amine-functionalized mesoporous silica materials, which will be used as the support onto which the POM will be immobilized.

Immobilization of the POMs

A 50 ml sample of methanol solution containing 0.25 g of POM (equivalent to 0.108 mmol of 10-MVPA and 0.106 mmol of 11-MVPA), was added to 0.7 g of freshly

acid-treated amine-functionalized silica aerogels and refluxed for 3 h. It was then filtered, washed by methanol and dried under vacuum. The resulting product is designated by either '10' or '11' for those prepared from the immobilization of 10-MVPA and 11-MVPA, respectively. The color of the starting material of POM has changed from a dark orange to a dark green for the supported catalyst materials when 10-MVPA was used and the color became light green from an orange color when 11-MVPA was used. Scheme 5.2 depicts the immobilization process conducted in this thesis.

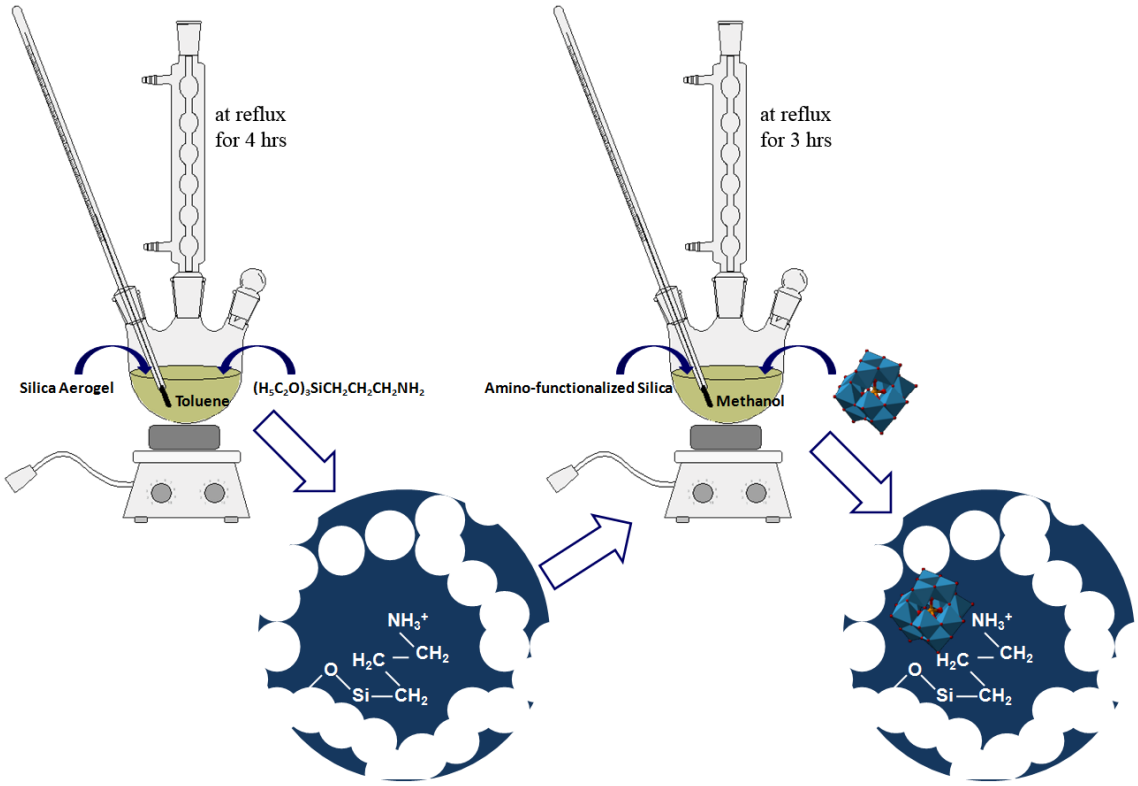

Scheme 5. 2. POM immobilization process onto surface-modified silica aerogels

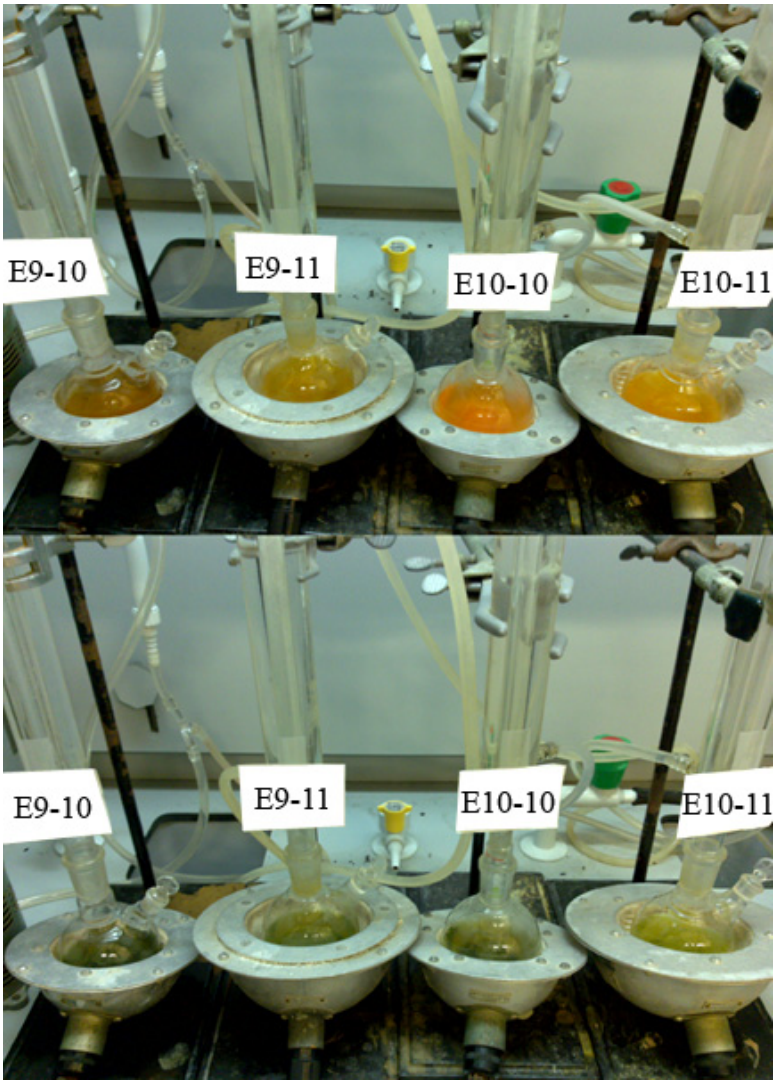

Fig. 5. 8. The change in color from orange to green after immobilization, as prepared in our laboratory

5.3.3. Characterization

The Mo content in these newly synthesized catalysts is the most important for the analysis of these immobilized materials, which is quantified by atomic absorption spectroscopy (AAS) using a SOLAAR atomic absorption spectrophotometer. This technique was used for the quantification of the immobilized POMs within the mesoporous silica materials. These obtained immobilized materials were characterized by FTIR spectroscopy using a Nicolet^{TM} 4700 FTIR spectrometer. The specific surface

areas of these new catalysts were measured by N_2 physisorption at liquid nitrogen temperature using a Quantachrome NOVA-2200 surface area analyzer and standard multipoint BET analysis methods, where the procedure is the same as that explained in Chapter Four. X-Ray diffraction (XRD) patterns of the immobilized materials were obtained in detector scan mode with a BRUKER D8 Discover diffractometer scanned in the range $2\Theta = 20°–80°$, same as the procedure followed for the analysis of the POMs. Diffuse reflectance UV–Vis (DR UV–Vis) spectra of the catalyst samples were obtained using a JASCO, V-570 UV/VIS/NIR spectrometer equipped with a diffuse–reflectance accessory, where the procedure is the same as that explained in section 5.2.3.

5.3.4. Results and discussion

All the obtained results for the characterization of the immobilized materials are labeled and color-coded in such a way that the silica aerogel materials categorized as previously assigned into those prepared in TMOS shown in blue and those prepared in TEOS shown in red. Meanwhile, the amino-functionalized silica aerogel materials are designated by a letter 'N' next to the silica aerogel's name and are shown in violet. Moreover that synthesized catalysts are as well categorized with those prepared by the immobilization of 10-MVPA are designated by a '10' shown in dark green and those prepared by the immobilization of 11-MVPA are designated by an '11' shown in light green. The green color is not chosen haphazardly, however the dark green color as seen in the previous sections is the color of the immobilized materials, as seen, obtained from 10, and similarly the light green of the materials prepared from 11. In this section, only the characterization spectra and experiments for the silica aerogels M1 and E1 will be presented, the rest are included in Appendix C.

5.3.4.1. AAS spectroscopy

Using atomic absorption spectroscopy technique, the POM content within the pores of these synthesized materials have been tested and quantified. Prior to AAS analysis, the solid material has been digested using a microwave digestion routine in order to convert our samples into liquid medium to be analyzed. This is done in this way since the solid materials couldn't be used directly in AAS, since only liquid sample could be analyzed with the flame AAS technique. Such analyses have resulted into absorbance values specific of Mo, which is the element tested in the materials due to its abundance with 10 equivalent Mo atoms in 10-MVPA and 11 equivalent Mo atoms in 11-MVPA. These experiments allowed for the calculation of the amount of POM present inside the synthesized materials. Table 5.2 presents the percent immobilization of 10-MVPA and 11-MVPA inside the different silica aerogels. The percent POM immobilized within the materials ranged from 14.8–32% which is very indicative that following the suggested synthesis, the 10-MVPA and 11-MVPA have been successfully integrated in the network of the different silica mesoporous materials.

Table 5. 2. AAS data for the immobilization of 10-MVPA and 11-MVPA on the different silica aerogel materials

Sample	% POM Immobilized	Sample	% POM Immobilized
E1-10	32.0	E1-11	28.9
E9-10	31.5	E9-11	21.5
E10-10	22.5	E10-11	14.8
E11-10	30.6	E11-11	27.2
E12-10	26.2	E12-11	24.0
E13-10	21.6	E13-11	19.6
E14-10	19.9	E14-11	18.3
E15-10	23.4	E15-11	26.0
M1-10	31.2	M1-11	28.3
M10-10	28.6	M10-11	27.2
M11-10	27.2	M11-11	27.9

5.3.4.2. FTIR Spectroscopy

FTIR spectra of M1, M1-N, M1-10, and M1-11 are shown in figure 5.9. The FTIR study was performed to identify the presence of 10-MVPA and 11-MVPA in the amino-functionalized mesoporous silica aerogels. The FTIR spectrum of M1-10 and M1-11 were compared with the spectra of M1-N and neat 10-MVPA. The 10-MVPA showed four peaks characteristic as explained in the previous sections. Most of the IR bands of M1-N, the amino-functionalized silica aerogel materials 1073, 951, 870, 795, and 489 cm^{-1} overlapped with the IR bands of 10-MVPA (the characteristic bands of POMs at 1050, 959, and 882 cm^{-1}); thus, these bands are not clearly seen in IR spectra of M1-10 and M1-11. However, an increase in intensity of the IR bands at 882, 959, and 1050 cm^{-1} and the appearance of a new band at 870 cm^{-1} in M1-10 and M1-11 corresponding to M1-N may be considered an indication of the presence of 10-MVPA in the mesopores of the amino-functionalized mesoporous silica materials [54]. The same rational may be applicable to the E1 immobilized materials with their respective spectra seen in figure 5.10, the peaks appearing exclusively for the E1-10 and E1-11 which are similarly attributed to the peaks of the 10-MVPA and 11-MVPA are an indicative evidence of the presence of these POMs inside the aerogels. This further assures that the synthesis of these new catalysts has been successful, yet much more properties need to be tested in order to analyze their surface upon which the reaction and the oxidative catalysis would take place eventually.

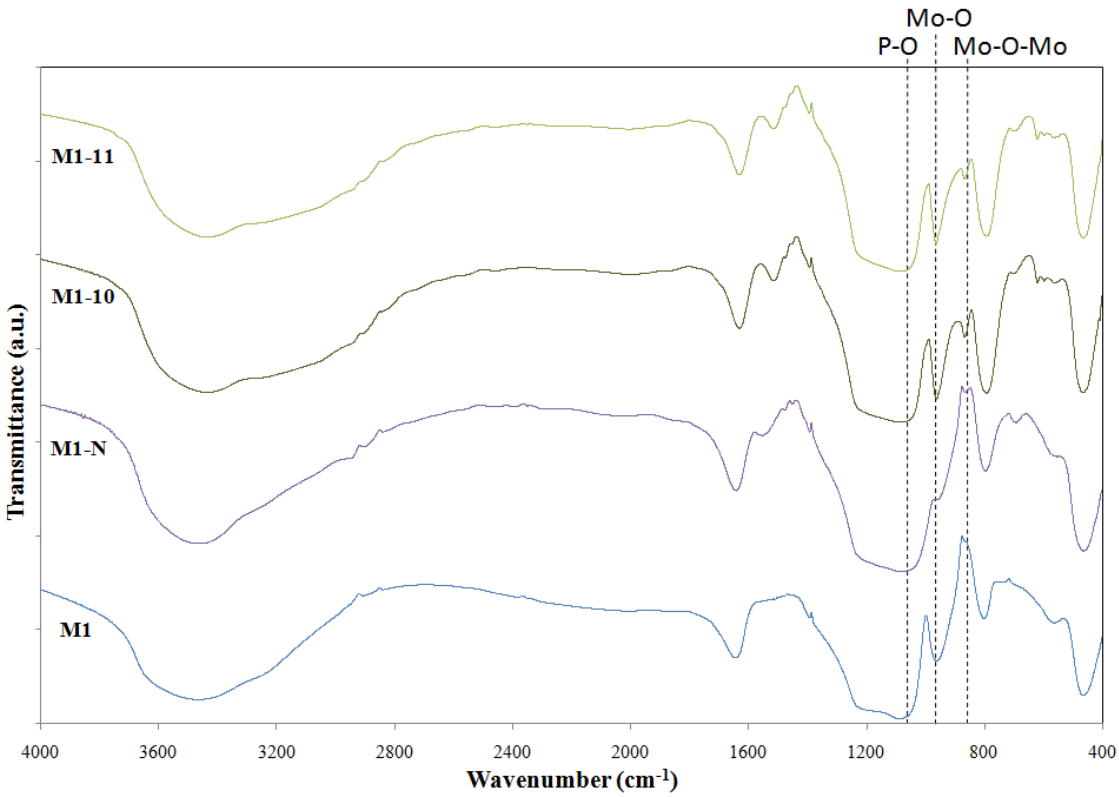

Fig. 5. 9. FTIR spectra of the M1 immobilized materials

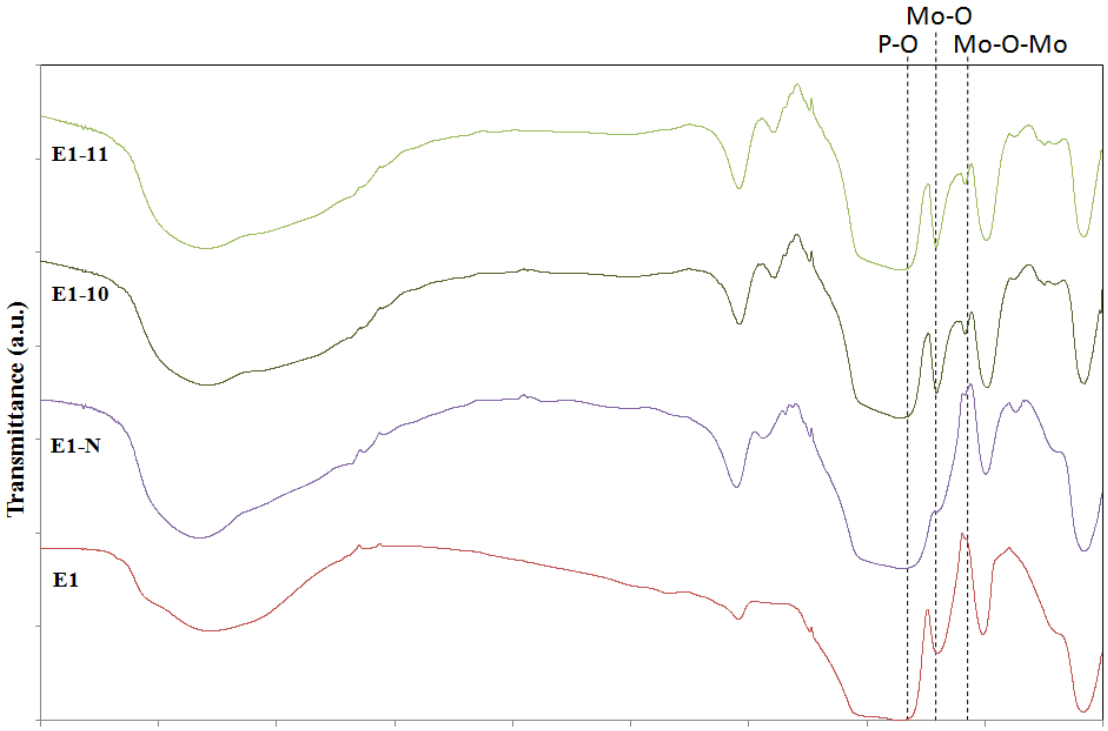

Fig. 5. 10. FTIR spectra of the E1 immobilized materials

5.3.4.3. Nitrogen physisorption experiments

The nitrogen adsorption/desorption experiments conducted into testing the surfaces of these supported materials has resulted into interesting results. The isotherms for the M1, M1-N, M1-10, and M1-11 that are compared in figure 5.11 clearly show a type IV isotherm with H2 hysteresis. Based on these observations, one can conclude that the obtained supported materials M1-10 and M1-11 have a mesoporous type character different from the non-porosity of the neat 10-MVPA and 11-MVPA. The M1-N however has experienced a slightly different isotherm trend than the pure silica M1, due to the existence of the amine groups on its surface, as it was expected. The specific surface area is a key parameter to our analysis; one can easily notice the decrease in surface area from 574 $m^2.g^{-1}$ for the M1 to a 277 $m^2.g^{-1}$ for the M1-N then the values decreased even more for the supported materials to 267 and 243 $m^2.g^{-1}$ for M1-10 and M1-11 respectively. The same trend is experienced for the total pore volume and the mesoporous volume, which is decreasing from M1 to M1-N to M1-10 and M1-11. The great resemblance and similarity that is seen between the obtained results for M1-10 and M1-11 assures the reproducibility of the work achieved. These exhibited trends, which are the decrease in surface area and pore volumes is a direct indication of a change undergoing on the surface. As a conclusion, surface being functionalized by amino groups has caused a decrease of the surface by occupying the surface and filling up the available pores. Moreover the immobilization of the POMs onto the amino-functionalized silica materials have caused further decrease in values which is again because the pores are being now impregnated by these supported POMs on the surface of the silica aerogel materials. The pore size distributions (Figure 5.12) however, have just indicated the presence of a porous structure of mesoporous character with sufficient

amount of pores to host a reaction at its surface. The nitrogen sorption experiments for the E1 supported materials (Figures 5.13 and 5.14) have shown very similar trends and the same conclusion could easily be drawn. However, the specific surface areas showed a clearer decreasing trend as follows: E1 545 $m^2.g^{-1}$, E1-N 310 $m^2.g^{-1}$, E1-10 230 $m^2.g^{-1}$, and E1-11 219 $m^2.g^{-1}$. In general, it can be concluded that 10-MVPA immobilized materials have always experienced slightly higher specific surface areas and total pore volumes than those immobilized with 11-MVPA, yet the values remain very relatable.

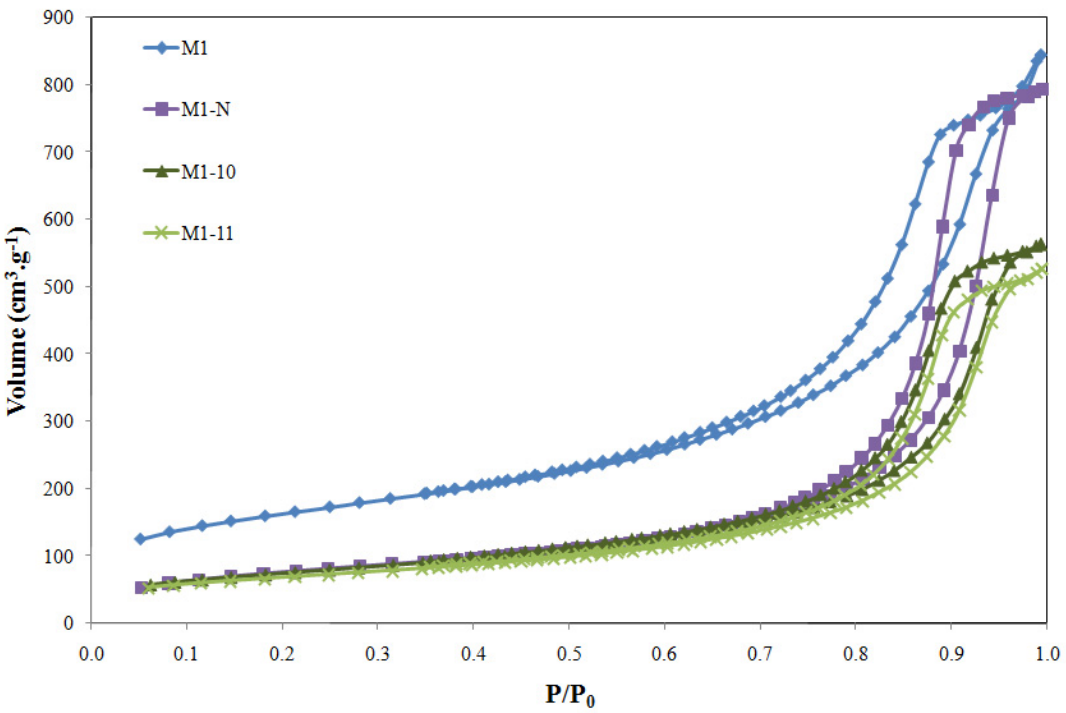

Fig. 5. 11. Nitrogen adsorption/desorption isotherms of the M1 immobilized materials

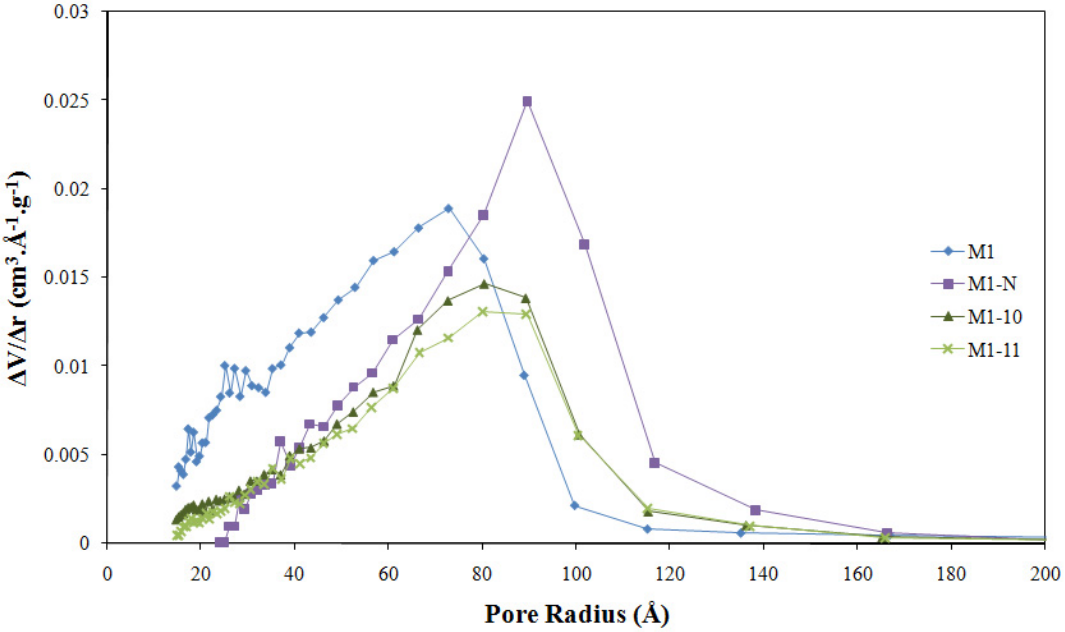

Fig. 5. 12. Pore size distribution of the M1 immobilized materials

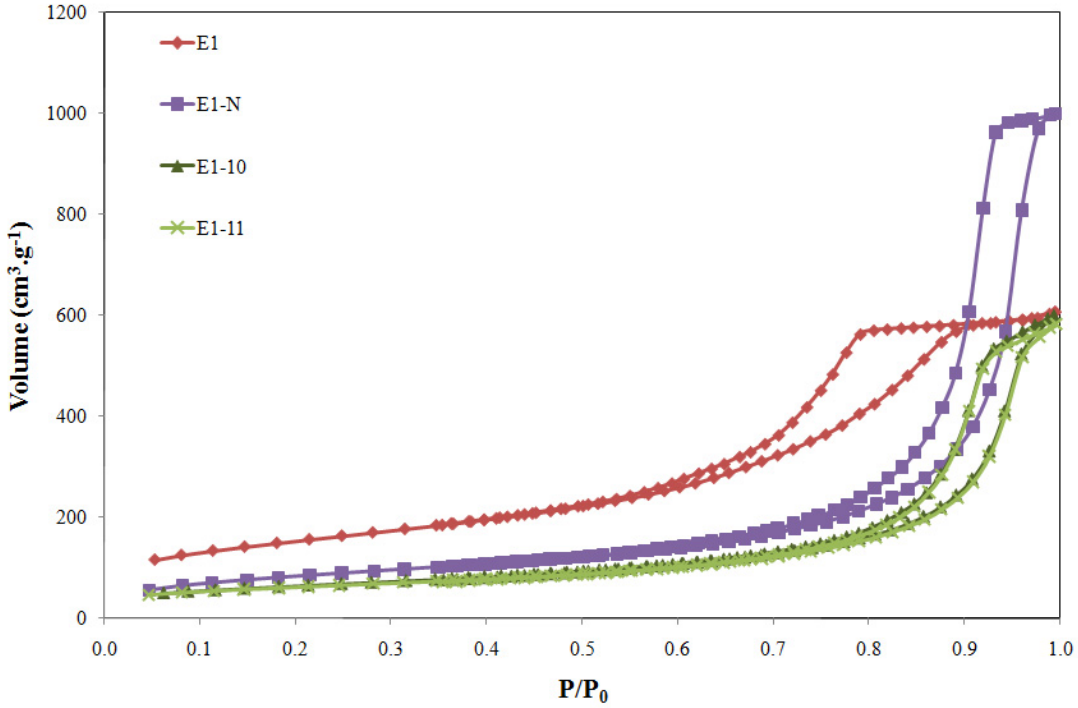

Fig. 5. 13. Nitrogen adsorption/desorption isotherms of the E1 immobilized materials

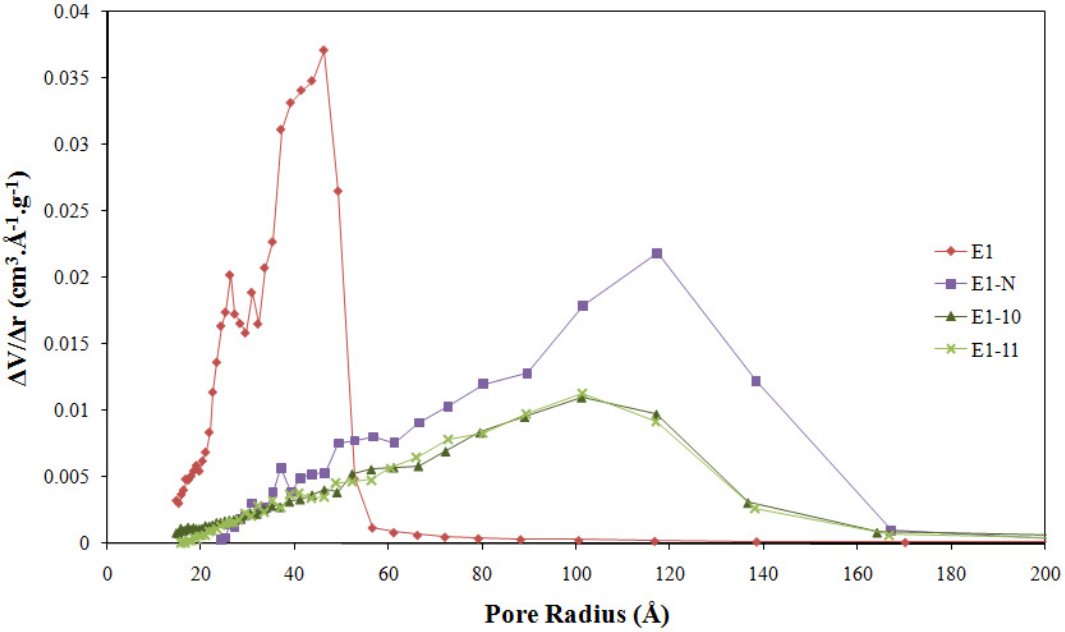

Fig. 5. 14. Pore size distribution of the E1 immobilized materials

5.3.4.4. X-ray diffraction

The x-ray diffraction patterns obtained for M1-10 and M1-11 are presented in figure 5.15. Comparing these patterns to those obtained earlier for 10 and 11, the diffraction patterns observed are inconclusive since they appear in both the 10 and M1-10 samples, which is an invalid result. Such invalidity of XRD results could be very well attributed to the lack of the machine itself by which it is not equipped with holders specifically for powder materials, and the technique might seem inadequate. In the case of the 11-MVPA however, the M1-11 did not show any identifiable peaks that are related to the pattern of the 11-MVPA. This could possibly be due to a very valid reason that the immobilized 11-MVPA onto the surface of the M1 has been dispersed in a very diffuse manner, and did not allow for any formation of aggregation of these crystals. Therefore, the 11-MVPA POMs were very well distributed within the pores of the

mesoporous silica materials and therefore no x-ray diffraction peaks would appear in the pattern due to the very small crystallites. Another explanation could well be that the peaks that are obtained from the supported POMs in the material are of a very small intensity and thus are neither identifiable nor deciphered from the baseline. Since it has been already shown and identified that these POMs are indeed present and immobilized on the surface as explained and analyzed earlier by the AAS, FTIR, and nitrogen sorption experiments.

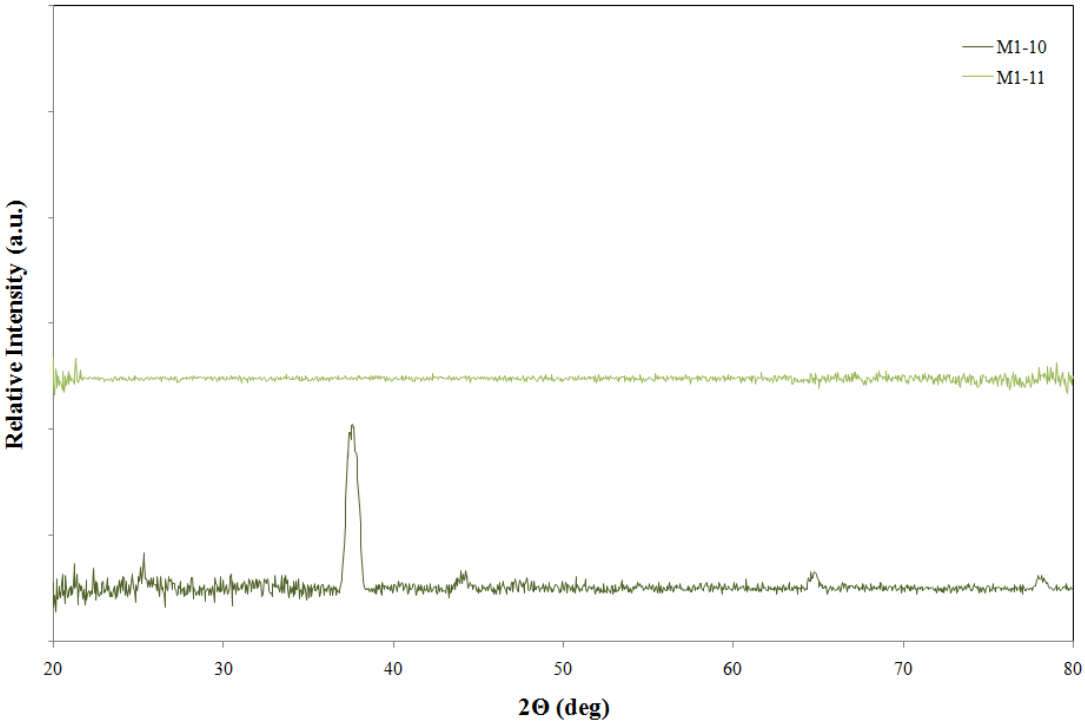

Fig. 5. 15. X-ray diffraction patterns of the M1-10 and M1-11

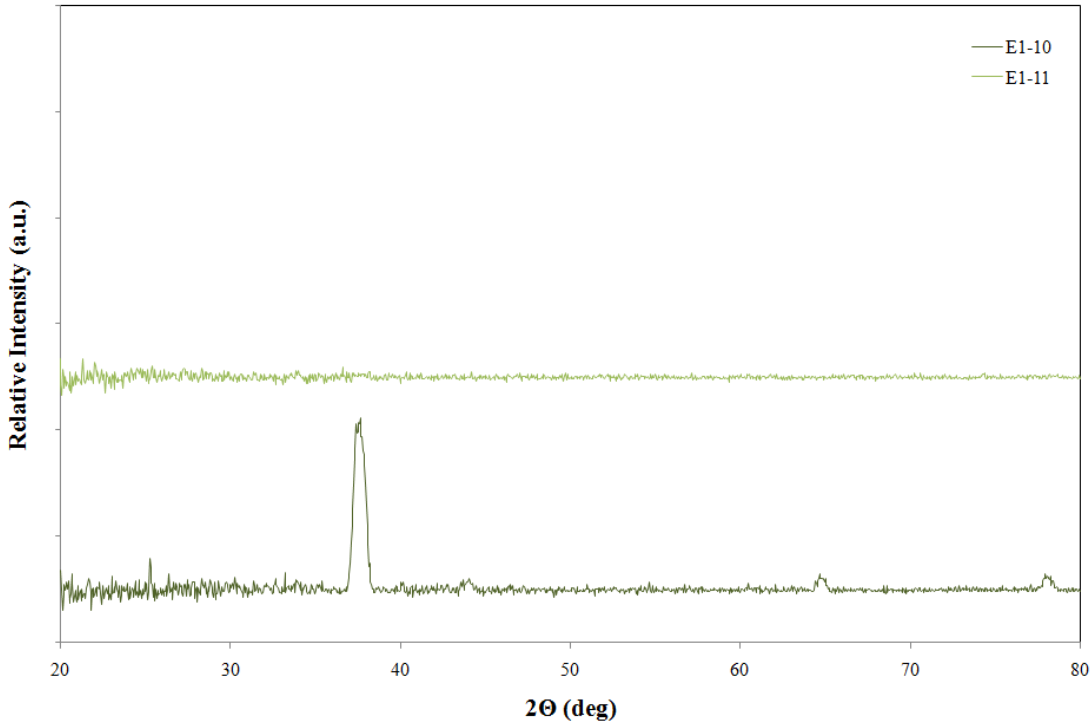

Fig. 5. 16. X-ray diffraction patterns of the E1-10 and E1-11

5.3.4.5. DR UV-Vis spectroscopy

The DR UV-Vis spectra for M1-10 and M1-11 are shown in figure 5.17. As seen in earlier sections, 10 and 11 experience characteristic absorption bands in the UV–Vis region. However, the pure silica and the amine-functionalized silica aerogels do not show any characteristic absorption bands in UV–Vis region (Appendix C, Figure C.41). M1-10 and M1-11 exhibit bands that are compared with the characteristic bands of neat 10-MVPA and 11-MVPA at around 234 and 322 nm, with a distinct shoulder appearing at 422 nm that could be attributed to the large absorption bands of the 10 and 11. On anchoring of 10 and 11 onto M1-N, these bands shifted slightly, and the shoulder appeared. These obtained bands are weak due to the low concentration of 10 and 11 in the immobilized sample. The presence of these bands indicates the existence of 10 and 11 within the M1 silica network, and these bands exhibit small shifts in

wavelength. The broadness of the POM bands after immobilization may be due to different reasons. It is often thought that definite interactions in fact exist between the POMs and mesoporous silica, and that POMs are under the constraint environment of mesoporous silica after immobilization. The bands were shifted slightly (~2 nm) with respect to neat 10-MVPA and 11-MVPA, possibly due to interactions between the respective 10 and 11 with the solvent in the constraining environment of mesoporous silica aerogels [247].

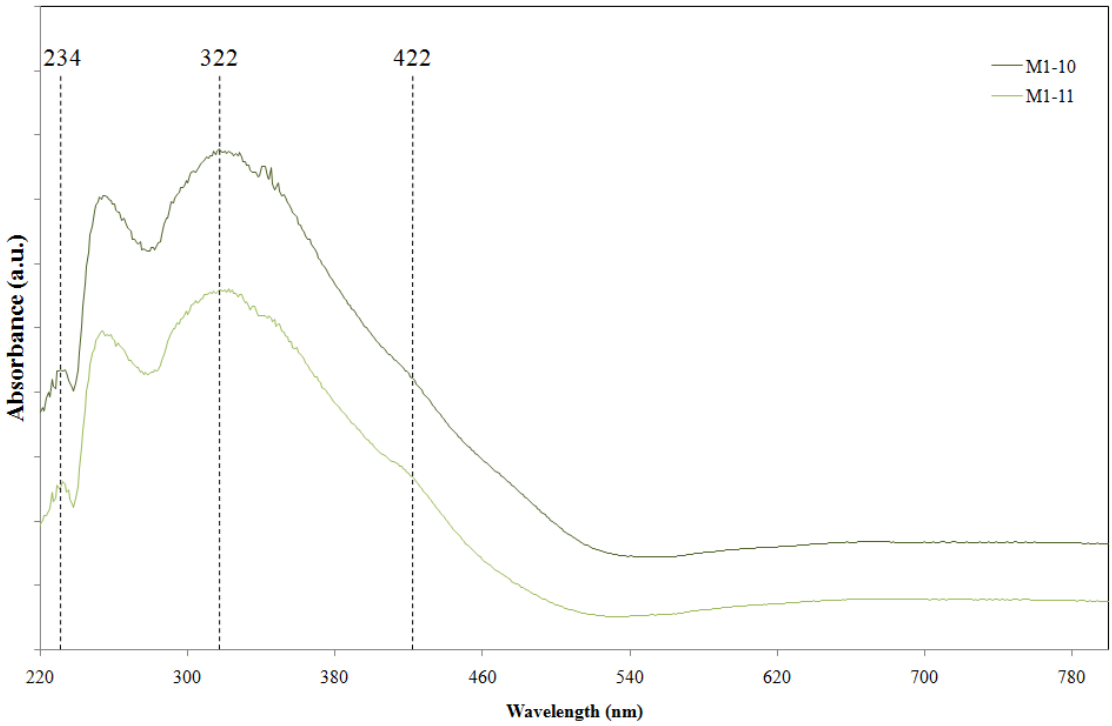

Fig. 5. 17. DR UV-Vis spectra of the M1-10 and M1-11

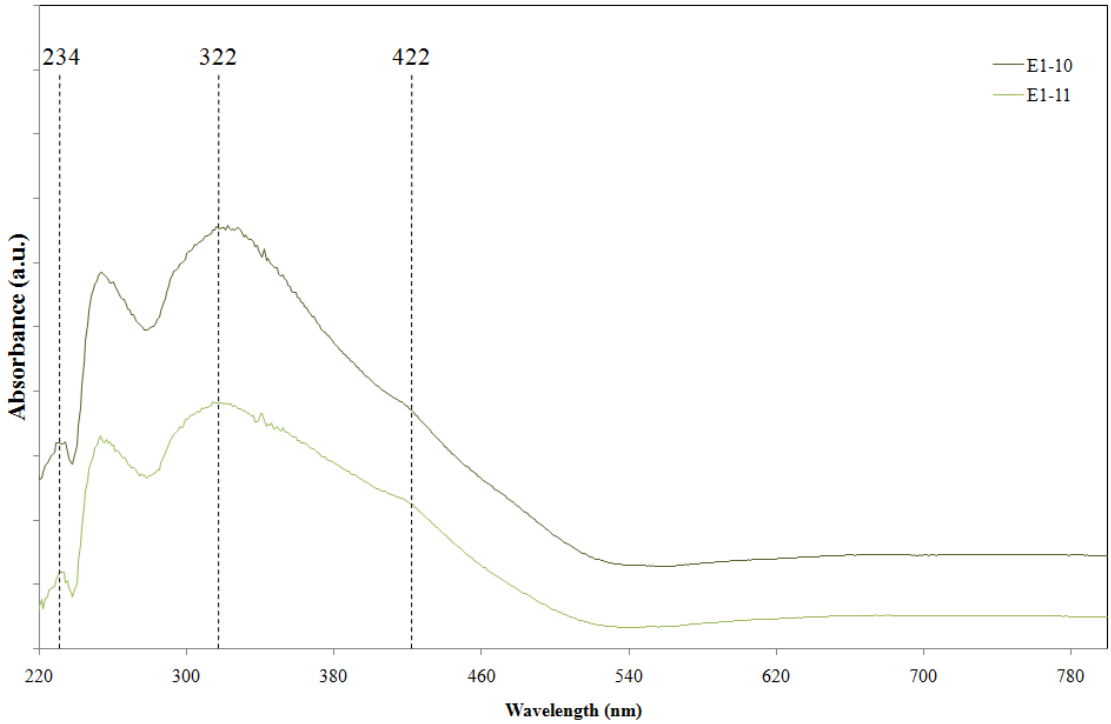

Fig. 5. 18. DR UV-Vis spectra of the E1-10 and E1-11

5.4. Catalysis

5.4.1. Reaction significance

Anthracene was oxidized to anthrone, oxanthrone and anthraquinone with *tert*-butyl hydroperoxide (TBHP) as oxidant and the immobilized 10-MVPA and 11-MVPA onto surface organically-modified silica aerogels as catalysts. In all cases anthraquinone was identified as the major end product of anthracene oxidation. Anthraquinones represent a large family of compounds having diverse biological properties. Anthraquinone ($C_{14}O_2H_8$) in particular, is an intermediate in the manufacture of pigments and dyes, an additive in the pulping process of paper industry, and is also applied in the synthesis of hydrogen peroxide [249]. On a small scale, it is used as a catalyst in the isomerization of vegetable oils, an accelerator in nickel electroplating and as a bird repellant [250-252]. A variety of methods exists to produce anthraquinone, by

which 85% of the world production is based on the vapor phase oxidation of anthracene with air. The industrial process is performed over a supported iron vanadate-potassium catalyst at 390°C with a 99% yield to the quinone [249, 252].

In another perspective, the clinical treatment of neoplastic diseases relies on the complementary procedures of surgery, radiation treatment, immunotherapy and chemotherapy. The latter technique has developed from its earliest applications of mustard alkylating agents in the 1940s to being used in an increasingly valuable discipline, which is the combating of human malignancies. As the field of chemotherapy progressed, several promising natural anticancer agents were identified [253]. Although most common anticancer drugs have clinically high toxicity limits, however a more urgent need into the development of less toxic drugs is therefore a necessity. Thus, medicinal chemistry turned towards development analogs and derivatives of certain anthraquinones. Hence, the most commonly used cytotoxic anticancer agent is doxorubicin, an anthracycline, which is still amongst the most widely prescribed and effective of anticancer agents [253].

Many publications and patents have been devoted to investigate the vapor-phase oxidation of anthracene over vanadium based materials that contain additives such as iron, manganese, molybdenum, cesium, potassium, chromium and others [249, 254-256]. However, no information about the catalytic activity of vanadium pentoxide without additives is reported in the literature. Other studies and investigations have been put forth to study and investigate the use of POMs in the oxidation catalysis of anthracene such as the work of Bordoloi *et al.* [54] and Bonfranceschi *et al.* [249]. Hand-in-hand with this considerable synthetic effort, the aim of the present study is to

investigate the selective oxidation of anthracene with TBHP over pure POMs supported on novel silica aerogels.

5.4.2. Materials

AN, benzene, and toluene were obtained from Fluka, AQ and AT were from Acros Organics, methanol from Sigma Aldrich, all of which were of research grade and used as received without further purification.

5.4.3. Procedure and analysis technique

In a typical experiment, a reaction mixture of 0.0713 g (0.4 mmol) of AN dissolved in 40 ml of benzene, resulting into an AN concentration of 10 mM, are added in a 250 ml round-bottomed flask containing 0.25 g of heterogeneous catalyst (immobilized POMs onto different silica aerogel supports), to which 274 μl of 70% aqueous TBHP (2 mmol) was added and heated to 80°C (benzene boiling temperature), where it is kept at this temperature for 24 hours. During the course of this experiment, 10 μl aliquot samples were taken at different time intervals which were then diluted 100 times with methanol before being analyzed. However, dilution with benzene in this step is to be avoided to prevent the overwhelming intense solvent benzene peak. The molar ratios of AN/catalyst and TBHP/AN were maintained throughout this reaction. Scheme 5.3 schematically represents the oxidation of AN to give mainly AQ. A blank experiment carried out without catalyst, with the same composition of the reaction mixture as earlier, showed no oxidation of AN, demonstrating that a catalyst is needed for the reaction to take place.

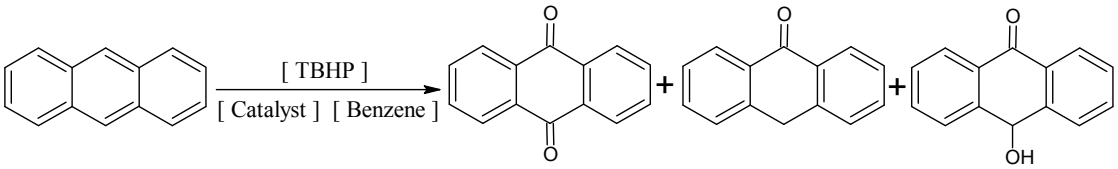

Anthracene (AN) 9,10-Anthraquinone (AQ) Anthrone (AT) Oxanthrone (O)

Major Product

Scheme 5. 3.

High-performance liquid chromatography (HPLC) analyses were recorded with a computer-controlled chromatograph supplied with a computing integrator quaternary pump high performance liquid chromatography (AGILENT 100 Series) with a diode array UV detector Discovery HSC_{18} column (250 mm × 4.6 mm, 5 μm particles, from Supelco). Mobile phase was a mixture of methanol and 10 mM phosphate buffer (82%:18% (v/v)) at a flow rate of 1 $ml.min^{-1}$. The 10 mM phosphate buffer (pH 7) prepared from the acidic solution of NaH_2PO_4 and the basic solution of Na_2HPO_4 was employed in the mobile phase in order to avoid any pH fluctuations that could affect the reactions. The AN, AQ, AT, and O were detected at 246 nm. Reaction products were identified by injection of reaction solutions containing assumed products. Based on these set of conditions, the obtained retention times for the AN, AQ, AT, O, methanol, benzene, and toluene were at ~17.1, ~8.1, ~6.5, ~3.8, ~2.7, ~5, ~6.5 min, respectively (Appendix C, Figure C.51). The retention times for AN, AQ, and AT were based on calibration curves (Appendix C, Figures C.52, C.53, C.54) that have been conducted in order to be used in the calculations of the AN conversion and AQ production later on.

5.4.4. Results and discussion

5.4.4.1. Catalysis

In previous studies, it was shown that with the $[PV_2Mo_{10}O_{40}]^{5-}$ catalyst oxygenation was possible by an initial activation of a hydrocarbon by electron transfer [257, 258]. Substrates oxygenated in this manner however included polycyclic aromatic compounds such as anthracene, which is why AN has been chosen as this thesis's study case. The use of $^{18}O_2$ and isotopically labeled POMs, as well as carrying out stoichiometric reactions under anaerobic conditions provided strong evidence for a homogeneous Mars-van Krevelen type mechanism and clear verification that precluded autooxidation and oxidative nucleophilic substitution as alternative possibilities [258].

The catalysis reactions would therefore give, in a non-selective type reaction, AQ which is the major product in addition to the by-products AT and O. However, after running the same series of reactions with these catalysts with AQ as the reactant instead of AN, which is to enable the study of the adsorption of the AQ on the surface of our catalyst, it was found that the concentrations of AQ used initially very slightly changed and therefore the effect of the adsorption of AQ on the outcome of these reactions is typically negligible. The testing for adsorption is done, since due to conservation of matter in any system, it is expected that the quantities of the remaining AN and AQ with all the by-products at the end of the reaction to be conserved. That being said, the only valid conclusion thereafter, for obtaining lower quantities in the reaction ends, would be attributed to the adsorption of rather AN on the surface of the reaction. However, testing for the adsorption of AN is quite impossible due to the circumstances of the current reaction conditions, hence the obtained results would only be monitored by the production of AQ rather than by the AN conversion.

The oxidation catalysis reactions for 10-MVPA and 11-MVPA resulted in a typical non-selective reaction where all the products after 4 hours of reaction would be present in the solution (Appendix C, Figure C.51 top). The resulting amounts of AQ produced are merely 0.109 and 1.607 mM for 10-MVPA and 11-MVPA respectively after 1 hour of reaction. Using the supported catalysts in a heterogeneous mode in the oxidation of AN reactions has significantly resulted into a highly selective type reaction giving only the desired major product AQ with essentially no appearance of any of the by-products. The amounts of AQ produced (Tables 5.4 and 5.5) have significantly increased with the best of them at 2.813 and 4.211 mM for M1-10 and E1-10 respectively in the 10-MVPA immobilized series, and in the 11-MVPA immobilized series 2.090 and 3.664 mM for M1-11 and E1-11 respectively. The highly activity especially for E1-10 and M1-10 explains why these only two catalysts, from the complete series, were chosen as the templates for the characterization of these materials in the previous sections. The trends of AQ production (Figures 5.19 and 5.20) clearly show that the most highly active two catalysts are indeed the E1-10 and M1-10.

Many conclusions may be made here based on the type of the material and the way the POMs are loaded on the silica aerogel materials. This would subsequently affect the number of active sites existing at the surface, where the reaction would take place. In general, the supported POMs onto the mesoporous silica materials have enabled them to be more dispersed and better distributed on the surface which in turn would facilitate the access of AN and thus the availability of more active sites leading to more reactions and eventually to higher activities. However E1-10, M1-10, E1-11, and M1-11 experienced the best activity out of the rest silica materials because their respective surface is not organically modified and this could help the loading of more

POM on the surface as attested by the AAS results. Therefore, fewer groups on the surface would enable more amine functionalization to the silica's surface, which would in this case enhance the loading of the POMs. In another side of the story, one can conclude that the reaction of free POMs has a less adequate environment for a high activity reaction to take place, while the supported clusters of POMs onto these mesoporous silica materials ensured a better environment for the easy access of AN.

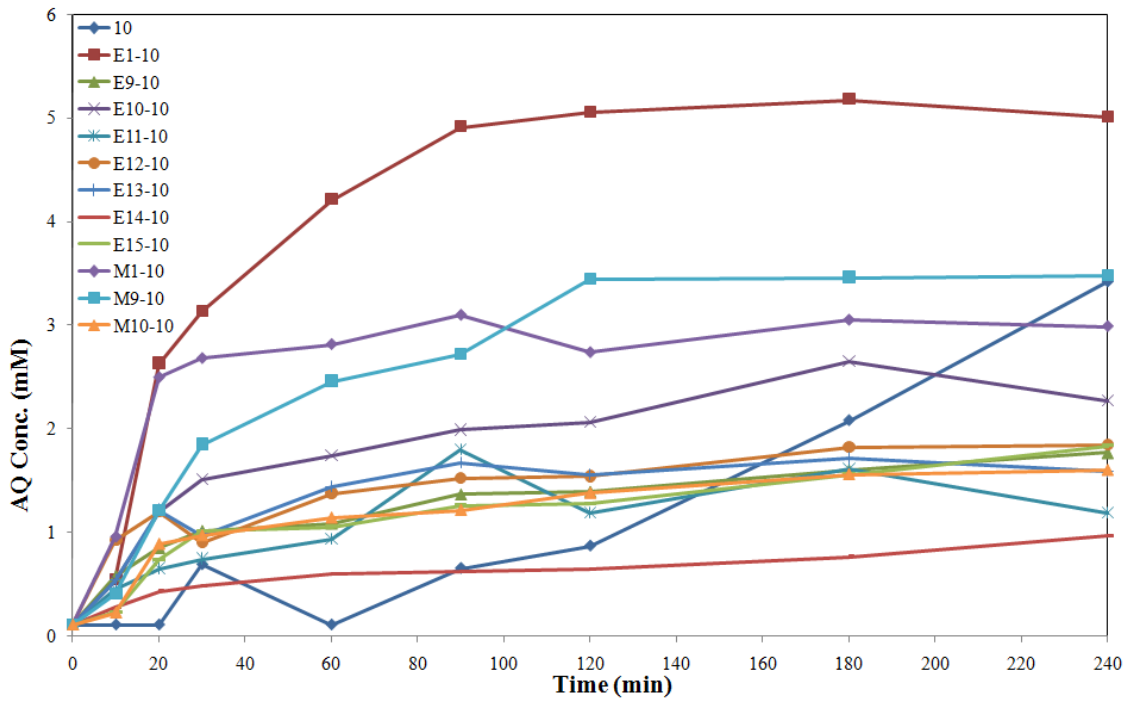

Fig. 5. 19. Anthraquinone production as a function of time with the 10-MVPA immobilized materials

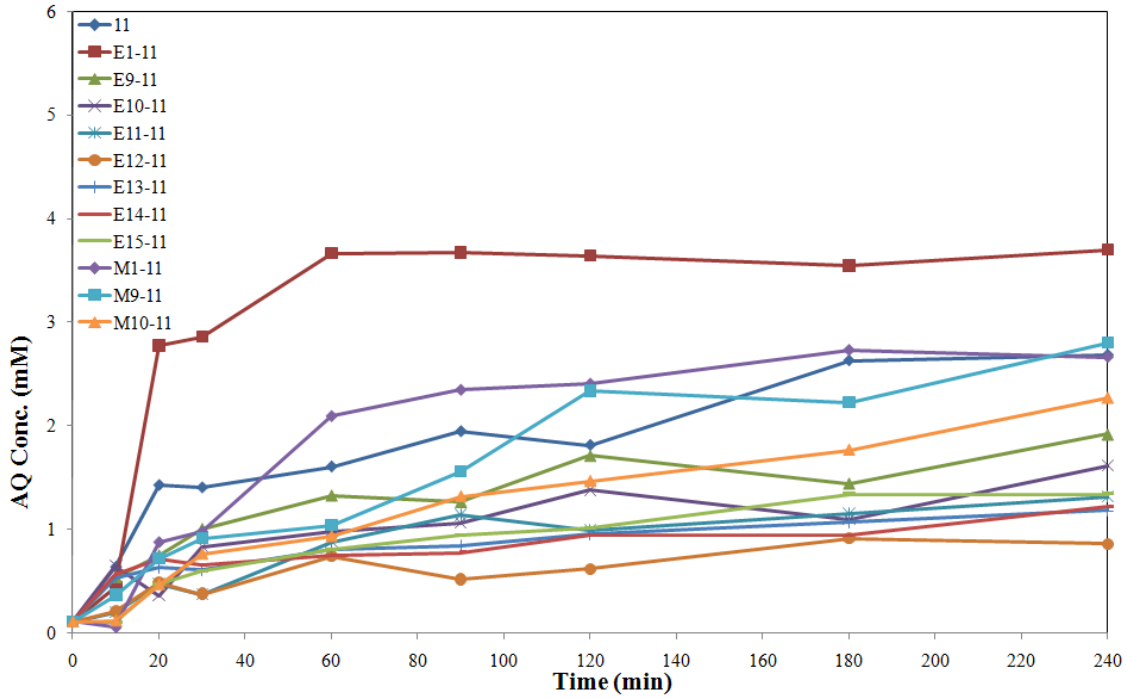

Fig. 5. 20. Anthraquinone production as a function of time with the 11-MVPA immobilized materials

Table 5. 3. Catalytic activity of 10-MVPA

Sample	AQ produced after 1h (mM)	AQ produced after 4h (mM)
10	0.109	3.417
E1-10	4.211	5.006
E9-10	1.085	1.767
E10-10	1.736	2.270
E11-10	0.932	1.186
E12-10	1.376	1.841
E13-10	1.439	1.585
E14-10	0.603	0.966
E15-10	1.055	1.837
M1-10	2.813	2.986
M10-10	2.458	3.475
M11-10	1.143	1.604

Table 5. 4. Catalytic activity of 11-MVPA

Sample	AQ produced after 1h (mM)	AQ produced after 4h (mM)
11	1.607	2.686
E1-11	3.664	3.699
E9-11	1.327	1.918
E10-11	0.980	1.612
E11-11	0.878	1.312
E12-11	0.739	0.857
E13-11	0.810	1.183
E14-11	0.754	1.217
E15-11	0.806	1.342
M1-11	2.090	2.660
M10-11	1.039	2.802
M11-11	0.936	2.272

5.4.4.2. Oxidant and solvent effects

Hydrogen peroxide is a readily available, inexpensive and benign oxidant and therefore has been targeted, since long time ago, for use as a preferred oxidant in many oxidation catalysis systems [259]. When considering biomimetic systems, for instance with iron(III) porhyrins, iron(IV)-oxo porphyrin cation radical species may be formed [260]. Moreover, some platinum based catalysts could react with hydrogen peroxide resulting into nucleophilic species capable of oxygen transfer to alkenes with electron withdrawing moieties [261]. The original use of POMs in hydrogen peroxide oxidation dates way back to the mid-late 1980's when Ishii and co-workers [262] described the epoxidation of alkenes by $[PW_{12}O_{40}]^{3-}$ in biphasic media. This research and many others conducted later have came to the conclusion that this POM under the given reaction condition was transformed to $[PO_4(WO(O_2)_2)_4]^{3-}$ compound, which was previously discovered and used for epoxidation by Venturello and co-workers [263]. The realization that $[PW_{12}O_{40}]^{3-}$ was not stable to hydrogen peroxide, conducted in an

aqueous solution, led to three conclusions: (i) The Keggin type POMs are thought to be unstable to aqueous H_2O_2, and are poor compounds for activation of H_2O_2. (ii) The analysis of the POM should be carefully examined and inspected, especially in the identification of the actual catalyst [244]. (iii) This is a very clear and valid explanatory basis for the results obtained of the oxidation catalysis reactions conducted in this research.

Although these conclusions seem quite reasonable and inclusive, it should be noted nevertheless that the stability of the Keggin type POMs depends on the solvent, as the trends formulated in previous sections. There are certain solvents where the stability would be much higher. Stability as well depends on the specific POM that is being used [244]. Furthermore, Keggin type POMs do have some catalytic activity for easy to oxidize substrates such as those investigated in this thesis. The realization that Keggin type POMs are inherently unstable to hydrogen peroxide has led to the use of TBHP instead. The stability of the POMs can be measured by using a combination of techniques including elemental analysis (AAS), FTIR, XRD and kinetic analysis. With a combination of these methods, already presented in previous sections, it is clear that the catalysts appear to be stable and much more active under reaction conditions when TBHP is used as the oxidant compared to the instability and lower activity of the Keggin type species with hydrogen peroxide. It remains therefore a very significant challenge to elucidate the mechanism of the more reactive POMs and the discovery of more reactive compounds is certainly a surplus [244].

The catalyst E1-10, with its highest activity out of the whole materials series, was chosen as the template model for the testing for the different variables that could affect the reaction. The effect of the oxidant is tested by utilizing hydrogen peroxide

instead of TBHP for the reaction, however the results are self-explanatory showing a drastic decrease of the amounts of produced AQ from 5.014 mM in TBHP to 0.364 mM after 1 hour. Possible conclusions on this behavior have been already been suggested. Now moving on to test for the solvent effect, which as explained earlier would have a significant effect on both the stability and structure of the catalyst being used and this would directly affect the activity of these catalysts in different solvent media. The reactions conducted in benzene (B) as the solvent resulted into 5.014 mM as the amount of AQ produced after 1 hour, it was observed that by utilizing toluene (T) in different proportions as the solvent did in fact have an effect on the outcome of these reactions. The 75%:25% benzene to toluene ratio had a very similar decreased amount of AQ formation as that of 50:50 ratio, however this amount decreased even further for the B25:T75 ratio and reached a 1.884 mM of AQ produced for when the toluene was solely used as the solvent. Another conclusive argument about the preferable use of benzene as the solvent instead of any other solvent such as toluene is because the oxidation catalysis reactions are not selective for AQ in the case of toluene [54]. This clearly shows the effect of the solvent on the conducted reactions due to many reasons and explanations, explained earlier, that are now rationally verified.

Table 5. 5. Effect of oxidant and solvent on the catalytic activity of E1-10

Sample	Variable	AQ produced after 1h (mM)	AQ produced after 4h (mM)
E1-10	TBHP	5.014	6.090
E1-10	H_2O_2	0.364	0.472
E1-10	B	5.014	6.090
E1-10	B75:T25	3.553	2.721
E1-10	B50:T50	3.552	5.736
E1-10	B25:T75	3.257	3.316
E1-10	T	1.884	3.903

5.4.4.3. Catalyst reuse

The aim of transforming these catalyst into using them on suitable supports and conducting these oxidative reactions in heterogeneous media was to recycle and regenerate these catalysts in order to reuse them more than once, for industrial and ecological purposes. Again by using E1-10 for the first reaction, it resulted into 3.131 mM of AQ produced after 1 hour, after filtration and washing of the reaction mixture with toluene, the same used catalyst was regained and used for a second reaction resulting into 1.811 mM as the amount of AQ produced, and again was recycled and used for a third reaction giving now 0.675 mM of AQ produced. The results obtained clearly emphasize that these immobilized POMs have been successfully regenerated and used several times, where the activity shown after three uses was always higher than the unsupported bulk POMs. Although the amounts of AQ produced were not retained as is for the reuse reactions is certainly not a problem at all, many explanations would be put forth why these catalysts were not as active as the time where they are used for the first time. This could possibly be due to the loss of some of the quantity of the amount used each time, which is the case, since it was difficult to obtain all the used amount of the catalyst due to experimental drawbacks of simple filtration.

Table 5. 6. Catalytic activity for the reuse of E1-10

Sample	Reaction #	AQ produced after 1h (mM)	AQ produced after 4h (mM)
E1-10	1	3.131	3.651
E1-10	2	1.811	2.299
E1-10	3	0.675	1.122

5.5. Conclusion

Consequently, to conclude the picture that has been tailored in this chapter, highly active molybdovanadophosphoric acids have been successfully dragged from homogeneous based reactions into heterogeneous mediated oxidation catalysis, where it has been exploited and investigated. The advantage of using supported catalysts as previously explained is the capability of recycling the catalyst and reusing it all over again for economical goals, as well as resulting into the 100% selectivity for AQ, the major product, rather than obtaining any of the other by-products would further assert on the purposes achieved. Moreover, the supported POMs showed significantly higher AQ formation and subsequently were more active catalysts than the neat POMs. Although the oxidant and solvent change would have an effect on the outcome of these reactions and the activity of these catalysts, however the correct use of reaction conditions shouldn't limit the user from obtaining the desired activity from the use of these heterogeneous based catalysts. This chapter has fully explained the immobilization technique and the respective characterization of the different materials thus obtained. These supported catalysts synthesized were tested for catalysis of the oxidation of AN reaction and resulted into higher activities and enhanced selectivities, which again once more reassure that these POMs were successfully immobilized onto the mesoporous silica aerogel materials.

CHAPTER SIX

CONCLUSION

Surface organically-modified silica aerogels were successfully synthesized by following the sol-gel process and drying under supercritical carbon dioxide conditions. These silica materials were first characterized by FTIR spectroscopy, the results of which, has enabled the identification of the different functional groups on the surface due to the different organic groups functionalized on different silica surfaces. The FTIR spectra showed that the general structures of the obtained silica aerogel materials are very relatable with peaks that are characteristic of such materials. Since the aim of this thesis is to load two active POMs on the surface of these materials, then there was a need to test the physical and chemical properties of the surfaces onto which these POMs will be impregnated. Hence, liquid nitrogen physisorption experiments were conducted to show the different aspects of the surface structure of these materials. This allowed for the surface characterization and study of these materials by resulting into information about the porous structure and nature of these materials, it also allowed for qualifying the type, shape and nature of these pores. In addition the specific surface areas, total pore volumes, and mesoporosity percentage were successfully calculated using the BET technique. Conclusively, these organo-modified silica aerogels had interesting properties of very high specific surface areas, and relatively high pore volumes which would eventually aid the loading of the POMs on its surface. Moreover, all of the synthesized silica aerogels had a very nice mesoporous character with pore structures that could vary from one material to another depending on the type of the organic group present on the surface. The synthesis and characterization of such silica materials with

high specific surface areas and pore volumes made them very good candidates for hosting and acting as supports for the immobilization of two active polyoxometalates.

The synthesis of two polyoxometalates 10-MVPA and 11-MVPA has been effectively achieved based on previous synthetic routes to a very high reproducibility end. These two POMs were chosen to be used as the catalysts in the reaction of anthracene oxidation to anthraquinone and other by-products. This could be easily done in homogeneous type reactions. However, the aim here is to transform these reactions into heterogeneous based media where the POMs will be readily available for regeneration and recycling, which would enhance the productivity and ultimately the economic and production-cost would surely benefit from that. The POMs were immobilized onto the synthesized silica aerogel materials by first functionalizing their surfaces by amino groups, which essentially enhance the POM loading, and then the immobilization took place under reflux condition enabling the production of supported These ecologically benign material were tested for reactivity in a template reaction which is the oxidation of AN to AQ. The results of which made successful the 100% selectivity to AQ with interestingly high activity compared to free POMs. Many variables that could affect the reaction were tested such as the change of oxidant or solvent. Both of these variables appeared to have an effect on the outcome of the reactions, where the use of another oxidant or solvent lowered the material's effective activity and the use of other solvents did not allow for the selectivity that has been desired. However, our study suggests that more complicated kinetics and mechanisms are being followed here, and yet as such remains inconclusive.

Over the last two decades, there has been a tremendous rush in the use of POMs in oxidation catalysis. Future objectives and explorations have to be subjected

into deciphering the mechanistic understanding that could lead to new “green” syntheses. Unfortunately, only a few of the POM structure types have been investigated in the framework of oxidation catalysis. Since it is expected that structure-activity relationships would have a significant effect, yet such understanding is still in the developing stages. Therefore, the field of catalytic oxidation with POMs has barely seen any bloom. Subsequently, this current investigation has been a very valid attempt into broadening the scope of POM application into heterogeneously based reactions by developing these new catalyst systems with very special physicochemical properties. Moreover the never-ending exploitation of these newly developed catalytic systems in applications such as the prominent photocatalysis degradation, which is one of the research studies currently undertaken at our laboratory. Most important, however, is that POMs along with the support of these clusters onto mesoporous silica aerogel materials promise to be a productive area for chemists to explore well in the 21st century. Thus much blooming in this field is expected and much more innovations are yet to come.

APPENDIX A

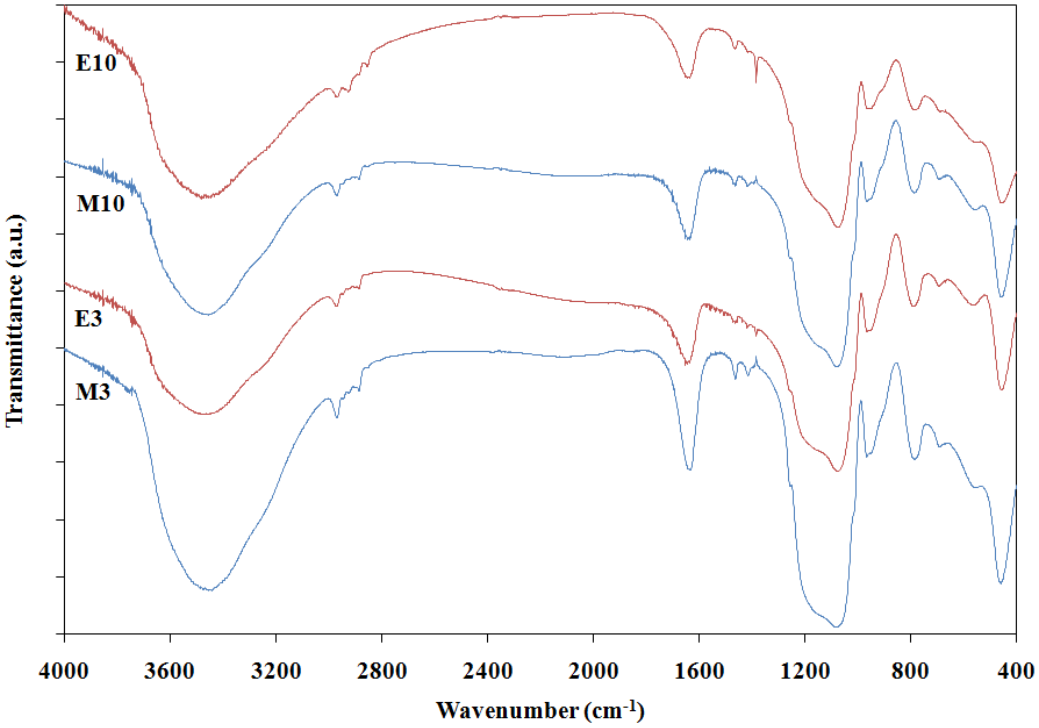

Fig. A. 1. FTIR spectra of the ethyl-modified silica aerogels

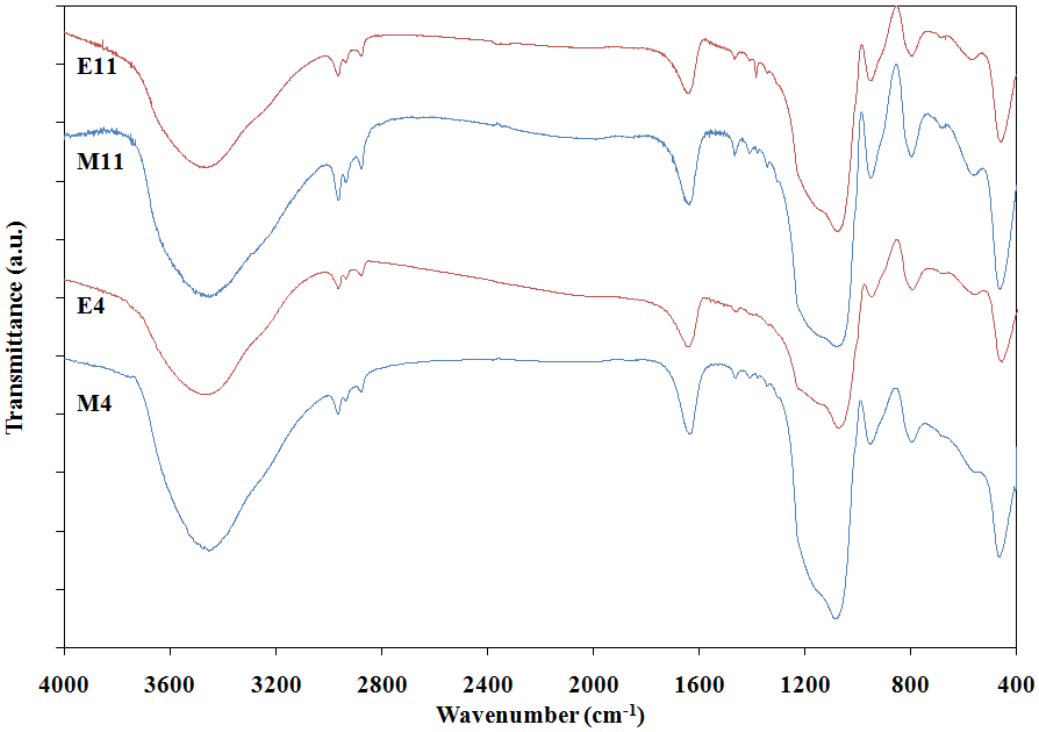

Fig. A. 2. FTIR spectra of the propyl-modified silica aerogels

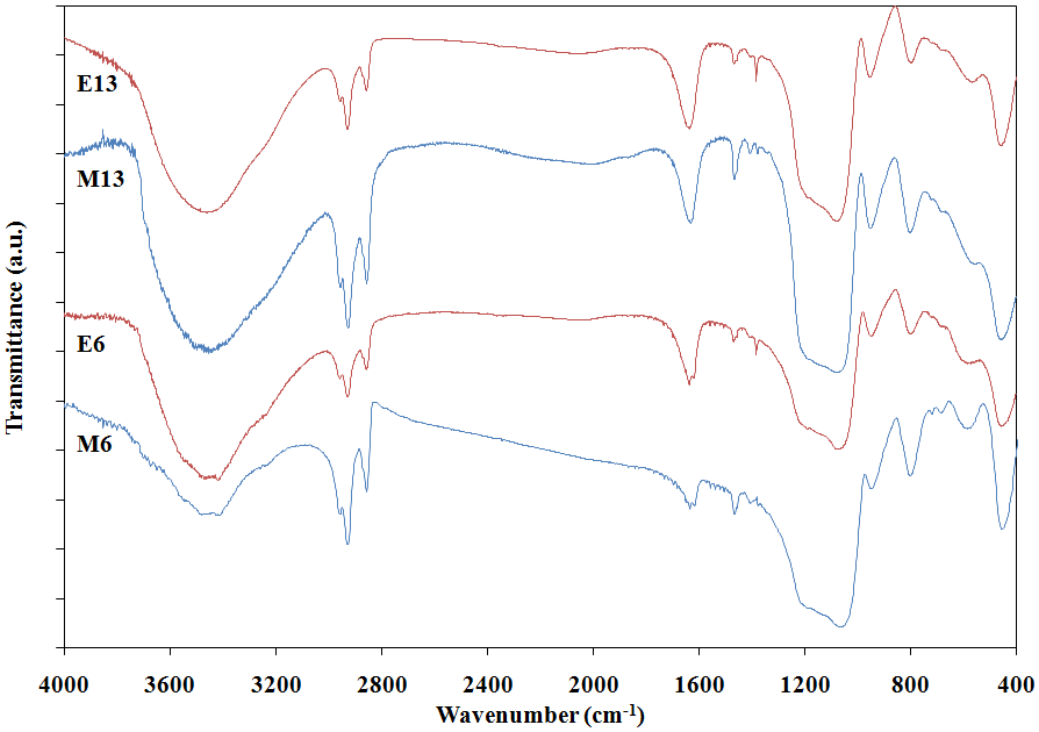

Fig. A. 3. FTIR spectra of the octyl-modified silica aerogels

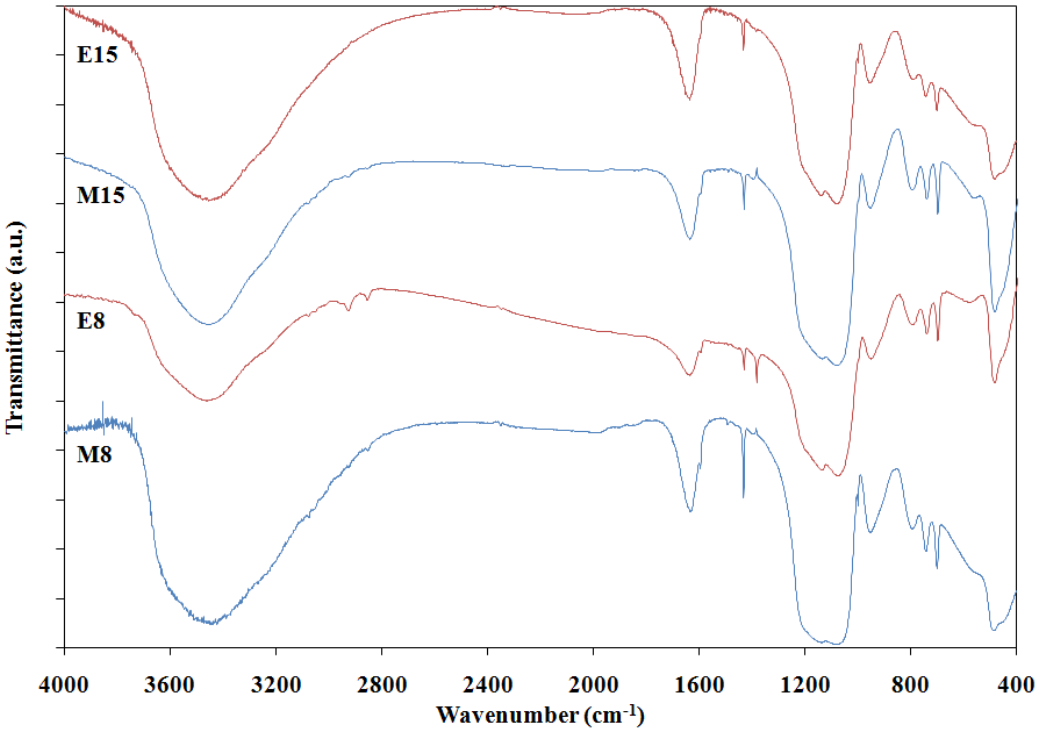

Fig. A. 4. FTIR spectra of the phenyl-modified silica aerogels

Table A. 1. Characteristic vibration frequencies (cm^{-1}) in FTIR spectra of synthesized silica aerogels

M1	E1	M2	E2	M9	E9	M3	E3	M10	E10	M4	E4	M11	E11	Type of vibration	Structural unit	Ref.
3451	3472	3450	3457	3462	3464	3455	3470	3457	3475	3455	3465	3451	3471	O-H and SiO-H	H-O-H…H_2O and ≡SiO-H…H_2O	[5]
		2977	2977	2979	2977	2969	2971	2969	2970	2964	2965	2962	2964	ν_s C-H	$-CH_3$	[222]
						2946	2946	2946						ν_{as} C-H	$-CH_2$	[222]
		2924		2930		2925	2924	2923	2927	2936	2936	2933	2935	ν_{as} C-H	$-CH_2$	[222]
						2885	2885	2886	2885	2876	2877	2876	2876	ν_{as} C-H	$-CH_3$	[222]
		2857		2854	2857	2855		2854	2855					ν_s C-H	$-CH_2$	[222]
1634	1653	1645	1654	1636	1642	1636	1652	1634	1635	1636	1646	1636	1637	δ H-O-H	H-O-H	[227]
						1462	1464	1464	1464	1466	1465	1466	1466	δ_{as} C-H δ_s C-H	$-CH_3$ $-CH_2$	[222]
		1407	1413	1409	1413	1415	1418	1418	1415	1406	1410	1409	1408	δ_{as} C-H	Si-R	[227]
1384		1384	1384	1385	1384	1384	1384	1385	1384	1379		1380	1384	δ_s C-H	$-CH_2$	[222]
										1341	1341	1341	1341	δ $-CH_2-$	R	[235]
		1279	1280	1279	1280	1258	1256	1258	1258					δ_s C-H	Si-R	[227]
~1200	~1200	~1170	~1160	~1173	~1154	~1170	~1156	~1157	~1176	~1185	~1160	~1160	~1157	ν_{as} Si-O-Si (LO mode)	≡Si-O-Si≡	[231]
1095	1089	1076	1073	1076	1078	1080	1076	1078	1077	1084	1075	1075	1076	ν_{as} Si-O-Si (TO mode)	≡Si-O-Si≡	[231]
961	965	951	951	951	951	965	964	966	952	952	951	950	951	ν_β Si-O	≡Si-OH	[229]
						~910	~910	~910	~910	~910	~910	~910	~910	ν_β Si-O	Free $Si-O^-$	[228]
		834	834	831	834									ν Si-C	Si-R	[227]
799	800	800	799	800	800	785	788	785	783	796	795	798	793	ν_s Si-O	≡Si-O-Si≡	[5]
						692	693	692	698		682	685	682	ν_s Si-O-Si	≡Si-O-Si≡	[229]
~560	558	555	556	557	558	556	565	554	554	561	557	562	569	ν Si-O	SiO_2 defects	[5]
469	467	453	456	459	455	459	453	456	455	466	459	463	459	δ O-Si-O	-O-Si-O-	[230]

M5	E5	M12	E12	M6	E6	M13	E13	M7	E7	M14	E14	M8	E8	M15	E15	Type of vibration	Structural unit	Ref.
3458	3461	3468	3461	3450	3453	3454	3459	3457	3471	3474	3457	3450	3458	3458	3455	O-H and SiO-H	H-O-H…H_2O and ≡SiO-H…H_2O	[5]
								2964		2964	2965					ν_s C-H	Si-CH=CH_2	[232]
2960	2959	2960	2957	2959	2959	2957	2960									ν_s C-H	-CH_3	[222]
2932	2932	2933	2929	2930	2927	2926	2933						2927	2927		ν_{as} C-H	-CH_2	[222]
2875	2879	2875	2875	2875	2875	2875	2875			2866						ν_{as} C-H	-CH_3	[222]
			2858	2858	2857	2857		2854			2857		2855	2857		ν_s C-H	-CH_2	[222]
1636	1635	1636	1653	1636	1636	1632	1635	1636	1637	1635	1640	1634	1636	1637	1634	δ H-O-H	H-O-H	[227]
								1605		1605						ν_β C=C	Si-CH=CH_2	[232]
												1596	1596	1598	1598	ν_β C=C	Si-ph	[232]
												1492		1491		ν C=C + δ C-H in plane	Si-ph	[232]
1469	1471	1469	1468	1469	1469	1468	1471									δ_{as} C-H	-CH_3	[222]
												1431	1432	1432	1432	ν C=C + δ C-H in plane. 2ν Si-C	Si-ph	[226, 232]
								1413	1413	1413	1413					δ C-H in plane	Si-CH=CH_2	[232]
1402		1401	1405	1408	1410	1406	1399									δ_{as} C-H	Si-R	[227]
1385	1384	1384	1384	1385	1384	1379	1384		1384	1385	1384	1385	1384	1385	1384	δ_s C-H	-CH_2	[222]
1369	1369	1369	1369				1369									δ_s C-H	-CH_3	[222]
1336	1340	1336	1337			1341	1337									δ -CH_2-	R	[235]
								1278	1278	1278	1278					δ_s C-H	Si-R	[227]
~1180	~1180	~1180	~1195	~1192	~1194	~1195	~1173	~1176	~1160	~1170	~1160	1138	1137	1136	1136	ν_{as} Si-O-Si (LO mode)	≡Si-O-Si≡	[231]
1080	1076	1078	1080	1067	1074	1082	1079	1080	1078	1083	1078	1082	1078	1082	1081	ν_{as} Si-O-Si (TO mode)	≡Si-O-Si≡	[231]
												999	1000	1000	999	ν_s C=C	Si-ph	[233]
952	951	953	954	952	948	951	952	955	958	955	954	951	953	955	952	ν_β Si-O	≡Si-O	[229]
~910	~910		~910		~910	~910	~910				~910				~910	ν_β Si-O	Free Si-O^-	[228]
837	840	837		837			837									ν Si-C	Si-R	[227]
799	799	799	798	805	799	802	795	783	787	784	782	793	796	796	792	ν_s Si-O	≡Si-O-Si≡	[5]
												742	742	742	742	$\omega_{\delta,\gamma}$ C-H	Si-ph	[232]
736	739	740	723	723	723	723	735									*r* CH_2	-CH_2-	[222]
												700	700	700	700	*Φ* C-H	Si-ph	[226]
			682	688	685	685										ν_s Si-O-Si	≡Si-O-Si≡	[229]
								536	540	536	539					γ H	Si-CH=CH_2	[227]
561	580	573	568	590	574	561	560					565	582	559	561	ν Si-O	SiO_2 defects	[5]
												486	486	485	483	*Φ* C-H	Si-ph	[226]
466	462	466	459	458	458	460	458	459	459	459	456	448	~460	~450		δ O-Si-O	-O-Si-O-	[230]

ν, stretching vibration; ν_s, symmetric stretching vibration; ν_{as}, antisymmetric stretching vibration; δ, deformation vibration; δ_s, symmetric deformation vibration (bending); δ_{as}, antisymmetric deformation vibration (bending); ν_β, in-plane stretching vibration; *Φ*, out-of-plane ring deformation vibration; $\omega_{\delta,\gamma}$, in-phase out-of-plane wagging; *r*, rocking; γ, out-of-plane deformation vibration; LO, longitudinal optical; TO, transversal optical.

APPENDIX B

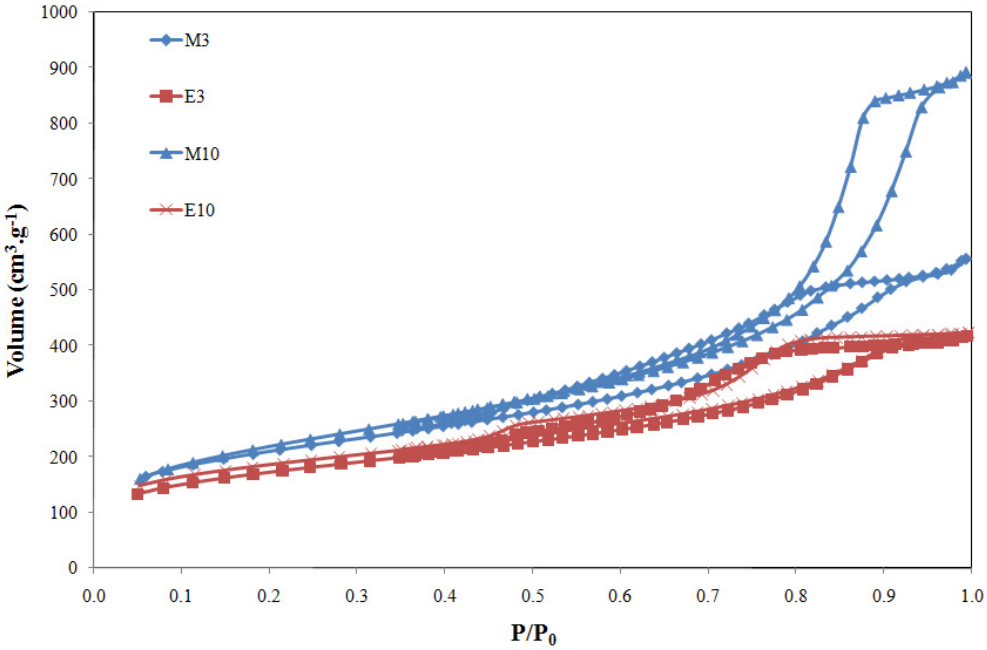

Fig. B. 1. Nitrogen adsorption/desorption isotherms of the ethyl-modified silica aerogels

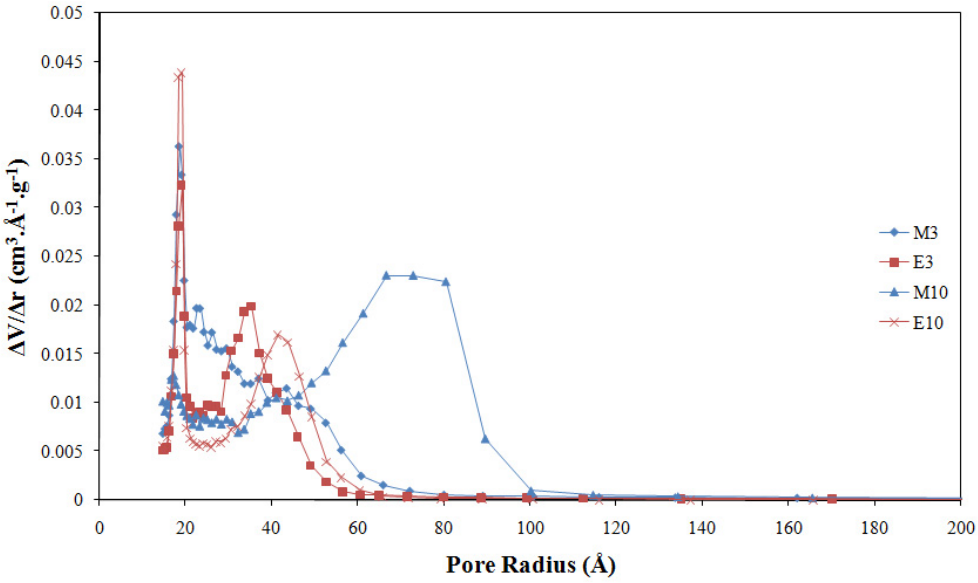

Fig. B. 2. Pore size distribution of the ethyl-modified silica aerogels

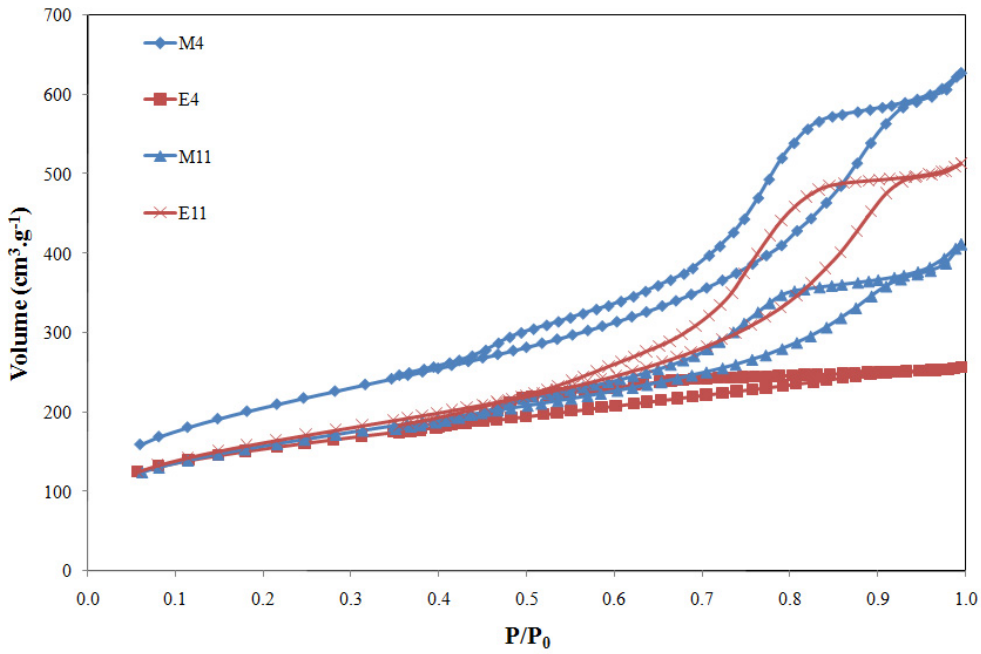

Fig. B. 3. Nitrogen adsorption/desorption isotherms of the propyl-modified silica aerogels

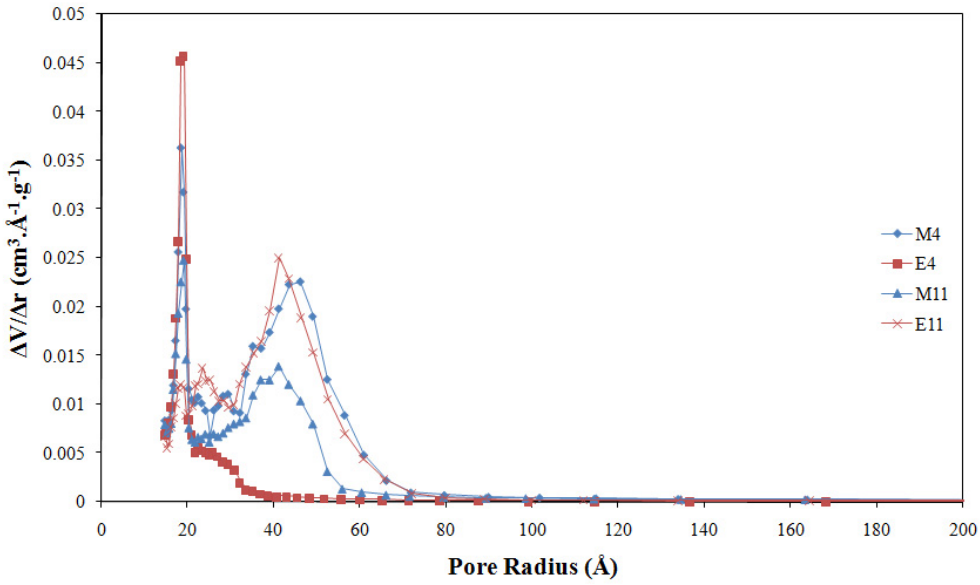

Fig. B. 4. Pore size distribution of the propyl-modified silica aerogels

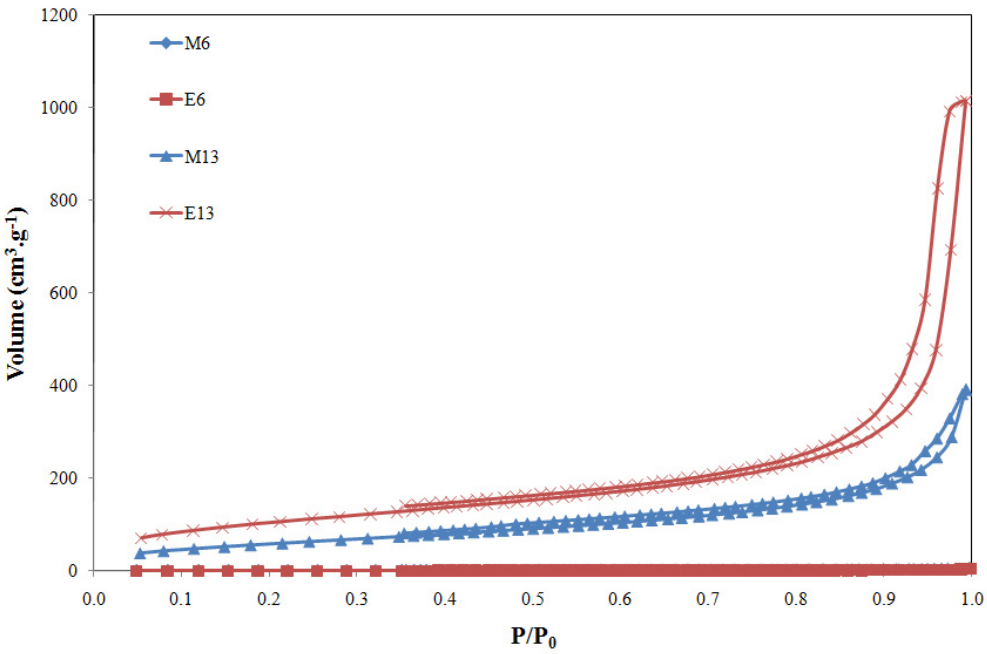

Fig. B. 5. Nitrogen adsorption/desorption isotherms of the octyl-modified silica aerogels

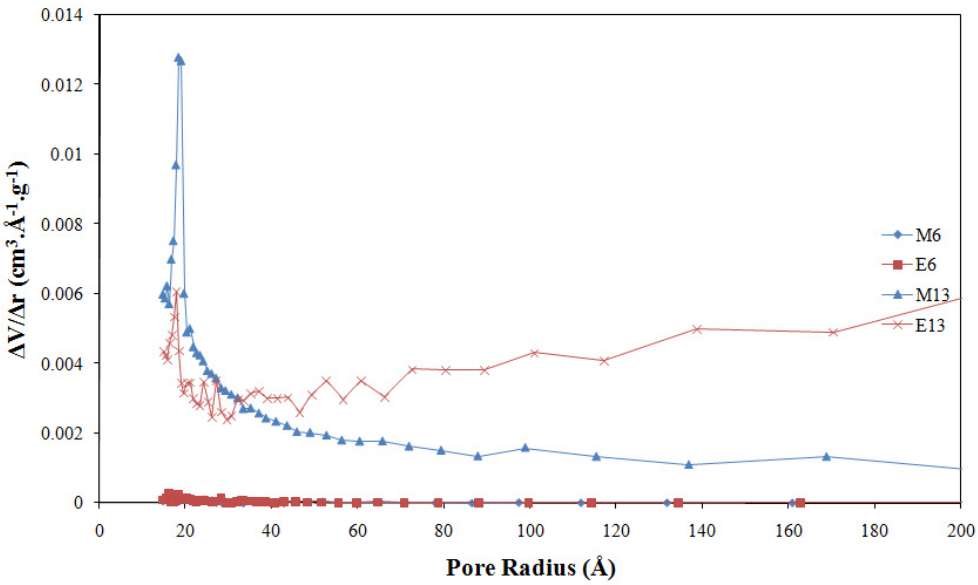

Fig. B. 6. Pore size distribution of the octyl-modified silica aerogels

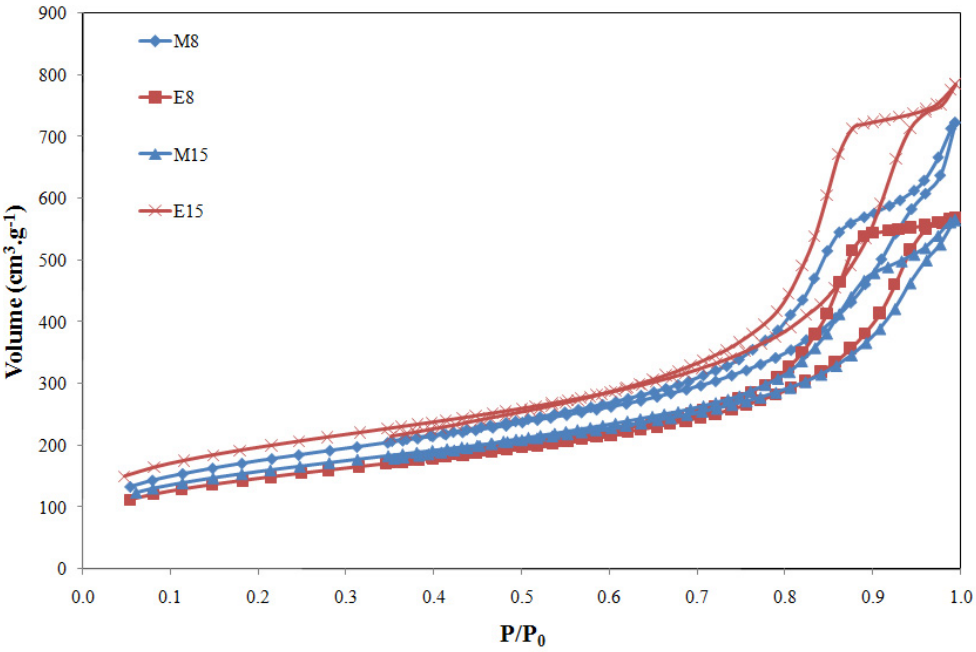

Fig. B. 7. Nitrogen adsorption/desorption isotherms of the phenyl-modified silica aerogels

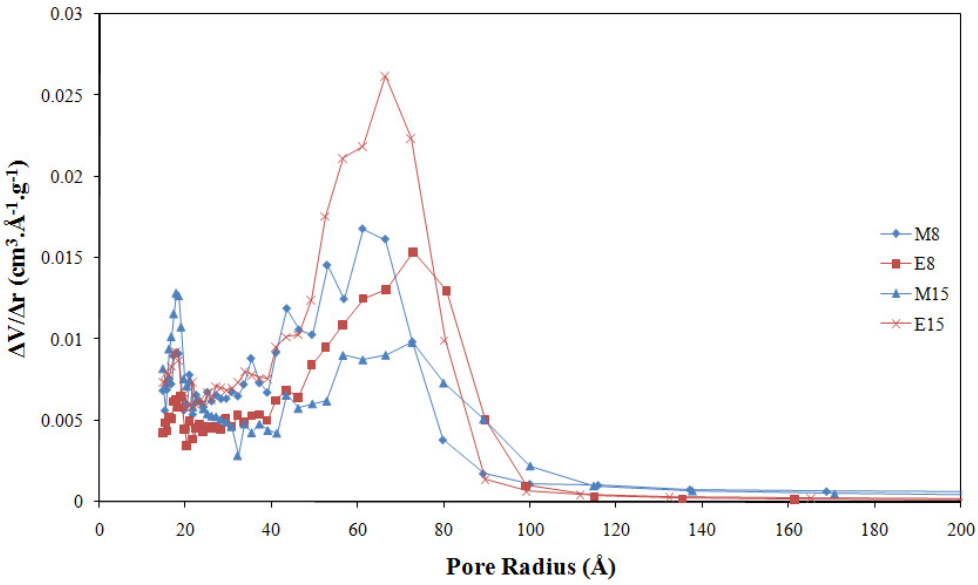

Fig. B. 8. Pore size distribution of the phenyl-modified silica aerogels

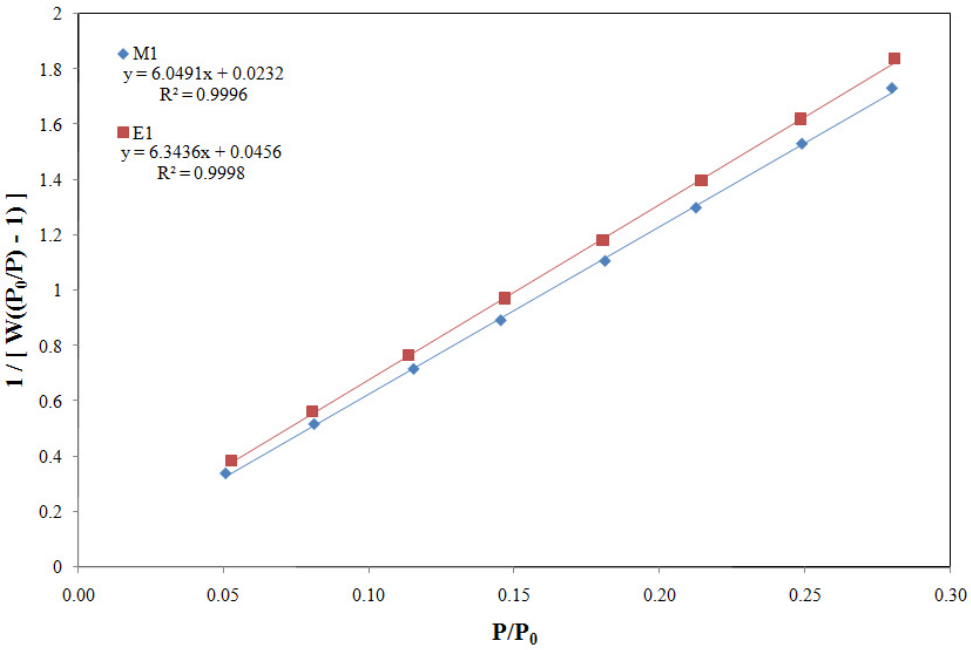

Fig. B. 9. BET plots of the silica aerogels from TMOS and TEOS

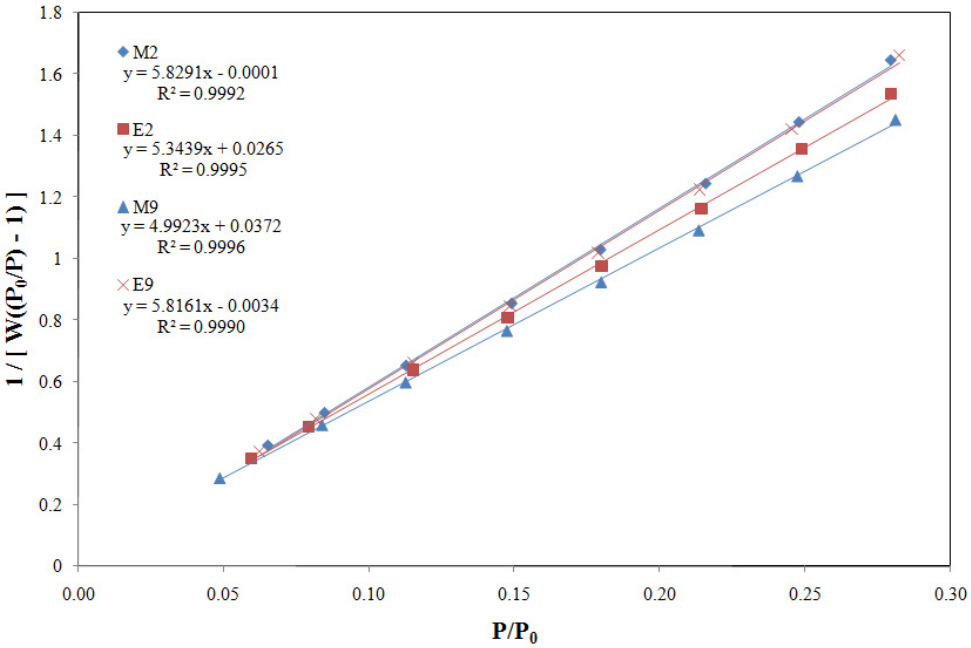

Fig. B. 10. BET plots of the methyl-modified silica aerogels

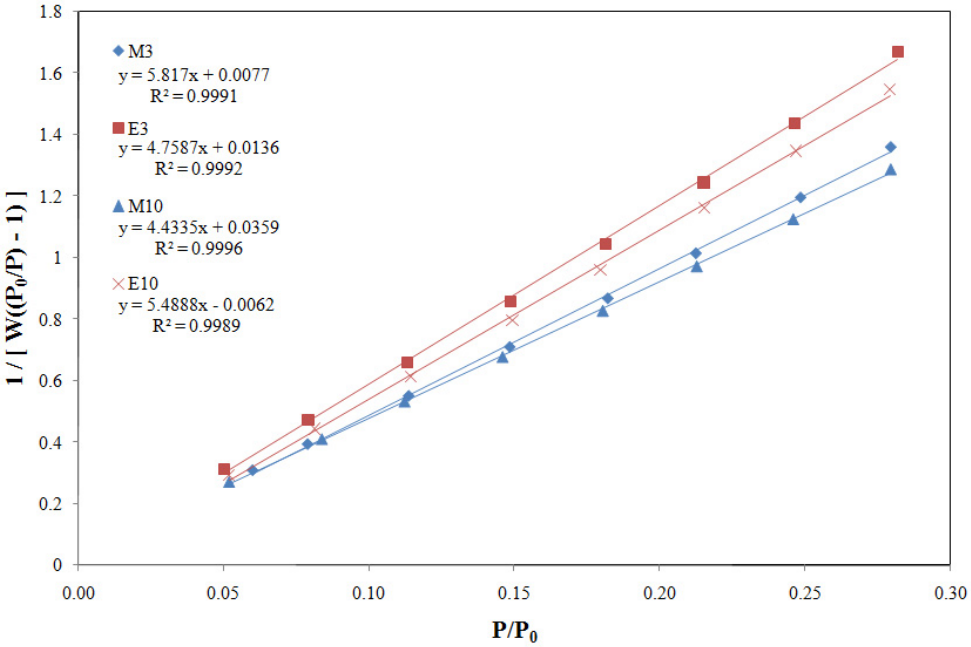

Fig. B. 11. BET plots of the ethyl-modified silica aerogels

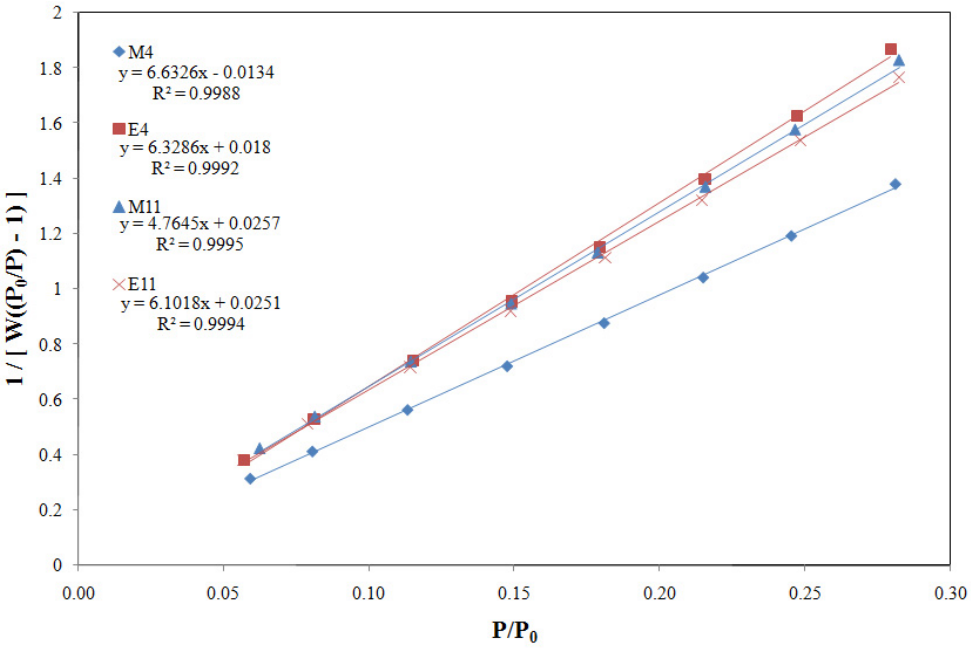

Fig. B. 12. BET plots of the propyl-modified silica aerogels

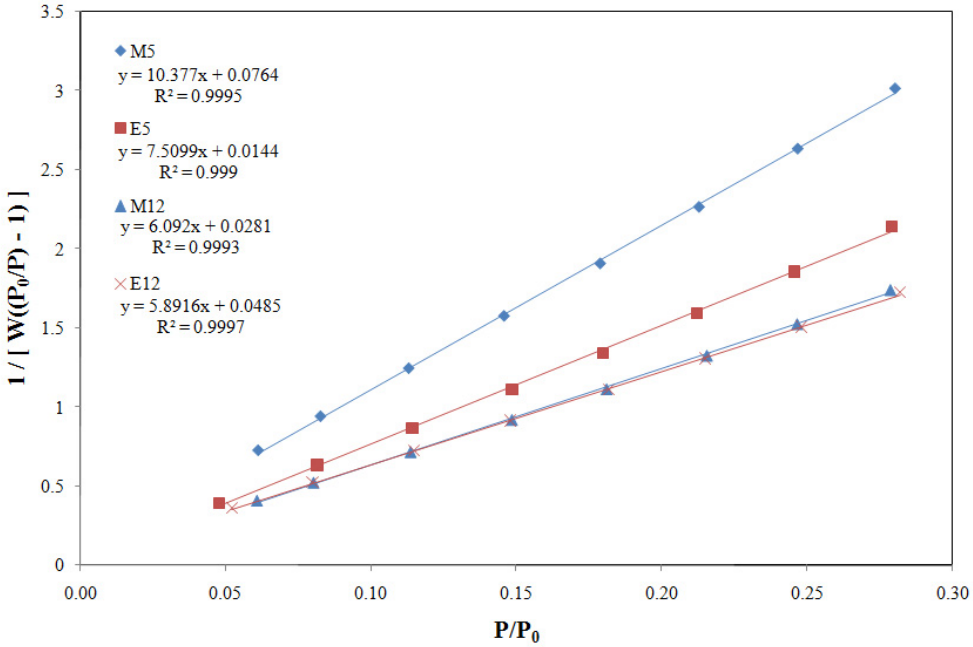

Fig. B. 13. BET plots of the iso-butyl-modified silica aerogels

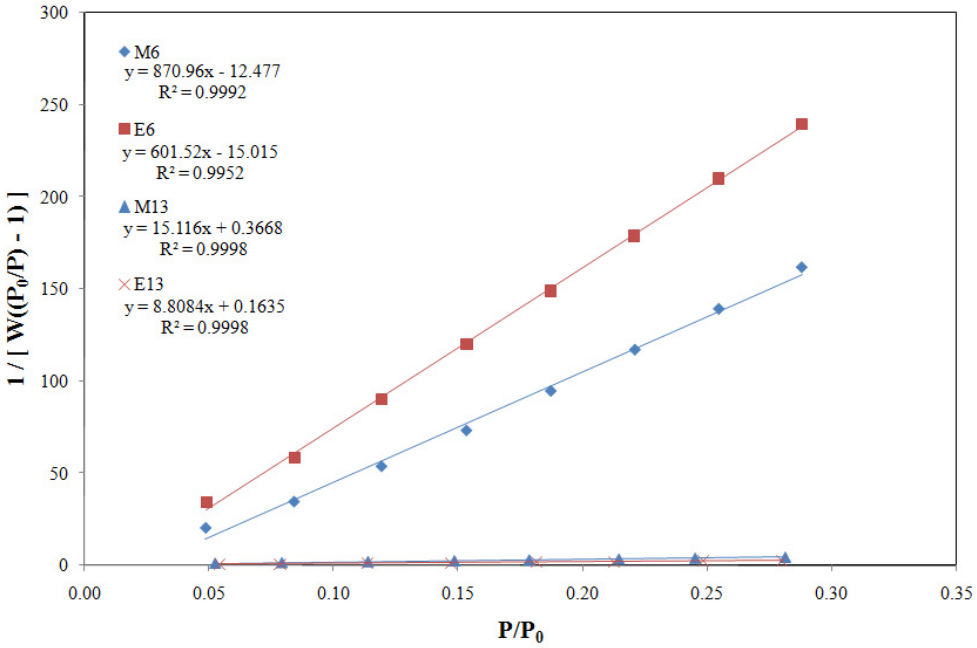

Fig. B. 14. BET plots of the octyl-modified silica aerogels

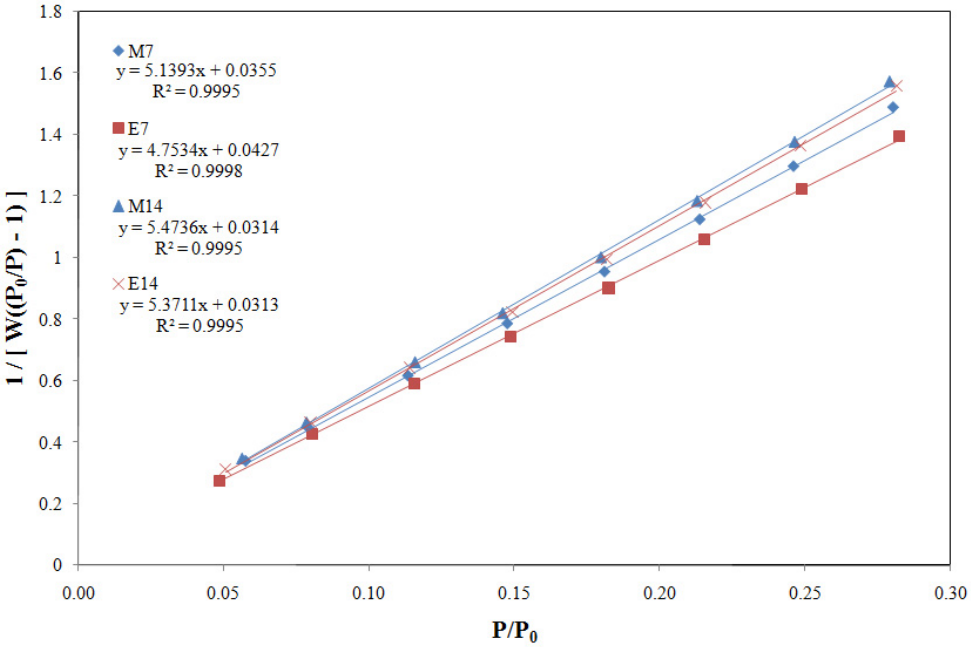

Fig. B. 15. BET plots of the vinyl-modified silica aerogels

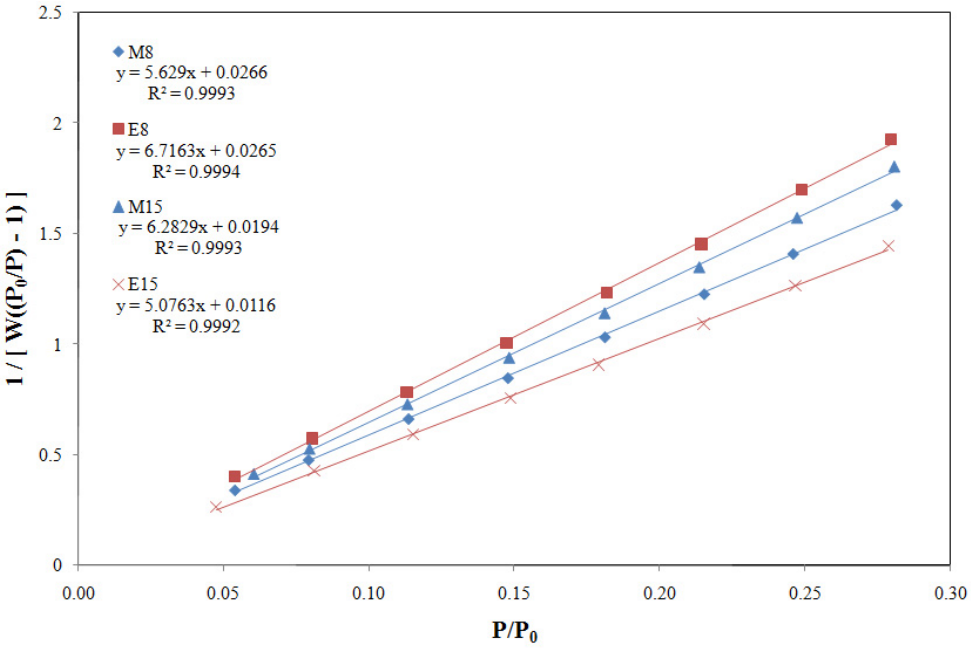

Fig. B. 16. BET plots of the phenyl-modified silica aerogels

APPENDIX C

Table C. 1. Physicochemical properties of the different immobilized materials

Sample	Specific surface area ($m^2.g^{-1}$)	Total pore volume ($cm^3.g^{-1}$)	Volume of mesopores ($cm^3.g^{-1}$)	Volume of micropores ($cm^3.g^{-1}$)	Maximum pore radius (Å)
M1	574	1.31	1.16	0.15	72.7
M1-N	277	1.23	1.23	0.00	89.6
M1-10	267	0.87	0.84	0.03	80.3
M1-11	243	0.82	0.79	0.03	80.0
E1	545	0.94	0.82	0.12	46.1
E1-N	310	1.55	1.55	0.00	117.2
E1-10	230	0.93	0.91	0.02	101.1
E1-11	219	0.90	0.89	0.01	101.2
M9	693	1.24	1.02	0.22	61.1
M9-N	357	1.41	1.41	0.01	101.3
M9-10	227	0.77	0.75	0.02	89.4
M9-11	209	0.76	0.76	0.00	80.5
E9	599	0.62	0.30	0.32	18.4
E9-N	244	0.77	0.75	0.02	80.1
E9-10	187	0.59	0.57	0.02	80.3
E9-11	165	0.57	0.56	0.01	79.7
M10	779	1.38	1.12	0.26	66.5
M10-N	375	1.17	1.13	0.04	72.8
M10-10	222	0.67	0.65	0.02	61.0
M10-11	197	0.64	0.63	0.01	66.0
E10	635	0.66	0.35	0.31	19.0
E10-N	325	0.85	0.82	0.03	56.7
E10-10	189	0.51	0.49	0.02	56.2
E10-11	210	0.57	0.55	0.02	49.0
E11	568	0.79	0.61	0.18	41.1
E11-N	395	1.09	1.05	0.04	60.9
E11-10	311	0.71	0.66	0.05	52.5
E11-11	260	0.62	0.58	0.04	49.2
E12	586	0.79	0.60	0.20	35.3
E12-N	388	0.86	0.81	0.04	46.2
E12-10	232	0.48	0.44	0.04	33.7
E12-11	263	0.54	0.50	0.04	37.0
E13	388	1.57	1.44	0.13	72.5
E13-N	164	1.59	1.58	0.01	99.9
E13-10	224	0.75	0.72	0.03	89.5
E13-11	213	0.72	0.70	0.02	89.5
E14	645	1.06	0.83	0.24	66.4
E14-N	313	1.08	1.06	0.02	89.7
E14-10	130	1.10	1.09	0.01	89.2
E14-11	126	0.99	0.98	0.01	79.6
E15	685	1.22	1.02	0.20	66.3
E15-N	535	1.30	1.30	0.00	72.5
E15-10	220	0.72	0.69	0.03	66.4
E15-11	193	0.65	0.64	0.01	72.3

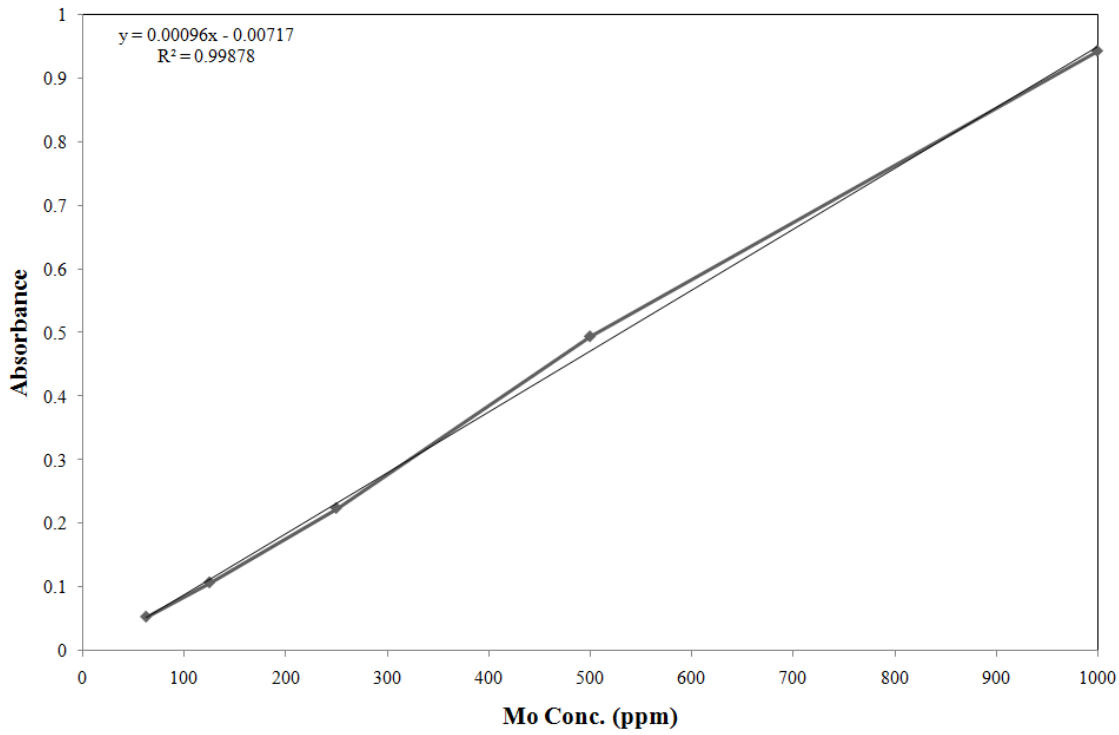

Fig. C. 1. Calibration curve for Mo AAS

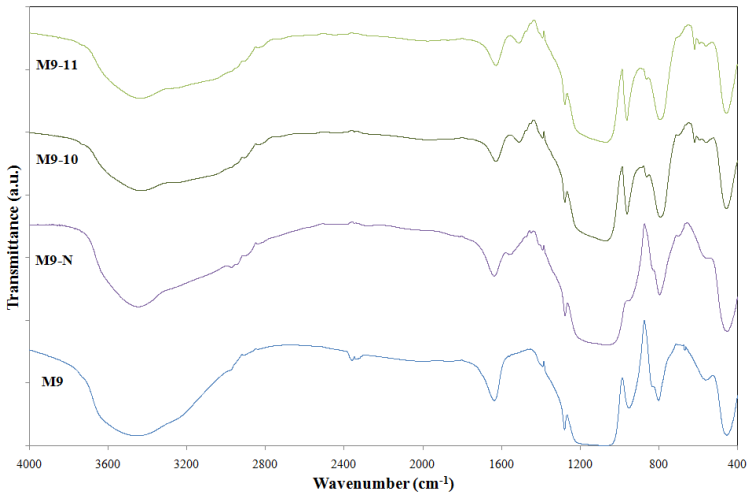

Fig. C. 2. FTIR spectra of the M9 immobilized materials

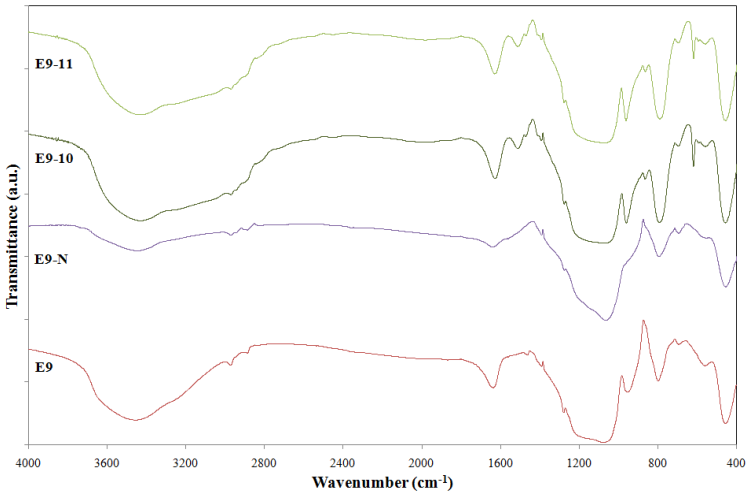

Fig. C. 3. FTIR spectra of the E9 immobilized materials

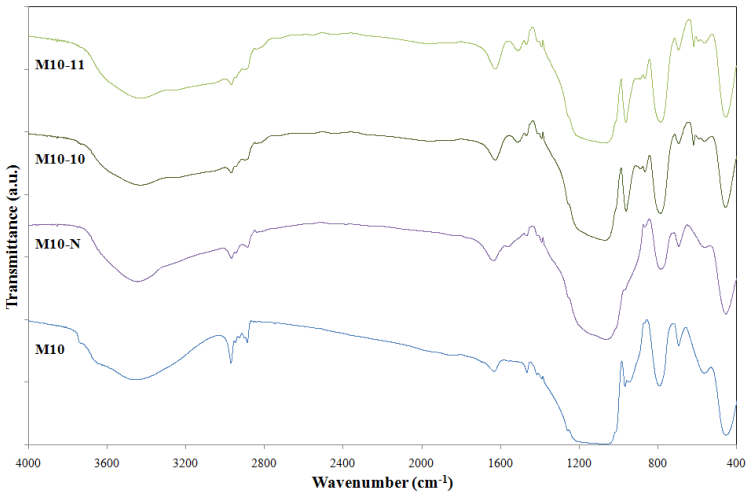

Fig. C. 4. FTIR spectra of the M10 immobilized materials

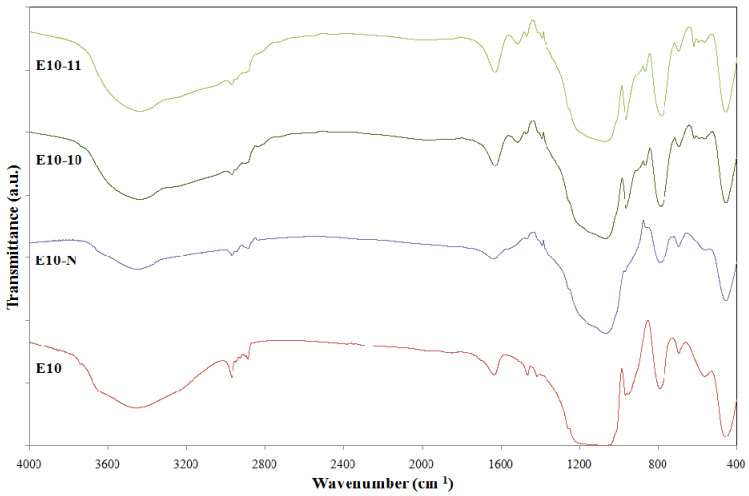

Fig. C. 5. FTIR spectra of the E10 immobilized materials

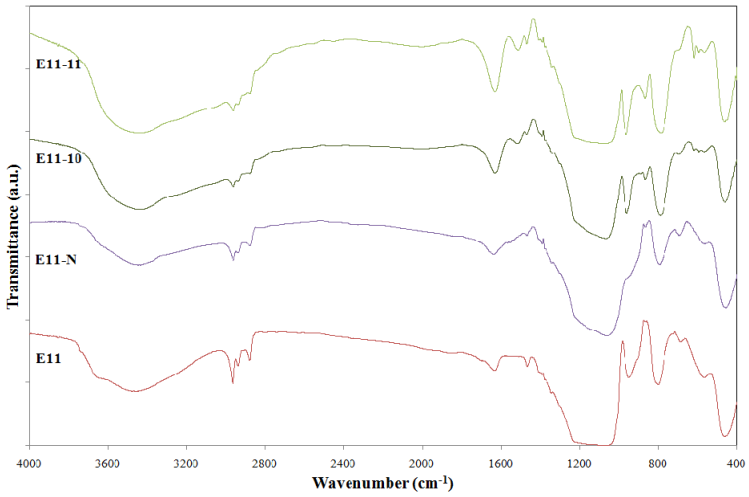

Fig. C. 6. FTIR spectra of the E11 immobilized materials

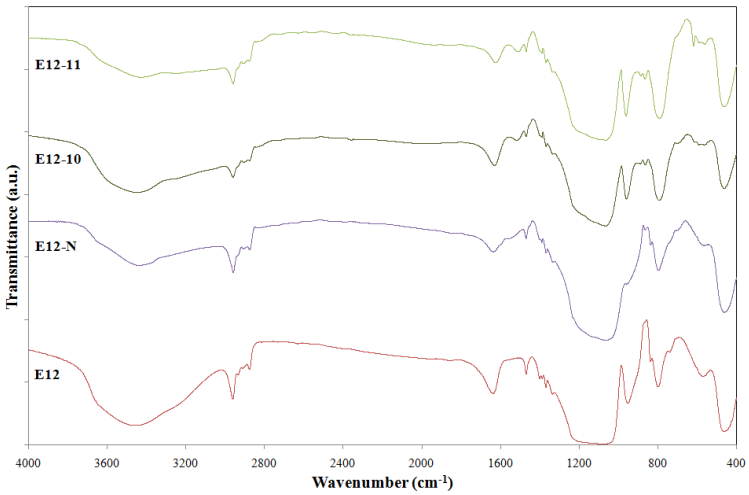

Fig. C. 7. FTIR spectra of the E12 immobilized materials

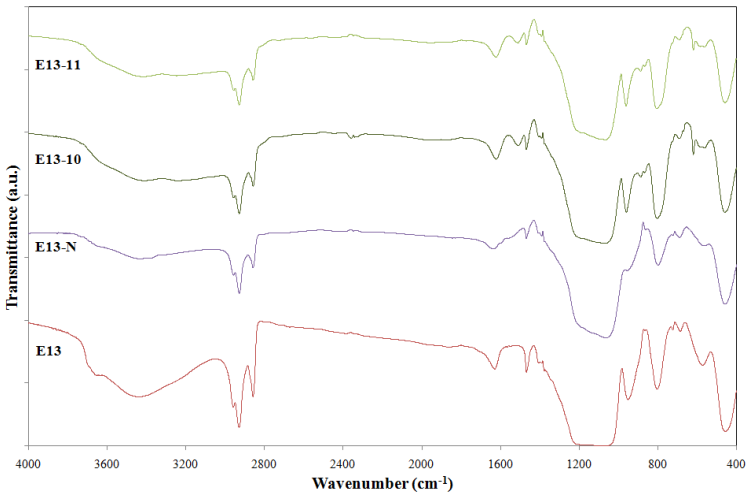

Fig. C. 8. FTIR spectra of the E13 immobilized materials

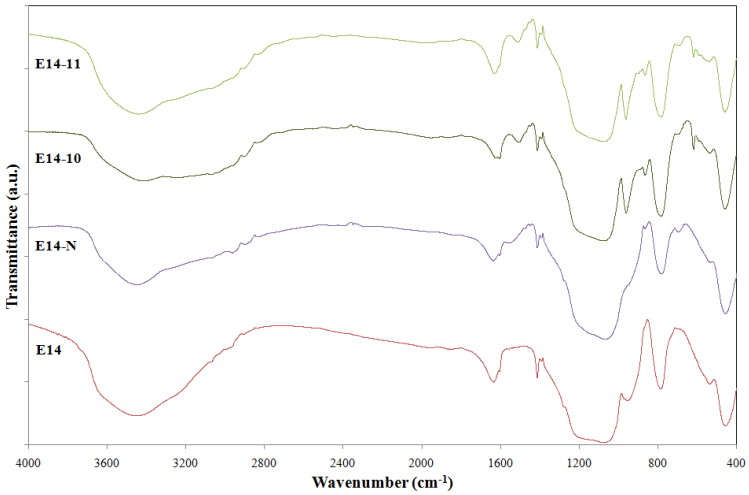

Fig. C. 9. FTIR spectra of the E14 immobilized materials

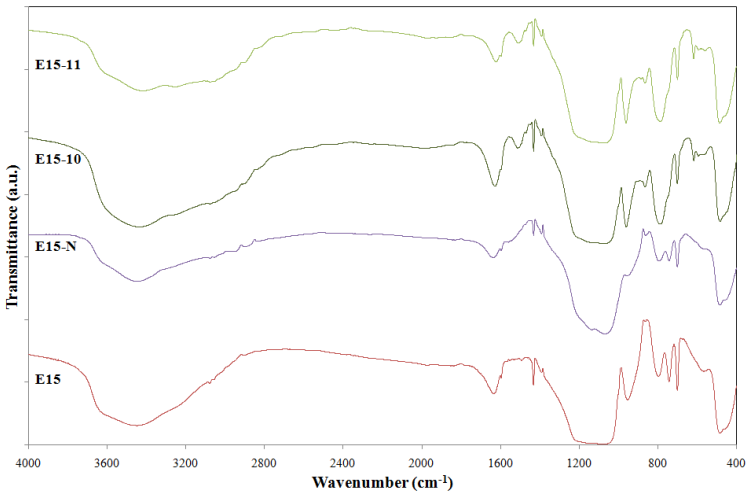

Fig. C. 10. FTIR spectra of the E15 immobilized materials

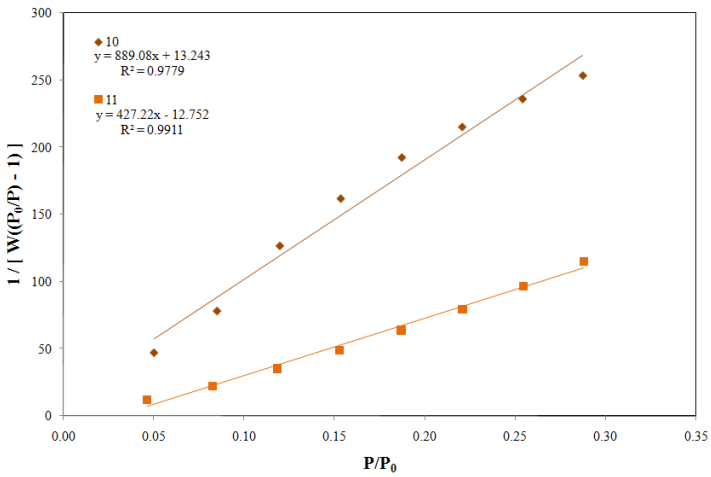

Fig. C. 11. BET plots of the 10-MVPA and 11-MVPA

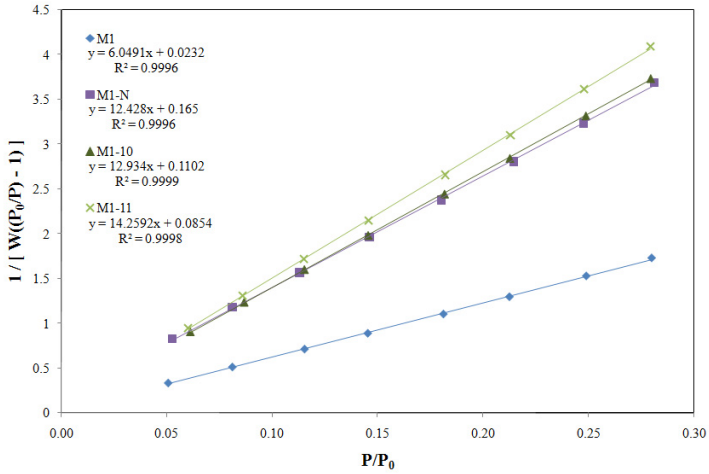

Fig. C. 12. BET plots of the M1 immobilized materials

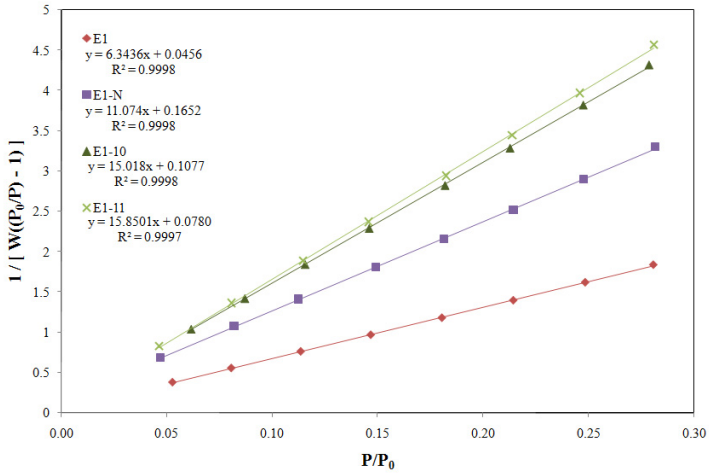

Fig. C. 13. BET plots of the E1 immobilized materials

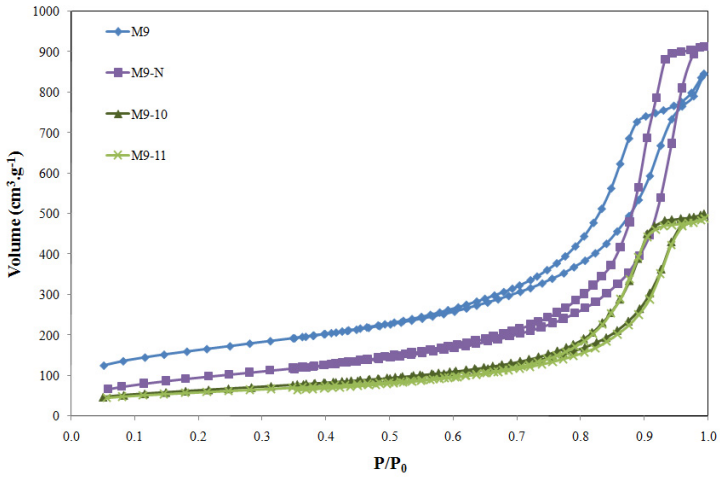

Fig. C. 14. Nitrogen adsorption/desorption isotherms of the M9 immobilized materials

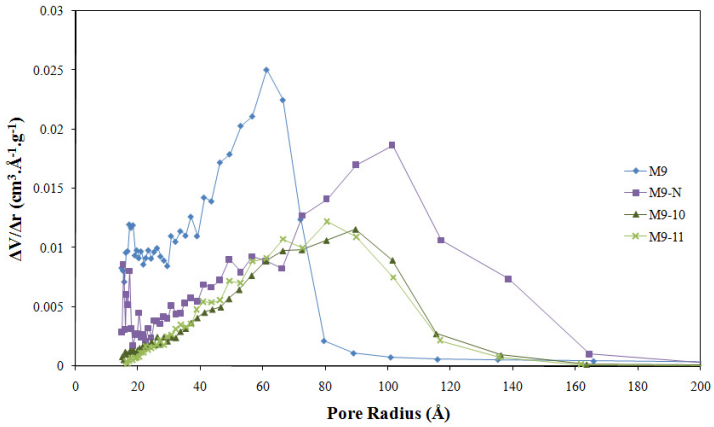

Fig. C. 15. Pore size distribution of the M9 immobilized materials

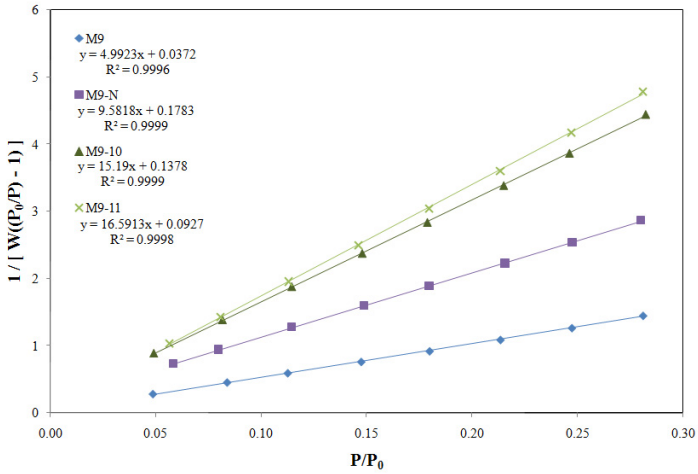

Fig. C. 16. BET plots of the M9 immobilized materials

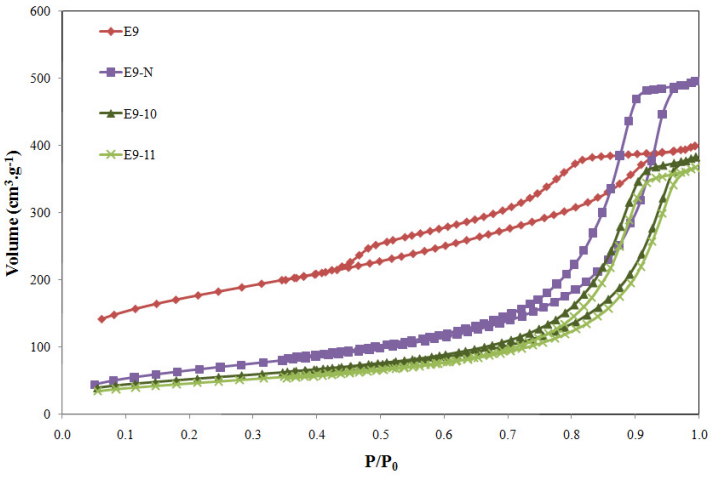

Fig. C. 17. Nitrogen adsorption/desorption isotherms of the E9 immobilized materials

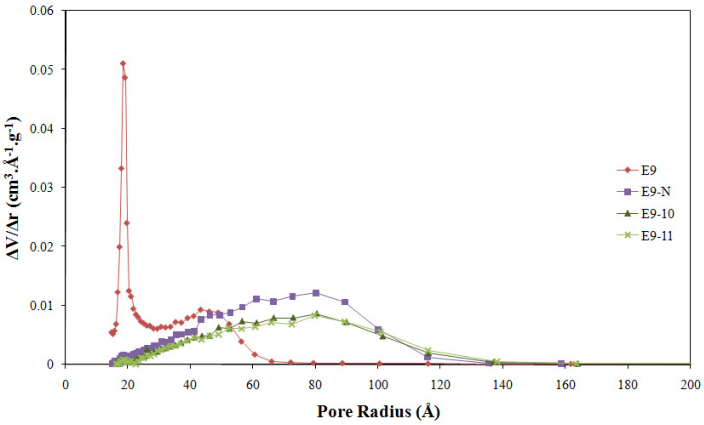

Fig. C. 18. Pore size distribution of the E9 immobilized materials

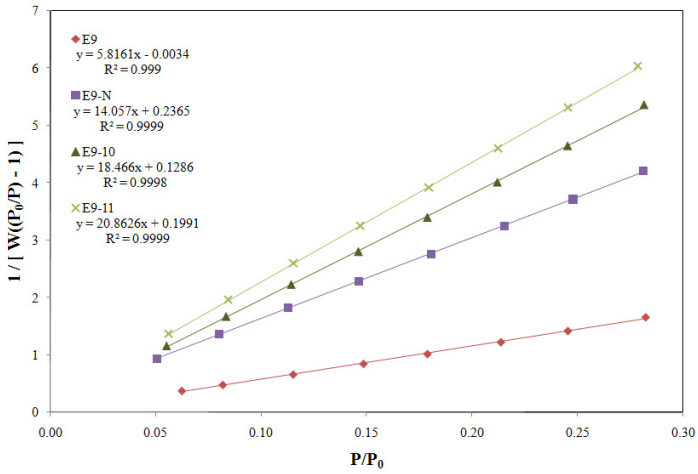

Fig. C. 19. BET plots of the E9 immobilized materials

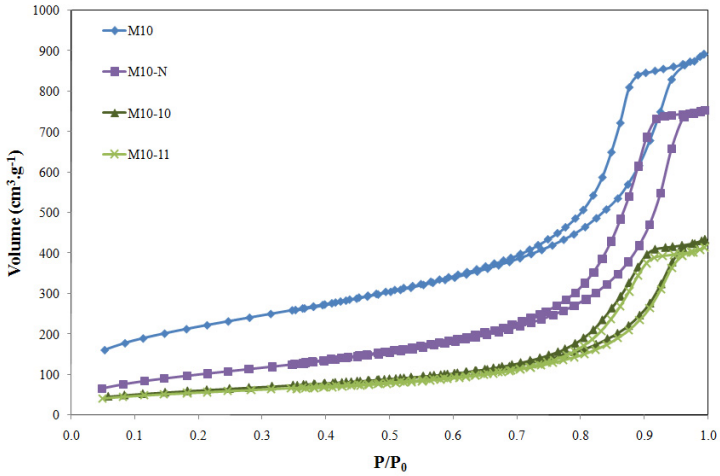

Fig. C. 20. Nitrogen adsorption/desorption isotherms of the M10 immobilized materials

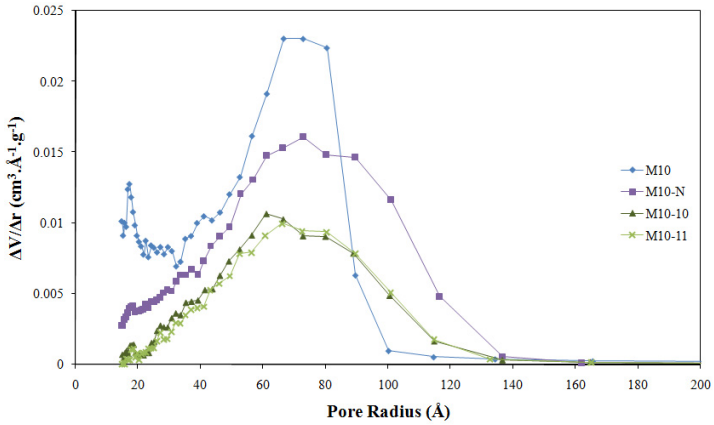

Fig. C. 21. Pore size distribution of the M10 immobilized materials

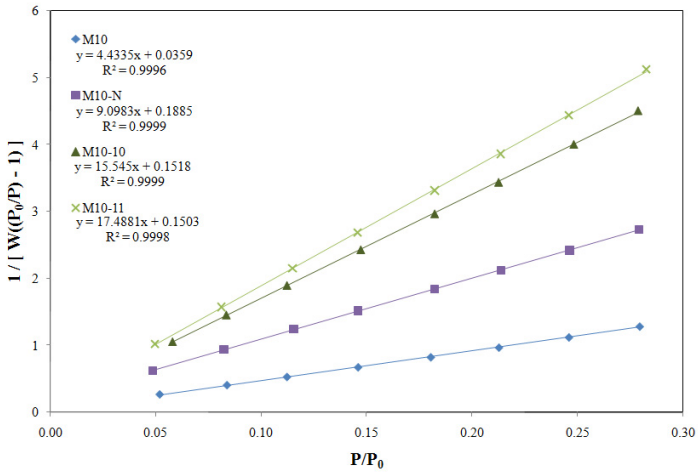

Fig. C. 22. BET plots of the M10 immobilized materials

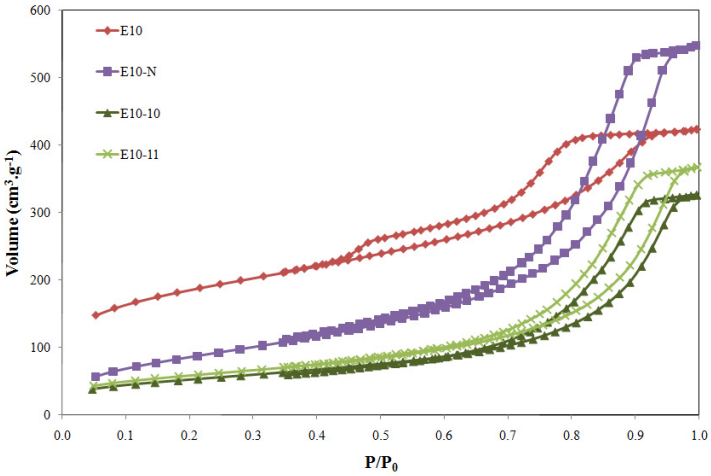

Fig. C. 23. Nitrogen adsorption/desorption isotherms of the E10 immobilized materials

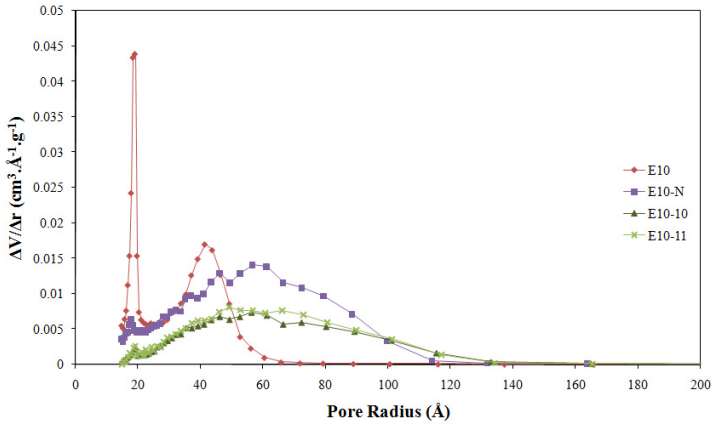

Fig. C. 24. Pore size distribution of the E10 immobilized materials

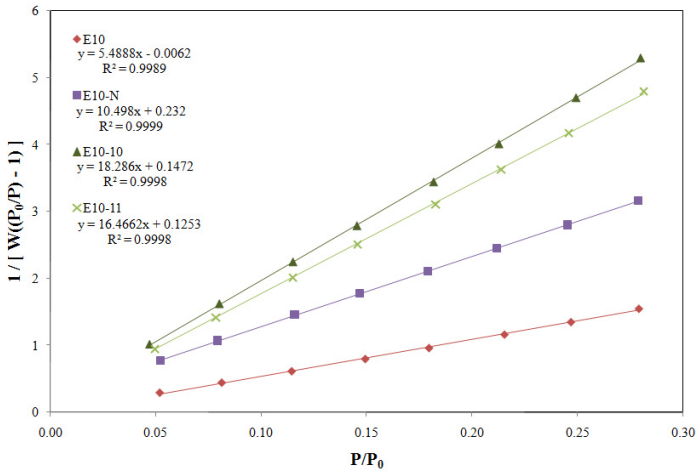

Fig. C. 25. BET plots of the E10 immobilized materials

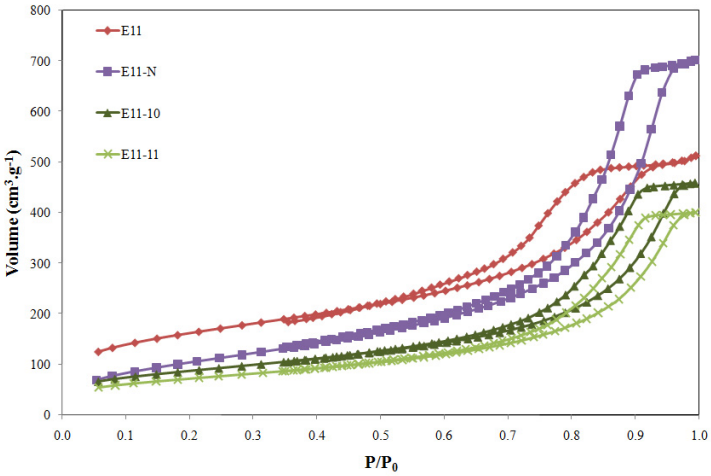

Fig. C. 26. Nitrogen adsorption/desorption isotherms of the E11 immobilized materials

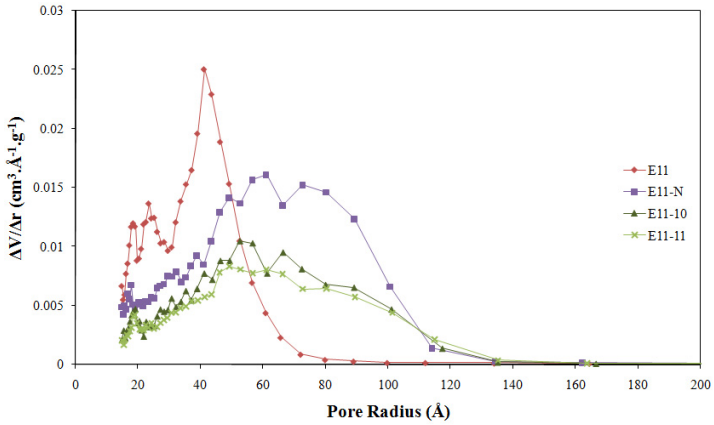

Fig. C. 27. Pore size distribution of the E11 immobilized materials

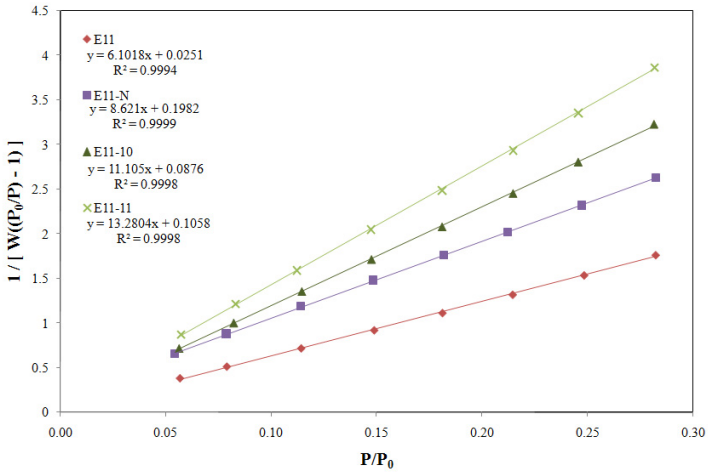

Fig. C. 28. BET plots of the E11 immobilized materials

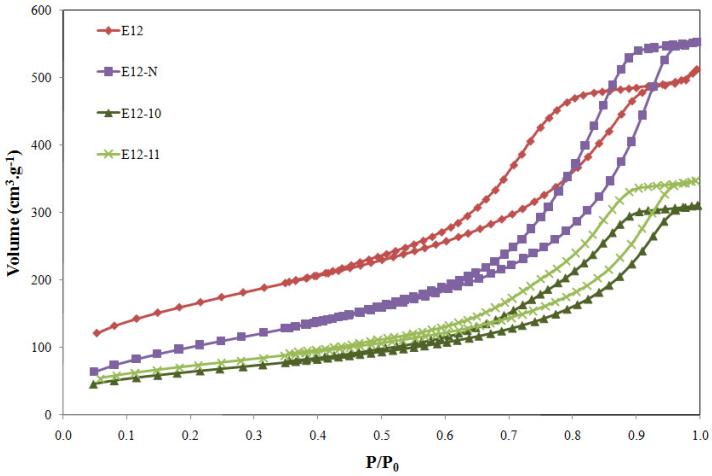

Fig. C. 29. Nitrogen adsorption/desorption isotherms of the E12 immobilized materials

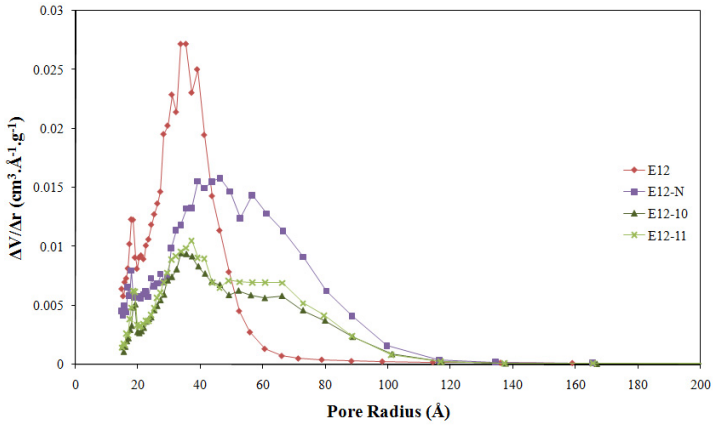

Fig. C. 30. Pore size distribution of the E12 immobilized materials

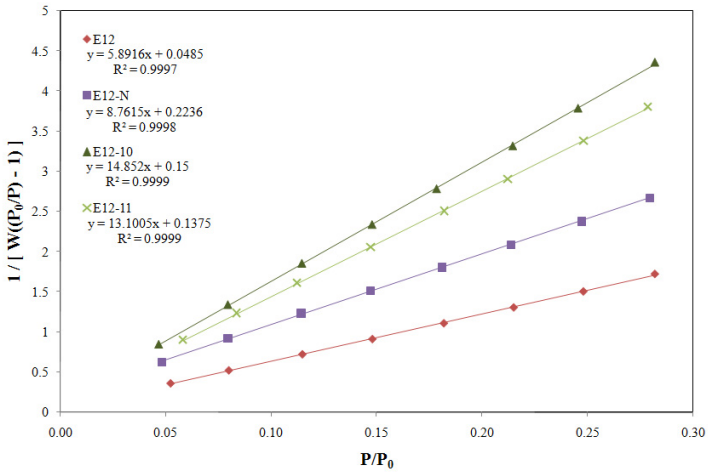

Fig. C. 31. BET plots of the E12 immobilized materials

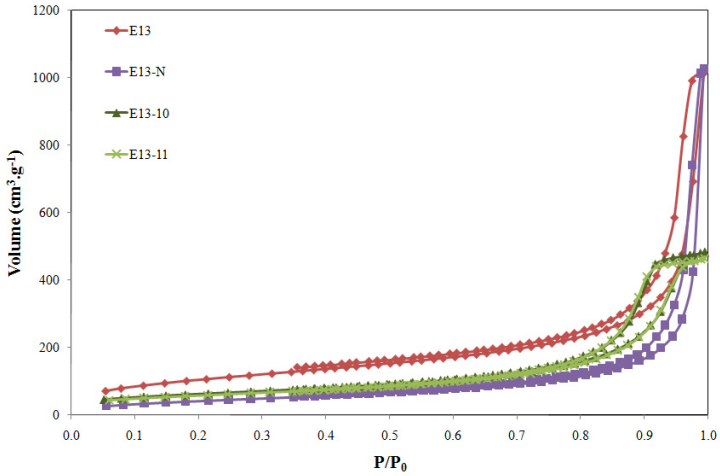

Fig. C. 32. Nitrogen adsorption/desorption isotherms of the E13 immobilized materials

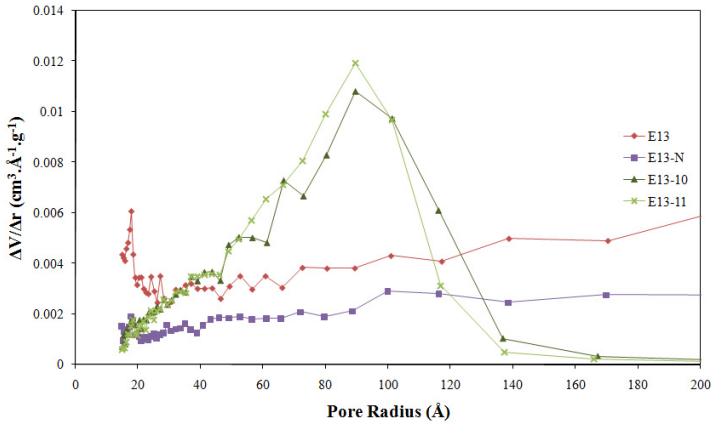

Fig. C. 33. Pore size distribution of the E13 immobilized materials

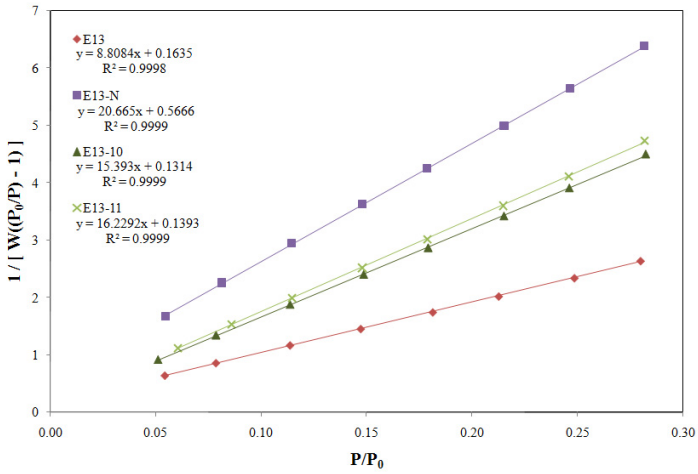

Fig. C. 34. BET plots of the E13 immobilized materials

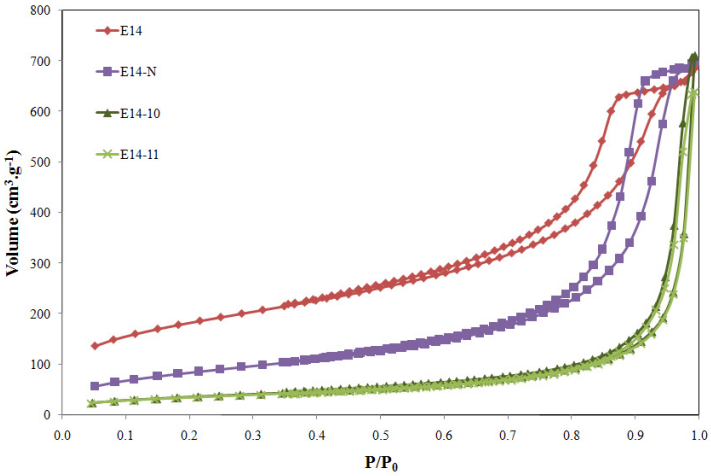

Fig. C. 35. Nitrogen adsorption/desorption isotherms of the E14 immobilized materials

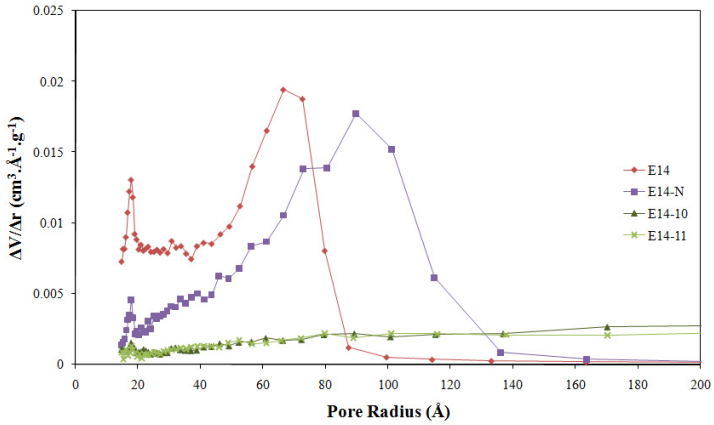

Fig. C. 36. Pore size distribution of the E14 immobilized materials

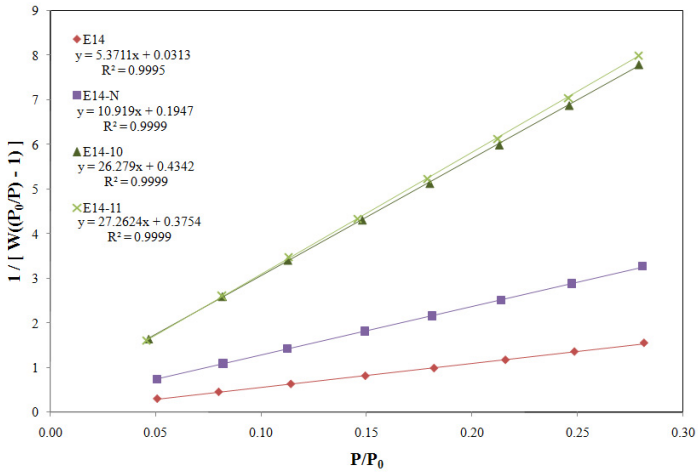

Fig. C. 37. BET plots of the E14 immobilized materials

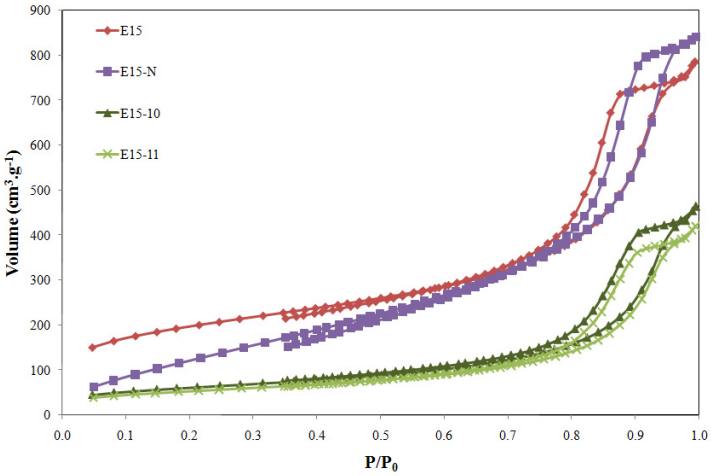

Fig. C. 38. Nitrogen adsorption/desorption isotherms of the E15 immobilized materials

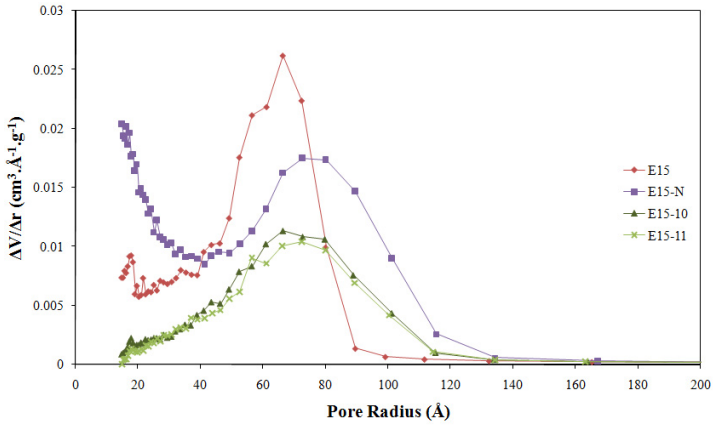

Fig. C. 39. Pore size distribution of the E15 immobilized materials

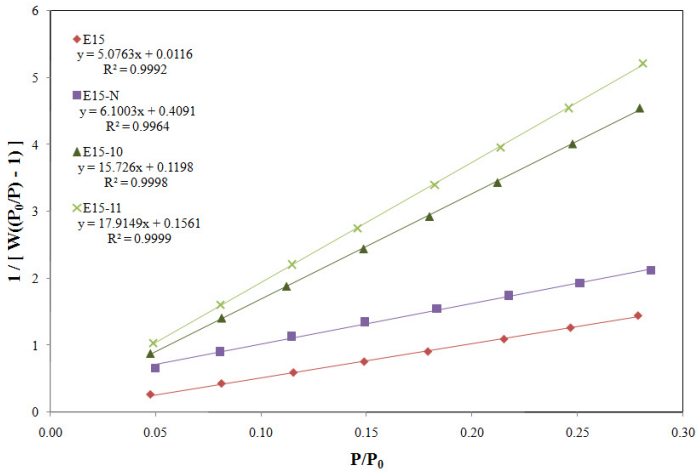

Fig. C. 40. BET plots of the E15 immobilized materials

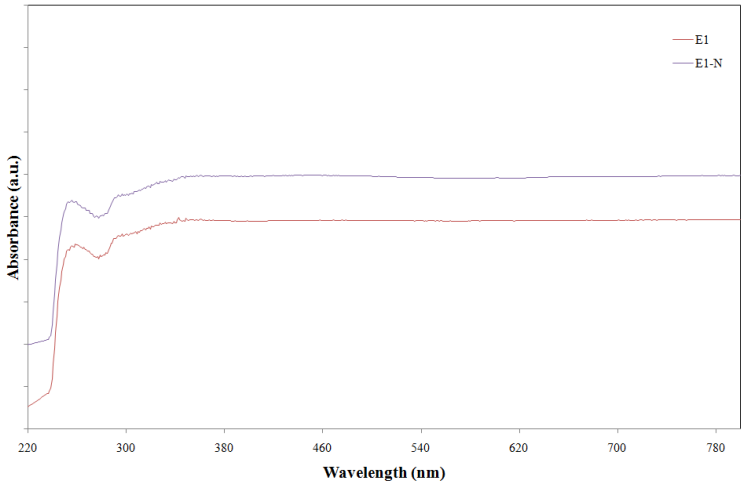

Fig. C. 41. DR UV-Vis spectra of the E1 and E1-N

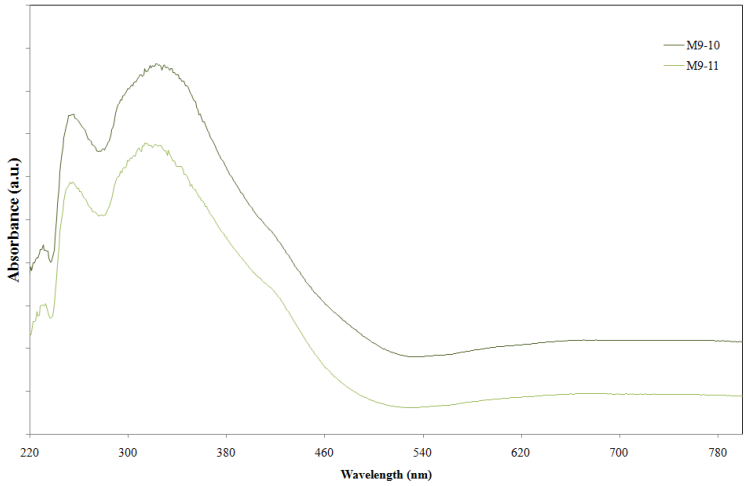

Fig. C. 42. DR UV-Vis spectra of the M9-10 and M9-11

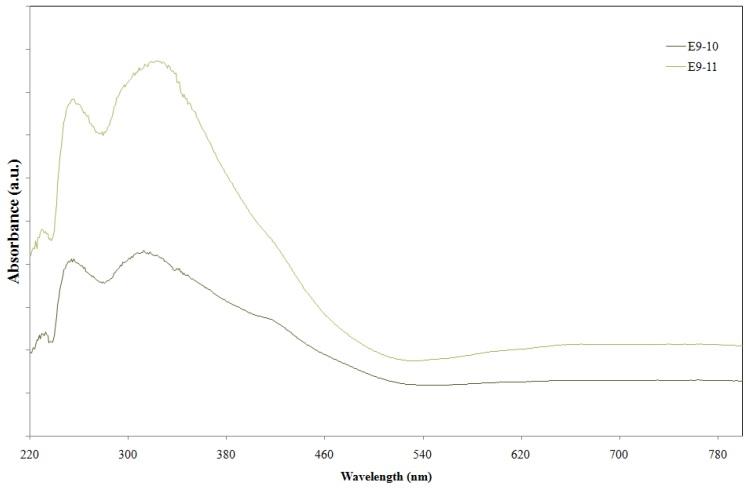

Fig. C. 43. DR UV-Vis spectra of the E9-10 and E9-11

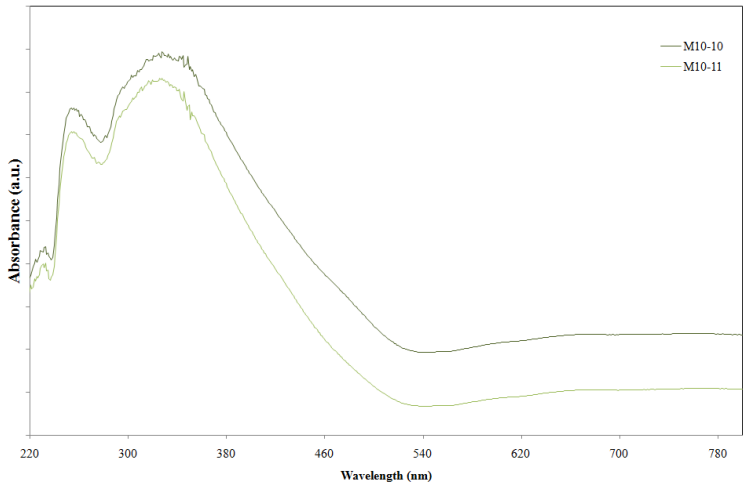

Fig. C. 44. DR UV-Vis spectra of the M10-10 and M10-11

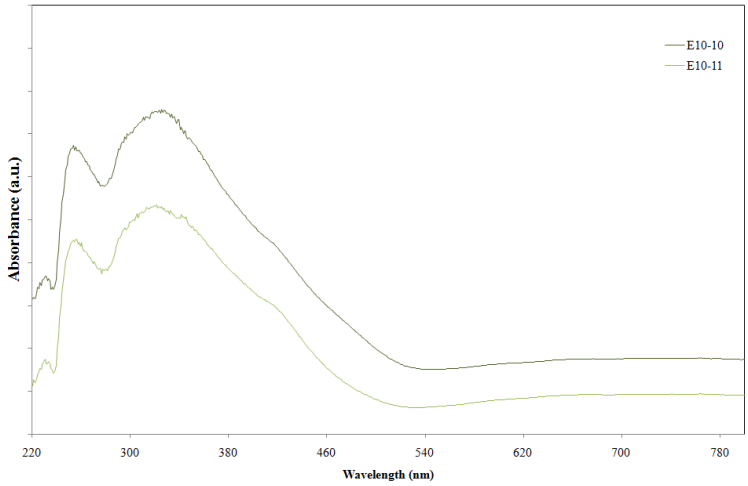

Fig. C. 45. DR UV-Vis spectra of the E10-10 and E10-11

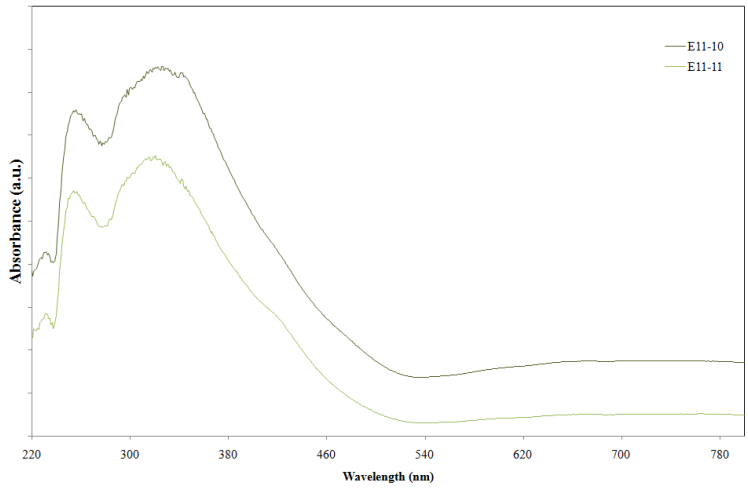

Fig. C. 46. DR UV-Vis spectra of the E11-10 and E11-11

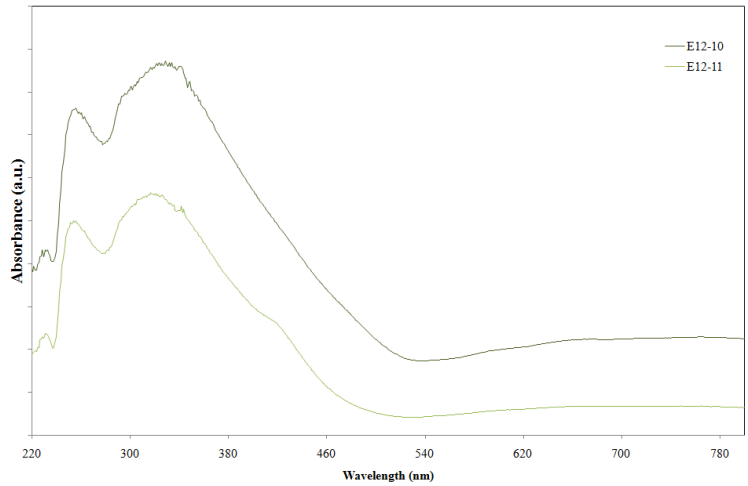

Fig. C. 47. DR UV-Vis spectra of the E12-10 and E12-11

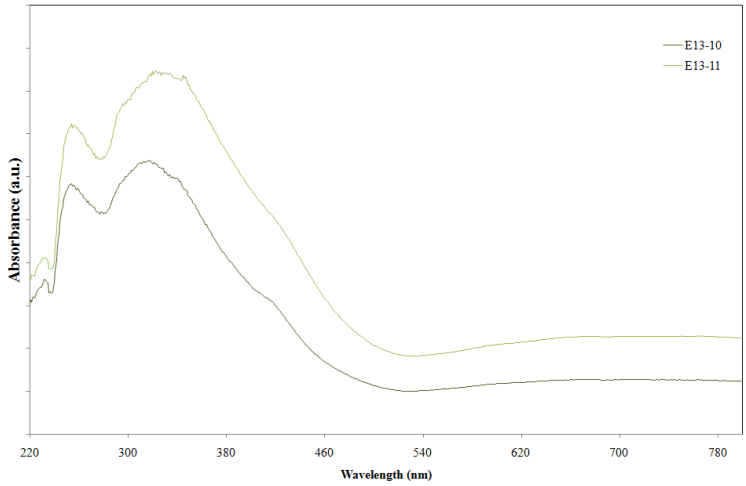

Fig. C. 48. DR UV-Vis spectra of the E13-10 and E13-11

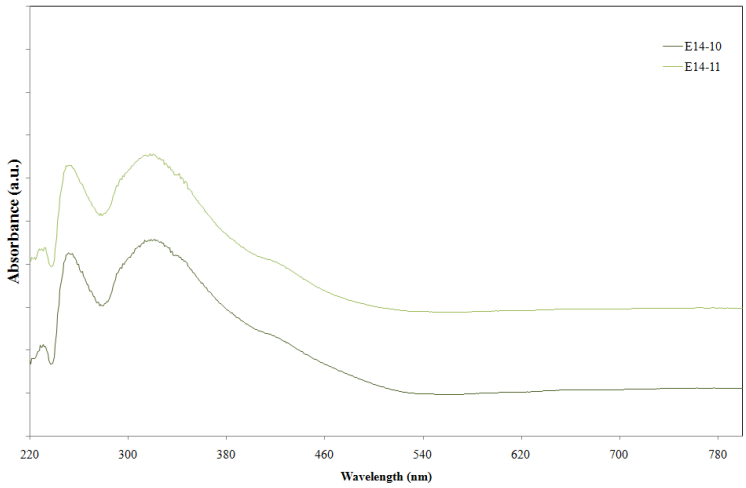

Fig. C. 49. DR UV-Vis spectra of the E14-10 and E14-11

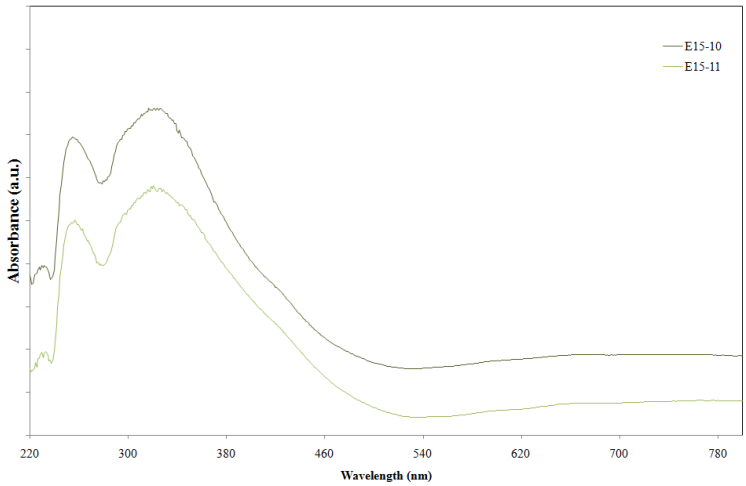

Fig. C. 50. DR UV-Vis spectra of the E15-10 and E15-11

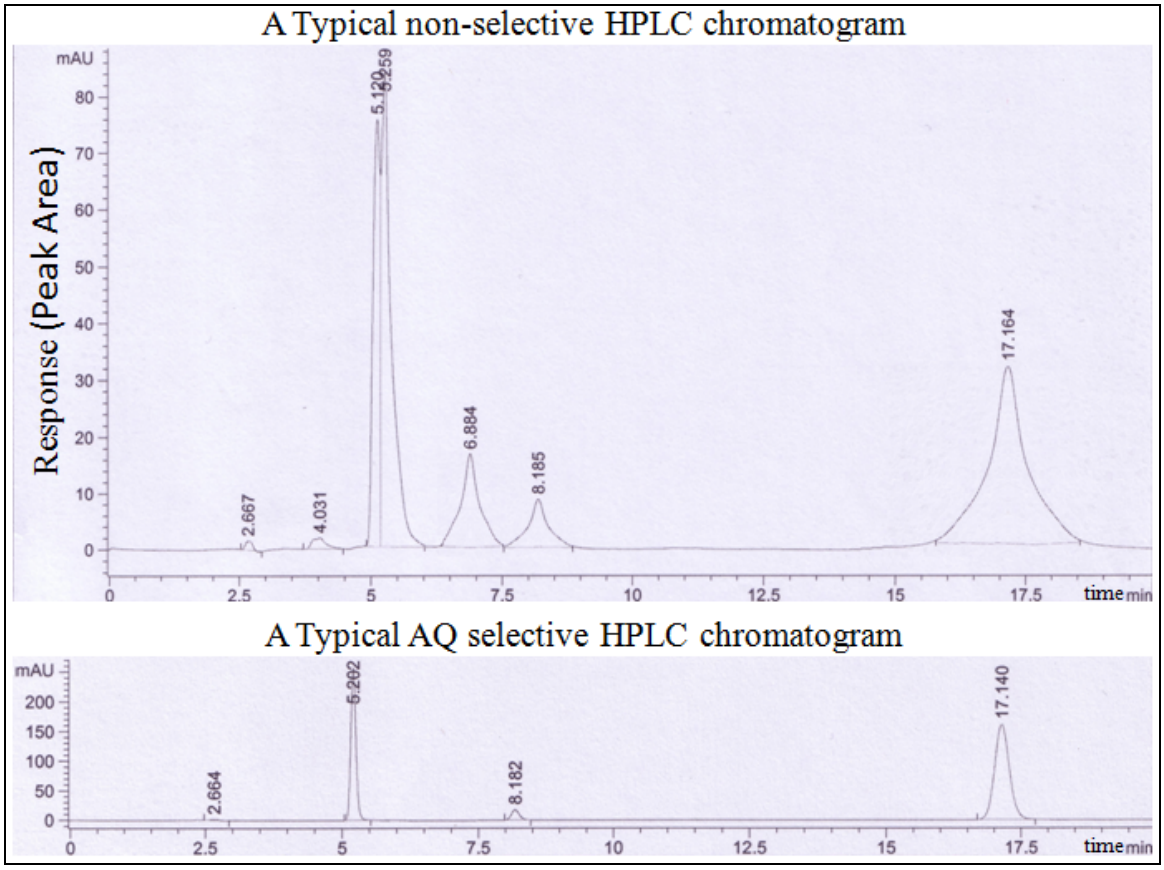

Fig. C. 51. Typical HPLC chromatograms as obtained during our analyses

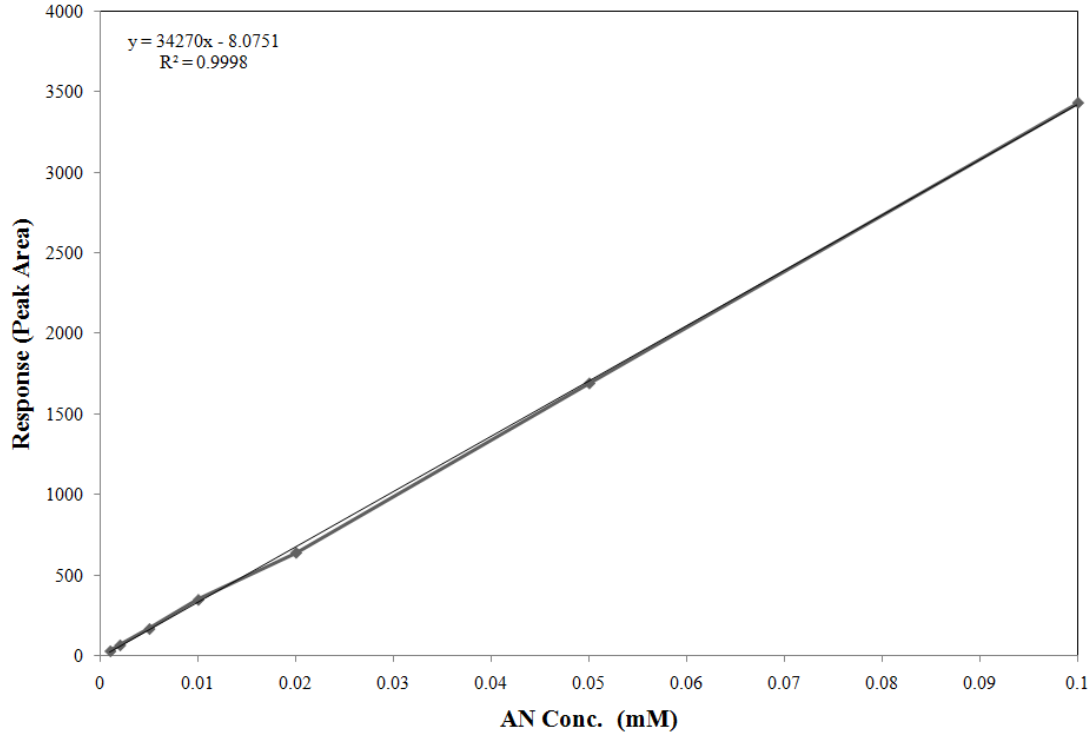

Fig. C. 52. HPLC calibration curve for AN

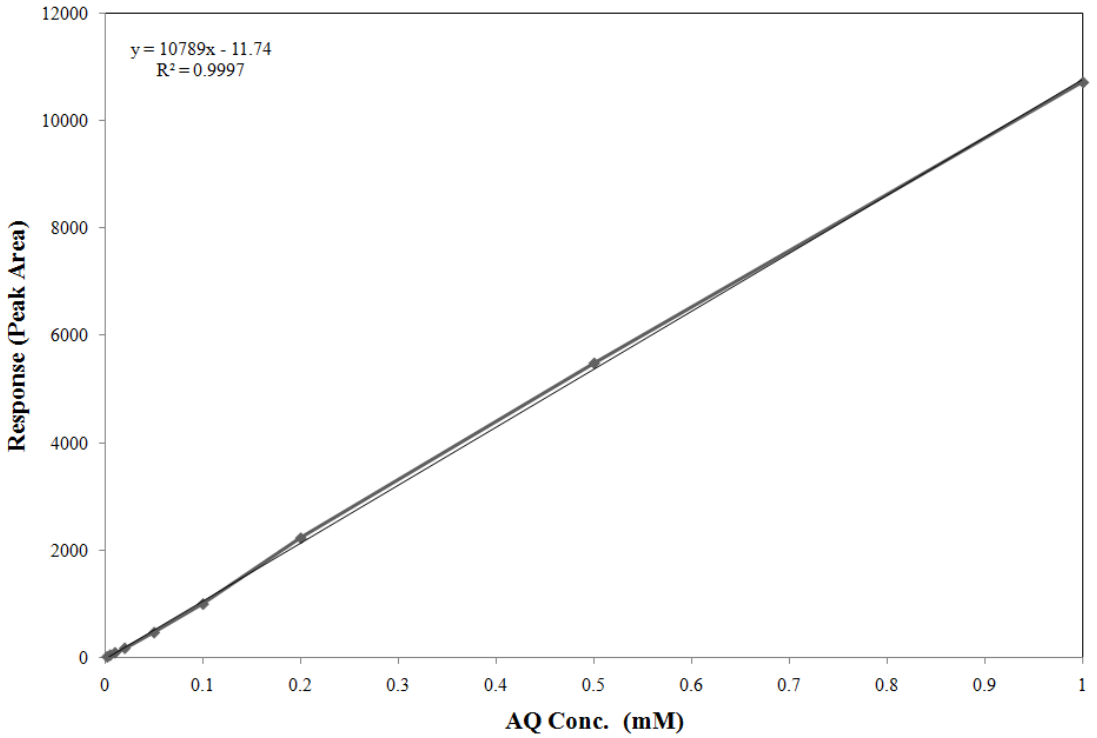

Fig. C. 53. HPLC calibration curve for AQ

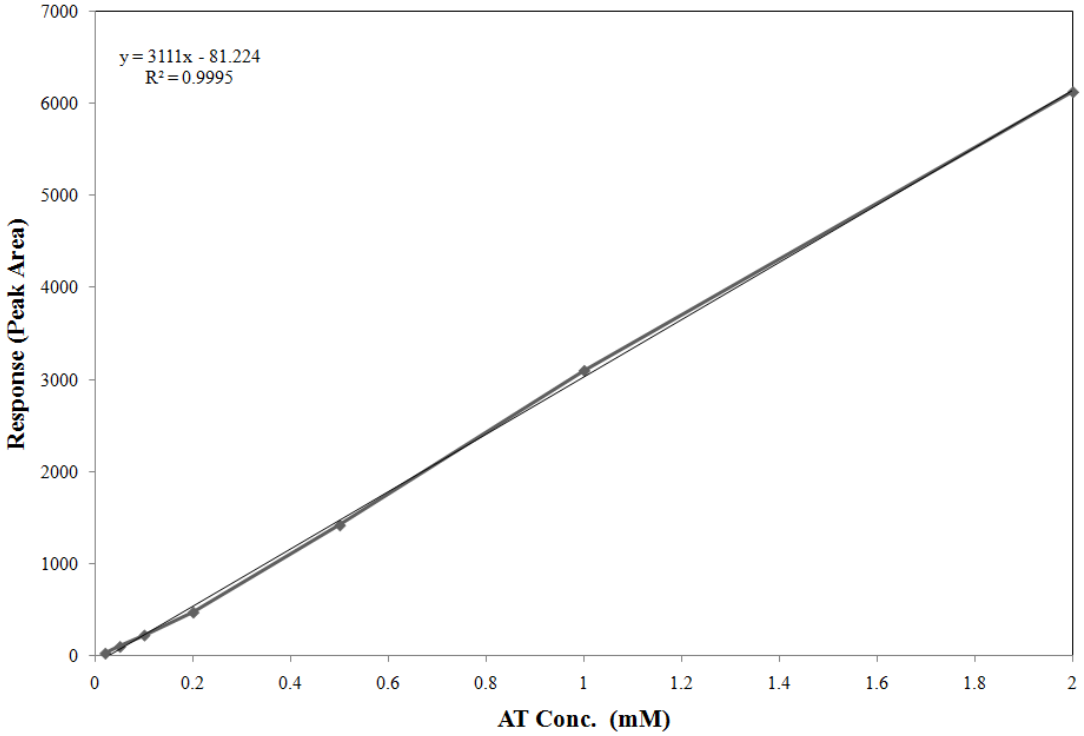

Fig. C. 54. HPLC calibration curve for AT

REFERENCES

1. Ebelmen, M. *Ann. Chim. Phys.* 16 (1846): 129.

2. Ebelmen, M. *C. R. Acad. Sci.* (1847).

3. Graham, T. *J. Chem. Soc.* (1864).

4. Pierre, A.C. *Introduction to Sol-Gel Processing*. Boston: Kluwer, 1998.

5. Brinker, C.J., and G.W. Scherer. *Sol-Gel Science: The Physics and Chemistry of Sol-Gel Processing*. New York: Academic Press, 1990.

6. Schmidt, H. "Chemistry of material preparation by the sol-gel process." *Journal of Non-Crystalline Solids* 100, no. 1-3 (1988): 51-64.

7. Livage, J., F. Beteille, C. Roux, M. Chatry, and P. Davidson. "Sol-gel synthesis of oxide materials." *Acta Materialia* 46, no. 3 (1998): 743-750.

8. Hiemenz, P.C. *Priciples of Colloid and Surface Chemistry*. New York: Marcel Dekker, 1977.

9. Dislich, H. *Journal of Non-Crystalline Solids* 57 (1983): 371-388.

10. Segal, D.L. *Journal of Non-Crystalline Solids* 63 (1984): 183-191.

11. Dash, S., S. Mishra, S. Patel, and B.K. Mishra. "Organically modified silica: Synthesis and applications due to its surface interaction with organic molecules." *Advances in Colloid and Interface Science* 140 (2008): 77-94.

12. Livage, J., and J. Lemerie. *Ann. Rev. Mater. Sci.* 12 (1982): 103-122.

13. Ebelmen, M. *Ann. Chim. Phys.* 15 (1845): 319.

14. Ebelmen, M. *Compte Rendus de l'Acd. des Sciences* 25 (1947): 854.

15. Cossa, A. *Il Nuovo Cimento* 3 (1870): 228-230.

16. Kistler, S.S. *Nature* 127 (1931): 742.

17. Kistler, S.S. *J. Phys. Chem.* 36 (1932): 52.

18. Mauritz, K.A., R.F. Storey, and C.K. Jones. "Multiphase Polymer Materials: Blends, Ionomers, and Interpenetrating Networks." edited by L.A. Utracki and R.A. Weiss, 401-417. Washington, DC: American Chemical Society, 1989.

19. Sanchez, C., and F. Ribot. *New J. Che,.* 18 (1994): 1007-1047.

20. Corma, A. *Chem. Rev.* 97 (1997): 2373-2419.

21. Cantin, M., M. Casse, L. Koch, R. Jouan, P. Mestran, D. Roussel, F. Bonnin, J. Moutel, and S. Teichner. *J. Nucl. Instrum. Methods* 118 (1974): 177.

22. Sumiyoshi, T., I. Adachi, R. Enomoto, T. Iijima, R. Suda, M. Yokoyama, and H. Yokogawa. *J. Non-Cryst. Solids* 225 (1998): 369-374.

23. Platzer, W., V. Wittwer, and M. Mielke. *Aerogels*, Edited by J. Fricke. Berlin Heidelberg New York: Springer, 1986.

24. Wittwer, V. *J. Non-Cryst. Solids* 145 (1992): 233.

25. Smith, D.M., A. Maskara, and U. Boes. *J. Non-Cryst. Solids* 225 (1998): 254.

26. Power, M., B. Hosticka, E. Black, C. Daitch, and P. Norris. *Journal of Non-Crystalline Solids* 285 (2001): 303.

27. Buisson, P., C. Hernandez, M. Pierre, and A.C. Pierre. *Journal of Non-Crystalline Solids* 285 (2001): 295.

28. Tsou, P. *J. Non-Cryst. Solids* 186 (1995): 415.

29. Tsou, P. In *6th international symposium on aerogels*, 8-11. Albuquerque, NM, USA, 2000.

30. Haertling, G.H., and C.E. Land. *Ferroelectrics* 3 (1972): 269-280.

31. Zelinski, B.J.J., and D.R. Uhlmann. *J. Phys. Chem. Solids* 45 (1984): 1069-1090.

32. Iler, R.K. *The Chemistry of Silica*: Wiley-Interscience, 1979.

33. LeVier, R.R., M.C. Harrison, R.R. Cook, and T.H. Lane. "What is Silicone?" *J. Clin. Epidemiol* 48, no. 4 (1995): 513-517.

34. Pope, M.T., and A. Müller. *Polyoxometalate Chemistry From Topology via Self-Assembly to Applications*. Dordrecht: Kluwer Academic Publishers, 2001.

35. Zhuravlev, L.T. "The surface chemistry of amorphous silica." *Colloids and Surfaces A: Physicochemical and Engineering Aspects* 173 (2000): 1-38.

36. Pierre, A.C., and G.M. Pajonk. "Chemistry of Aerogels and Their Applications." *Chemical Reviews* 102, no. 11 (2002): 4243-4266.

37. Livage, J., M. Henry, and C. Sanchez. "Sol-gel chemistry of transition metal oxides." *Progress in Solid State Chemistry* 18, no. 4 (1988): 259-341.

38. Yoshikawa, M., T. Ooi, and J. Izumi. "Novel membrane materials having EEE derivatives as a chiral recognition site." *Eur. Polym. J.* 37 (2001): 335-342.

39. Ansell, R.J. "Molecularly imprinted polymers for the enantioseparation of chiral drugs." *Adv. Drug Delivery Rev.* 57 (2005): 1809-1835.

40. Carabias-Martinez, R., E. Rodriguez-Gonzalo, E. Herrero-Hernandez, and M. Diaz-Garcia. "Development and characterisation of a molecularly imprinted polymer prepared by precipitation polymerisation for the determination of phenylurea herbicides." *J. Sep. Sci.* 28 (2005): 453-461.

41. Kempe, M. "Antibody-mimicking polymers as chiral stationary phases in HPLC." *Anal. Chem.* 68 (1996): 1948-1953.

42. Wulff, G., T. Gross, R. Schonfeld, T. Schrader, and C. Kirsten. "Molecular imprinting for the preparation of enzyme-analogous polymers." In *ACS Symp. Ser.*, 703, 10-28, 1998.

43. Piletsky, S.A., Y.P. Parhometz, N.V. Lavryk, T.L. Panasyuk, and A.V. El'skaya. "Sensors for low-weight organic molecules based on molecular imprinting technique." *Sens. Actuators, B* 19 (1994): 629-631.

44. Wei, X., and S.M. Husson. "Surface-Grafted, Molecularly Imprinted Polymers Grown from Silica Gel for Chromatographic Separations." *Ind. Eng. Chem. Res.* 46 (2007): 2117-2124.

45. El Rassy, H., S. Maury, P. Buisson, and A.C. Pierre. "Hydrophobic silica aerogel-lipase biocatalysts: Possible interactions between the enzyme and the gel." *Journal of Non-Crystalline Solids* 350 (2004): 23-30.

46. El Rassy, H., A. Perrard, and A.C. Pierre. "Behavior of silica aerogel networks as highly porous solid solvent media for lipases in a model transesterification reaction." *ChemBioChem* 4, no. 2-3 (2003): 203-210.

47. El Rassy, H., A. Perrard, and A.C. Pierre. "Application of lipase encapsulated in silica aerogels to a transesterification reaction in hydrophobic and hydrophilic solvents: Bi-Bi Ping-Pong kinetics." *Journal of Molecular Catalysis B: Enzymatic* 30, no. 3-4 (2004): 137-150.

48. Maury, S., P. Buisson, and A.C. Pierre. "Porous Texture Modification of Silica Aerogels in Liquid Media and Its Effect on the Activity of a Lipase." *Langmuir* 17 (2001): 6443-6446.

49. Shchipunov, Y.A. "Entrapment of Biopolymers into Sol-Gel derived Silica Nanocomposites." In *Bio-inorganic Hybrid Nanomaterials*, edited by E. Ruiz-Hitzky, K. Ariga and Y.M. Lvov, 75-103. Weinham: Wiley-VCH, 2008.

50. Choy, J., J. Oh, and S. Choi. "Bio-inorganic Conjugates for Drug and Gene Delivery." In *Bio-inorganic Hybrid Nanomaterials*, edited by E. Ruiz-Hitzky, K. Ariga and Y.M. Lvov, 401-415. Weinham: Wiley-VCH, 2008.

51. Forano, C., and V. Prevot. "Enzyme-based Bioinorganic Materials." In *Bio-inorganic Hybrid Nanomaterials*, edited by E. Ruiz-Hitzky, K. Ariga and Y.M. Lvov, 443-476. Weinham: Wiley-VCH, 2008.

52. Vallet-Regi, M., and D. Arcos. "Nanostructured Hybrid Materials for Bone Implants Fabrication." In *Bio-inorganic Hybrid Nanomaterials*, edited by E. Ruiz-Hitzky, K. Ariga and Y.M. Lvov, 367-393. Weinham: Wiley-VCH, 2008.

53. Vinu, A., N. Gokulakrishnan, T. Mori, and K. Ariga. "Immobilization of Biomolecules on Mesoporous Structured Materials." In *Bio-inorganic Hybrid Nanomaterials*, edited by E. Ruiz-Hitzky, K. Ariga and Y.M. Lvov, 113-150. Weinham: Wiley-VCH, 2008.

54. Bordoloi, A., F. Lefebvre, and S.B. Halligudi. "Selective oxidation of anthracene using inorganic-organic hybrid materials based on molybdovanadophosphoric acids." *Journal of Catalysis* 247, no. 2 (2007): 166-175.

55. Marugan, J., M.J. Lopez-Munoz, W. Gernjak, and S. Malato. "Fe/TiO2/pH Interactions in Solar Degradation of Imidacloprid with TiO2/SiO2 Photocatalysts at Pilot-Plant Scale." *Ind. Eng. Chem. Res.* 45 (2006): 8900-8908.

56. Gamelas, J.A.F., D.V. Evtuguin, and A.P. Esculcas. "Transition metal substituted polyoxometalates supported on amine-functionalized silica." *Transition Metal Chemistry* 32 (2007): 1061-1067.

57. Li, L., C. Liu, A. Geng, C. Jiang, Y. Guo, and C. Hu. "Preparation, characterization and photocatalytic applications of amine-functionalized mesoporous silica impregnated with transition-metal-monosubstituted polyoxometalates." *Materials Research Bulletin* 41 (2006): 319-332.

58. Popa, A., V. Sasca, E.E. Kiš, R. Marinkovic -Neducin, M.T. Bokorov, and J. Halasz. "Structure and Texture of Some Keggin Type Heteropolyacids Supported on Silica and Titania." *Journal of Optoelectronics and Advanced Materials* 7, no. 6 (2005): 3169 - 3177.

59. Glare, P.G.W. *Oxford Latin dictionary / edited by P.G.W. Glare*. Oxford [Oxfordshire], New York: Clarendon Press; Oxford University Press, 1982.

60. Fricke, J. "Aerogels -- highly tenuous solids with fascinating properties." *Journal of Non-Crystalline Solids* 100, no. 1-3 (1988): 169-173.

61. Fricke, J., and A. Emmerling. *J. Am. Ceram. Soc.* 75 (1992): 2027.

62. Kim, G.S., and S.H. Hyun. *Ceramist* 4 (2001): 5.

63. Carraher Jr., C.E. *Polym. News* 30, no. 12 (2005): 386.

64. Schultz, J.M., K.I. Jensen, and F.H. Kristiansen. *Sol. Energy Mat. Sol. Cells.* 89 (2005): 275.

65. Bhave, R.R. *Inorganic Membranes: Synthesis, Characteristics and Applications*. New York: Van Nostrand Reinhold, 1991.

66. Hrubesh, L.W. "Aerogel applications." *Journal of Non-Crystalline Solids* 225, no. 1 (1998): 335-342.

67. Hench, L.L., and J.K. West. "The sol-gel process." *Chemical Reviews* 90, no. 1 (2002): 33-72.

68. Brinker, C.J. *J. Non-Crystalline Solids* 100 (1988): 31-50.

69. Mauritz, K.A., and I.D. Stefanithis. "Microstructural evolution of a silicon oxide phase in a perfluorosulfonic acid ionomer by an in situ sol-gel reaction. 2. Dielectric relaxation studies." *Macromolecules* 23, no. 5 (1990): 1380-1388.

70. Engelhardt, V.G., W. Altenburg, D. Hoebbel, W. Weiker, and Z. Znorg. *Allgenines Journal der Chemie* 418 (1977): 43.

71. Keefer, K.D. *Silicon Based Polymer Science: A Comprehensive Resource* ACS Advances in Chemistry, Edited by J.M. Zeigler and F.W.G. Fearon. Washington, DC: American Chemical Society, 1990.

72. Ostwald, W. *Lehrbuch der Allgemeinen Chemie*. Vol. 2. Leipzig, Germany, 1896.

73. Brinker, C.J., and G.W. Scherer. *J. Non-Cryst. Solids* 70 (1985): 301.

74. Iler, R.K. *In Soluble Silicates* Symposium Series, Edited by J.S. Falcone. Washington, D.C.: ACS American Chemical Society, 1982.

75. Brinker, C.J., and G.W. Scfierer. *Sol-Gel Science*. New York: Academic Press, 1989.

76. Scherer, G.W. *In Better Ceramics Through Chemistry III*. Vol. 121, Edited by C.J. Brinker, D.E. Clark and D.R. Ulrich. Pittsburgh, PA: Materials Research Society, 1988.

77. Liu, S. *Aging of Gels*. University of Florida, 1989.

78. Wilson, M.J.R. "Drying Kinetics of Pure Silica Xerogels." Masters Thesis, University of Florida, 1989.

79. Soleimani Dorcheh, A., and M.H. Abbasi. "Silica aerogel: synthesis, properties and characterization." *Journal of Materials Processing Technology* 199, no. 1-3 (2008): 10-26.

80. Rao, A.P., G.M. Pajonk, and A.V. Rao. "Effect of preparation conditions on the physical and hydrophobic properties of two step processed ambient pressure dried silica aerogels." *Journal of Materials Science* 40, no. 13 (2005): 3481-3489.

81. Schwertfeger, F., D. Frank, and M. Schmidt. "Hydrophobic waterglass based aerogels without solvent exchange or supercritical drying." *Journal of Non-Crystalline Solids* 225, no. 1 (1998): 24-29.

82. Venkateswara Rao, A., A. Parvathy Rao, and M.M. Kulkarni. "Influence of gel aging and Na2SiO3/H2O molar ratio on monolithicity and physical properties of water-glass-based aerogels dried at atmospheric pressure." *Journal of Non-Crystalline Solids* 350 (2004): 224-229.

83. Hüsing, N. PhD Dissertation, University of Wurzburg, 1997.

84. Gao, G.-M., H.-F. Zou, D.-r. Liu, L.-n. Miao, S.-C. Gan, B.-C. An, J.-J. Xu, and G.-H. Li. "Synthesis of ultrafine silica powders based on oil shale ash by fluidized bed drying of wet-gel slurry." *Fuel* 88, no. 7 (2009): 1223-1227.

85. Guo, Q., S. Hikida, Y. Takahashi, N. Nakagawa, and K. Kato. "Drying of microparticle slurry and salt-water solution by a powder-particle spouted bed." *Journal of Chemical Engineering of Japan* 29, no. 1 (1996): 152-158.

86. Tatemoto, Y., M. Tsunekawa, Y. Mawatari, Y. Shiota, and K. Noda. "Drying characteristics of porous materials in a fluidized bed of hygroscopic porous particles." *Journal of Chemical Engineering of Japan* 38, no. 12 (2005): 976-982.

87. Bhagat, S.D., K.-T. Park, Y.-H. Kim, J.-S. Kim, and J.-H. Han. "A continuous production process for silica aerogel powders based on sodium silicate by fluidized bed drying of wet-gel slurry." *Solid State Sciences* 10, no. 9 (2008): 1113-1116.

88. Sing, K.S.W., D.H. Everett, R.A.W. Haul, I. Moscou, R.A. Pierotti, J. Rouquerol, and T. Siemieniewska. "Reporting physisorption data for gas/solid systems with

special reference to the determination of surface area and porosity." *Pure & Appl. Chem.* 57, no. 4 (1985): 603-619.

89. Dong, H. "Organic-Inorganic Hybrid Mesoporous Silica Materials and Their Application as Host Matrix for Protein Molecules." Doctor of Philosophy, Drexel University, 2002.

90. Pajonk, G.M., and S.J. Teichner. In *First International Symposium on Aerogels*, edited by J. Fricke, 193. Berlin: Springer, 1985.

91. Schmidt, M., and F. Schwertfeger. "Applications for silica aerogel products." *Journal of Non-Crystalline Solids* 225, no. 1 (1998): 364-368.

92. Tewari, P.H., A.J. Hunt, and K.D. Lofftus. *Springer Proc. Phys.* 6 (1986): 31.

93. Anappara, A.A., S. Rajeshkumar, P. Mukundan, P.R.S. Warrier, S. Ghosh, and K.G.K. Warrier. "Impedance spectroscopic studies of sol-gel derived subcritically dried silica aerogels." *Acta Materialia* 52, no. 2 (2004): 369-375.

94. Nyquist, R.A., and R.O. Kagel. *Handbook of Infrared and Raman Spectra of Inorganic Compounds and Organic Salts*. Vol. 4. San Diego: Academic Press, Inc, 1997.

95. Venkateswara Rao, A., M.M. Kulkarni, D.P. Amalnerkar, and T. Seth. "Superhydrophobic silica aerogels based on methyltrimethoxysilane precursor." *Journal of Non-Crystalline Solids* 330, no. 1-3 (2003): 187-195.

96. Pajonk, G.M. "Some applications of silica aerogels." *Colloid & Polymer Science* 281, no. 7 (2003): 637-651.

97. Grossemy, F., J. Borg, Z. Djouadi, A. Simionovici, L. Lemelle, D. Eichert, D. Deboffle, A.J. Westphal, and C.J. Snead. "In-situ Fe XANES of extraterrestrial grains trapped in aerogel collectors: An analytical test for the interpretation of Stardust samples analyses." *Planetary and Space Science* 55, no. 7-8 (2007): 966-973.

98. Allen, C., "Stardust", NASA http://www-curator.jsc.nasa.gov/seh/stardust.cfm.

99. Nemiroff, R., and J. Bonnell, "Astronomy Picture of the Day", NASA http://apod.nasa.gov/apod/ap990218.html.

100. Reetz, M.T., A. Zonta, and J.r. Simpelkamp. "Efficient immobilization of lipases by entrapment in hydrophobic sol-gel materials." *Biotechnology and Bioengineering* 49, no. 5 (1996): 527-534.

101. Livage, J., T. Coradin, and C. Roux. "Encapsulation of biomolecules in silica gels." *J. Phys.: Condens. Matter* 13 (2001): R673–R691.

102. Goksu, E.I., M.I. Hoopes, B.A. Nellis, C. Xing, R. Faller, C.W. Frank, S.H. Risbud, J.H. Satcher Jr, and M.L. Longo. "Silica Xerogel/Aerogel-Supported Lipid Bilayers: Consequences of Surface Corrugation." *Biochimica et Biophysica Acta (BBA) - Biomembranes* In Press, Accepted Manuscript.

103. Abramian, L., and H. El-Rassy. "Adsorption kinetics and thermodynamics of azo-dye Orange II onto highly porous titania aerogel." *Chemical Engineering Journal* 150, no. 2-3 (2009): 403-410.

104. Akl, J., T. Ghaddar, A. Ghanem, and H. El-Rassy. "Cobalt ferrite aerogels by epoxide sol-gel addition: Efficient catalysts for the hydrolysis of 4-nitrophenyl phosphate." *Journal of Molecular Catalysis A: Chemical* 312, no. 1-2 (2009): 18-22.

105. Venkateswara Rao, A., S.D. Bhagat, H. Hirashima, and G.M. Pajonk. "Synthesis of flexible silica aerogels using methyltrimethoxysilane (MTMS) precursor." *Journal of Colloid and Interface Science* 300, no. 1 (2006): 279-285.

106. Vioux, A., L. Viau, S. Volland, and J. Le Bideau. "Use of ionic liquids in sol-gel; ionogels and applications." *Comptes Rendus Chimie* In Press, Corrected Proof.

107. Liu, H., W. Sha, A.T. Cooper, and M. Fan. "Preparation and characterization of a novel silica aerogel as adsorbent for toxic organic compounds." *Colloids and Surfaces A: Physicochemical and Engineering Aspects* 347, no. 1-3 (2009): 38-44.

108. Center, K.S., "Aerogel Technology Advancements", NASA SBIR http://sbir.nasa.gov/SBIR/successes/ss/10-017text.html.

109. Aspen, "LapDesk With Aerogel Insulation", LapLogic, Inc. http://laplogic.com/.

110. "Aerogel Maintains Superior Thermal Performance In Intense Conditions", Aspen Aerogels, Inc. http://www.aerogel.com/markets/c_vasque.html.

111. "New Aerogel Technology", Dunlop Sport http://www.dunlopsport.com/Dunlop-Tennis/Technology/Aerogel-4D-technology/.

112. Schwertfeger, F., N. Hüsing, and U. Schubert. "Influence of the nature of organic groups on the properties of organically modified silica aerogels." *Journal of Sol-Gel Science and Technology* 2, no. 1 (1994): 103-108.

113. Venkateswara Rao, A., M.M. Kulkarni, D.P. Amalnerkar, and T. Seth. *Appl. Surf. Sci.* 206 (2003): 262.

114. Venkateswara Rao, A., and G.M. Pajonk. *J. Non-Cryst. Solids* 285 (2001): 202.

115. Al-Oweini, R., and H. El-Rassy. "Synthesis and characterization by FTIR spectroscopy of silica aerogels prepared using several Si(OR)4 and R"Si(OR')3 precursors." *Journal of Molecular Structure* 919, no. 1-3 (2009): 140-145.

116. Schwertfeger, F., W. Glaubitt, and U. Schubert. "Hydrophobic aerogels from Si(OMe)4/MeSi(OMe)3 mixtures." *Journal of Non-Crystalline Solids* 145 (1992): 85-89.

117. El Rassy, H., P. Buisson, B. Bouali, A. Perrard, and A.C. Pierre. "Surface characterization of silica aerogels with different proportions of hydrophobic groups, dried by the CO2 supercritical method." *Langmuir* 19, no. 2 (2003): 358-363.

118. El Rassy, H., and A.C. Pierre. "NMR and IR spectroscopy of silica aerogels with different hydrophobic characteristics." *Journal of Non-Crystalline Solids* 351, no. 19-20 (2005): 1603-1610.

119. Bhagat, S.D., C.S. Oh, Y.H. Kim, Y.S. Ahn, and J.G. Yeo. *Micro. Meso. Mater.* 100 (2007): 350.

120. Hegde, N.D., and A.V. Rao. *Appl. Surf. Sci.* 253 (2006): 1566.

121. Venkateswara Rao, A., G.M. Pajonk, S.D. Bhagat, and P. Barboux. *J. Non-Cryst. Solids* 350 (2004): 216.

122. Sumiyoshi, T., I. Adachi, R. Enomoto, T. Iijima, R. Suda, C. Leonidopoulos, D.R. Marlow, E. Prebys, R. Kawabata, H. Kawai, T. Ooba, M. Nanao, K. Suzuki, S. Ogawa, A. Murakami, and M.H.R. Khan. "Silica aerogel Cherenkov counter for the KEK B-factory experiment." *Nuclear Instruments and Methods in Physics Research Section A: Accelerators, Spectrometers, Detectors and Associated Equipment* 433, no. 1-2 (1999): 385-391.

123. Barnyakov, M.Y., V.S. Bobrovnikov, A.R. Buzykaev, A.F. Danilyuk, G. S.F., I.I. Goldberg, G.M. Kolachev, S.A. Kononov, E.A. Kravchenko, G.D. Minakov, A.P. Onuchin, G.A. Savinov, and V.A. Tayursky. *Nucl. Instrum. Methods Phys. Res., Sect. A* 453 (2000): 326-330.

124. Pope, M.T. *Heteropoly and Isopoly Oxometalates*. Berlin: Springer-Verlag, 1983.

125. Hill, C.L. "Introduction: Polyoxometalates Multicomponent Molecular Vehicles To Probe Fundamental Issues and Practical Problems." *Chemical Reviews* 98, no. 1 (1998): 1-2.

126. Bagno, A., and M. Bonchio. *Angew. Chem. Int. Engl. Ed.* 44 (2005): 2023.

127. Bonchio, M., M. Carraro, G. Scorrano, and A. Bagno. *Adv. Synth. Catal.* 346 (2004): 648.

128. Berzelius, J. *Pogg. Ann.* 6 (1826): 369-380.

129. Marignac, C. *C. R. Acad. Sci.* 55 (1862): 888.

130. Marignac, C. *Ann. Chim.* 25 (1862): 362.

131. Hill, C.L. "“Polyoxometalates” Special Issue (Ed.)." *Chem. Rev.* 98 (1998): 1-387.

132. Klemperer, W.G. "Scanning electron micrograph of ammonium phosphomolybdate." edited by Crystalstructure.jpg: Creative Commons, 2007.

133. López Fernández, X. "Theoretical Study of the Basicity and the Redox Properties of Heteropolyanions." PhD Thesis, Universitat Rovira i Virgili, 2003.

134. Kepert, D.L. *Inorg. Chem.* 4 (1962): 199.

135. Hervé, G.J. *Inorg. Nucl. Chem.* 39 (1977): 2151.

136. Colon-Ibanez, G., C. Belver-Coldeira, and M. Fernandez-Garcia. "Nanostructured Oxides in Photocatalysis." In *Synthesis, Properties, and Applications of Oxide Nanomaterials*, edited by J.A. Rodriguez and M. Fernandez-Garcia, 502. New Jersey: Wiley-Interscience, 2007.

137. Tsigdinos, G.A., and C.J. Hallada. "Molybdovanadophosphoric acids and their salts. I. Investigation of methods of preparation and characterization." *Inorganic Chemistry* 7, no. 3 (1968): 437-441.

138. Coronado, E., C. Giménez-Saiz, and C.J. Gómez-García. "Recent advances in polyoxometalate-containing molecular conductors." *Coordination Chemistry Reviews* 249, no. 17-18 (2005): 1776-1796.

139. Baker, L.C.W., and J.S. Figgis. *J. Am. Chem. Soc.* 92 (1970): 3794.

140. Cadot, E., V. Béreau, B. Marg, S. Halut, and F. Sécheresse. *Inorg. Chem.* 35 (1996): 3099.

141. Müller, A., C. Beugholt, P. Kögerler, H. Bögge, S. Bud’ko, and M. Luban. *Inorg. Chem.* 36 (2000): 5176.

142. Rowsell, J., and L.F. Nazar. *J. Am. Chem. Soc.* 122 (2000): 3777.

143. Bailar, J.C. *Inorganic Synthesis*. Vol. 1, Edited by H.S. Booth: McGraw Hill, 1939.

144. Kozhevnikov, I.V. "Catalysis by Heteropoly Acids and Multicomponent Polyoxometalates in Liquid-Phase Reactions." *Chem. Rev.* 98 (1998): 171-198.

145. Bailar, J.C. "Modern inorganic synthesis." *Pure and Applied Chemistry* 10, no. 4 (1965): 495.

146. Mizuno, N., and M. Misono. "Heterogeneous Catalysis." *Chemical Reviews* 98, no. 1 (1998): 199-218.

147. Katsoulis, D.E. "A Survey of Applications of Polyoxometalates." *Chemical Reviews* 98, no. 1 (1998): 359-388.

148. Ke Ping, H., and F. Jing Li. "A protective coating of P-Mo-V heteropoly acid on steel." *Journal of Electron Spectroscopy and Related Phenomena* 83, no. 1 (1997): 93-98.

149. Lin, Z., L. Zhongqun, C. Wenjun, and C. Shaojin. In *International Conference on Isotopes, Proceedings*, 205 49: J. Radioanal. Nucl. Chem., 1996.

150. Kamoshita, M., T. Fukazawa, and F. Kawamura. *Chem. Abstr.* 124 (1995): 129636.

151. Sheu, H.-C., and J.-S. Shih. "Organic ammonium ion selective electrodes based on 18-crown-6-phosphotungstic acid precipitates." *Analytica Chimica Acta* 324, no. 2-3 (1996): 125-134.

152. Polak, A., and P. Young. *Chem. Abstr.* 108 (1988): 95874.

153. Petty-Weeks, S. *Chem. Abstr.* 107 (1987): 69923.

154. Mazany, A.M. *Chem. Abstr.* 126 (1997): 200209.

155. Ishii, H., and T. Ogino. *Chem. Abstr.* 122 (1994): 220400.

156. Ishikawa, A., Y. Ito, H. Okamoto, T. Kudo, and K. Miyauchi. *Chem. Abstr.* 116 (1991): 224352.

157. Tomizawa, T., A. Tamaru, and A. Aoki. *Chem. Abstr.* 118 (1992): 224065.

158. Fukuda, M., H. Yamamoto, and I. Isa. *Chem. Abstr.* 117 (1992): 263043.

159. Judeinstein, P., and H. Schmidt. "Polymetalates based organic-inorganic nanocomposites." *Journal of Sol-Gel Science and Technology* 3, no. 3 (1994): 189-197.

160. Katsoulis, D.E., and J.R. Keryk. In *Abstract ACS National Meeting, Inorganic Chemistry Section*. Chicago, 1995.

161. Weinstock, I.A., R.H. Atalla, R.S. Reiner, M.A. Moen, K.E. Hammel, C.J. Houtman, and C.L. Hill. *New J. Chem.* 20 (1996): 269.

162. Rohm, H., J. Benedikt, and D. Jaros. "Comparison of Two Precipitation Methods for Determination of Phosphotungstic Acid Soluble Nitrogen in Cheese." *Lebensmittel-Wissenschaft und-Technologie* 27, no. 4 (1994): 392-393.

163. Vallance, D.T., D.J. Byrne, and A.F. Winder. "Precipitation procedures used to isolate high density lipoprotein with particular reference to effects on apo A-I-only particles and lipoprotein(a)." *Clinica Chimica Acta* 229, no. 1-2 (1994): 77-85.

164. Fabre, B., G. Bidan, and M.J. Lapkowski. *J. Chem. Soc.* 1509 (1994).

165. Rhule, J.T., C.L. Hill, D.A. Judd, and R.F. Schinazi. "Polyoxometalates in Medicine." *Chemical Reviews* 98, no. 1 (1998): 327-358.

166. Kozhevnikov, I.V. *Catal. Rev. Sci. Eng.* 37 (1995): 311.

167. Okuhara, T., N. Mizuno, and M. Misono. *Adv. Catal.* 41 (1996): 113.

168. Corma, A. *Chem. Rev.* 95 (1995): 559.

169. Hill, C.L., and C.M. Prosser-McCartha. *Chem. Rev.* 143 (1995): 407.

170. Zhou, Y., R. Bao, B. Yue, M. Gu, S. Pei, and H. He. "Synthesis, characterization and catalytic application of SBA-15 immobilized rare earth metal sandwiched polyoxometalates." *Journal of Molecular Catalysis A: Chemical* 270, no. 1-2 (2007): 50-55.

171. Hill, C.L. "Progress and challenges in polyoxometalate-based catalysis and catalytic materials chemistry." *Journal of Molecular Catalysis A: Chemical* 262, no. 1-2 (2007): 2-6.

172. Ballarini, N., F. Candiracci, F. Cavani, H. Degrand, J.L. Dubois, G. Lucarelli, M. Margotti, A. Patinet, A. Pigamo, and F. Trifir, "The dispersion of Keggin-type P/Mo polyoxometalates inside silica gel, and the preparation of catalysts for the oxidation of isobutane to methacrolein and methacrylic acid." *Applied Catalysis A: General* 325, no. 2 (2007): 263-269.

173. Bonchio, M., M. Carraro, A. Farinazzo, A. Sartorel, G. Scorrano, and U. Kortz. "Aerobic oxidation of cis-cyclooctene by iron-substituted polyoxotungstates: Evidence for a metal initiated auto-oxidation mechanism." *Journal of Molecular Catalysis A: Chemical* 262, no. 1-2 (2007): 36-40.

174. Bonchio, M., M. Carraro, A. Sartorel, G. Scorrano, and U. Kortz. "Bio-inspired oxidations with polyoxometalate catalysts." *Journal of Molecular Catalysis A: Chemical* 251, no. 1-2 (2006): 93-99.

175. Misono, M. *Catal. Rev. Sci. Eng.* 29 (1987): 269.

176. Misono, M. *Catal. Rev. Sci. Eng.* 30 (1988): 339.

177. Vazylyev, M., D. Sloboda-Rozner, A. Haimov, G. Maayan, and R. Neumann. *Top. Catal.* 34 (2005): 93.

178. Pope, M.T., A. Müller, and Eds. *Polyoxometalates: From Platonic Solids to Anti-RetroViral ActiVity*. Dordrecht: Kluwer, 1994.

179. Borrás-Almenar, J.J., E. Coronado, A. Müller, M.T. Pope, and Eds. *Polyoxometalate Molecular Science*. Dordrecht: Kluwer, 2004.

180. Bonchio, M., M. Carraro, G. Scorrano, and U. Kortz. "Microwave-Assisted Fast Cyclohexane Oxygenation Catalyzed by Iron-Substituted Polyoxotungstates." *Advanced Synthesis & Catalysis* 347, no. 15 (2005): 1909-1912.

181. Hill, C.L. *Compr. Coord. Chem. II* 4 (2003): 679.

182. Casan-Pastor, N., and P. Gomez-Romero. *Front. Biosci.* 9 (2004): 1759.

183. Okun, N.M., T.M. Anderson, and C.L. Hill. *J. Am. Chem. Soc.* 125 (2003): 3194.

184. Hermans, I., P. Jacobs, and J. Peeters. *Chem. Eur. J.* 13 (2007): 754-761.

185. Jones, M.D., R. Raja, J.M. Thomas, B.F.G. Johnson, D.W. Lewis, J. Rouzaud, and K.D.M. Harris. *Angew. Chem., Int. Ed.* 42 (2003): 4326.

186. Cao, Y., J.C. Hu, P. Yang, W.L. Dai, and K.N. Fan. *Chem. Commun.* 908 (2003).

187. Hess, C., M.H. Looi, S.B.A. Hamid, and R. Schlögl. *Chem. Commun.* 451 (2006).

188. Chen, L., K. Zhu, L. Bi, A. Suchopar, M. Reicke, G. Mathys, H. Jaensch, U. Kortz, and R.M. Richards. "Solvent-Free Aerobic Oxidation of n-Alkane by Iron(III)-Substituted Polyoxotungstates Immobilized on SBA-15." *Inorg. Chem.* 46 (2007): 8457-8459.

189. Mulder, C.A.M., and J.G. Van Lierop. *Aerogels* J. Fricke (Ed.). Berlin: Springer, 1986.

190. Novak, Z., M. Habulin, V. Krmelj, and Z. Knez. *J. Supercrit. Fluids* 27 (2003): 169.

191. Ganesan, R., and B. Viswanathan. *Bull. Catal. Soc. India* 10 (2000): 1.

192. Song, H., R.M. Rioux, J.D. Hoefelmeyer, R. Komor, K. Niesz, M. Grass, P. Yang, and G.A. Somorjai. *J. Am. Chem. Soc.* 128 (2006): 3027.

193. Kumar, D., and C.C. Landry. "Immobilization of a Mo,V-polyoxometalate on cationically modified mesoporous silica: Synthesis and characterization studies." *Microporous and Mesoporous Materials* 98 (2007): 309-316.

194. Chen, L., K. Zhu, L.-H. Bi, A. Suchopar, M. Reicke, G. Mathys, H. Jaensch, U. Kortz, and R.M. Richards. "Solvent-Free Aerobic Oxidation of n-Alkane by Iron(III)-Substituted Polyoxotungstates Immobilized on SBA-15." *Inorganic Chemistry* 46, no. 21 (2007): 8457-8459.

195. Maksimchuk, N.V., M.S. Melgunov, Y.A. Chesalov, J. Mrowiec-Białon, A.B. Jarzebski, and O.A. Kholdeeva. "Aerobic oxidations of α-pinene over cobalt-substituted polyoxometalate supported on amino-modified mesoporous silicates." *Journal of Catalysis* 246 (2007): 241-248.

196. Li, H.L., N. Perkas, Q.L. Li, Y. Gofer, Y. Koltypin, and A. Gedanken. *Langmuir* 19 (2003): 10409.

197. Wang, J., and H.O. Zhu. *Catal. Lett.* 93 (2004): 209.

198. Errington, R.J., S.S. Petkar, B.R. Horrocks, A. Houlton, L.H. Lie, and S.N. Patole. *Angew. Chem. Int. Ed.* 44 (2005): 1254.

199. Kato, N., A. Tanabe, S. Negishi, K. Goto, and K. Nomiya. *Chem. Lett.* 34 (2005): 238.

200. Kokorin, A.I. *J. Gen. Chem. USSR* 24 (1954): 697.

201. Krivy, I., and J. Krtil. *Colleclion Czech. Chem. Commun* 29 (1964): 587.

202. Charreton, B., F. Chauveau, G. Bertho, and P. Courtin. *Chim. Anal. (Paris)* 47 (1965): 17.

203. Courtin, M.P., F. Chauveau, and P. Souchay. *Compt. Rend.* 258 (1964): 1246

204. Mizuno, N., and M. Misono. *Chem. Rev.* 98 (1998): 199-217.

205. Guo, Y., Y. Wang, C. Hu, Y. Wang, Y. Whou, and F. S. "Microporous Polyoxometalates POMs/SiO2: Synthesis and Photocatalytic Degradation of Aqueous Organocholorine Pesticides." *Chemical Materials* 12 (2000): 3501-3508.

206. Izumi, Y., M. Ono, M. Kitagawa, M. Yoshida, and K. Urabe. *Microporous Materials* 5 (1995): 255.

207. Giles, G.I., and R.P. Sharama. *J. Peptide Sci.* 11 (2005): 417.

208. Cairns, D., E. Michalitsi, T.C. Jenkins, and S.P. McKay. *Bioorg. Med. Chem.* 10 (2002): 803.

209. Huang, H.S., J.F. Chiou, Y. Fong, C.C. Hou, Y.C. Lu, J.Y. Wang, J.W. Shih, Y.R. Pan, and J.J. Lin. *J. Med. Chem.* 46 (2003): 3300.

210. Preobrazhenskaya, M.N., A.E. Shchekotikhim, A.A. Shtil, and H.S. Huang. *J. Med. Sci.* 26 (2006): 4.

211. Bergiln, T., and N.H. Schiiiin. *Ind. Eng. Chem. Process Des. Dev.* 22 (1983): 150.

212. Goor, G., W. Kunkel, and O. Weiberg, *Ullman's Encyclopedia of Industrial Chemistry.* Weinheim:VCH, 1985.

213. Zollinger, H. *Colour Chemistry: Synthesis, Properties and Application of Organic Dyes and Pigment*. New York: Wiley, 1987.

214. Dijk, E.H.V., D.J.T. Myles, M.H.V. Veen, and J.C. Hummelen. *Org. Lett.* 8 (2006): 2333.

215. Tandon, P.K., R. Baboo, and A.K. Singh. *Gayatri. Appl. Organ. Chem.* 20 (2006): 20.

216. Dodor, D.E., H.M. Hwang, and S.I.N. Ekunwe. *Enzyme Microb. Tech.* 35 (2004): 210.

217. Baldrian, P., T. Cajthacm, V. Merhautova, J. Gabriel, F. Nerud, P. Stopka, M. Hruby, and M.J. Benes. *Appl. Catal. B* 59 (2005): 267.

218. Maayan, G., B. Ganchegui, W. Leitner, and R. Neumann. *Chem. Commun.* (2006): 2230.

219. Vogel, A., and A.G. Bayer, *Ullmann's Encyclopedia of Industrial Chemistry.* Weinheim:VCH, 1985.

220. Butterworth, B.E., O.B. Mathre, and K. Ballinger. *Mutagenesis* 16 (2001): 169.

221. Araȷo, R.S., F.S. Costa, D.A.S. Maia, H.B. Sant'Ana, and C.L. Cavalcante Jr. "Synthesis and characterization of Al- and Ti-MCM-41 materials: application to oxidation of anthracene." *Brazilian Journal of Chemical Engineering* 24 (2007): 135-141.

222. Günzler, H., and H.U. Gremlich. *IR Spectroscopy: An Introduction*. Translated by M.-J. Blumich. Weinheim, Germany: Wiley-VCH Verlag GmbH, 2002.

223. Sherman Hsu, C.P. *Infrared Spectroscopy* Handbook of Instrumental Techniques for Analytical Chemistry, Edited by F. Settle. Upper Saddle River, New Jersey: Prentice-Hall, Inc., 1997.

224. *Introduction to Fourier Transform Infrared Spectrometry*. Verona Road, Madison - USA: Thermo Nicolet Corporation, 2001.

225. Skoog, D.A., F.J. Holler, and S.R. Crouch. *Principles of Instrumental Analysis*. 6 ed. Australia: Brooks Cole, 2007.

226. Colthup, N.B., L.H. Daly, and S.E. Wiberley. *Introduction to Infrared and Raman Spectroscopy*. second ed. New York: Academic Press, 1975.

227. Socrates, G. *Infrared and Raman Characteristic Group Frequencies: Tables and Charts*. third ed.: Wiley, 2001.

228. Chmel, A., E.K. Mazurina, and V.S. Shashkin. "Vibrational spectra and deffect structure of silica prepared by non-organic sol-gel process." *Journal of Non-Crystalline Solids* 122, no. 3 (1990): 285-290.

229. Gopal, N.O., K.V. Narasimhulu, and J.L. Rao. "EPR, optical, infrared and Raman spectral studies of Actinolite mineral." *Spectrochimica Acta Part A: Molecular and Biomolecular Spectroscopy* 60, no. 11 (2004): 2441-2448.

230. Bertoluzza, A., C. Fagnano, M. Antonietta Morelli, V. Gottardi, and M. Guglielmi. "Raman and infrared spectra on silica gel evolving toward glass." *Journal of Non-Crystalline Solids* 48, no. 1 (1982): 117-128.

231. Duran, A., C. Serna, V. Fornes, and J.M. Fernandez Navarro. "Structural considerations about SiO2 glasses prepared by sol-gel." *Journal of Non-Crystalline Solids* 82, no. 1-3 (1986): 69-77.

232. Ou, D.L., and A.B. Seddon. "Near- and mid-infrared spectroscopy of sol-gel derived ormosils: vinyl and phenyl silicates." *Journal of Non-Crystalline Solids* 210, no. 2-3 (1997): 187-203.

233. Jones, C.W., K. Tsuji, and M.E. Davis. "Organic-functionalized molecular sieves as shape-selective catalysts." *Nature* 393, no. 6680 (1998): 52-54.

234. Sato, K., F. Kurosawa, and O. Kammori. "Effect of Particle Size on Infrared Spectra of Inorganic Powders." *Bulletin of the Chemical Society of Japan* 42, no. 12 (1969): 3593-3596.

235. Matko, S., A. Toldy, S. Keszei, P. Anna, G. Bertalan, and G. Marosi. "Flame retardancy of biodegradable polymers and biocomposites." *Polymer Degradation and Stability* 88, no. 1 (2005): 138-145.

236. Lowell, S., J.E. Shields, M.A. Thomas, and M. Thommes. *Characterization of Porous Solids and Powders: Surface Area, Pore Size and Density*. Dordrecht, The Netherlands: Kluwer Academic Publishers, 2004.

237. McCash, E.M. *Surface Chemistry*. New York: Oxford University Press Inc., 2001.

238. *Chemical Processes on Solid Surfaces*. The Royal Swedish Academy of Sciences, 2007.

239. Brunauer, S., P.H. Emmett, and E. Teller. "Adsorption of Gases in Multimolecular Layers." *Journal of the American Chemical Society* 60, no. 2 (1938): 309-319.

240. Ertl, G. *Reactions at surfaces: From atoms to complexity*. The Royal Swedish Academy of Sciences, 2007.

241. Rouquerolt, J., D. Avnir, C.W. Fairbridge, D.H. Everett, J.H. Haynes, N. Pernicone, J.D. Ramsay, K.S.W. Sing, and K.K. Unger. "Recommendations for the characterization of porous solids." *Pure & Appl. Chem.* 66, no. 8 (1994): 1739-1758.

242. *NOVA Win2: Operation manual*. Quantachrome Instruments, 2003.

243. D'Souzae, J.I., and D.H.N. More, "Mercury Intrusion Porosimetry : A Tool for Pharmaceutical Particle Characterization" http://www.pharmainfo.net/reviews/mercury-intrusion-porosimetry-tool-pharmaceutical-particle-characterization.

244. Neumann, R. "Applications of Polyoxometalates in Homogeneous Catalysis." In *Polyoxometalate Molecular Science*, edited by J.J. Borrás-Almenar, E. Coronado and A. Müller, 98. Dordrecht: Kluwer Academic Publishers, 2003.

245. Misono, M. "Unique acid catalysis of heteropoly compounds (heteropolyoxometalates) in the solid state." *Chemical Communications*, no. 13 (2001): 1141-1152.

246. Marta, G., E. Gianotti, and S. Coluccia. "The Application of UV-Visible-NIS Spectroscopy to Oxides." In *Metal oxide catalysis*, edited by S.D. Jackson and J.S.J. Hargreaves, 1. Weinheim: Wiley-VCH, 2009.

247. Bordoloi, A., S. Sahoo, F. Lefebvre, and S.B. Halligudi. "Heteropoly acid-based supported ionic liquid-phase catalyst for the selective oxidation of alcohols." *Journal of Catalysis* 259, no. 2 (2008): 232-239.

248. Joseph, T., and S.B. Halligudi. "Oxyfunctionalization of limonene using vanadium complex anchored on functionalized SBA-15." *Journal of Molecular Catalysis A: Chemical* 229, no. 1-2 (2005): 241-247.

249. Bonfranceschi, A., L.E. Briand, and H.J. Thomas. "Selective oxidation of anthracene to 9,10-anthraquinone over silica supported vanadium catalyst." *Reaction Kinetics and Catalysis Letters* 77, no. 1 (2002): 59-64.

250. Casey, J.P. *Casey´s Report on Paper and the Paper Industry*. New York: Chemical and Mechanical Pulping. Marcel Dekker, 1984.

251. Albers, R.E., M. Nystrm, M. Siverstrm, A. Sellin, A.C. Dellve, U. Andersson, W. Hermann, and T. Berglin. *Catal. Today* 69 (2001): 247.

252. *Ullmans's Encyclopedia of Industrial Chemistry.* Germany:Wiley-VCH Verlag Gmbh, 1998.

253. Lown, J.W. "Anthracycline and anthraquinone anticancer agents: current status and recent developments." *Pharmacol Ther* 60, no. 2 (1993): 185-214.

254. Baerns, M., H. Borchert, R. Kalthoff, P. Kaβner, F. Majunke, S. Trautmann, and A. Zein. *Stud. Surf. Sci. Catal.* 72 (1992): 57.

255. Brükner, A., and M. Baerns. *Appl. Catal.* 157 (1997): 311.

256. Deo, G., and I.E. Wachs. *J. Catal.* 146 (1994): 323.

257. Khenkin, Alexander M., and R. Neumann. "Low-Temperature Activation of Dioxygen and Hydrocarbon Oxidation Catalyzed by a Phosphovanadomolybdate: Evidence for a Mars-van Krevelen Type Mechanism in a Homogeneous Liquid Phase13." *Angewandte Chemie* 39, no. 22 (2000): 4088-4090.

258. Khenkin, A.M., L. Weiner, Y. Wang, and R. Neumann. "Electron and Oxygen Transfer in Polyoxometalate, H5PV2Mo10O40, Catalyzed Oxidation of Aromatic and Alkyl Aromatic Compounds: Evidence for Aerobic Marsâˆ’van Krevelen-Type Reactions in the Liquid Homogeneous Phase." *Journal of the American Chemical Society* 123, no. 35 (2001): 8531-8542.

259. Strukul, G. *Catalytic Oxidations with Hydrogen Peroxide as Oxidant*. Dordrecht: Kluwer Academic Publishers, 1992.

260. Ortiz de Montellano, P.R. *Cytochrome P450*. New York: Plenum Press, 1995.

261. Strukul, G., and R.A. Michelin. "Catalytic epoxidation of 1-octene with diluted hydrogen peroxide. On the basic role of hydroxo complexes of platinum(II) and related species." *Journal of the American Chemical Society* 107, no. 25 (2002): 7563-7569.

262. Ishii, Y., K. Yamawaki, T. Ura, H. Yamada, T. Yoshida, and M. Ogawa. "Hydrogen peroxide oxidation catalyzed by heteropoly acids combined with

cetylpyridinium chloride. Epoxidation of olefins and allylic alcohols, ketonization of alcohols and diols, and oxidative cleavage of 1,2-diols and olefins." *The Journal of Organic Chemistry* 53, no. 15 (2002): 3587-3593.

263. Venturello, C., E. Alneri, and M. Ricci. "A new, effective catalytic system for epoxidation of olefins by hydrogen peroxide under phase-transfer conditions." *The Journal of Organic Chemistry* 48, no. 21 (2002): 3831-3833.